Assessing the Potential of Small Molecules of Natural Origin in Emerging Biological Targets

Inauguraldissertation

zur

Erlangung der Würde eines Doktors der Philosophie

vorgelegt der

Philosophisch-Naturwissenschaftlichen Fakultät

der Universität Basel

von

Maria Teresa Faleschini

aus Süd-Afrika

Basel, 2017

Genehmigt von der Philosophisch-Naturwissenschaftlichen Fakultät

auf Antrag von

Prof. Dr. Matthias Hamburger

Prof. Dr. Jürg Gertsch

Basel, den 20.06.2017

Prof. Dr. Martin Spiess

Dekan

Attribution-NonCommercial-NoDerivatives 3.0 Switzerland

(CC BY-NC-ND 3.0 CH)

You are free to Share — to copy, distribute and transmit the work

Under the following conditions:

Attribution — You must attribute the work in the manner specified by the author or licensor (but not in any way that suggests that they endorse you or your use of the work).

Noncommercial — You may not use this work for commercial purposes.

No Derivative Works — You may not alter, transform, or buildup on this work.

With the understanding that:

- **Waiver** — Any of the above conditions can be **waived** if you get permission from the copyrightholder.
- **Public Domain** — Where the work or any of its elements is in the **public domain** under applicable law, that status is in no way affected by the license.
- **Other Rights** — In no way are any of the following rights affected by the license:
  - Your fairdealing or **fairuse** rights, or other applicable copyright exceptions and limitations;
  - The author's **moral** rights;
  - Rights other persons may have either in the work itself or in how the work is used, such as **publicity** or privacy rights.
- **Notice** — For any reuse or distribution, you must make clear to others the license terms of this work. The best way to do this is with a link to this webpage.

Quelle: creativecommons.org/licenses/by-nc-nd/3.0/ch/deed.en Datum: 12.11.2013

Acknowledgements

First and foremost, I am deeply indebted to Professor Dr. Matthias Hamburger, for his continuous support, sharing of knowledge and experiences which have tremendously expanded my view of science, it was a privilege to work under his supervision. My deepest and immense gratitude extends to PD Dr. Olivier Potterat for his continuous encouragement, productive guidance, most fruitful discussions, friendliness and cherished dedication he has provided me with throughout my research. Also, my heartfelt gratitude extends to Dr. Maria De Mieri, for all her pronounced and continuous support on NMR and ECD, her devoted inspiration and profound friendship she provided me with in every step of my research. Additionally, I would like to deeply thank Dr. Samad Ebrahimi and Dr. Niels Guldbrandsen for their help and fascinating discussions during the beginning of my research. I would like to convey my deepest appreciation to Dr. Mouhssin Oufir, for the discussions and support in all aspects of lab work and life; as well as Orlando Fertig, for his never-ending dedicated technical assistance and organisation. I would like to extend my warmest gratitude to Manuela Rogalski, for her outstanding manifold assistance and support, she is extraordinary. My deepest thanks go to Prof. Dr. Jürg Gertsch for taking the time to review my thesis and to Prof. Dr. Daniel Ricklin for chairing my defence.

I would like to express my utmost gratitude to my numerous collaborators – of which none of this work would have been possible: Prof. Dr. Michael Sinnreich and Dr. Ruben Herrendorff (in DM1-project), Prof. Dr. Jean Pieters, Dr. Rajesh Jayachandran and Dr. Saumya Mazumder (in TB-project), Prof. Dr. Michael Detmar, Dr. Epameinondas Gousopoulos and Jihye Kim (in Lymphatic-project), as well as Prof. Dr. Fürst and his team (in CHF-project). Furthermore, the successful completion of my PhD thesis was possible thanks to the encouragement of all my colleagues in the lab, of which I would like to acknowledge some of them here; Justine, Alen, Daniela, Fahimeh, Evelyn, Elisabetta, Jakob, Yoshie, Diana, Olga, Nova, Marzieh, Halim, Maryam, Sara, thank you for the amazing environment and the friendships we have formed. I would also like to acknowledge Ms Delpho for the support during my scholarship time as well as the Switzerland Government Excellence Scholarship, South African National Research Foundation and Oppenheimer Memorial Trust for their financial support.

During the years of my doctorate I had the privilege to live with and enjoy all my single days with my Swiss mother figure Maria Rutz. I am forever grateful to her, for her exceptional kindness, encouragement and support she has provided and shared with me. I am also grateful to Maria Rutz's family. I also had an unforgettable privilege to spend my time with the amazing Sonnenweg family: Hans and Sibylle Kohler, Michael Kierdorf, Dorli, Pepita, Mützli, Maggie, Soleia and Chiamo - who shared their lives with me and opened their hearts. Danke, dass du mir das Gefühl, zu Hause zu sein, gibst. Lastly, thank you to my family and friends back in South Africa and all of those who welcomed me in Switzerland, for their love and support throughout my PhD research.

Table of Contents

Abbreviations

AC	Absolute Configuration
APCI	Atmospheric Pressure Chemical Ionisation
ASE	Accelerated Speed Extraction
BBO	Double resonance Broad Band probe (5 mm)
CCC	Countercurrent Chromatography
$CHCl_3$	Chloroform
^{13}C	Carbon NMR
CHF	Chronic Heart Failure
CLCN1	Chloride channel
COR-1	Coronin-1
COSY	Correlation Spectroscopy
CPC	Centrifugal Partition Chromatography
CS	Countercurrent Separation
CUG_{78}	Cytosine Uracil Guanine (78 basepair hairpin loop)
DAD	Diode Array Detector
DCM	Dichloromethane
DM1	Myotonic Dystrophy type I
DMPK	Dystrophia Myotonica Protein Kinase
DMSO	Dimethylsulfoxide
DMSO-*d6*	Deuterated dimethylsulfoxide
DNP	Dictionary of Natural Products
EC	Effective Concentration
ECD	Electronic Circular Dichroism

EIC	Extracted Ion Chromatogram
ELSD	Evaporative Light Scattering Detector
EMB	Ethambutol
ESI-MS	Electron Spray Ionisation – Mass Spectroscopy
ETH	Ethionamide
EtOAc	Ethyl acetate
FAO	Fatty Acid β-Oxidation
GC	Gas Chromatography
GFP	Green Fluorescence Protein
^{1}H	Proton NMR
H_2O	Deionised Water (HPLC grade)
HMBC	Heteronuclear Multiple Bond Correlation
HPLC	High Performance Liquid Chromatography
HR	High Resolution
HSQC	Heteronuclear Single Quantum Coherence
INH	Isoniazid
INSR	Insulin Receptor
IPA	Isopropanol
IS	Internal Standard
LECs	Lymphatic Endothelial Cells
MBNL1	Muscleblind-like 1
MDR-TB	Multidrug Resistant TB strain
MeCN	Acetonitrile
MeOH	Methanol
MP	Mobile Phase

MTB	*Mycobacterium tuberculosis*
NCE	New Chemical Entity
NMR	Nuclear Magnetic Resonance
NOESY	Nuclear Overhauser effect spectroscopy
NYHA	New York Heart Association
OD_{450}	Optical Density at 450 nm
PDA	Photodiode Array
PZA	Pyrazinamide
qHNMR	quantitative ^{1}H-NMR
RIF	Rifampicin
RFP	Red Fluorescence Protein
ROESY	Rotating frame nuclear Overhauser effect spectroscopy
RR-TB	Rifampicin-Resistant TB strain
TB	Tuberculosis
TCM	Traditional Chinese Medicine
TLC	Thin Layer Chromatography
TNNT2	Cardiac Troponin type 2
TOF	Time-Of-Flight
TXI	Triple resonance probe (1 mm)
SCPC	Speed-Centrifugal-Partition-Chromatography
SD	Standard Deviation
SERCA1	Sarcoplasmic/endoplasmic reticulum Ca^{2+} ATPase 1
S/N	Signal-to-Noise ratio
SP	Stationary Phase
UTR	Untranslated Region (gene)

UV-Vis	Ultraviolet-Visible
VCD	Vibrational Circular Dichroism
VEC	Vascular Endothelial Cells
XDR-TB	Extensively Drug Resistant TB strain

Summary

Since the post-genomics era, our understanding of intracellular and intercellular processes, and interaction mechanisms has increased, this has led to the discovery of new biological targets for drug discovery. Generally modern medicinal chemistry and pharmacognosy research seek to identify new small molecules which can selectively modulate the functions of these biological targets. Natural products (such as substances extracted from plants or animals) are a vast reservoir of complex and highly structurally diverse chemical compounds. As a result they remain to play a vital role in the discovery of novel bioactive molecules (lead compounds) which could have therapeutic benefit in medicinal chemistry, and/or structures that could be used as chemical probes for understanding certain unknown biological processes. Especially following technological advances on instruments that are used for characterisation of natural products as well as in extraction and screening methods, the field of natural products is growing fast and making significant contributions in areas of biochemistry and drug discovery. Given the facts discussed so far, natural products need to be continually tested on emerging biological targets, via processing them and analysing their results with modern technologies such as HPLC-UV-MS-ELSD and microprobe NMR.

Based on aforementioned background, the main aims of this study are: (a) to test the activity of various plant and fungal extracts on four emerging biological targets (assays), and (b) to characterise the active extracts and to distinguish the molecules which are possibly responsible for observed biological activities on each of the four biological targets (assays). These four emerging biological targets (assays) and their purposes are: (1) inhibition of complex formation between CUGn-RNA and MBNL1; which was identified as an important target for the treatment of Myotonic Dystrophy type 1 (DM1); (2) inhibition of the expression of a protein named coronin-1, since expression of coronin-1 is essential for the survival of pathogenic *Mycobacterium tuberculosis* in the human host, thus inhibiting this expression is identified as an important target for the treatment of Tuberculosis (TB); (3) promotion of Lymphatic Endothelial Cell (LEC) growth, which was identified to be an important testing platform for pinpointing bioactive molecules which could possibly be used for the treatment of lymphedema or chronic skin inflammation; and (4) inhibiting thrombin-induced [Ca^{2+}] influx, since the underlying mechanism through which *Crataegus* WS 1442 extracts treat Chronic Heart Failure (CHF) was found to be via inhibiting thrombin-induced [Ca^{2+}] influx which leads to a reduction in

endothelial hyperpermeability. Thus this assay was identified to be an important testing platform for pinpointing bioactive molecules which could possibly be used for the treatment of CHF. Based on the respective biological targets given above, this study was divided into four projects, namely: DM1-project, TB-project, Lymphatic-project, and CHF-project. Three of these projects (DM1, TB, and Lymphatic) started with an extract library screening; whereas the last project (CHF) was initiated due to the use of *Crataegus* WS 1442 extracts as an adjuvant therapy. Moreover, in each of these projects, to track activity and characterise selected natural products that exhibit an interaction with the biological targets, the approach known as HPLC-based activity profiling is utilised. The main findings and concluding remarks of these four projects are summarised as follows:

[1] DM1-project: based on the screening results, harmine (from *Peganum harmala*) as well as 1,2-dihydrotanshinquinone I and methylenetanshinquinone (from *Salvia miltiorrhiza*) were identified as the most active compounds in inhibiting CUGn-RNA and MBNL1 complex formation. Also subsequent to the identification of active scaffold of harmine; planar-nitrogen-based compounds (such as protoberberine alkaloids) were projected to possess higher activity. Thus an alkaloid library was tested and berberine was found to be another main active compound. These bioactive alkaloids (i.e., harmine and berberine) are able to ameliorate certain aspects of the DM1 pathology, whereas the compounds from *Salvia* species (i.e., *S. miltiorrhiza*) exhibit some activities with certain degrees of toxicity, thereby these compounds need further investigation. Notably, the findings of this study exhibited that compounds with planar scaffolds which contain mostly nitrogen were more active in inhibiting CUGn-RNA–MBNL1 complex formation and restoring MBNL1 function. It was projected that the mechanism through which these active molecules restore MBNL1 function is due to these bioactive molecules-induced reversible intercalation into the RNA hairpin loop via electrostatic interactions, thereby blocking the binding of MBNL1 and allowing it to carry out its normal function. Overall the hit compounds found in this study may have the potential for drug discovery in RNA-mediated diseases.

[2] TB-project: following the feedback from extract library screening, HPLC-based activity profiling (bioactivity tracking) was carried out on prioritised extracts. This led to the identification of active constituents (class of compounds) that are feasibly responsible for inhibition of coronin-1 expression, namely: alkaloids (from *Pancratium*

littorale MeOH extract) and furanocoumarins (from *Dorstenia contrajerva* EtOAc extract). Furthermore, a compound named 'dorstenin' was isolated from *D. contrajerva* EtOAc extract and it was found that the compound is active only at a much higher concentration; this implied that dorstenin was not the major contributor for activity observed from *D. contrajerva* extract. On the other hand, 15 alkaloids were isolated from *P. littorale* MeOH extract. Subsequently their activities were tested using Green Fluorescence Protein (GFP) as a readout for coronin-1 inhibition as well as their toxicities were tested using Red Fluorescence Protein (RFP). Activity/toxicity correlated structural analysis of these pure alkaloids showed that molecules with secondary nitrogen and methylenedioxy groups are higher in toxicity, whereas molecules which contain a hemiacetal ring and acetylation of some hydroxy functions are active. Moreover further examination using western blotting illustrates that alkaloid compounds which showed highest activity in GFP assay were inactive in inhibiting coronin-1 expression at the protein level. Because of these contrasting GFP assay and western blotting activity outcomes, this study recommends that (a) after GFP testing, it is crucial to confirm coronin-1 expression on a genetic level while identifying lead compounds, such as via RT-PCR tests; and (b) it is important to re-evaluate the utilisation of GFP assay for testing coronin-1 inhibition, which may include the need of conducting further investigation on understanding the interaction mechanism of compounds with GFP and its responses. This is also important to provide insights into the use of natural products as chemical probes in cell biology.

[3] Lymphatic-project: based on the extract library screening, DCM extract of *Daphne giraldii* was identified as an active extract in inducing LEC growth. Afterwards this extract underwent a series of fractionation and assaying. The results of this profiling showed that activities are localised in lipophilic regions of the *D. giraldii* DCM extract. Also, each active micro-fraction contains trace amounts of potent bioactive constituents; as a result this study was unable to isolate the active compounds that are responsible for observed activities. However, through various correlative analysis techniques (such as using minimum effective concentration as a reference, clustering script and NMR), this study projected that daphnetoxin could be (at least one of) the main contributing factors for observed activities. In addition to this, fatty acid signals were identified in the active micro-fractions, these fatty acids might also play a role in

overall observed activity. To certainly identify this and other constituents of *D. giraldii* active micro-fractions, this study recommends the need of working with large amounts of optimally prepared extracts; which will allow bioassay-guided refined separations to end up with suitable amounts of pure compounds for identification.

[4] CHF-project: *Crataegus* WS 1442 extract was separated into 9 fractions and their activities were tested via calcium imaging assay. The results exhibited that only 2 fractions were active in inhibiting thrombin-induced [Ca^{2+}] influx which leads to a reduction in endothelial hyperpermeability. Further fractionation of the two active fractions (via semi-preparative HPLC-UV chromatography) and analysis on the resulting active sub-fractions showed that all of them contain fatty acids and triterpenes. Moreover selective analysis on one of the active sub-fractions showed that it constituted 40% fatty acids (stearic acid and palmitic acid) and 50% of a triterpene (hyptatic acid A). These constituents which comprise almost 90% of this active sub-fraction were tested in their pure form and were found to be inactive in inhibiting thrombin-induced calcium influx. This implies that minor compounds which comprise maximum 10% of the active sub-fraction constituents were responsible for observed activities. Based on the results given so far, this study deduced that the activities of *Crataegus* WS 1442 extracts were possibly induced by: (a) a minor constituent with potent activity; or (b) minor constituents with moderate activity which act synergistically. This study thus recommends further research on large amounts of optimally prepared *Crataegus* extracts to be able to certainly identify the molecule(s) responsible for observed activity and to assess their biological interactions.

Overall each of the studies presented in this thesis were one of the first to employ natural products in assessing their interactions or abilities to interact with the four emerging biological targets which are summarised above. The final remark of this study is that there are very few or no known drugs on the market to treat these specific diseases that are associated with the aforementioned four projects. In this context, this study makes significant contributions, via providing: (a) new hit compounds; (b) possible constituents of potently active fractions; (c) activity correlated structural analysis and extract characterisation; as well as (d) by identifying challenges and providing possible recommendations. Lastly, besides presenting the findings of this study on different conferences, parts of the results presented in this thesis have been published.

Zusammenfassung

Seit der postgenomischen Ära hat sich unser Verständnis von intrazellulären und interzellulären Prozessen und Interaktionsmechanismen verbessert, was zur Entdeckung neuer biologischer Targets geführt hat. Im Allgemeinen versucht die moderne medizinische Chemie- und Pharmakognosieforschung, neue Kleinmoleküle zu identifizieren, die die Funktionen dieser biologischen Ziele selektiv modulieren können. Dafür ist die Gesamtheit der Naturstoffe (wie z. B. Moleküle aus Pflanzen und Tieren) ein riesiges Reservoir an komplexen und stark strukturell verschiedenen chemischen Verbindungen. Daher spielen sie eine wichtige Rolle bei der Entdeckung neuartiger bioaktiver Moleküle (Leitstrukturen) mit therapeutischem Nutzen in der medizinischen Chemie. Andererseits können solche Strukturen als chemische Sonden zum Verständnis bestimmter unbekannter biologischer Prozesse verwendet werden. Die technologischen Fortschritte von modernen Instrumenten, die zur Charakterisierung von Naturstoffen sowie für Extraktions- und Screening-Methoden eingesetzt werden, sind im Bereich der Naturstoffe substanziell und leisten einen wichtigen Beitrag in der Biochemie und der Wirkstoffforschung. Angesichts dessen, müssen Naturstoffe kontinuierlich auf neu entdeckten biologischen Zielen getestet werden. Dabei helfen moderne Technologien wie HPLC-UV-MS-ELSD und Mikrosonden-NMR, um möglichst viele Informationen zu bekommen und auszuwerten.

Vor diesem Hintergrund sind die Hauptziele dieser Arbeit: (a) die Aktivität verschiedener Pflanzen- und Pilz-Extrakte auf vier neuen biologischen Targets (Assays) zu testen und (b) die aktiven Extrakte zu charakterisieren und die Moleküle zu identifizieren, die möglicherweise für die beobachteten biologischen Aktivitäten verantwortlich sind. Diese vier neuen biologischen Ziele (Assays) und ihre Anwendungen sind: (1) Hemmung der Komplexbildung zwischen CUGn-RNA und MBNL1, was als wichtiges Ziel für die Behandlung der Myotonischen Dystrophie Typ 1 (DM1) identifiziert wurde; (2) Hemmung der Expression des Proteins Coronin-1, da Coronin-1 für das Überleben von pathogenen *Mycobacterium tuberculosis*-Bakterien im menschlichen Wirt essentiell ist, sodass die Expressionshemmung als wichtiges Ziel für die Behandlung von Tuberkulose (TB) gesehen wird; (3) Förderung des Lymphatischen Endothelzell (LEC) -Wachstums, das als eine wichtige Testplattform für die Lokalisierung von bioaktiven Molekülen identifiziert wurde, die möglicherweise für die Behandlung von Lymphödemen verwendet werden könnten; Und (4) Hemmung des Thrombin-induzierten [Ca^{2+}] -Einstroms, was der

zugrundeliegende Mechanismus ist, durch den *Crataegus* WS 1442 Extrakte chronische Herzversagen (CHF) behandeln. Dabei wurde eine Hemmung des Thrombin-induzierten [Ca^{2+}] -Zustroms gefunden, was zu einer Reduktion der Hyperpermeabilität des Endothels führt. Damit wurde dieser Assay als eine wichtige Testplattform für die Lokalisierung von bioaktiven Molekülen identifiziert, die für die Behandlung von CHF verwendet werden könnten. Auf Grundlage der oben genannten biologischen Ziele wurde diese Studie in vier Projekte unterteilt: DM1-Projekt, TB-Projekt, Lymphatic-projekt und CHF-Projekt. Drei dieser Projekte (DM1, TB und Lymphatic) begannen mit einem Extrakt-Bibliotheks-Screening, während das letzte Projekt (CHF) aufgrund der Verwendung von *Crataegus* WS 1442-Extrakten als adjuvante Therapie initiiert wurde. Darüber hinaus wird in jedem dieser Projekte, um die Aktivität zu verfolgen und ausgewählte Naturstoffe zu charakterisieren, die eine Wechselwirkung mit den biologischen Targets aufweisen, der Ansatz, der als HPLC-basierte Aktivitätsprofilierung bekannt ist, verwendet. Die wichtigsten Erkenntnisse und Schlussbemerkungen dieser vier Projekte sind wie folgt zusammengefasst:

[1] DM1-Projekt: Basierend auf den Screening-Ergebnissen wurden Harmin (aus *Peganum harmala*) sowie 1,2-Dihydrotanshinchinon I und Methylentanshinchinon (aus *Salvia miltiorrhiza*) als die aktivsten Verbindungen bei der Inhibierung von CUGn-RNA und MBNL1-Komplexbildung identifiziert. Nach der Identifizierung des aktiven Gerüstes von Harmin wurde eine höhere Aktivität bei planaren Stickstoffverbindungen (wie Protoberberin-Alkaloiden) vermutet. Daher wurde eine Alkaloidbibliothek getestet und Berberin als ein weiterer Hauptwirkstoff gefunden. Diese bioaktiven Alkaloide (d.h. Harmin und Berberin) sind in der Lage, bestimmte Aspekte der DM1-Pathologie zu lindern während die Verbindungen aus *Salvia*-Spezies (d.h. *S. miltiorrhiza*) Aktivität verbunden mit einer gewissen Toxizität aufweisen, so dass diese Verbindungen weiter genauer werden müssen. Bemerkenswerterweise zeigten die Ergebnisse dieser Studie, dass Verbindungen mit planaren Gerüsten, die meistens Stickstoff enthalten, bei der Hemmung der CUGN-RNA und MBNL1-Komplexbildung und der Wiederherstellung der MBNL1-Funktion aktiver waren. Es wurde prognostiziert, dass der Mechanismus, durch den diese aktiven Moleküle die MBNL1-Funktion wiederherstellen, auf der Interkalation in die RNA-Haarnadelschleife über elektrostatische Wechselwirkungen beruht. Dadurch wird die Bindung von MBNL1 blockiert und ihm ermöglicht wird, seine normale Funktion

auszuführen. Insgesamt können die in dieser Studie gefundenen Hit-strukturen das Potenzial für die Wirkstoffforschung bei RNA-vermittelten Erkrankungen haben.

[2] TB-Projekt: Nach den Ergebnissen aus dem Extrakt-Bibliotheks-Screening wurde ein HPLC-basiertes Aktivitätsprofiling (Bioaktivitätsverfolgung) auf priorisierten Extrakten durchgeführt. Dies führte zur Identifizierung von aktiven Bestandteilen (Klasse von Verbindungen), die für die Hemmung der Coronin-1-Expression verantwortlich sind, nämlich: Alkaloide (aus *Pancratium littorale* MeOH-Extrakt) und Furanocumarinen (aus *Dorstenia contrajerva* EtOAc-Extrakt). Weiterhin wurde eine Verbindung namens 'Dorstenin' aus *D. contrajerva* EtOAc-Extrakt isoliert und es wurde gefunden, dass die Verbindung nur in hohen Konzentrationen aktiv ist. Dies bedeutet, dass Dorstenin nicht den Hauptbeitrag zur Aktivität leistet, die im *D. contrajerva*-Extrakt beobachtet wurde. Auf der anderen Seite wurden 15 Alkaloide aus *P. littorale* MeOH-Extrakt isoliert. Anschließend wurden die Aktivitäten mit Green Fluorescence Protein (GFP) getestet und ihre Toxizitäten wurden mit Red Fluorescence Protein (RFP) getestet. Aktivität / Toxizität korrelierte Strukturanalyse dieser reinen Alkaloide zeigte, dass Moleküle mit sekundären Stickstoff- und Methylendioxygruppen eine höhere Toxizität aufweisen während Moleküle, die einen Hemiacetalring und eine Acetylierung von einigen Hydroxyfunktionen enthalten, aktiver sind. Darüber hinaus zeigt die weitere Untersuchung mit Western-Blotting, dass Alkaloidverbindungen, die die höchste Aktivität im GFP-Assay zeigten, bei der Inhibierung der Coronin-1-Expression auf Proteinebene inaktiv waren. Aufgrund dieser kontrastierenden GFP-Assay- und Western-Blotting-Aktivitätsergebnisse empfiehlt diese Studie, dass (a) nach dem GFP-Testen entscheidend ist, die Coronin-1-Expression auf genetischer Ebene etwa mit RT-PCR-Tests zu bestätigen, um Leitstrukturen zu identifizieren; Und (b) es ist wichtig, die Verwendung des GFP-Tests zur Prüfung der Coronin-1-Hemmung neu zu bewerten, was die Notwendigkeit einer weiteren Untersuchung des Verständnisses des Interaktionsmechanismus von Verbindungen mit GFP und deren Reaktionen einschließen kann. Dies ist auch wichtig, um Einblicke in die Verwendung von Naturstoffen als chemische Sonden in der Zellbiologie zu bekommen.

[3] Lymphatic-projekt: Auf der Basis des Extraktbibliotheks-Screenings wurde der DCM-Extrakt von *Daphne giraldii* als aktiver Extrakt bei der Induktion des LEC-Wachstums identifiziert. Danach wurde dieser Auszug einer Reihe von Fraktionierungen und

Untersuchungen unterzogen. Die Ergebnisse dieses Profilings zeigen, dass die Aktivität in den lipophilen Regionen des *D. giraldii* DCM-Extrakts lokalisiert ist. Auch enthält jede aktive Mikrofraktion Spurenmengen von stark bioaktiven Bestandteilen; Infolgedessen war diese Studie nicht in der Lage, die Wirkstoffe zu isolieren, die für beobachteten Aktivitäten verantwortlich sind. Allerdings prognostiziert diese Studie durch verschiedene Korrelatanalysetechniken (z. B. die Verwendung von minimaler effektiver Konzentration als Referenz, Clustering-Skript und NMR), dass Daphnetoxin einer der wichtigsten Faktoren für die beobachtete Aktivität sein könnte. Darüber hinaus wurden in den aktiven Mikrofraktionen Fettsäure-Signale identifiziert, die auch bei der Gesamtaktivität eine Rolle spielen könnten. Um diese und andere Bestandteile von *D. giraldii* aktiven Mikrofraktionen sicher zu identifizieren, empfiehlt diese Studie, mit größeren Mengen optimierten Extrakten zu arbeiten, die es ermöglichen, Bioassay-geführte verbesserte Trennungen mit geeigneten Mengen an reinen Verbindungen zur Identifizierung zu beenden.

[4] CHF-Projekt: *Crataegus* WS 1442-Extrakt wurde in 9 Fraktionen aufgetrennt und die Aktivität wurde mittels Calcium-Imaging-Assay getestet. Die Ergebnisse zeigten 2 aktive Fraktionen, die den Thrombin-induzierten [Ca^{2+}] - Einstrom hemmen, der zu einer Verringerung der endothelialen Hyperpermeabilität führt. Eine weitere Fraktionierung der beiden aktiven Fraktionen (über semi-präparative HPLC-UV-Chromatographie) und die Analyse der resultierenden aktiven Teilfraktionen zeigte, dass alle Fettsäuren und Triterpene enthalten. Darüber hinaus zeigte die selektive Analyse an einer der aktiven Teilfraktionen, dass sie aus 40% Fettsäuren (Stearinsäure und Palmitinsäure) und 50% Triterpen (hyptatische Säure A) besteht. Diese Bestandteile, die fast 90% dieser aktiven Teilfraktion ausmachten, wurden in ihrer reinen Form getestet und es wurde festgestellt, dass sie bei der Inhibierung des Thrombin-induzierten Calcium-Zustroms inaktiv waren. Dies bedeutet, dass für beobachtete Aktivitäten andere Verbindungen, die maximal 10% der aktiven Teilfraktionsbestandteile enthalten, verantwortlich sind. Auf der Grundlage der bisherigen Ergebnisse ergab diese Studie, dass die Aktivitäten von *Crataegus* WS 1442-Extrakten möglicherweise durch: (a) einen Bestandteil, der in geringfügigen Mengen vorliegt aber eine hohe Aktivität aufweist, induziert wurden; Oder (b) geringfügig vorliegende Bestandteile mit mäßiger Aktivität, die synergistisch wirken. Diese Studie empfiehlt daher, weitere Mengen an optimal vorbereiteten

Crataegus-Extrakten zu untersuchen, um das für die beobachtete Aktivität verantwortliche(n) Molekül(e) sicher zu identifizieren und ihre biologischen Wechselwirkungen zu beurteilen.

Insgesamt war jede der in dieser Arbeit vorgestellten Studien eine der ersten, die die Interaktion von Naturstoffen mit den vier oben beschriebenen biologischen Targets untersuchen. Das Fazit dieser Studie ist, dass es nur wenige oder keine bekannten Medikamente auf dem Markt gibt, um diese spezifischen Krankheiten zu behandeln, die mit den vorgenannten vier Projekten verbunden sind. In diesem Zusammenhang leistet diese Studie erhebliche Beiträge, indem sie: (a) neue Hit-strukturen identifiziert hat, (b) mögliche Bestandteile von stark aktiven Fraktionen gefunden hat, (c) Aktivitätskorrelierte Strukturanalyse und Extraktcharakterisierung durchgeführt hat sowie (d) Hindernisse identifiziert und mögliche Lösungsstrategien genannt hat. Schließlich wurden neben der Präsentation der Erkenntnisse auf verschiedenen Plattformen auch Teile der in dieser Arbeit vorgestellten Studien veröffentlicht.

Chapter 1

1. Introduction

1.1 Drug Discovery and Development

Medicine is considered as one of the most important necessity to all of us. It is derived from the Latin words '*ars medicina'* meaning "the art of healing". It's a branch of the health sciences and is the sector of public life concerned with maintaining or restoring human health through the study, diagnosis, treatment and possible prevention of disease, injury and other damage to our body or mind[1]. This area encompasses an understanding of the body system, its diseases, and treatment by drugs, diet, exercise and other nonsurgical means, which is used to maintain our health. An agent such as a drug is employed to treat a disease or injury[1]. A drug can be defined as a chemical that interacts with a biological system and produces a biological response[2]. Drug discovery and development is a complex process where chemistry, preclinical, and clinical pharmacology have a prevalent role but it is also supported by the knowledge of several other life science disciplines such as genetics, physiology, pathology, microbiology, and molecular biology[2]. Generally, drug discovery and development is a time- and financially- consuming process and can be divided into three main stages (see Fig. 1.2): drug discovery, drug development, and registration; which are briefly discussed below[3].

The process of drug discovery starts because there is a continuous unmet need for new medicine to combat diseases or clinical conditions with insufficient medical products available. This is the underlying motivation that drives drug discovery efforts[4]. Generally, discovery of the biological target and validation, hit identification, as well as lead optimisation are the main steps in the drug discovery process. During these processes chemistry is involved in various fundamental forms such as synthesis or extraction, drug analysis, formulation and pharmaceutical technologies[2]. Historically, the first medicinal drugs came from natural sources and existed in the form of herbs, plants, roots, vines and fungi[5]. Medicinal value of these natural sources were discovered through traditional means or by serendipitous discovery[5].

The initial research of drug discovery involves two main approaches as depicted in Fig. 1.1: classical pharmacology[6], and reverse pharmacology[7]. In the classical approach (also known as phenotypic drug discovery[8]), synthetic molecules or natural extracts are screened in intact cells

or whole organisms for biological activity without knowledge of the biological target. Only after an active substance was identified to have a desirable therapeutic effect is an effort made to identify the target. This approach is quick but often leads to various time consuming mode of action studies and challenging lead optimisation[9]. An additional challenge is effectively incorporating new screening technologies to address the limitation of considerably lower throughput than target-based assays[7]. The second approach, reverse pharmacology (also known as target-based drug discovery[10]), is the most frequently used approach today[7]. This approach first identifies a target (such as a protein or pathway) which is hypothesised that upon its inhibition or activation, a therapeutic effect will be observed in the disease state[4]. Cloning of the human genome made possible the screening of large libraries of compounds against specific targets thought to be linked to specific diseases. The advantage of this approach is that once a lead is found the mode of action is already known, therefore easier medicinal chemistry and lead optimisation[9]. Also, since the protein target is already known the hits can immediately be tested in further cell or animal models[7]. The strengths of the target-based approach include the ability to apply molecular and chemical knowledge to investigate specific molecular hypotheses[7]. However, many potential leads may be lost because they act on different targets, and protein expression and assay development can be challenging[9]. Additionally, the solution to the specific molecular hypotheses may not be relevant to the disease pathogenesis or provide a significant therapeutic index[7]. During drug discovery, ADMET (Absorption, Distribution, Metabolism, Elimination, and Toxicity) properties are also assessed[11]. Based on these data, lead structures are optimised, before they enter the drug development phase.

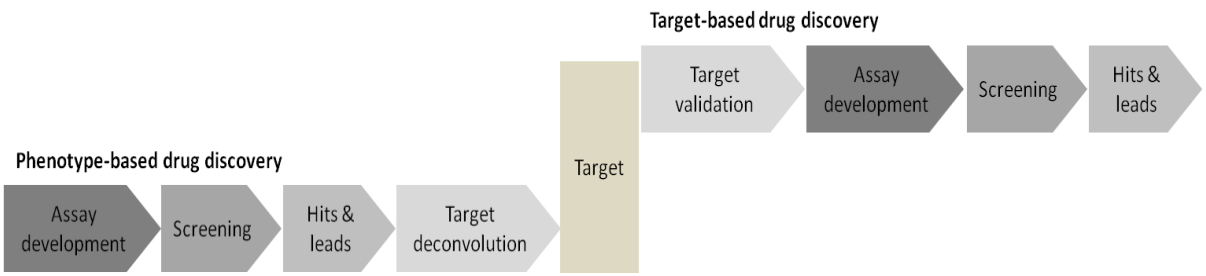

Figure 1.1: Phenotype- versus target- based drug discovery. In the phenotype-based approach, lead molecules are first obtained, followed by target deconvolution to identify the molecular targets that underlie the observed phenotypic effects. Conversely, in the target-based approach, molecular targets are identified and validated before lead discovery starts (adapted from[10]).

Generally, the origin of lead compounds can be from natural or synthetic sources. Natural products and their derivatives have been recognised for many years as a source of therapeutic agents and structural diversity[12]. In addition to their structural diversity and bioactivity, the development of new technologies has revolutionised the screening of natural products for the discovery of new drugs. Applying these technologies compensates for the inherent limitations of natural products and offers a unique opportunity to re-establish natural products as a major source of lead compounds for drug discovery. Accordingly, natural products are an enormous source of effective drug compounds that is unsurpassed by synthetic libraries[12]. The development and formulation of various novel drugs from natural sources, as an alternative to conventional synthetic products, increases the scientific community's interest in medicinal plants[13]. Further discussion on natural products and technologies which improve the use of natural products in drug discovery is provided in section 1.2 and 1.3, respectively. Overall, once these lead compounds are identified, they are evaluated for their potential to be developed into pharmaceutical drugs for a particular disease. This is an important initial step which links drug discovery and drug development. The drug development process is divided into three main stages: preclinical testing in animals, phase I (first in man studies), and full clinical trials (phase II and III); before the compound finally enters the registration phase. Prior to market launch, new drugs undergo a long and complicated series of steps, including an evaluation of efficacy and safety, application for approval, and investigation and approval of drug applications by regulatory authorities. A new active principle that has received marketing authorisation is usually protected by a patent and can be marketed only by the company owning the patent or by licensed companies. However, when the patent expires, generic drugs can be developed and, under some given rules, can be produced and marketed by any other company[2].

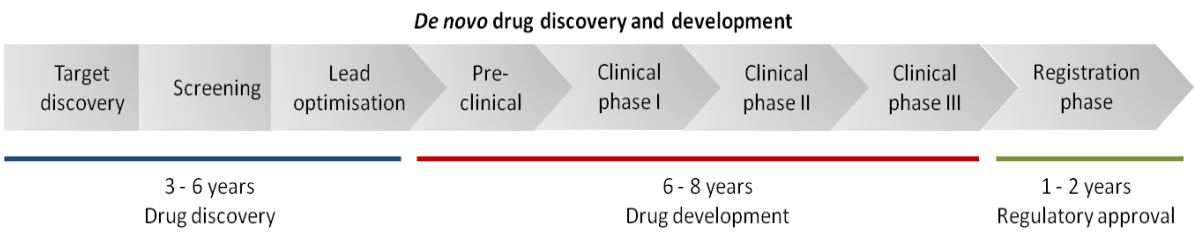

Figure 1.2: Simplified process of drug discovery and development with an estimate of the time required for the three main stages (adapted from[14,15]).

1.2 Natural Products in Drug Discovery

1.2.1 The Importance of Natural Products

Since ancient times, man has relied on nature to sustain his basic needs, and for curing or relieving various maladies or symptoms. Natural products include a large and diverse group of secondary metabolites from a variety of sources, such as marine organisms, bacteria, fungi, and plants. Not only do natural products provide sustenance or medicine but also possess a plethora of novel molecular scaffolds and interrogate a different and wider chemical space with structural and chemical diversity that is unsurpassed by synthetic derivatives[16–20]. Many natural products have gone onto become current drug candidates[20].

The history of natural products in drug discovery is full of noteworthy accounts on how the discovery of a natural compound impacted advances in biology and therapies. Isolation of the well-known drug, morphine, from *Papaver somniferum* (the opium poppy) in 1817 spurred interest in identifying the active principles of plant-based medicines[21]. Following this breakthrough many alkaloids were discovered from plant sources, such as emetine from *Carapichea ipecacuanha* in 1817, which is nowadays used for its emetic properties[22]. Coniine, first isolated in 1826 from *Conium maculatum*[23] (poison hemlock), is still a candidate today for current drug discovery, this time being a model for induction of apoptosis in trypanosomal infections[24]. Commercialisation of the antibiotic penicillin in the 1940s was a significant milestone in drug discovery research, and spurred an enormous amount of effort in this field[25]. The structures of the above discussed compounds can be found in Fig. 1.3.

Many interesting biologically active secondary metabolites are alkaloids. However, not all drugs derived from natural products are nitrogen based. One natural product, salvinorin A (see Fig. 1.3), first isolated in 1982 from *Salvia divinorum*, a *trans*-neoclerodane diterpene[26], is a hallucinogenic molecule that acts as a κ-opiod selective agonist, making it the first known compound acting on this receptor that is not an alkaloid[27]. Additionally, salvinorin A has no action at the 5-HT_{2A} serotonin receptor, which is the principal molecular target responsible for the action of classical hallucinogens such as LSD or mescaline[27]. The most extraordinary examples of natural products making it to a marketable drug unchanged clearly emphasises the importance of continuing the search of new drugs using nature as a source. On average natural products represent 34 ± 9% of New Chemical Entity (NCE) approvals (from 1999 to 2014)[28]. Not

only are natural products used for treating various diseases but, nowadays play advantageous roles in understanding biological processes[25].

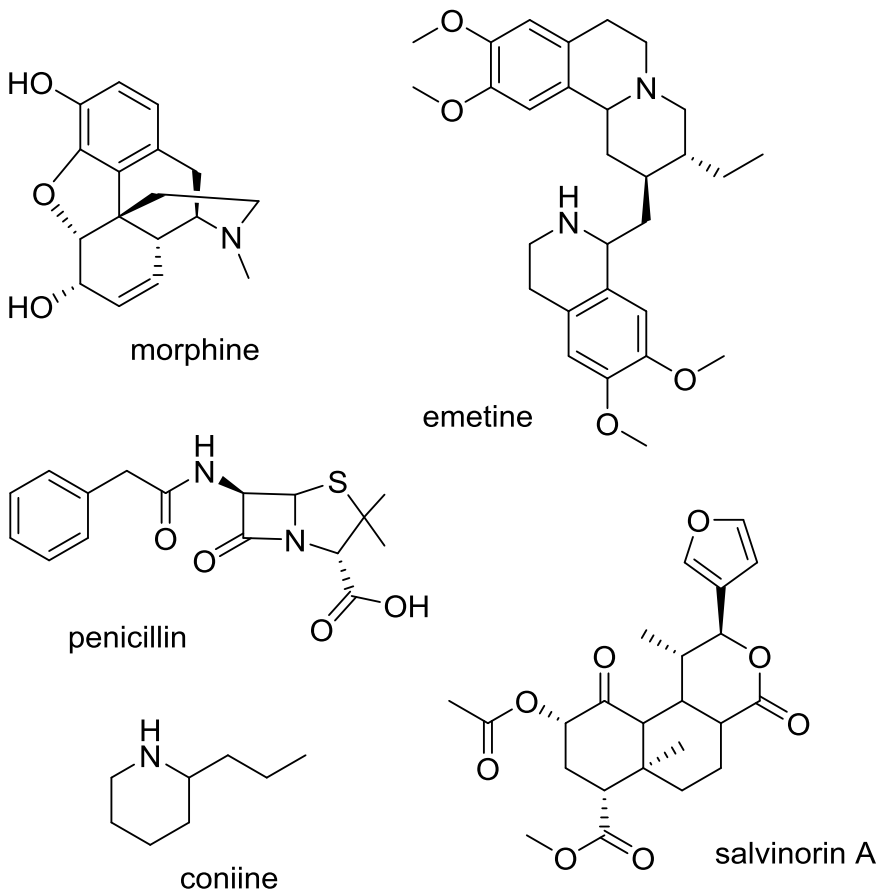

Figure 1.3: Structures of selected natural products namely morphine, emetine, coniine, penicillin, and salvinorin A.

1.2.2 Natural Products as Chemical Probes of Cell Biology

Substances that were identified as late as the 1970s are still influencing chemists and biologists to use the 'native product' either as probes for specific targets or as a treatment in its own right[21]. Natural products have been central to the discovery of novel drug targets and represent a unique source of chemical tools to investigate proteins and signalling networks[25]. It is believed that compounds found in nature are often far more superior to even the best synthetic moieties in terms of diversity, specificity, binding efficiency, and propensity to interact with biological targets[25,29,30]. It is these characteristics that have lead researchers to use natural products in studies that facilitate the exploration of a biological system (that is to use them as chemical probes) and not only for the identification of potential therapeutic agents[31]. Various

review articles[25,32–36] have summarised the plethora of natural products used as chemical probes to explore biological phenomena and assemble biochemical pathways, below only a select few will be discussed (see Fig. 1.4 for structures of the natural products discussed below).

The understanding of how natural products affect normal biological processes at the molecular level has often guided new strategies for drug design[31]. The relationship between histone deacetylases, transcription regulation and cell cycle progression was established by understanding the molecular targets of trichostatin A and trapoxin B[31,32]. This knowledge lead to the development of histone deacetylase inhibitors for the treatment of cancer at the transcription level[31,37]. Trichostatin A, initially isolated from *Streptomyces hygroscopicus* in 1976 on the basis of its anti-proliferative activity[38]; and trapoxin B, a cyclic tetrapeptide isolated from the fungus *Helicoma ambiens* which caused cell cycle arrest in mammalian cells, were found to inhibit histone deacetylation[39].

The mechanism of information transfer or signalling through the cytoplasm of the cell is one of the great mysteries of cell biology. Natural products that inhibit this process offer a unique window into fundamental aspects of how extracellular molecules influence events[34]. Rapamycin, a macrolide lactone produced by *Streptomyces hygroscopicus*, and its derivatives have played a pivotal role in the clarification of several cellular processes including cell growth, proliferation, survival, protein synthesis, and transcription[40,41]. It was first identified as an antibiotic/anti-fungal agent but due to its immunosuppressive properties was rejected and later rediscovered for its potent immunosuppressive and anti-proliferative properties. In 1999 it was approved as an immunosuppressive drug[42]. Studies on the mode of action of rapamycin revealed a new signalling pathway which is central to cell growth[31]. Rapamycin was shown to bind to mTOR (mammalian Target Of Rapamycin), a protein which subsequently appeared critical for the regulation of major events regarding cell growth. This triggered more in-depth studies of mTOR and its essential function in cells was clarified thanks to the use of rapamycin[31,43].

The molecular mechanisms through which cyclosporine suppresses an immune response pioneered the field of chemical biology. Cyclosporine was isolated from the fungus *Tolypocladium inflatum* on the basis of its anti-fungal properties, but its spectrum was too narrow to be of any clinical use. Thereafter, its immunosuppressive action was found and it became the first immunosuppressive drug that allowed selective immunoregulation of T cells

without excessive toxicity[44]. Elucidating the mode of action provided insights into understanding the mechanism leading to T-cell activation. This natural product was shown to associate with intracellular receptors that inhibit the regulation of cytokine gene expression, leading to a general immunosuppressive activity[31,34]. Macrocyclic immunosuppressive natural products such as rapamycin and cyclosporine have been valuable not only as therapeutic agents but also as lead structures for studying the regulatory processes of cell proliferation[33].

Natural products have also played a crucial role in the identification and characterisation of thermo-sensitive ion channels[31,45]. For example, the mechanism through which capsaicin, the pungent ingredient of hot chilli peppers, elicits a hot sensation remained unknown for many years, until capsaicin was used as a molecular probe for pain/heat signal propagation[32]. Its receptor was cloned and named transient receptor potential vanilloid 1 (TRPV1)[46], which is strongly activated by capsaicin and when neurons are subjected to temperatures above a pain-threshold[32]. Additionally, this receptor was shown to be a heat-activated ion channel involved in pain sensation, opening a new field of research on temperature-dependent ion channels[31,46] and understanding the mechanisms involved in the heat-stimulated pain pathway[32]. Similarly, menthol was found to activate the cold-sensitive receptor TRPM8 in a comparable manner as its natural stimulus[31,47]. TRPM8 was later shown to be permeable to ions (Na^+, K^+, Ca^{2+}, or Ba^{2+}) under both natural and provoked stimuli[31,48].

Much of what is currently known about the structure and organisation of the mitotic spindle was determined by the use of small molecules, such as colchicine and taxol[49]. Generally, these compounds are tubulin-binding agents (e.g. taxol) and have been developed into successful cancer therapeutic agents[25].

In general, chemical probes are an essential component of research and are utilised to dissect complex biological processes, to wield temporal control over biochemical pathways, and to identify novel therapeutic targets. The studies above highlight the use of natural products as biological probes given their innate ability to interact with high affinity and selectivity with biological targets and will continue to map important biochemical networks and identify novel therapeutic strategies[25]. Biologically active natural products have proven to be invaluable in the exploration of systems that cannot be studied by traditional genetic manipulations[32].

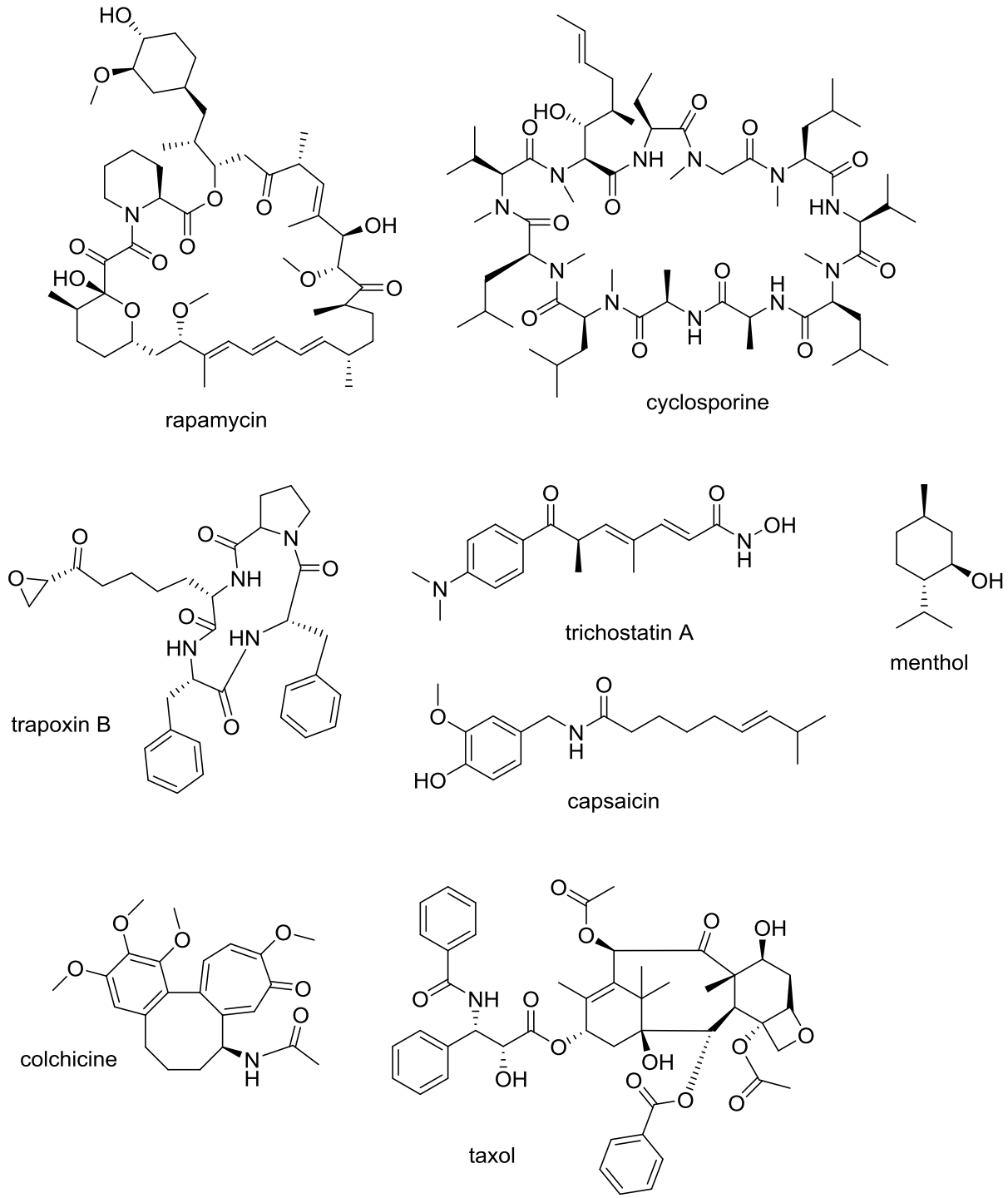

Figure 1.4: Structures of selected natural products that have played a significant role in chemical biology acting as chemical probes, namely trichostatin, trapoxin B, rapamycin, cyclosporine, capsaicin, menthol, colchicine, and taxol.

1.2.3 Main Steps Employed for the Study of Natural Products in Drug Discovery

In the investigation of natural products, various crucial steps need to be followed, which will be briefly discussed below.

(**i**) Plant Selection Criteria and Supply

The criteria used for the selection of plants to be studied sets the course of the work. There are four basic types of approaches: randomised, ecological, chemotaxonomic, and ethno-directed approaches. The random approach consists of an indiscriminate selection and collection of plant species according to the plant availability. The second approach consists of observing the interactions between organisms in their ecological environment, such as observing animals in their eating habits could lead researchers to test certain plants. The chemotaxonomic approach consists of identifying groups of constituents present in plants, by considering the taxonomic organisation of these plants. The ethno-guided approach consists of selecting plant species in accordance to their traditional use. This allows collaboration between traditional healers, botanists and researchers[50]. The issue when working with natural products is that populations of plants possessing potent substances are in danger of becoming extinct especially if the active secondary metabolites are present in minor quantities – which is most often the case. For industrial exploitation of plant derived metabolites to be used as such or as starting material for synthesis, economically viable and ecologically responsible production is a necessity[51]. Finding alternative ways of producing the active compound isolated from nature may be difficult, due to the extreme complexity of chemistry that can be present in a natural compound such as taxol that was isolated in 1971 from *Taxus brevifolia* (Taxaceae) for its anti-cancer properties[51].

About two decades ago, the legalities of obtaining samples of plants, microbes, and animals were straightforward. A researcher could arrive at a field, collect samples and take them home. An example of this was the discovery of the anti-fungal compound, cyclosporine. A soil sample collected from employees of Sandoz during their business trips or holidays were catalogued and later screened. In 1970, the fungus *Tolypocladium inflatum* was isolated from two soil samples, thereby leading to the discovery of cyclosporine based on its anti-fungal properties. Nowadays, cyclosporine is used in organ transplant patients to prevent organ rejection due to its potent immunosuppressive properties[44]. However, in 1992, the Convention on Biological Diversity (CBD) was signed; which lead to various forms of regulations and legislation which control the

acquisition of biological materials and indigenous knowledge. The implementation of these regulations had a profound impact on academic and industrial research groups. Agreements to access biological materials required lengthy negotiations on intellectual property and benefit sharing. The CBD was conceived with the aim to facilitate a higher level of international collaboration, but it lead to several pharmaceutical companies abandoning their natural product screening efforts. Alternatively, there have been a number of successful cooperative agreements between academic groups, pharmaceutical industries and governmental institutions in biodiversity-rich countries[51–53]. Afterwards, the Nagoya Protocol was implemented for fair, reliable, simple, and transparent access regulations[54]. These provisions should be viewed as an opportunity to carry out natural product research in an ethical way, within an agreed legal framework, however lengthy the process may take[54]. In this sense it protects the institution or company involved from charges of biopiracy and in addition, provides the possibility of doing some good for a developing country[51–53].

(**ii**) Extraction of Plant Metabolites

The study on medicinal plants starts with an efficient extraction procedure that plays a critical role in the outcome and also on the consequent assays performed. The term extraction, used in its pharmaceutical sense, involves the removal of plant secondary metabolites from the inert components by using selective solvents through standard procedures. A wide range of technologies with different methods of extraction is available nowadays. Both fresh and dried plant materials such as leaves, barks, roots, fruits, and flowers can be utilised for extract sample preparation; however pre-extraction preparation of plant samples such as drying (air-drying, oven-drying, freeze-drying) and grinding processes can influence the preservation of secondary metabolites in the final extract. Therefore, the selection of proper extraction procedures requires thorough evaluation that accomplishes the intended objectives of the research. There are various types of extraction methods which have their own principle, equipment needs, strengths and limitations[13,55]. Traditional methods such as maceration, percolation, and soxhlet extraction (hot continuous extraction) are commonly used at research settings or small level manufacturing. Accelerated Solvent Extraction (ASE)[56] and supercritical fluid extraction are also being used in the extraction of plant materials. These methods are less common due to high cost despite the efficiency of the methods. On the other hand, following technological advances, modern extraction methods which increase yields with lower costs have emerged

such as Microwave-Assisted Extraction (MAE)[57] and Ultrasound-Assisted Extraction (UAE)[55,58]. These extraction methods are usually applicable for selective needs such as extracting polar molecules and for large scale extraction at low cost. All the methods that employ solvents in their procedures (maceration, MAE, UAE and ASE) are critically influenced by the solvent types[13]; thus in these methods the selection of suitable solvent type and volume is crucial. For further discussion on the strengths and limitations of different extraction methods the reader is referred to[13,59] and references therein. Extracts which are produced from various plant materials through different methods and solvents can be stored in stock solutions (typically 10 mg/mL in DMSO) at lower temperatures; this is known as an extract library. It is a useful way to store extracts and repeatedly screen the collection of extracts for various biological activities[60].

(**iii**) Biological Screening

Before pursuing the separation of pure compounds from plant extracts, biological screening (analysis on biological assay outcome) is carried out in order to assess the presence of active compounds in the extracts. Biological assay (also known as bioassay) is a test method employed to determine the biological activity of a substance such as a drug on tissue or cell lines (*in vitro*), or live animal or plants (*in vivo*). An analytical *in vitro* procedure used to detect, quantify and/or study the binding or activity of a biological molecule, such as an enzyme, is commonly known as a biochemical assay. Generally, bioassays (biochemical assays) are typically conducted to examine the biological activity of a substance on an organism, tissue, cell, or target protein (enzyme or receptor), via determining the relative strength of the induced biological response/changes on the target of interest while compared to a standard preparation (positive and negative controls). Biological assays can be qualitative or quantitative. Qualitative assays are used for assessing the physical effects or mechanism of action of a substance that may not be quantified. Quantitative assays involve estimation of the dose-response curve, which allows estimation of the concentration of a substance associated with a specific biological response. For example the half maximal inhibitory concentration (IC_{50}) represents the concentration of a particular drug (inhibitor) that is required for 50% *in vitro* inhibition of a given biological process (biochemical function). Overall quantitative assays are essential for toxicological information, extract/compound screening (cell-based and/or isolated target screening[61]) or for developing drug candidates with therapeutic value.

A variety of assays can be used to evaluate or screen the selected *in vitro* activity of an extract or pure compound. However, on various screening results, a high number of false positives might be observed, this is due to the common presence of compounds with non-specific activities or interference with the assay format. Polyphenolic compounds, such as tannins, form tight complexes with metal ions and a wide array of proteins, while polysaccharides often give a false-positive result in most assays involving a purified protein. Saponins and fatty acids, widely distributed in plants, have the propensity to disrupt membranes causing a misleading result. In assays based on light measurements, pigments, ultraviolet (UV) quenchers and auto-fluorescent compounds are prone to interfere with the readout of the assay[51,62].

(**iv**) Isolation of Active Constituents and Structure Elucidation

Natural product extracts are composed of a complex mixture of various types of bioactive compounds and phytochemicals with different polarities. Therefore separation of bioactive pure compounds and their characterisation requires further processing utilising different chromatographic and structural elucidation techniques. Various chromatographic techniques exist such as silica gel column chromatography, sephadex chromatography, Thin Layer Chromatography (TLC), and preparative or semi-preparative High Performance Liquid Chromatography (HPLC). Each technique is based on the principle that certain compounds have different migration rates given a particular stationary and mobile phase. Separation is achieved by exploiting the affinities of different compounds for the mobile or stationary phases. More details on these techniques can be found in numerous reviews[59,63,64]. Furthermore, to characterise the effluent as it moves through the flow cell such as in terms of mass and/or functional groups (bonds), some of these chromatographic techniques are coupled to different detectors. For example, HPLC is most commonly combined with a UV-Vis absorbance detector (UV) and/or a mass spectrometer[65]. In addition to these, tracking activity in complex plant extracts using the bioassay-guided approach or the miniaturised approach (HPLC-based activity profiling) of small amounts of samples has been developed with the advancement of analytical techniques[66–68]. Throughout the research of this thesis, HPLC-based bioassay-guided activity profiling has been employed; thus this technique will be further discussed in section 1.3.2. Once pure compounds are obtained their chemical structure needs to be determined. One of the most common instruments used for this purpose is a nuclear magnetic resonance (NMR), which will be discussed in more detail in section 1.3.3.

Besides the aforementioned technological advancements, the isolation of a bioactive compound from natural products faces a number of technical challenges. These include variability of source material, difficulty of isolating the active constituents, possibility of isolating an already known active compound or otherwise uninteresting compounds, loss of bioactivity during the purification process, and costs of collection[51,69]. An extract may show a high activity and contain large quantities of only very few moderately active major constituents; or a moderately active extract could lead to minor compounds with high potent activity[70]. Extremely low yields of compounds that may be active make detection and identification challenging. The comparison of fractions generated, whether it is for finding similarities and/or differences in metabolites present in active/inactive fractions or for targeting isolation of unique compounds present in some fractions, may also be somewhat tricky depending on the number of fractions and the complexity or overlapping of compounds present in the fractions. At present, this process is tackled manually, which often results in overlooking of compounds[51,68]. Additionally, the complexity of structures poses difficulties for structural modifications and practical synthesis[51,68].

(**v**) Testing of Pure Compounds Against Intended Target

Once pure compounds are obtained and their structures characterised, it is important to test their activity. Thus the biological response of pure metabolites should be tested in the bioassay that has been used for the extract screening (see section 1.2.3–iii). Following this step, pure metabolites will be further subjected to secondary bioassays (which assess their IC_{50}, toxicity, and selectivity). After this, the drug candidate goes on to the drug development procedure which has been discussed in section 1.1. Identifying a potential drug candidate and processes that follow this step have quite a number of time consuming and labour intensive challenges. A lead compound that was discovered using the cell-based approach has to be subjected to mode of action studies because the molecular target is unknown[10,25,71]. There is a great need for new techniques to facilitate the rapid identification of cellular targets for biologically active natural products[30]. Recent advances in proteomics, three-hybrid systems, phage and mRNA display technologies, chemical synthesis, and affinity chromatography-based methods have greatly accelerated target identification[10,25,72,73]. However, most of these methods require derivatisation of the lead compound to facilitate either covalent interactions between the natural product and the target biomolecule or conjugation of the natural product to a read-out

tag such as biotin or a fluorophore[10,25,71]. This process often requires either total synthesis or semi-synthesis of lead structures. The functionalised natural product could suffer dramatic decrease in the desired bioactivity[25].

Overall, in the fields of natural products and drug discovery, advances in extraction and isolation techniques, biological screening methods, and the development of sensitive instrumentation that are employed for structure elucidation, provide a crucial benefit for the continual growth of novel bioactive molecule identification from natural products. Researchers are constantly working to provide new tools to make identification, functional annotation, and synthesis more straightforward. Even though the pharmaceutical industry expanded its resources to both high-throughput screening (HTS) and combinatorial chemistry which occupied a well-defined area in chemistry, overall in the last 30 years only 30% of NCEs were found to be synthetic, while 52% of these compounds were either a natural product, a mimic, or a chemical modification of an existing natural product pharmacophore[28]. Additionally, natural products are evolutionarily optimised as drug-like molecules and have been designed to interact with biomolecules, which is why so many natural products have gone on to become current drugs[18,28,74]. Forty percent of the chemical scaffolds published in the Dictionary of Natural Products database (Chapman & Hall) are absent from today's synthetic chemistry[75,76]. Only about one-fifth of the ring systems found in natural products are represented in current trade drugs[77]. The declining number of NCEs showed that *de novo* combinatorial chemistry approaches in drug discovery over the past few years were not as efficient as expected and classified as structurally simplistic and poorly designed[78,79]. The power of nature's small molecules far outweighs their challenges, and it has become clear that renewed interest in natural products is essential to the future of both biological studies and drug development[25].

1.3 Tracking Bioactivity in Extracts

Interest in natural product-based drug discovery efforts experienced a decline in the 1980s and 1990s due in part to the advent of combinatorial chemistry coupled with high-throughput screening methods. This however marked a decline in the number of new drug candidates[80]. With the advancement of new techniques used for tracking activity in complex plant extracts, natural products drug discovery was able to meet the demand of high-throughput screening and thus interest was rekindled[25].

1.3.1 Bioassay-guided Approach

Between the 19th century to around the 1980s natural product discovery relied mainly on traditional knowledge, pharmacological observations, well documented usage (evidence-based phytotherapy), and serendipity[54]. During these times, the classical approach for the study and isolation of natural products was used, which comprised of working on few plant samples, testing the extracts for observed activity and 'blindly' isolating as many pure compounds as possible. This classical phytochemical approach is basically based on testing of the extract initially, then carrying out numerous column chromatographic purification steps until a pure compound was obtained. Thereafter, pure compounds were tested for their activity. Generally, this approach targeted mainly the major compounds that were easier to purify and it was not always the case that the specific pure compound that was isolated happened to be the active compound. This approach also often lead to duplication of previously isolated compounds that were already known for a specific activity[51]. Moreover, the biological activity is frequently lost once the pure compound was isolated since it was not possible to know exactly which compound or substances gave rise to the initial observed activity of the extract. This major concern of loss in biological activity lead to the development of a new technique which implements activity testing throughout the separation process, which is known as the bioassay-guided approach[67]. Generally, in modern natural product-based drug discovery processes, a common procedure to isolate active metabolites from an extract is based on bioassay-guided fractionation. This means through different chromatographic techniques, a given extract is separated into a number of smaller quantities (called fractions) in which the composition varies according to their physicochemical properties; and subsequently the biological activity of these fractions will be tested. On the fractions that exhibit activity, further fractionation will be carried out. This loop of separation and assaying method (also known as bioassay-guided approach) will step-by-step lead to isolation of active pure metabolites. Bioassay-guided approach is time consuming, however relative to the classical method it is an advanced approach that made natural product chemistry more targeted towards identification (and purification) of novel bioactive molecules[81]. Particularly, automated assays in microtiter plates allow testing of large numbers of samples in a short time; this makes bioassay-guided approaches more effective in terms of time and specification. Overall, equipped with an array of sensitive and rapid assays and advancement of analytical methods, natural product chemistry became more facilitated to explore the vast chemical wonders present in Nature[82].

As highlighted in section 1.2.3–iv, there are various types of chromatographic techniques that are used for the separation of compounds from a given extract. Different chromatographic techniques have different separation performances[51] and in some cases in order to obtain a decent amount of pure compound after numerous purification steps, a large amount of plant material is needed at the extraction point such as in the case of silica gel chromatography[83]. In addition, some of the classical chromatographic techniques do not allow dereplication of known bioactive molecules or otherwise uninteresting compounds[51]. Considering these and other issues, preparative or semi-preparative HPLC techniques which combines UV and MS becomes one of the most advantageous methods for separation and characterisation of compounds, along with activity localisation in extracts.

1.3.2 HPLC-based Activity Profiling – Miniaturised Approach

Natural products are extraordinary reservoirs of complex novel molecules, of which only one or several compounds may be responsible for the biological activity. Recent advances in analytical techniques opened new possibilities for natural product research[84]. It was imminent that localising activity in complex extracts at an early stage was an important step to further advance research with natural products. The combination of biological data with chemo-analytical information obtained in parallel is key to localising the activity in extracts[51]. HPLC-based activity profiling has been successfully implemented to overcome this major setback. This offline strategy is directly applicable to a broad range of mechanism-based and cellular assays, and has increased in popularity in the context of industrial natural product screening[67]. Miniaturisation of the approach combined with sensitive biological assays decreases the total amount of plant material required and allows researchers to work more effectively, thus decreases sample demand.

During the HPLC-based activity profiling approach, on-line spectroscopy is linked with an off-line bioassay in a microtiter format, via automated micro-fractionation in 96-well plates, followed by removal of solvent prior to biological testing[62]. The retrieval of spectroscopic information during the chromatographic separation, combined with database searches allows early dereplication of possibly known or otherwise uninteresting compounds[62,85]. Semi-preparative HPLC fractionation of peaks of interest is thereafter undertaken for off-line microprobe NMR spectroscopy and high resolution mass spectrometry (HR-MS) data for scaffold and molecular formula prediction. Full structure analysis by NMR involves the

measurement of 1D ^{1}H and ^{13}C and 2D COSY, NOESY, edited HSQC and HMBC spectra, and additional experiments depending on the specific structural issues to be resolved[51]. This approach, which is depicted in Fig. 1.5, allows the interfacing of chemo-analytical and biological data allowing researchers to make significant advances in identifying the active compounds or at least the class of targeted molecules; thus making isolation and purification of the specific class of compounds more efficient (e.g. using alkaloid extraction technique to enrich alkaloidal compounds in a quick and easy step, or polyamide for separation of tannins and diaion for the removal of sugars, etc.). Detailed dereplication strategies are discussed in the review article by Dias and co-workers (2012)[20].

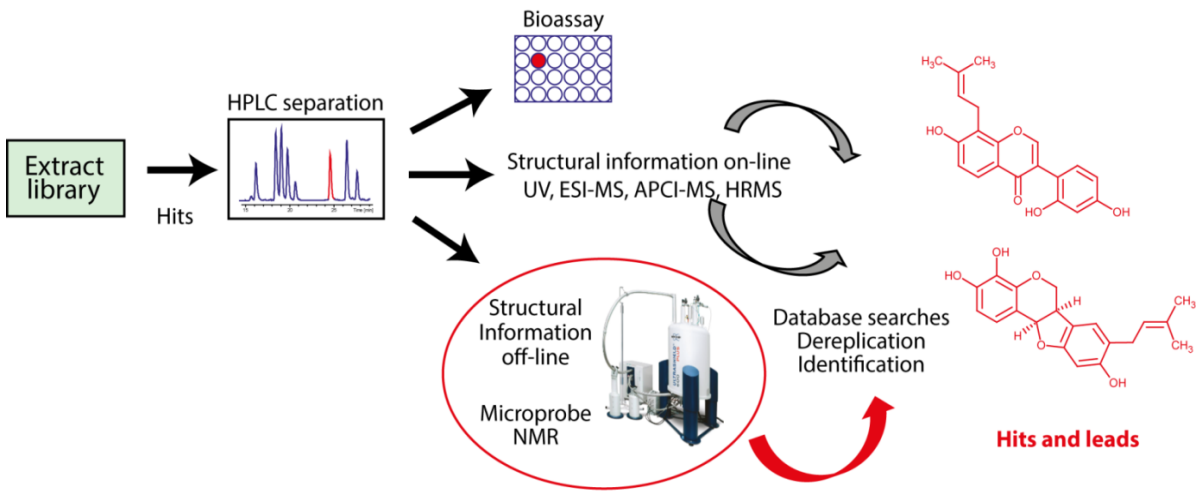

Figure 1.5: Overview of the setup and approach when using HPLC-based activity profiling of bioactive extracts[62].

Besides those which involve adsorption chromatography (e.g. HPLC)[86], partition chromatography is a powerful tool in both early and advanced stages of the fractionation process[70,87]. Generally, Countercurrent Chromatography (CCC) and Centrifugal Partition Chromatography (CPC) are collectively referred to as Countercurrent Separation (CS)[88]. These techniques can handle complex polar or a-polar plant extracts equally well as purified fractions and sample amounts are versatile[87]. Basically, the principle is partitioning solutes between two immiscible liquid phases; separation is achieved due to the affinities of the solutes for the upper or lower liquid phases[89]. The attrition rates in loss of compounds during fractionation steps, as well as loss of bioactivity can be overcome with the use of CCC or CPC since no stationary phase is present (see Fig. 1.6) thus eliminating the chance of irreversible adsorption of compounds and perhaps loss of activity[70].

Figure 1.6: One disc showing the chamber arrangement of the CPC instrument. Photo courtesy of Dr. Thomas Pfeiffer (AlphaCrom AG).

1.3.3 Structure Elucidation and Absolute Configuration of Natural Products

Structure elucidation is an important step for isolated molecules. Various techniques are used to determine the structure, such as UV spectroscopy, MS, and NMR, all of which when taken together can allow the relative configuration of a molecule to be established. UV absorption can be used to allocate compounds to certain classes of secondary metabolites due to the presence of characteristic chromophores which give specific patterns of maximal absorption[66]. Absorption for most natural products occurs in the range of 200 – 550 nm[66], thus also encompassing the Visible region (which is from about 380 – 700 nm). Among all the HPLC detectors, UV is the simplest and most widely used, even though it has some limitations, particularly for natural products that do not possess a chromophore. Compounds that possess a weak chromophore (for example, one double bond as in the case of most triterpene glycosides) can be detected by UV at short wavelengths (λ_{max} 203 nm); however the UV cut-off of certain solvents should be taken into consideration[66]. For compounds with weak/no chromophores evaporative light scattering detector (ELSD) can be employed. This technique can detect any analyte less volatile than the mobile phase. A light beam is directed onto the particles entering the detection cell and will cause scattering of the incident light which is detected by a photodiode or photomultiplier[66]. This technique also gives an estimate quantity of the compounds present, i.e. a higher peak represents a compound with a higher quantity present.

Alternatively, MS provides important structural information online for example molecular weight, molecular formula (achieved with the use of HR-MS) and fragmentation patterns which are crucial for dereplication and characterisation of natural products[66]. Different ionisation sources and mass analysers are available, most commonly electrospray ionisation (ESI) and

atmospheric pressure chemical ionisation (APCI) are used for polar, labile and non-polar, thermally-stable molecules respectively. For mass analysers, single/ triple quadrupole, ion trap, and time-of-flight (TOF) spectrometers are commonly used. Generally TOF is routinely used for accurate mass measurements, and allows assignment of molecular formula with high confidence on sub-nanogram amounts of compound[66].

This information along with 1D ^{1}H-NMR and ^{13}C-NMR experiments, and 2D homonuclear (^{1}H-^{1}H-COSY) and heteronuclear (^{1}H-^{13}C) correlation NMR experiments such as HSQC and HMBC are standard in determining the covalent structure of a small molecule. NOESY and ROESY experiments provide information of the 3D structure of a molecule and are used for the assignment of the relative configuration of the molecules. Sensitivity in NMR instruments is a major setback for identification of metabolites. Nonetheless, with the further development of NMR, in particular the advent of new probe technology and higher magnetic fields, structure elucidation on amounts less than a milligram has become a more routine process[90]. NMR is considered a leading non-destructive analytical tool in structural analysis[91]. These techniques can also be used for the quantification of specific compounds present in the extracts, for example, quantification by ^{1}H-NMR (qHNMR). Some reviews on optimisation of parameters for qHNMR provide useful considerations for the quantification of constituents in an extract[90,91].

For natural products with chiral centres, determination of the absolute configuration (AC) is one of the most challenging features in the elucidation process[92]. AC is the spatial arrangement of the atoms of a chiral carbon and its stereochemical description. Determination of AC of chiral molecules is an important step in any field related to the pharmaceutical industry. The mainly used methods for AC assignment include X-ray crystallography, chiral derivatisation, or stereo-controlled organic synthesis[93]. However, for X-ray crystallography a suitable single crystal is often difficult to obtain especially for some natural products, chiral derivatisation is not always possible on small amounts of sample, and chemical synthesis is hampered by the cost and challenges[92,93]. The use of electronic circular dichroism (ECD) has been shown to be a powerful chiroptical tool for the AC assignment of natural products with various chromophores since the 1960s. CD is the phenomena of a chiral molecule that absorbs left and right circularly polarised light beams to a different extent. The principle is based on the comparison of experimental and calculated ECD spectra; i.e. the more closely they match, the more reliable the AC assignment can be drawn[92]. Vibrational circular dichroism (VCD) is the extension of ECD into infrared and

near-IR regions of the spectrum where vibrational transitions occur within the ground electronic state of the molecule[94]. This technique has many advantages since there is no need for single crystals, derivatisation, or UV-Vis chromophores – the latter being essential for ECD[93]. By comparing the sign and intensity of the experimental spectrum with the *ab initio* DFT calculated spectrum of a chosen configuration, one can unambiguously assign the AC of a chiral molecule.

1.4 Emerging Targets

Understanding the complexities that underline the interactions between the human body and different diseases or disorders is forever growing. The world of science is constantly unravelling new potential drug targets. Along with the advancement of technologies and techniques, researchers can carry out more in-depth investigations. Using the target-based drug discovery approach, identification of the target that is hypothesised that upon its inhibition or activation a therapeutic effect will be observed in the disease state should be well characterised – this information is then transposed into a model assay to screen for potential lead candidates[4]. With emerging targets – the impact of discovering a lead is tremendous to the advancement of science in the related field and to understanding the disease and its interactions on a deeper level. Researchers are now advancing drug discovery, particularly in the fields of hit identification, examination of new targets and exploration of novel chemical space[4]. The following subsections describe the targets of the projects that are encompassed in this thesis.

1.4.1 Myotonic Dystrophy Type I

1.4.1.1 Background

Myotonic dystrophy type I (DM1) is a disabling neuromuscular disorder, characterised by progressive muscle wasting, weakening, cataracts, cardiac conduction defects and myotonia (see Fig. 1.7). Affected individuals have muscle weakness and difficulty with muscle relaxation after a sustained period of contraction[95]. DM1 has a prevalence of 1:8000 people worldwide and is genetically inherited[95]. Due to the many symptoms experienced by patients, DM1 is characterised as a multisystemic disorder. The condition is transmitted as an autosomal dominant trait and becomes more severe as the gene mutation is passed from generation to generation, a phenomenon known as anticipation[96].

The underlying mechanism for anticipation was unknown for a long time however, with the discovery of a group of disorders associated with triplet repeat expansions in a variety of genes; the fundamentals of anticipation could be understood[96].

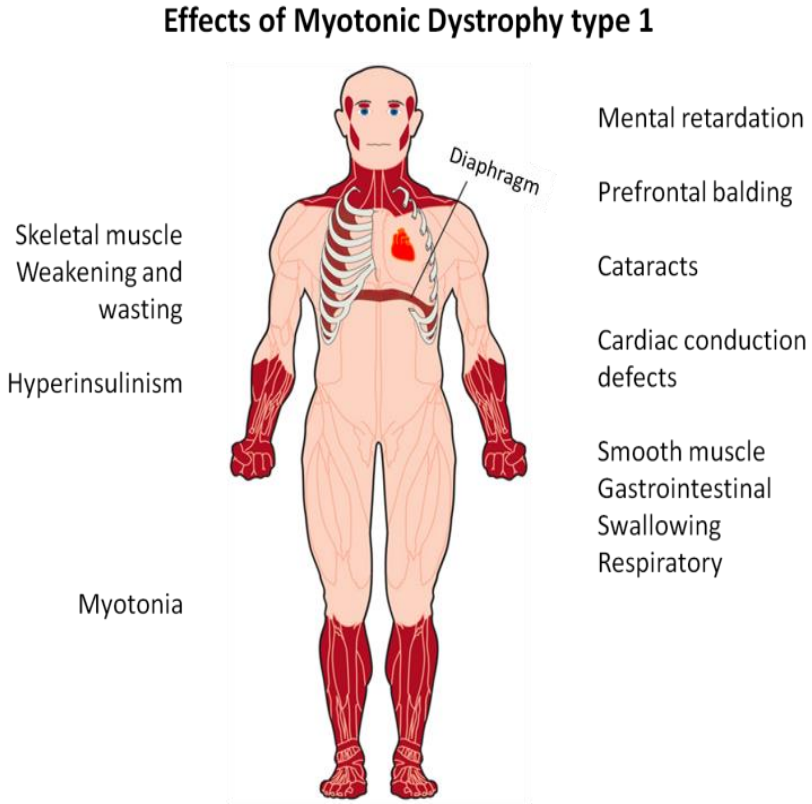

Figure 1.7: Major effects of Myotonic Dystrophy type 1.

1.4.1.2 The Underlying Cause of DM1

In the early 1990s the identification of a new class of disease-causing mutations caused considerable excitement in the scientific community. The mutations were inherited trinucleotide repeat expansions on the DNA level. There is a subset of genes, with trinucleotide repeats in which expansion of the number of repeats beyond a threshold leads to abnormal gene function[96]. The number or triplet repeat expansion is directly linked to the disease severity. Over 20 neurological diseases have now been assigned to this group. Each disease is associated with a single defective gene, which triggers the process of pathogenesis through aberrant expression or toxic properties of mutant transcripts or proteins. Although researchers have been making efforts to develop treatments for these diseases for nearly two decades, they remain incurable. Examples are fragile X syndrome which is an expansion of CGG in the 5' untranslated region (UTR) of the FMR1 gene (Fragile X mental retardation 1 gene) or DM1

which is caused by an expansion of CTG codon in the 3' UTR of the dystrophia myotonica protein kinase (DMPK) gene[97,98] (see Fig. 1.8). DMPK is a protein kinase enzyme part of the rho family of kinases and forms a protein that is almost exclusively expressed in smooth, skeletal, and cardiac muscles in humans.

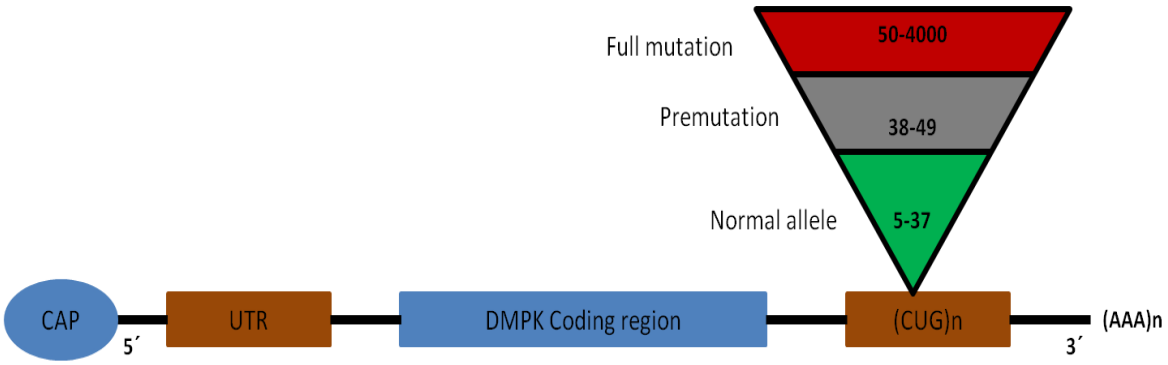

Figure 1.8: Expansion of CTG repeats on the 3' untranslated region of the DMPK gene (adapted from[96]).

As depicted in Fig. 1.9, on the RNA level, expanded $(CUG)_n$ repeats form hairpin structures, which lead to ribonuclear inclusions. More specifically, the RNA with expanded $(CUG)_n$ repeats sequesters splicing-factors such as muscleblind-like 1 (MBNL1), which is involved in alternative splicing. Lack of available MBNL1 leads to miss-regulated alternative splicing of many other pre-mRNA targets, which have been shown to be linked to the multisystemic defects associated with the DM1 pathology.

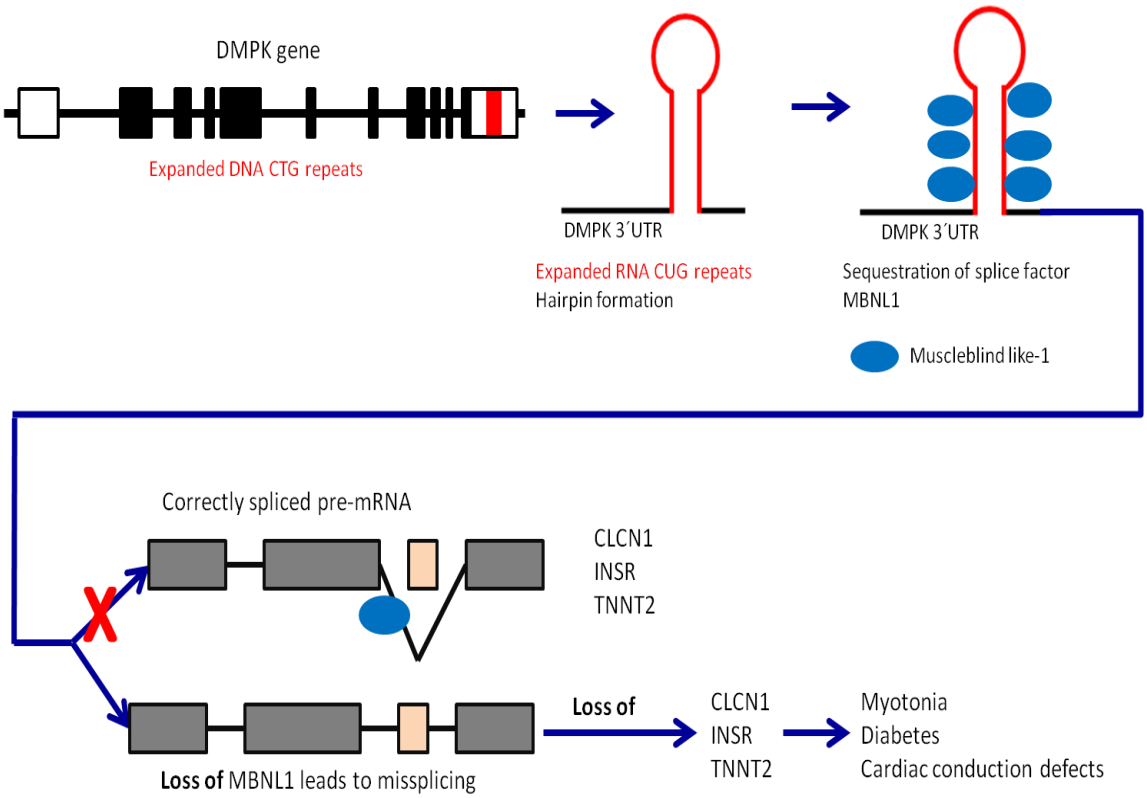

Figure 1.9: Underlying mechanism of DM1, showing the hairpin loop on RNA formed by expanded CUG repeats, which sequester MBNL1 leading to miss-splicing of pre-mRNA targets (adapted from[97]).

MBNL1 proteins control the alternative splicing of specific exons during mammalian postnatal development[99]. This process is dysregulated in DM1 because MBNL1 is sequestered by $(CUG)_n$ RNAs expressed from mutant DMPK genes. This observation suggests that MBNL1 has a higher affinity for pathogenic RNAs rather than their normal splicing targets. However, it has been demonstrated that MBNL1 proteins preferentially recognize CG-rich RNA helices containing a pyrimidine mismatch on both normal splicing substrates and pathogenic RNAs. MBNL1 binds selectively to the stem region of the $(CUG)_n$ RNA which results in a stacked ring complex that effectively traps MBNL1 and inhibits its role as an alternative splicing factor during postnatal development[99], an example of this is shown in Fig. 1.10. Thus, the splicing of a multitude of pre-mRNAs is miss-regulated, including the skeletal muscle chloride channel (CLCN1)[100], the insulin receptor (INSR)[101], sarcoplasmic/endoplasmic reticulum Ca^{2+} ATPase 1 (SERCA1)[102], and cardiac troponin type 2 (TNNT2) pre-mRNA[103]. The miss-splicing of some of these pre-mRNAs can be

linked directly to a certain disease symptom, e.g. myotonia results from the miss-splicing of CLCN1 pre-mRNA.

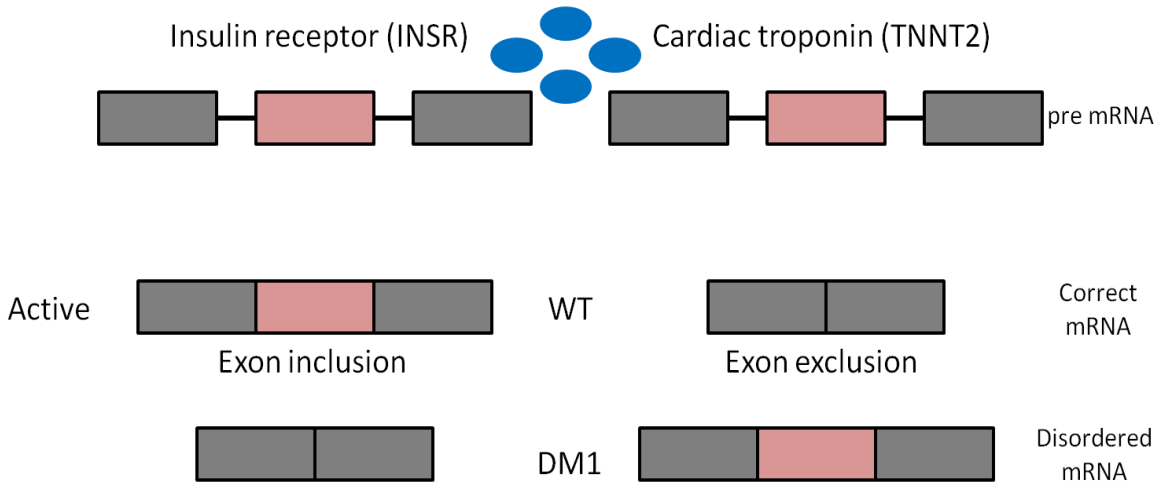

Figure 1.10: Mechanism of miss-splicing due to lack of MBNL1 (in blue), leading to exon exclusion or inclusion (disordered) mRNA in the insulin receptor (INSR) and cardiac troponin (TNNT2), respectively (adapted from[97]).

1.4.1.3 Current Therapies and State of Research

Current therapies include symptomatic therapy which involves visits to the neurologist, the cardiologist, ophthalmologist and endocrinologist, related to the symptoms of DM1. Presently there is no drug on the market with the ability to reverse the defects associated with DM1. Since there is no cure more focus is given to the management of individuals with DM1, which very much depends on the severity and includes vigilant cardiac monitoring and implantation of a pacemaker when indicated, cataract removal, and treatment of diabetes and of pain. Emphasis is on respiratory care and treatment of cardiological complications[97]. Early detection of cardiomyopathy in DM1 is important and treatment of the symptoms includes conventional use of diuretics, angiotensin-converting-enzyme inhibitors, and digitalis glycosides[104]. The most treatable symptom of DM1 is cataract development, which commonly begins in the second decade or later and is characterised by multicoloured lens opacities on slit-lamp examination[104]. Adaptation of assistive devices as the disease progresses is helpful[97].

The hairpin loops formed by expanded triplet repeats that bind and sequester MBNL1 proteins could be targeted by low molecular weight compounds with the idea of disrupting the hairpin structure, and thus interfering with MBNL1 binding. To date, many studies aiming to identify

small molecules targeting the MBNL1-CUGn complex have been focusing on synthetic molecules. Different therapeutic strategies involve development of agents degrading the toxic RNA or blocking its pathogenic interaction with proteins[105] and have been tested in *in vitro* or *in vivo* experiments using animal models[97]. Synthesis of antisense oligonucleotides which are single stranded RNA complimentary to the target RNA are currently being followed. These target the DMPK-$(CUG)_n$ transcripts[106]. Various other approaches include viral over-expression of MBNL1[107], RNA interference[108], ribozyme technology[109], as well as peptides[110], and small molecular compounds[111,112].

Pentamidine has been shown to improve splicing defects associated with DM1[112]. Biochemical experiments in cell and mouse model studies of the disease have indicated that pentamidine and related compounds may bind to the DNA-motif and inhibit transcription[113].

1.4.1.4 Natural Products and DM1

Most of the described $(CUG)_n$ RNA targeting molecules are synthetic. Only a few natural compounds have been described, such as neomycin B[112] and lomofungin[114]. Neomycin B was shown to disrupt MBNL1 binding to CUG repeats *in vitro*, however in tissue culture cells neomycin B was not able to reduce the formation of ribonuclear foci, nor release MBNL1 from the foci in the treated cells[112]. Lomofungin and its dimer dilomofungin were identified as inhibitors of MBNL1-(CUG)n binding. However, in secondary cellular assays the dimer actually increased the expression of CUG^{exp} RNA and the monomer slightly rescued the splicing defects. These results showed the feasibility of identification of novel small molecules targeting toxic RNA, but also demonstrated that ligands for repetitive sequences may have unexpected effects on RNA decay[114]. The structures of these compounds, as well as the synthetic pentamidine are depicted in Fig. 1.11.

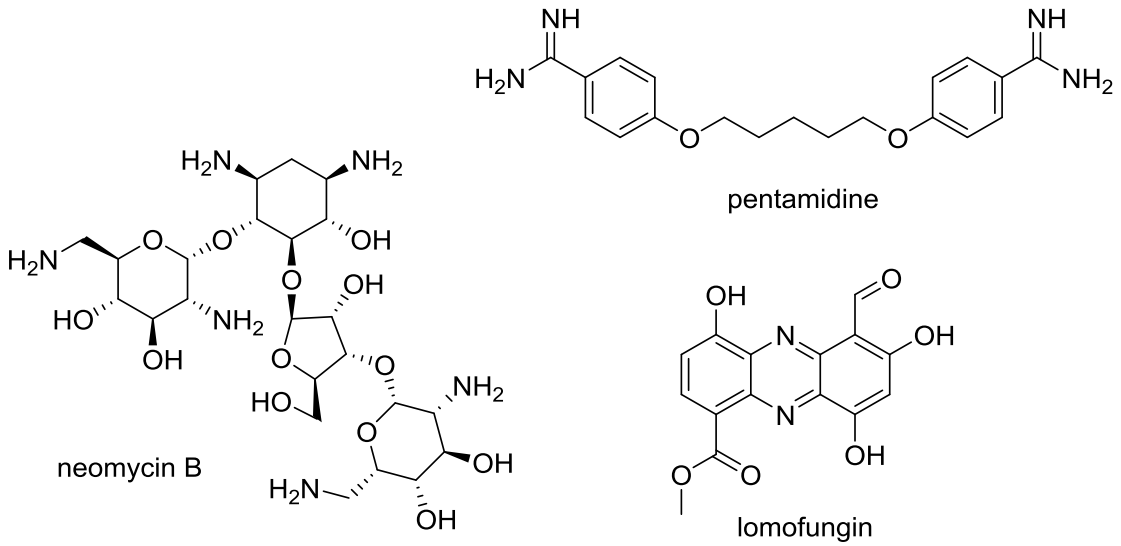

Figure 1.11: Structures of the compounds used in DM1 namely, pentamidine, neomycin B, and lomofungin.

1.4.2 Tuberculosis

1.4.2.1 Background

Tuberculosis (TB) is a widespread infectious disease caused by various strains of mycobacteria, predominantly *Mycobacterium tuberculosis* (MTB) – which generally affects the lungs (see Fig. 1.12). Despite the availability of multiple anti-TB drugs for over 50 years, TB remains the leading infectious killer worldwide, resulting in death of over 1.4 million people per year[115]. The emergence of multidrug resistant- (MDR-) and extensively drug resistant- (XDR-) TB strains warrants the need for new strategies at combating the disease. Globally in 2015, an estimated 480 000 people developed MDR-TB, and an additional 100 000 people with rifampicin-resistant TB (RR-TB)[115], while XDR-TB was detected in over 105 countries[116].

MTB is transmitted from person to person by droplets of air, particularly when people who have an active TB infection cough, sneeze, or otherwise transmit respiratory fluids through the air. Most infections do not exhibit symptoms, which is called latent TB. About one-third of the world's population has latent TB. One in ten of these latent infections will eventually progress to the active disease, which if left untreated, kills more than 50% of those so infected. Individuals with compromised immune systems, such as people living with HIV, have an increased risk of falling ill[116]. The classical symptoms of an active TB infection are chronic

coughing with blood-containing sputum, fever, night sweats, fatigue, loss of appetite and weight loss[116,117].

The causative agent – MTB – is a very persistant pathogen, which can withstand weak disinfectants and survive in a dry state for weeks. MTB is a slow growing, obligate aerobe and has an extremely lipid-rich cell wall which may contribute to its pathogenesis[118,119]. MTB has developed various strategies to persist within the hostile environment of the host macrophage, thereby enabling it to survive[120]. Although most humans and experimental animals develop appropriate immune responses after infection, these immune responses do not reliably eradicate the bacteria. Instead, such responses cause MTB to adopt a clinically silent, latent state of infection, from which the bacteria can be reactivated[121].

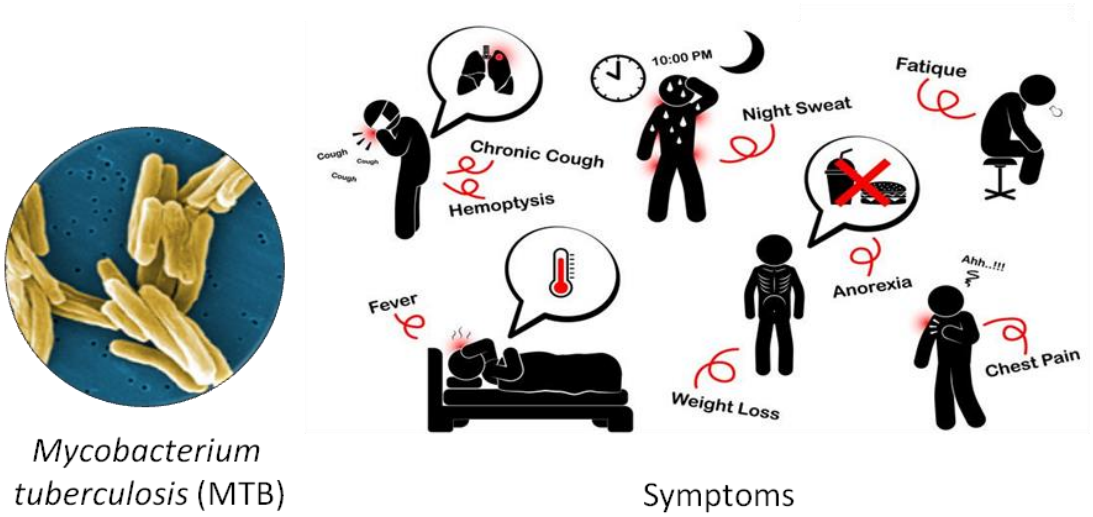

Figure 1.12: *Mycobacterium tuberculosis* bacilli (MTB) as viewed under scanning electron micrograph and symptoms of a patient with an active MTB infection.

1.4.2.2 Current Therapies

Effective TB treatment is difficult due to the unusual structure and chemical composition of the mycobacterial cell wall (an impermeable waxy cell envelope), which hinders the entry of drugs and makes many antibiotics ineffective[122], and thus only a few drugs have emerged in the past 30 years[123]. The two most commonly used antibiotics for TB are isoniazid (INH) and rifampicin (RIF) however drug treatment regimens are long – lasting up to 2 years. Latent TB is usually treated with a single antibiotic, while active TB is treated with combinations of several antibiotics to reduce the risk of bacteria developing antibiotic resistance. Antibiotic combinations include INH, RIF, pyrazinamide (PZA) and ethambutol (EMB) (first-line drugs) for

at least 18 to 24 months (see Fig. 1.13 for their structures). INH is a prodrug which is activated by a bacterial catalase-peroxidase enzyme in MTB, and works by blocking fatty acid synthase thus inhibiting mycolic acids that are part of the resistant mycobacterial cell wall. PZA is also a prodrug that diffuses into the granuloma of MTB and stops its growth. EMB is bacteriostatic against actively growing TB bacilli. It obstructs the formation of the cell wall of MTB leading to increased permeability of the mycobacterial cell wall. First-line drugs have the greatest activity against mycobacterium and are particularly used in patients with active TB disease that have not had any previous TB drug treatments.

A person with fully susceptible MTB may develop secondary (acquired) resistance during therapy because of inadequate treatment, lack of compliance to drug regimen, or using low-quality medication. MDR-TB is defined as resistant to the two most effective first-line drugs (INH and RIF). XDR-TB, defined as MDR-TB plus resistance to three or more second-line drugs, currently has no treatment. For cases with MDR-TB, bedaquiline and linezolide (second-line drugs) are currently being used. The second-line drugs are only used to treat infections that are resistant to first-line therapy, for e.g. XDR-TB or MDR-TB infections. A drug is classified as second-line instead of first-line for one of three possible reasons, (i) it may be less effective than first-line drugs (e.g. *p*-aminosalicycylic acid), (ii) may have toxic side-effects (e.g. cycloserine), or (iii) may be effective, but unavailable in many developing countries (e.g. fluoroquinones). There are currently ten drugs that are approved by the FDA for TB treatment and various drug regimens exist[124]. As of 2016, delamanid has been introduced in combination with first-line and second-line drug regimens for the treatment of patients with MDR-TB[125]. Pretomanid is a drug currently under clinical evaluation[123]; and in the latest news of 2017, researchers have discovered a spiroisoxazoline family of Small Molecules Aborting Resistance (SMARt) that induce the expression of an alternative bioactivation pathway of ethionamide (ETH), which reverts the acquired resistance of MTB to this antibiotic[123].

The only available vaccine developed in the early twentieth century is Bacillus Calmette-Guérin (BCG), which is live, attenuated (virulence-reduced) *Mycobacterium bovis*. Even though the BCG vaccine has limited efficacy in preventing active TB, it was still administered to over 3.5 billion people[121]. There are several TB vaccines in Phase I and Phase II trials, however for the time being a vaccine that is effective in preventing TB in adults remains elusive[116].

Despite all the advances made in treatment and management of TB, it still remains one of the main public health threats[126]. Even though there may seem to be many approved drugs for the treatment of TB, each drug has limited benefits and can only be used under specific conditions and duration. Repurposing an existing antibiotic class that is already known to be safe and effective in other infections but that has not demonstrated anti-TB activity is an attractive strategy as outlined in some recent reports[122,127].

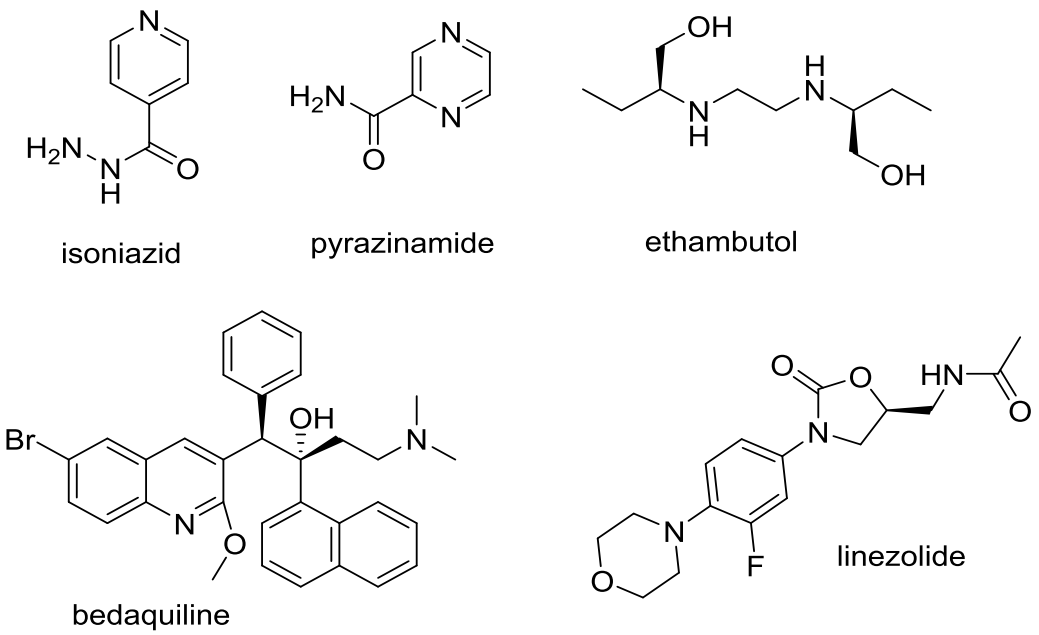

Figure 1.13: Structures of first-line (isoniazid, pyrazinamide, and ethambutol), and second-line (bedaquiline, and linezolide) drugs used for Tuberculosis treatment[128].

Combating TB is a multi-faceted effort that requires improvement of various aspects such as diagnostics, vaccine development, development of new technologies, combination drug therapies, reduction of drug regimen time, reduction of antibiotic resistant TB strain emergence, discovery of new markers and mediators of human immune responses, finding new target strategies for combating TB in the human body, and growing commitments by funding agencies, regulatory offices and pharmaceutical companies to TB vaccine development. There is an unmet need for new drugs addressing novel MTB targets to provide different therapy options for patients with drug-resistant TB and also to shorten and simplify treatment of drug-sensitive TB[129]. Ideally, these new drugs would be included in combination regimens tackling both drug-sensitive and drug-resistant TB, representing a paradigm shift towards a universally useful TB treatment regimen[129].

1.4.2.3 The Target – Coronin-1 Inhibition

Understanding host-mycobacterial interactions is important for identifying new targets that could potentially destroy MTB. To find new targets, studies should focus on the lifecycle of the pathogen once it has entered the host system and the interaction that takes place between the host's immune system and mycobacterial infection.There are multiple stages in the human immune response to MTB and these distinct stages of MTB infection have been defined as an 'immunological life cycle'[121]. During an immune response to a foreign pathogen, most microbes – once internalised by macrophages – are rapidly transported to lysosomes in which they are destroyed. In contrast, pathogenic mycobacteria do not avoid capture by macrophages but rather prevent fusion of phagosomes to lysosomes, thereby surviving intra-cellularly for prolonged periods of time[120]. MTB have developed strategies to circumvent the normal trafficking routes in macrophages in order to increase their chances of survival by manipulating normal host cell biology[119]. This is a crucial point for the persistence of MTB because they manage to lie dormant inside the human body for prolonged periods of time. Efforts in understanding host-mycobacteria interactions have provided vital insights into these survival tactics[119–121,130].

Generally, once a pathogen is engulfed into macrophages, phagosomal content is delivered to lysosomes either by maturation or through vesicular traffic of intermediate vesicles. In contrast to normal phagocytosis, mycobacteria resist their lysosomal delivery once MTB is engulfed into macrophages[119]. The inhibition of lysosomal delivery is an active process exerted by the mycobacteria themselves[119,131,132]. Once mycobacteria are inhaled, they come in contact with the alveolar macrophages and are engulfed into vacuoles called phagocytes[133,134]. The entry of MTB into the macrophages involves binding to one or more specific receptor molecules and interaction with plasma membrane steroid cholesterol[135]. Cholesterol was shown to help increase the viscosity of the membrane that is in contact with the hydrophobic cell wall, thereby accelerating phagocytic uptake[135]. MTB use cholesterol-rich domains of the plasma membrane to enter the host cells[135].

Intensive research into the interaction between MTB and the immune system have lead to the discovery of a coat protein, known as coronin-1, which was found to be essential for the survival of MTB within macrophages in the human body[120,136,137]. Pieters *et al*. (2008) showed that killed mycobacteria were readily found in lysosomes, while living mycobacteria were found

in mycobacterial phagosomes (vacuoles that are morphologically distinct from lysosomes)[130]. By analysing different macrophage proteins present in phagosomes containing live mycobacteria, coronin-1 was consistently identified which was absent from phagosomes harbouring killed bacilli[119,137]. Coronin-1 was shown to prevent phago-lysosome fusion by regulating calcium-dependent signalling processes[130,138]. After *in situ* killing of the bacilli coronin-1 initially associates with the phagosomal surface but is rapidly released concomitant with lysosomal degradation of the phagosome and its contents (see Fig. 1.14). Coronin-1 coated phagosomes may open novel perspectives for strategies designed to interfere with the normal course of MTB in the host cell[119]. In a coronin-1 knockout mouse model, macrophages lacking coronin-1 did not display any abnormalities in their number or functional responses including proliferation, phagocytosis of beads and bacteria, migration, chemotaxis, activation, membrane ruffling, and morphology[136,138]. The coronin-1 deficient macrophages did however efficiently kill MTB upon mycobacterial challenge, which was found to occur through a defect in the Ca^{2+}/calcineurin activation pathway[138]. Trimerisation of coronin-1 is a prerequisite for the mycobacterial-mediated calcineurin activation and subsequent mycobacterial survival[139,140].

The role of coronin-1 in the maintenance of immune cell diversity and function is extensively described in a review article by Jayachandran and Pieters (2015)[136]. The authors describe how various immune cells namely; macrophages, T cells, B cells, neutrophils, natural killer cells, dendritic cells, and mast cells are affected by coronin-1 deficiency[136]. The exact mechanism of coronin-1 retention at the mycobacterial phagosome remains to be elucidated, but may involve an enzyme (lipoamide dehydrogenase) that is secreted by MTB and is known to be involved in resisting toxic effects generated by the host cell[141]. Since activation-induced phosphorylation of coronin-1 acts as the molecular switch, manipulation of this pathway with therapeutics may be useful to induce cargo transfer to and elimination within lysosomes[120,137,142,143]. Therapeutic interventions in the inhibition of coronin-1 may provide an alternative mode to achieve pathogen clearance through manipulation of the host rather than trying to eliminate MTB from an infected phagosome[143]. A strategy in targeting the host rather than the pathogen may also help to overcome drug resistance, which is an increasing challenge in anti-TB efforts[143].

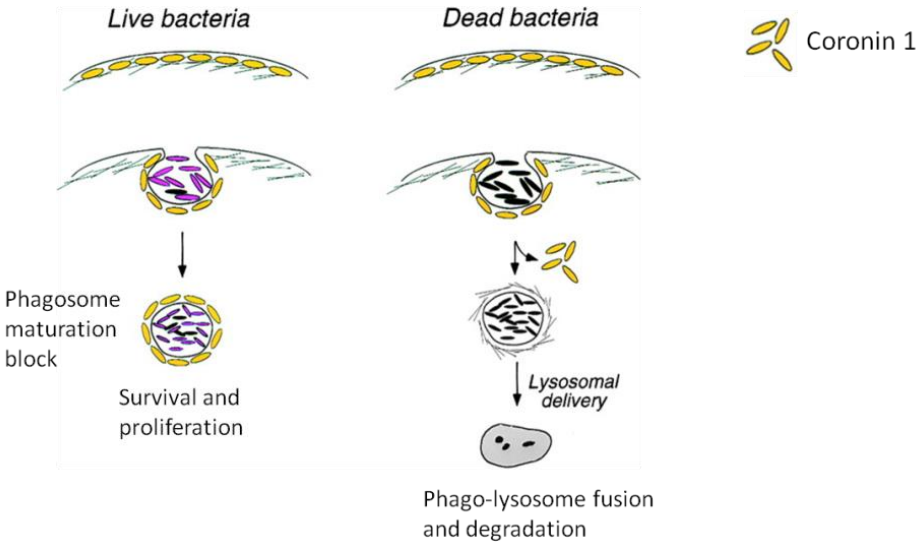

Figure 1.14: Model describing the role of coronin-1 in intracellular survival of *Mycobacteria*. Phagocytosis triggers the recruitment of coronin-1 (yellow) around the particle to be ingested, possibly as a result of its initial association with microtubules (black lines) at the cell cortex. In the case of viable bacteria (violet), coronin-1 is actively retained on the phagosomal membrane, while it dissociates from the microtubule network, perhaps as a consequence of a conformational change. In contrast, during phagocytosis of killed bacteria (black) or after *in situ* killing of the bacilli, coronin-1 initially associates with phagosomes but is rapidly released concomitant with lysosomal delivery of the bacilli (adapted from[137]).

1.4.2.4 Natural Products and TB

Natural products represent a diverse and powerful tool for anti-TB drug discovery, in the form of potential anti-microbial leads, and as a means of identifying biochemical targets that are most vulnerable in the bacterium[144]. Natural products have long provided a rich source of effective anti-TB agents. Many drugs on the market that act against Mycobacterium are synthetic compounds or derived from natural products to increase their potency. The most commonly used first-line TB drug is RIF, which is a more stable, semi-synthetic product based on rifamycins. Rifamycins, which are produced by soil bacteria (*Amycolatopsis rifamycinica*) were discovered based on their antibiotic activity in 1957 by researchers in Milan. Rifampicin-resistant mycobacteria develop quickly when the patient is given RIF without another antibiotic. Rifampicins are among the few drugs that can kill dormant strains of MTB[128]. The discovery of RIF was the biggest advance in TB chemotherapy. Prior to the use of RIF, the duration of anti-TB regimens with 2 or 3 different agents in combination was 18-24 months for active forms of TB and 9 months for latent TB[122]. Following the introduction of RIF to combination therapy with 3

other agents, the standard therapy duration was knocked down to only 6 months for active TB and 3 months for latent TB[122,128].

The discovery of streptomycin, produced by *Streptomyces griseus*, founded the age of TB therapy and is a second-line treatment commonly used in combination with INH, RIF and PZA[129]. Spectinomycin, a natural product isolated from *Streptomyces*, showed little activity against MTB, but was found to bind to an independent site on the ribosome than that of streptomycin[127]. Derivatives of spectinomycin, called spectinamides, have been shown to display potent anti-TB activity both *in vitro* and in mice[122,127]. Pyridomycin, a natural compound produced by *Dactylosporangium fulvum*, shows activity against MTB growing within macrophages and shows low toxicity to human cells and mice[128,144,145]. It was shown to have a dual action that eventually leads to the inhibition of mycolic acid synthesis in MTB[144]. Furthermore, majority of INH-resistant MTB are sensitive to pyridomycin[128,144]. The chemical structures of rifampicin, streptomycin, and pyridomycin can be found in Fig. 1.15.

Griselimycin, a natural product isolated half a century ago from the same organism that produced streptomycin, was discovered to possess anti-mycobacterial activity, but showed poor pharmacological properties[129,146]; thus was not investigated further at that time. However, recently, a synthetic derivative has shown improved oral uptake and penetrates cells of the immune system that harbour MTB[129]. In combination with other drugs, the cyclohexyl derivative of griselimycin displayed a different mechanism of action, and high potency *in vitro* and *in vivo*[147]. This new series of derivatives have the potential to contribute to drug regimens for patients with both drug-sensitive and drug-resistant TB[129]. Another series of compounds emerging to tackle MTB are the synthetic analogues of the sansanmycin uridylpeptide natural products[148]. Earlier in 2017, Tran and co-workers created a library of synthetic sansanmycin analogues that possessed potent and selective inhibition of MTB both *in vitro* and in macrophages with MTB co-infection[148]. The analogues were shown to inhibit peptidoglycan biosynthesis[148].

Some of the most effective anti-TB antibiotics require bioactivation by MTB enzymes to acquire their anti-bacterial effect[123]. However, bioactivation of pro-antibiotics is vulnerable to mutational inactivation or attenuation of the corresponding bioactivating enzymes, as observed for INH-, PZA-, and ETH-resistant clinical isolates[123]. The bromotyrosine-derived spiroisoxazolines represent a structurally diverse class of physiologically active natural

products[123]. The compound SMARt-420 (see Fig. 1.15), a representative member of the spiroisoxazoline family has been recently discovered to induce the expression of an alternative bioactivation pathway of ETH, which reverts the acquired resistance of MTB to this antibiotic[123]. This first-of-its-kind molecule, is not only fully capable of reversing and clearing ethionamide-acquired resistance in mice, but was also shown to increase basal sensitivity of bacteria to ethionamide[123].

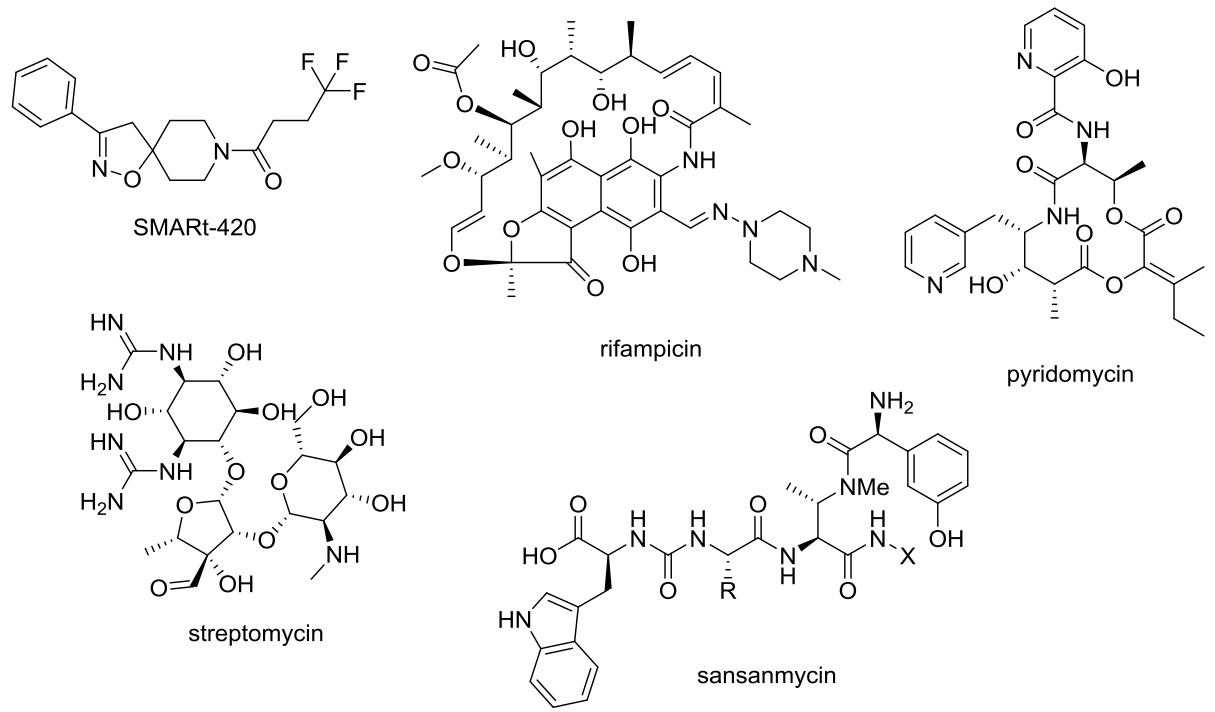

Figure 1.15: Structures of the natural product compounds that have been recently discovered (SMARt-420, sansanmycin) or used (rifampicin, pyridomycin, streptomycin) for the treatment of TB.

The Global Alliance for TB Drug Development (TB Alliance) has various ongoing joint research projects, however only a few of these projects aim at discovery of novel compounds from natural products. These studies mostly target MTB in phenotypic assays rather than target-specific assays. Overall, current methods have led to numerous natural product lead compounds for which non-specific toxicity towards host cells other than the mycobacterium has been reported[70]. Simultaneous determination of cytotoxicity and selectivity during the process of fractionation of active principles is important in the course of discovering new anti-TB leads[70].

1.4.3 Lymphangiogenesis

Interest in basic lymphatic research was boosted by the growing evidence that the lymphatic system contributes to a number of diseases, such as lymphedema, cancer metastasis, and different inflammatory disorders[149]. This emphasises the emerging importance of the lymphatic vasculature as a therapeutic target[149]. The formation of lymphatic vessel sprouts is one of the first and essential steps in the development of new lymphatic vessels.

1.4.3.1 Formation of Lymphatic Vessels

Lymphangiogenesis is the process through which new lymphatic vessels are formed. Lymphatic vessels are lined by Lymphatic Endothelial Cells (LECs) and are critical for health. They control tissue fluid homeostasis, immune surveillance, lipid transport, and inflammation[150,151]. Blood and lymphatic vascular systems partially develop by separate molecular mechanisms even though they are structurally related and function in concert[152]. To initiate lymphangiogenesis, selected tip cells from the wall of preexisting vessels send out protrusions and sprout into the extracellular matrix on their basolateral site. Lymphangiogenesis is induced by vascular endothelial growth factor (VEGF) -C and VEGF-D via VEGFR-3 signaling, which acts on LECs that differentiate from venous endothelial cells at mid-gestation[151]. After their formation, lymphatic vessels mature and remodel into a branched network that covers the skin and most internal organs of the body[152]. The formation of lymphatic vessel sprouts is one of the first and essential steps in the development of new lymphatic vessels. To initiate lymphangiogenesis, selected tip cells from the wall of preexisting vessels send out protrusions and sprout into the extracellular matrix on their basolateral site. This process is similar to the first steps of blood vessel angiogenesis[153] and incorporates several mechanistic steps including cell–cell communication with neighbouring cells, cell polarisation, matrix degradation, migration, and invasion[154]. VEGF-A, VEGF-C, VEGFR-3, neurophilin-2, and Notch signaling play an important role in mediating sprout formation[153–155]. The dorsolateral sprouting, migration, and survival of the first LECs and the formation of lymph sacs are dependent on VEGF-C[151]. VEGF-C co-receptor neurophilin-2 (NRP-2)[156] and the Eph tyrosine kinase ligand ephrin B2[157] are required for efficient sprouting of lymphatic capillaries, while the Notch1-DII4 signaling pathway is essential for postnatal lymphatic development[158] (see Fig. 1.16).

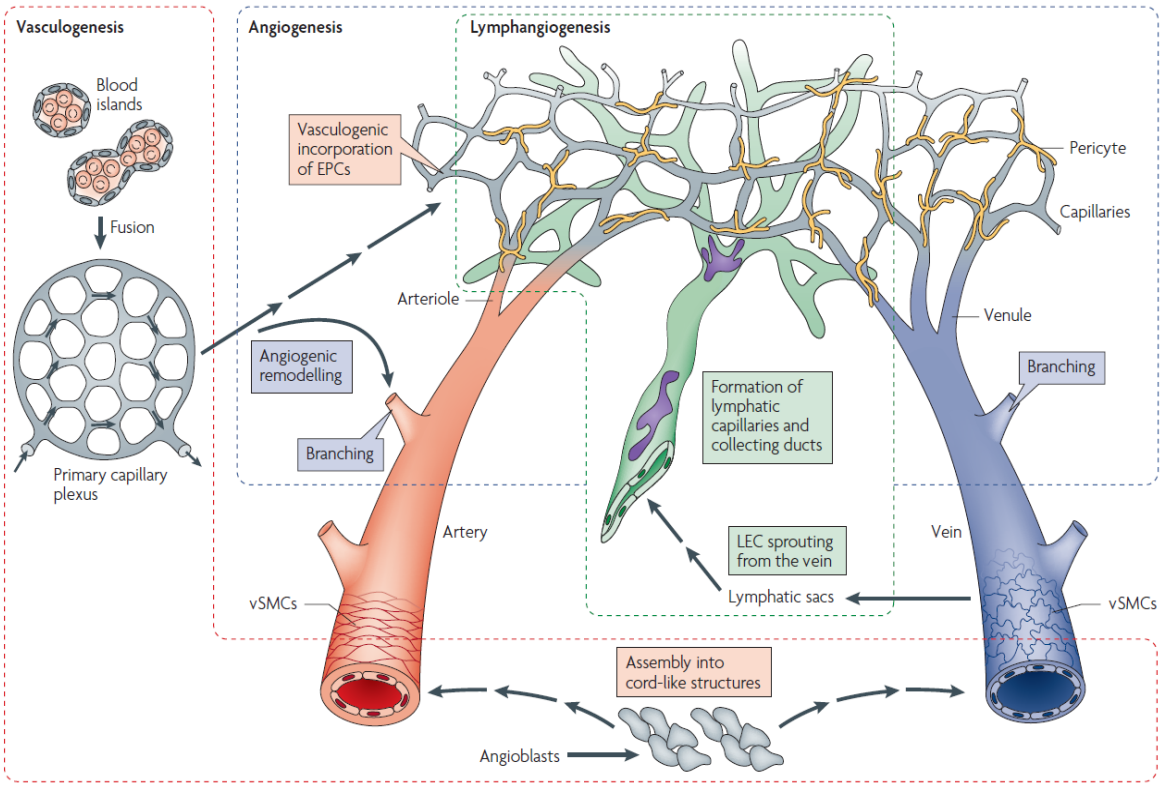

Figure 1.16: Origin of endothelial cells and assembly of the vasculature. Mesodermal cells in the early embryo differentiate into endothelial precursor cells (EPCs, angioblasts) and form aggregates, known as blood islands (left). Fusion of blood islands leads to the vasculogenic formation of honeycomb-shaped primary capillary plexi in the yolk sac and embryo itself. Blood circulation is established and primary plexi are remodeled into a hierarchical network of arterioles and arteries (red), capillaries (grey), and venules and veins (blue). The dorsal aorta and cardinal vein are directly formed through the assembly of angioblasts. The vasculogenic incorporation of circulating EPCs into growing blood vessels may contribute to regenerative or pathological neovascularization in the adult. Vascular smooth-muscle cells (vSMCs) are associated with arteries and veins, whereas capillaries are covered by pericytes (yellow). The first lymphatic endothelial cells (LECs) sprout from the embryonic veins, then migrate and form lymphatic sacs. Further steps of lymphangiogenic growth involve sprouting, branching, proliferation, differentiation and remodeling processes. The recruitment of lymphangioblasts from the adjacent mesenchyme has been speculated to be a further source of LECs. Blind-ending lymphatic capillaries (green) feed into collecting vessels and ducts. These larger lymphatics are sparsely covered by SMCs (purple) and contain valves that prevent backflow[155].

1.4.3.2 Diseases Associated with Lymphangiogenesis

A multitude of diseases are linked to an insufficient or overactive vasculature (vascular network)[159]. Among them are many inflammatory diseases, such as psoriasis[160]. Defects in

lymphatic vessel formation or function cause lymphedema[151] and has recently been linked to chronic skin inflammation[160], whereas excess lymphangiogenesis promotes cancer metastasis[150,161] and organ transplant rejection[162]. Lymphatic vessels dynamically participate in inflammatory reactions, modulate immune responses and immune tolerance, and respond to increased fluid loads in tissues. They expand (but do not show sprouting lymphangiogenesis) during inflammation and their activation (induction of sprouting) reduces the severity of tissue inflammation, highlighting an emerging role of the lymphatic vasculature as a therapeutic target[149,163].

Lymphatic vessels allow the drainage of interstitial fluid from tissues[164]. Functional impairment of the lymphatic system results in reduced drainage of extravasated fluid and macromolecules, leading to a condition known as lymphedema which most commonly occurs in the subcutaneous space[165]. Edema formation, a cardinal sign of inflammation and clinically significant feature of inflammatory disease, results when the amount of leakage from inflamed blood vessels exceeds the capacity of lymphatic vessels for drainage[164]. Blocking VEGFR-3, that is mainly expressed on the lymphatic endothelium[166], has been shown to enhance mucosal edema in a mouse model of chronic airway inflammation[164], increase severity of chronic inflammatory arthritis in a mouse model[167], and also prolong the course of inflammatory ear swelling in a mouse model for chronic skin inflammation[168]. Lymphatic insufficiency results in chronic fluid stasis with subsequent disruption of cutaneous tissue architecture and profound inflammation[163]. Lymphedema is characterised by adipose tissue and progressive tissue fibrosis[169]. The accumulation of protein-rich fluid in the tissues causes swelling of the extremities and is in most patients also associated with inflammatory reactions, fibrosis, overgrowth of adipose and connective tissues in the affected areas, increased risk of infection, and impaired wound healing[149]. Lymphatic injury (even minor lymphatic damage) acts as the initial trigger for the multistep procedure resulting in lymphedema[163]. It has been shown that lymphatic vessel morphology was profoundly altered during the course of lymphedema development and was associated with a gradual impairment of lymphatic vessel function and a distinct immune cell infiltration[163].

Lymphedema is a chronic, disabling, and disfiguring condition, which is classified into primary and secondary (acquired) lymphedema and is based on its cause[149]. Primary lymphedema further categorised by the age of onset as congenital (present at birth), praecox (very early), or

tarda (late onset), is a rare, autosomal dominant disorder with an estimated prevalence rate of 1.15 per 100 000 patients in North America[170]. It originates from missense mutations affecting lymphatic development[170,171]. Milroy's disease, a form of congenital lymphedema with autosomal dominance inheritance was ascribed to kinase-inactivating mutations in the VEGFR-3 gene[171,172]. Secondary lymphedema, which is more frequent than the primary form, represents a common complication after operative procedures in oncologic surgery (such as lymph node dissection in the context of breast cancer or melanoma treatment[173]), or any other traumatic, inflammatory, or neoplastic disruption or obstruction of lymphatic pathways[169]. Up to 30% of women treated for breast cancer and around 20% of patients after lymph node dissection for melanoma develop lymphedema[174]. Secondary lymphedema has also been described after sentinel lymph node biopsies[174]. Radiation, infectious diseases (e.g. lymphatic filariasis) or chronic inflammation may also cause secondary lymphedema[175]. According to WHO report, over 15 million people were reported in 2014 to suffer from lymphedema because of lymphatic filariasis, making it the most important cause of secondary lymphedema in developing countries, while in industrialised countries, cancer treatment is the most frequent cause of secondary lymphedema[176]. Despite advances in all fields of surgery, physiotherapy (e.g. lymph drainage, compressive bandages) remains the standard symptomatic treatment for both primary and secondary lymphedema[175].

1.4.3.3 Natural Products and Lymphangiogenesis

There has been reported benefit of coumarin (5,6-benzo-pyrone) in lymphedema, which is ascribed to its stimulatory effect upon cutaneous macrophages and, thereby, upon local proteolysis[177]. Coumarins stimulate other cellular elements of the immune system and may promote protein reabsorption[177]. Flavonol glycosides, particularly rutin derivatives, are thought to benefit lymphedema through protective effects on vascular endothelium and general improvement in the microcirculation[169]. Dietary restriction of long-chain triglycerides provides some relief of edema in patients[178].

Fatty acid β-oxidation (FAO) was shown to promote LEC proliferation through the same mechanism as vascular endothelial cell (VEC) proliferation. Endothelial cells oxidize fatty acids to produce acetyl-CoA for epigenetic modifications critical to lymphangiogenesis[162]. Fatty acids provide acetyl-CoA, which helps to sustain the Krebs cycle and histone acetylation that is

required for lymphangiogenesis[162]. Alternatively, statins were shown to inhibit lymphangiogenic sprouting *in vitro*, and *in vivo* for corneal and cutaneous lymphangiogenesis[154].

1.4.4 Chronic Heart Failure

1.4.4.1 Background

According to the New York Heart Association (NYHA), heart failure (HF) is classified into four different functional classes (I to IV). Patients are classified by a doctor based on their HF symptoms and functional limitations. The severity of HF depends on the ability of the heart to pump blood to the rest of the body. HF, which is often referred to as congestive or chronic heart failure (CHF), is a progressive and severe cardiovascular health condition, of which there is no cure for. Patients experience shortness of breath during daily activities, general tired or weak feeling, weight gain with water retention and swelling (edema) in the feet, legs, ankles (peripheral edema), and stomach (ascites), as well as troubles with breathing while lying down (pulmonary edema). The term 'acute' means rapid onset and 'chronic' refers to a long-term condition, which is usually kept stable by the treatment of symptoms. Current therapy – based on the NYHA classification – includes symptomatic therapy which consists of managing the symptoms, such as control of blood pressure, regular visits from cardiac nurses, attending specific exercise programs with specific lifestyle changes, and use of a pacemaker or implantable cardiac defibrillator[179]. Approximately 20 million people are affected worldwide, and at the age of 40 years the lifetime risk of developing HF is 1 in 5 (for both men and women)[180].

1.4.4.2 Underlying Pathology

HF is a physiological state in which cardiac output is insufficient to meet the needs of the body and lungs. The basic pathophysiology in HF involves changes in neurohormonal system with increasing activity in rennin-angiotensin-aldosterone system (RAAS), which results in sodium retention (edema formation), and sympathetic activation (increase in heart rate and peripheral vascular resistance)[181]. There is a cascading effect resulting in myocardial fibrosis which leads to impaired relaxation and filling problems, and vascular fibrosis which leads to impaired arterial compliance as well as baroreceptor dysfunction and alterations in renal function[181].

In CHF, endothelial hyperpermeability has been linked to edema formation. The endothelium plays a crucial role in various physiological and pathological processes[182]. Calcium ions are an important second messenger system in the endothelium and play a pivotal role in regulation of endothelial permeability[183]. The most important mechanisms that cause elevated calcium levels in the endothelium are moderated by the activation of phospholipase C (PLC) through G-protein coupled receptors[184,185] provoking the formation of inositol 1,4,5-triphosphate (IP_3) and diacylglycerol[186]. IP_3 generates calcium depletion from the endoplasmic reticulum, whereas diacylglycerol activates calcium influx from the extracellular space through transient receptors potential (TRP) channels[187].

1.4.4.3 *Crataegus* species for Cardiovascular Disease

Several species of hawthorn (*Crataegus* species) have been used in traditional medicine for a variety of purposes. The dried fruits (from *Crataegus pinnatifida*) are used as a digestive aid in Traditional Chinese Medicine (TCM), while other species such as *C. laevigata* are believed to strengthen cardiovascular function[188,189]. Hawthorn is one of the oldest known medicinal plants in the Western world[190]. The most prominent extract of *Crataegus*, called WS 1442, is an aqueous alcoholic special extract from leaves and flowers of *C. monogyna/laevigata*[186]. *Crataegus* extract WS 1442 is approved for the treatment of mild forms of CHF according to the New York Heart Association functional class II[191]. The *Crataegus* special WS 1442 extract has been evaluated for its function in cardiovascular disease, and its efficacy has been shown in various clinical trials[192,193]. Treatment with WS 1442 has been reported to improve ankle edema in CHF[194,195]. Studies into the underlying mechanism of action for *Crataegus* extracts are rare, even though considerable clinical knowledge exists[186]. In recent studies, WS 1442 was shown to prevent vascular leakage by affecting endothelial barrier-regulating systems[196], thus protecting against edema formation via the inhibition of thrombin-induced endothelial barrier dysfunction in human endothelial cells[197]. Additionally, WS 1442 displayed a barrier-protective activity *in vivo* in a murine model of endothelial hyperpermeability[196,197]. Detailed investigations showed WS 1442 extract was able to prevent endothelial hyperpermeability via a dual mechanism[196,197]. The hawthorn extract inhibits the barrier-disruptive pathway by reduction of thrombin-induced intracellular calcium rise, PKC, and RhoA activity; while on the other hand barrier-protective signalling was activated by increasing cAMP levels, activation of Rap1/Rac1 signalling, and cortactin rearrangement at the borders of the endothelial cells (see Fig. 1.17)[186,196,197].

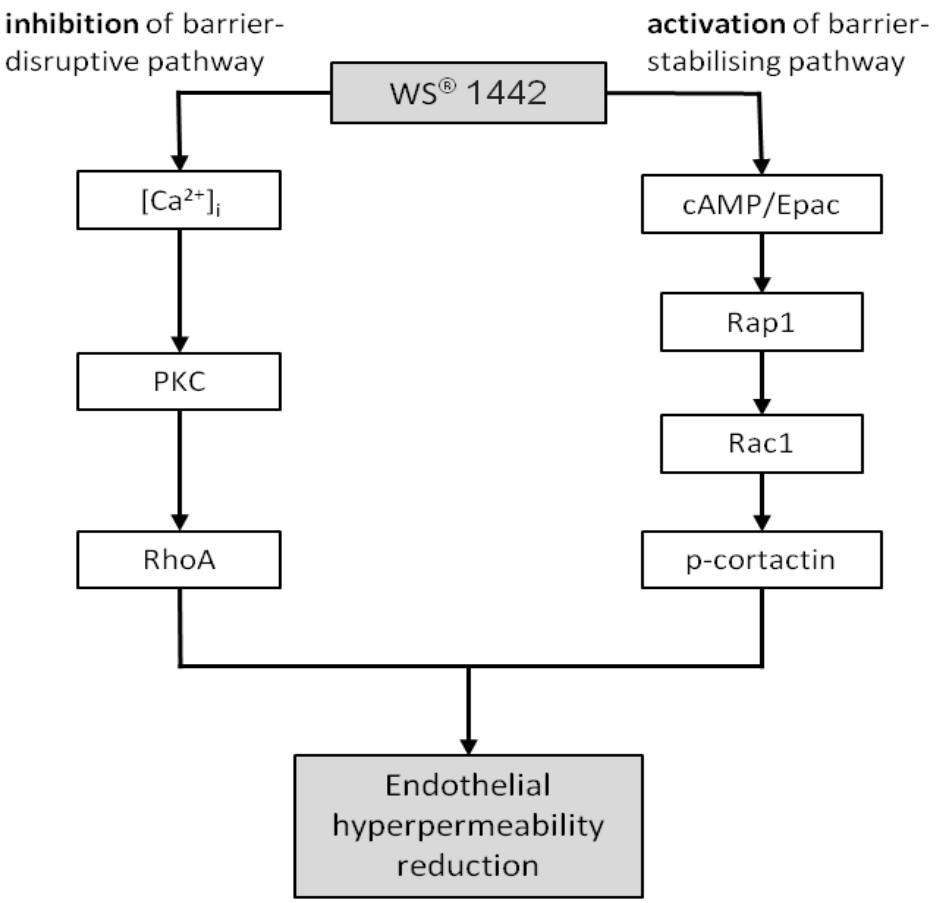

Figure 1.17: Summary of the two pathways activated and inhibited by hawthorn extract that leads to the reduction of endothelial hyperpermeability (adapted from[197]).

1.5 Aim of this Thesis

Based on the discussion given so far, natural products have a crucial role in drug discovery and need to be continuously tested against various molecular targets that have emerged by the progress in genetics and molecular biology. Accordingly, the main objective of this thesis is to assess the role natural products play in key targets of four different disease areas. The approach known as HPLC-based activity profiling will be employed in each project to track activity and identify small molecules of natural origins that exhibit an interaction with the identified four emerging biological targets, which are:

CUGn-RNA and MBNL1 complex: directed in disease area of Myotonic Dystrophy type 1 (this is referred to as the DM1 project; the investigation was carried out in collaboration with Prof. Sinnreich of the Neurobiology Department at the University of Basel),

Coronin-1 expression: directed in the disease area of Tuberculosis (this is referred to as the TB project; the research was conducted in collaboration with Prof. Pieters at the Biozentrum of the University of Basel),

Lymphatic endothelial cells: directed in the disease area of lymphedema (this is referred to as the Lymphatic project; it was carried out in collaboration with Prof. Detmar of the Pharmacogenomics group at the ETH Zürich), and

Thrombin: directed in the disease area of Chronic Heart Failure (this is referred to as CHF project; it was conducted in collaboration with Prof. Fürst from the Institute of Pharmaceutical Biology at the Goethe University in Frankfurt).

The DM1 project focuses on identifying small molecules which have the ability to inhibit the formation of the pathogenic complex between CUGn-RNA and MBNL1 in a novel complex-inhibition assay. Results and discussion of this project will be presented in Chapter 2.

The TB project targets the identification of small molecules of natural origin which have the ability to inhibit the expression of coronin-1 protein that has an essential role for the survival of MTB in the host cell. The results of this project will be addressed in Chapter 3.

The Lymphatic project assesses the potential of plant secondary metabolites in promoting lymphatic vessel growth. Results and discussion of this project will be presented in Chapter 4.

The CHF project focuses on characterising the secondary metabolites present in active sub-fractions of *Crataegus* species which have the ability to inhibit endothelial hyperpermeability. Results and discussion of this project will be addressed in Chapter 5.

In Chapter 6 of this thesis, all materials and methods used for each project are described.

Finally, concluding remarks and general outlook of the thesis will be presented in Chapter 7.

Chapter 2

2. Results and Discussion: Myotonic Dystrophy type I

As highlighted in section 1.5, the main focus of the DM1 project is to identify small molecules which have the ability to inhibit the formation of the pathogenic complex between CUGn-RNA and MBNL1, in a novel complex-inhibition assay. In the following sections, extract library screening and hit prioritisation, the results of prioritised plant extracts (*Lamium album*, *Salvia miltiorrhiza* and *Peganum harmala*) as well as isolated compounds and alkaloid library are presented. Finally, summarised discussion and conclusions of the DM1 project are given.

2.1 Extract library screening and hit prioritisation

A library containing just over 2100 plant and fungal extracts, selected based on their chemotaxonomy and/or traditional uses were screened in the complex inhibition assay at 100 µg/mL and 100 µM, respectively. The results were analysed for optical density readout at 450 nm (OD_{450}) in a competitive binding ELISA assay. Extract prioritisation was based on the criteria of at least 50% CUG_{78}-MBNL1 complex binding inhibition (effect shown as a decrease of OD_{450} signal, high OD_{450} values represent no effect).

Ten plant extracts were prioritised and further investigated for their active principles, namely methanol (MeOH) extract of roots from *Peganum harmala* (Nitrariaceae), ethyl acetate (EtOAc) extract of roots from *Salvia miltiorrhiza* (Lamiaceae), MeOH extract of leaves from *Bathysa veraguensis* (Rubiaceae), EtOAc extract of leaves from *Lamium album* (Lamiaceae), MeOH extract of the herb from *Pistacia lentiscus* (Anacardiaceae), MeOH extract of stems from *Henriettella tuberculosa* (Melastomataceae), MeOH extract of the leaves from *Henriettella tuberculosa* (Melastomataceae), MeOH extract of leaves from *Casearia arborea* (Flacourtiaceae), MeOH extract of leaves from *Coccoloba* spp. (Polygonaceae), and MeOH extract of aerial parts from *Struthanthus orbicularis* (Loranthaceae).

Seven of the ten extracts belong to families that are commonly known to contain tannins, so to remove the possibility of false positive interactions due to tannins present in the extracts polyamide filtration was done and the resulting tannin-free fractions were tested. The tannin-free fractions displayed no further activity thus the activity from these extracts could be

assigned to tannin interactions with protein-based screens. The 7 extracts subjected to polyamide filtration were from *Bathysa veraguensis*, *Pistacia lentiscus*, *Henriettella tuberculosa* stems and leaves, *Casearia arborea*, *Coccoloba* species, and *Struthanthus orbicularis*. As an example to exhibit the presence of tannins in various extracts, the figure below (Fig. 2.1) shows the HPLC-based activity profile of *B. veraguensis* MeOH extract overlaid with UV chromatogram at 254 nm. The HPLC-activity profile in Fig. 2.1 displays the activity spread over numerous fractions and also the characteristic tannin-like bump that is visible in the UV chromatogram at 254 nm.

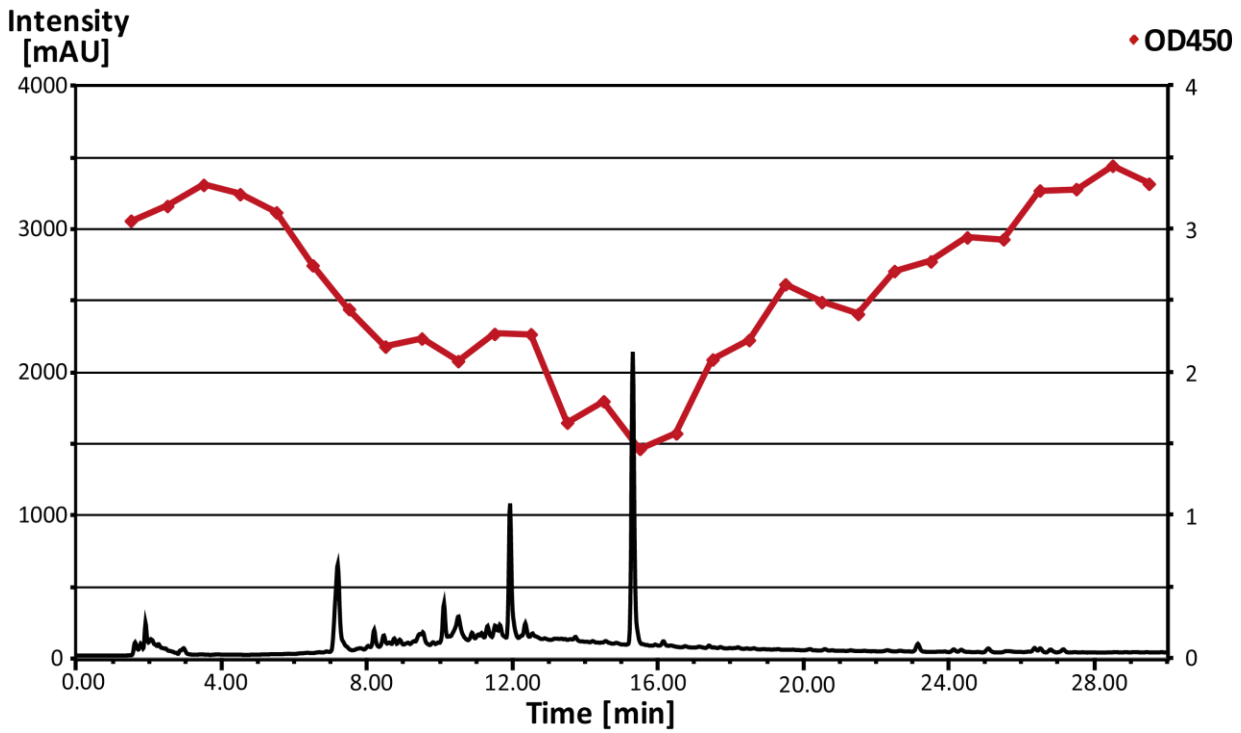

Figure 2.1: HPLC-based activity profile of *Bathysa veraguensis* methanol extract displaying UV chromatogram at 254 nm (in black) on the y-axis on the left and OD_{450} signal (in red) on the right y-axis.

After removal of tannins by filtration over polyamide, the resulting tannin-free extracts were tested and found to lose their activity (Fig. 2.2). Accordingly, the remaining three active extracts were the EtOAc extract of leaves from *Lamium album*, the EtOAc extract from roots of *Salvia miltiorrhiza*, and the MeOH extract of roots from *Peganum harmala* which were investigated further.

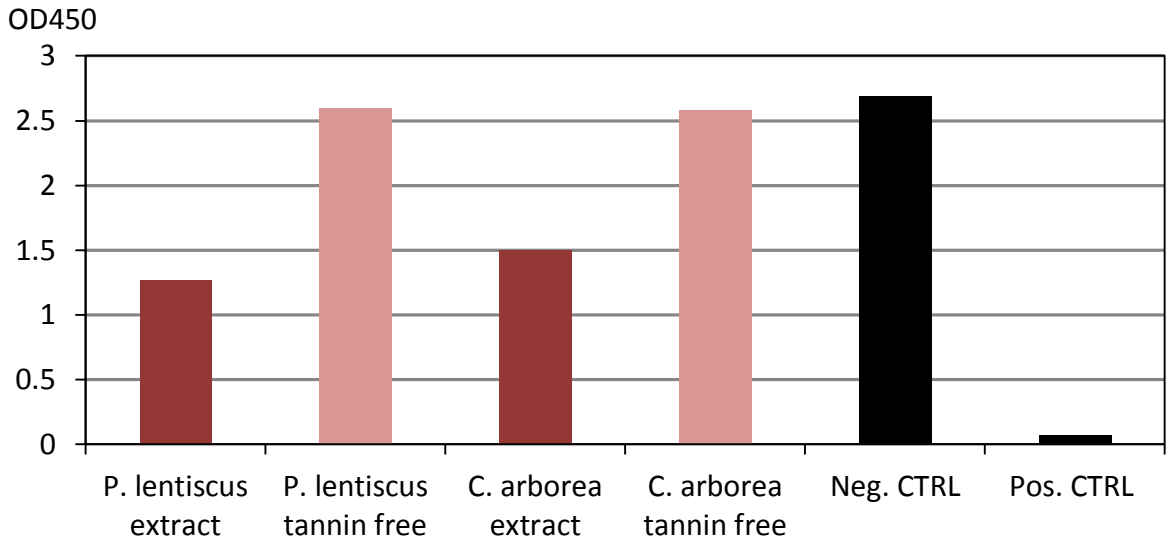

Figure 2.2: OD_{450} values for some extracts and their tannin free fractions tested at 100 µg/mL.

2.2 *Lamium album* (Lamiaceae)

Investigation of *L. album* was assigned as a second priority plant since only a minor effect was observed with the fractions. The maximum decrease in OD_{450} signal for *L. album* (but not high enough to be considered as a top priority) was observed in fraction 8 (minute 7.00-8.00) which corresponds to the compound auroside, an iridoid-glycoside (**La-1**). Fig. 2.3 below exhibits the structure of auroside along with HPLC-based activity profile of *L. album* EtOAc extract superposed with the UV chromatogram at 254 nm.

(a)

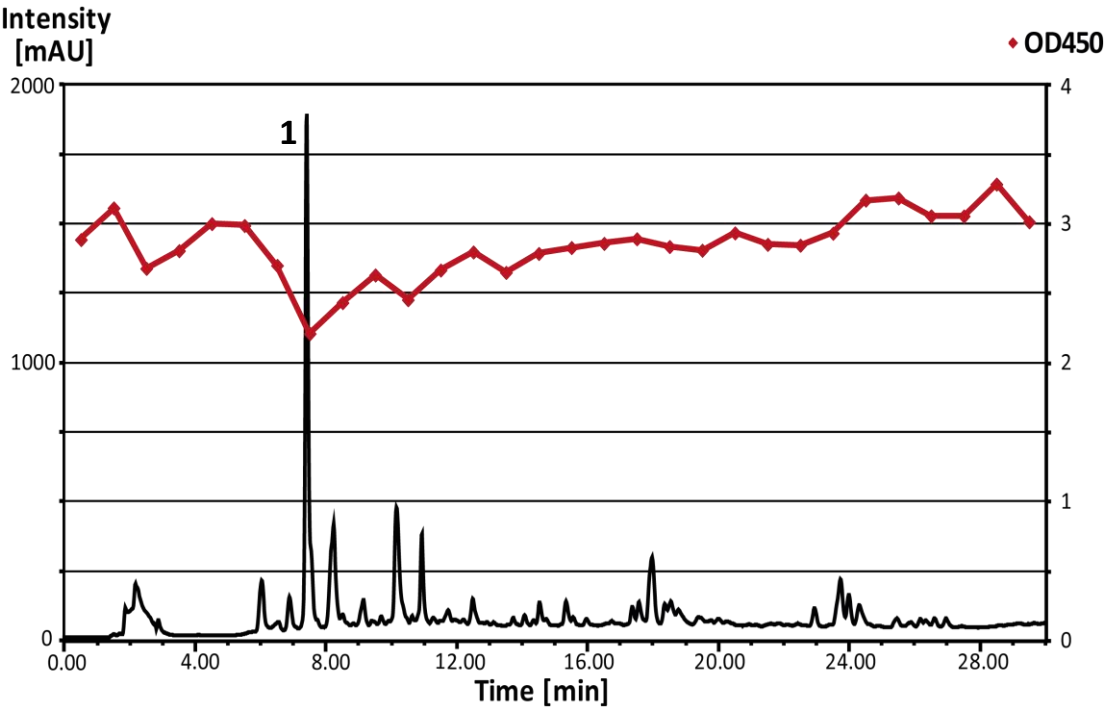

(b)

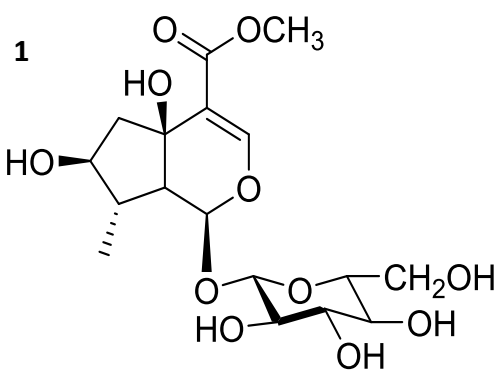

Figure 2.3: (**a**) HPLC-based activity profile of *Lamium album* EtOAc extract displaying UV chromatogram at 254 nm (in black) on the y-axis on the left and OD_{450} signal (in red) on the right y-axis. (**b**) **peak-1**: auroside structure.

Though auroside was not active enough for further tests, its absolute configuration was determined to be 1*S*,5*R*,7*S*,8*S*,9*R* (see Fig. 2.4) for the aglycone.

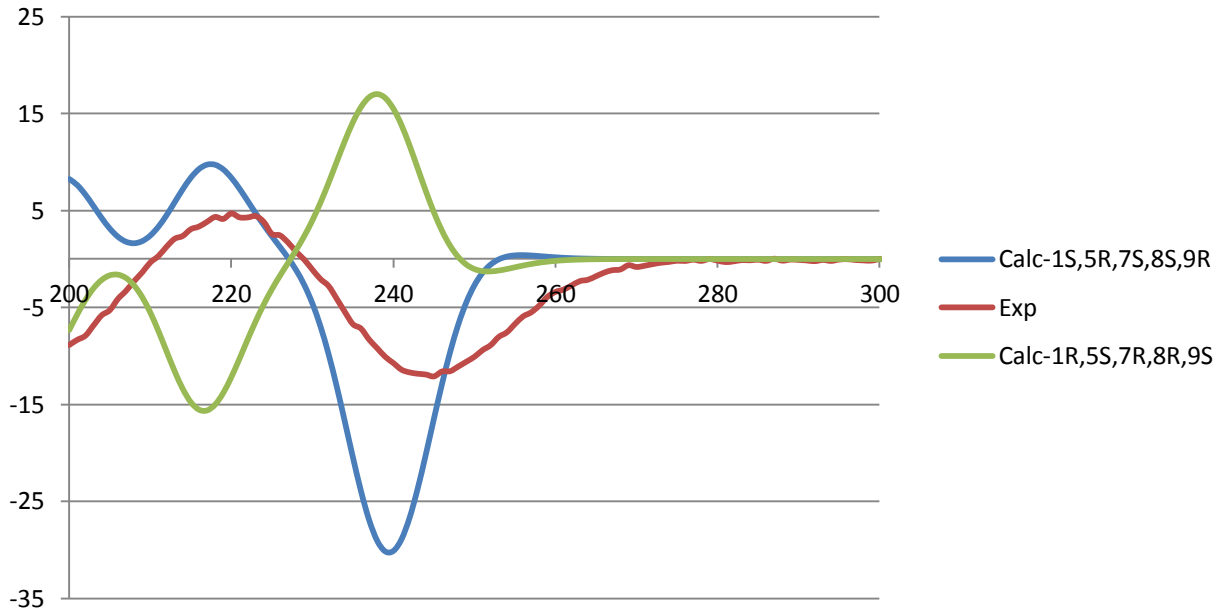

Figure 2.4: Overlay of experimental and calculated ECD spectra for auroside 1*S*,5*R*,7*S*,8*S*,9*R* and 1*R*,5*S*,7*R*,8*R*,9*S* aglycone enantiomers.

2.3 *Salvia miltiorrhiza* (Lamiaceae)

The main activity for the EtOAc extract for *S. miltiorrhiza* was found in fraction 26 (corresponding within the minute 26.00 to 27.00) which could be assigned to the two positional isomers that co-elute (compounds **4** and **5**). HPLC-based activity profile of *S. miltiorrhiza* EtOAc extract overlaid with UV chromatogram at 254 nm as well as the structure of isolated compounds are shown in Fig. 2.5.

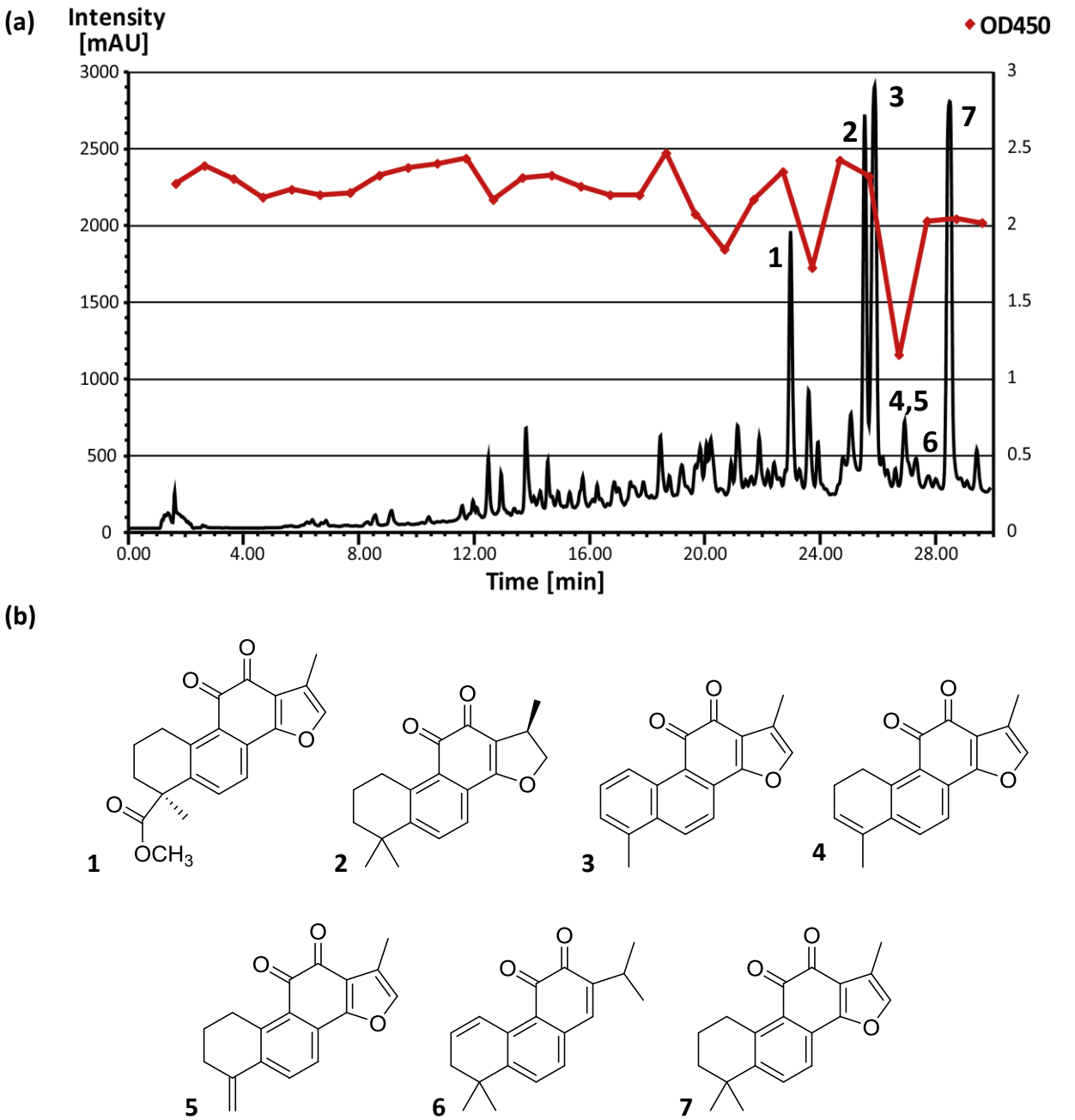

Figure 2.5: (**a**) HPLC-based activity profile of *Salvia miltiorrhiza* ethyl acetate extract displaying UV chromatogram at 254 nm (in black) on the y-axis on the left and OD_{450} signal (in red) on the right y-axis. (**b**) The structure of isolated compounds which are represented by peak numbers on the profile: (**peak-1**) methyltanshinoate, (**peak-2**) cryptotanshinone, (**peak-3**) tanshinone I, (**peak-4**) 1,2-dihydrotanshinquinone I, (**peak-5**) methylenetanshinquinone, (**peak-6**) dehydromiltirone, and (**peak-7**) tanshinone IIA.

In general, difficulties in solubility of the compounds were experienced especially with compound **7** (tanshinone IIA). The dicarbonilic group of tanshinone IIA, isolated in a large amount from *S. miltiorrhiza*, and of the commercially available 9,10-phenanthrenquinone were transformed into oxazole and methyl-imidazole groups, respectively, by reductive amination with methyl amine[198]. The figure below (Fig. 2.6) shows the reaction on 9,10-phenanthrenquinone and tanshinone IIA together with the resulting synthetic structures. The resulting compounds named PQ-I and TA-II were further tested in cell-based assays. These two molecules can be considered as part of a preliminary structure-activity relationship (SAR) study, where the imidazole and oxazole groups were introduced.

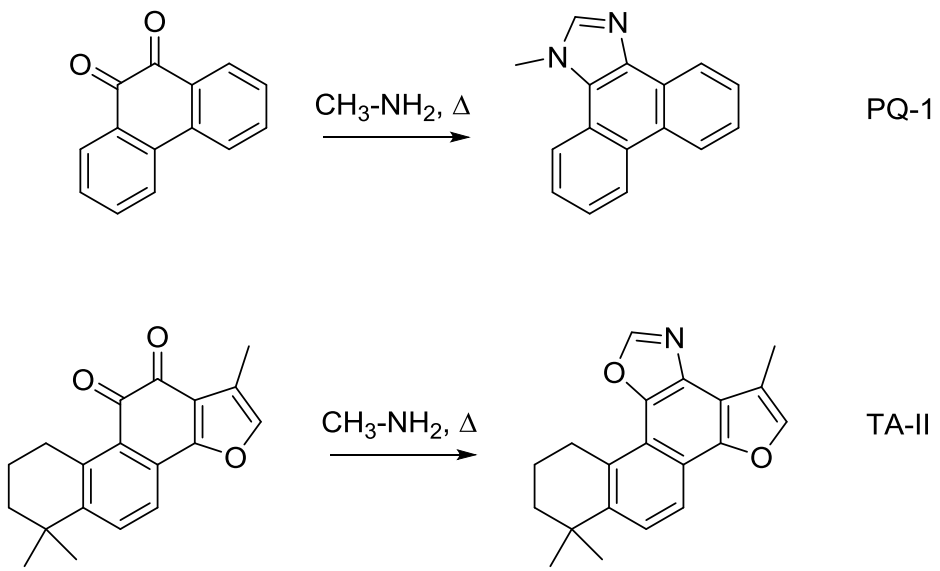

Figure 2.6: Reaction on 9,10-phenanthrenquinone (top left) and tanshinone IIA (bottom left) and resulting synthetic structures (PQ-1 and TA-II).

2.3 *Peganum harmala* (Nitrariaceae)

The main activity of the extract from *P. harmala* was assigned to harmine (peak 3) between 8.00-9.00 minutes (fraction 8) as depicted in the HPLC-activity profile in Fig. 2.7. Further Fig. 2.7 shows the structure of isolated compounds which are represented by numbers on the HPLC profile.

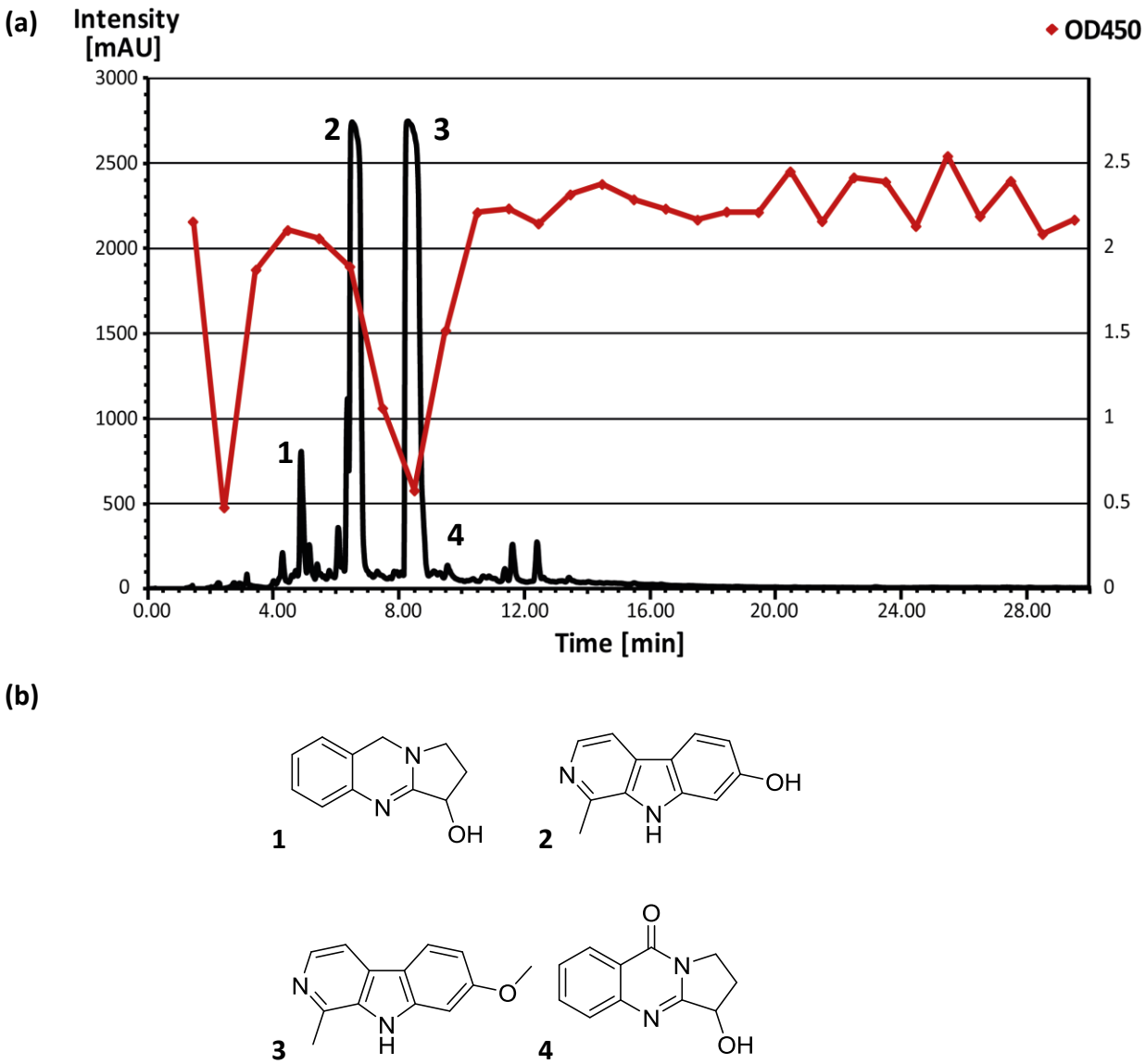

Figure 2.7: (**a**) HPLC-based activity profile of *Peganum harmala* methanol extract displaying UV chromatogram at 254 nm (in black) on the y-axis on the left and OD_{450} signal (in red) on the right y-axis. (**b**) The structures of isolated compounds which are represented by numbers on the profile: (**peak-1**) vasicine, (**peak-2**) harmol, (**peak-3**) harmine, and (**peak-4**) vasicinone.

2.4 Isolated compounds, synthetic tanshinones, and alkaloid library

All isolated compounds presented so far as well as a collection of selected in-house alkaloid compounds which are chosen based on the active scaffold of harmine were tested. As shown in Fig. 2.8, the complex inhibition assay results for isolated compounds exhibits that harmine, 1,2-dihydrotanshinquinone I, and methylenetanshinquinone were the most active compounds, this

is in line with their observed HPLC-based activity profiles. Moreover these results illustrate that the type of compounds that would more likely be active would be planar and nitrogen based.

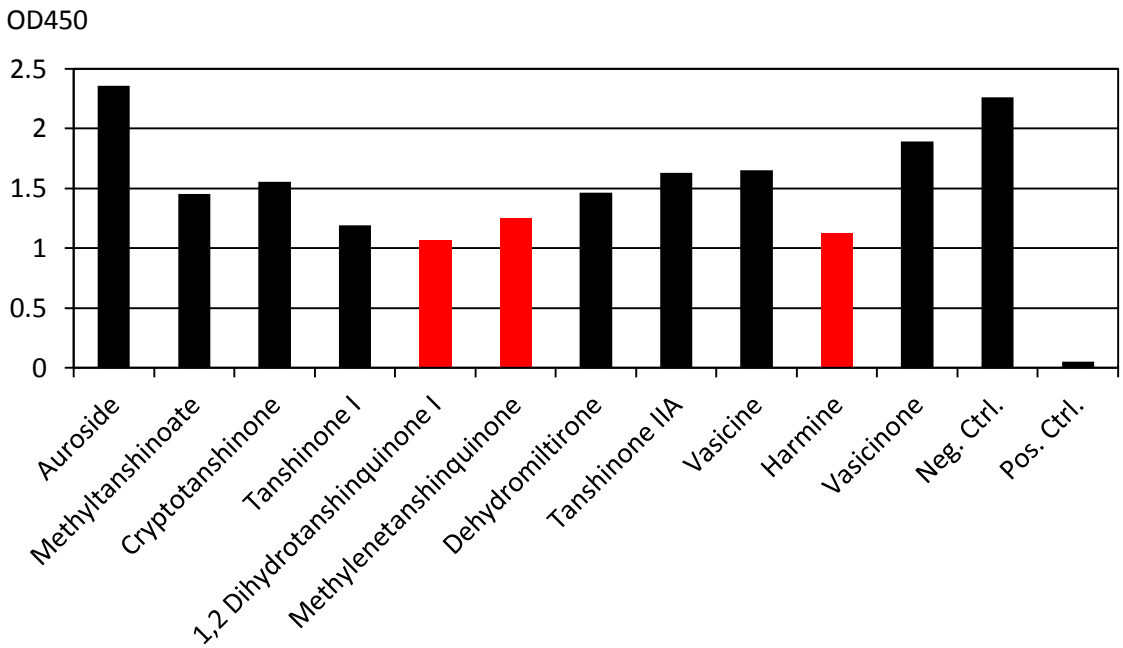

Figure 2.8: Complex inhibition results for isolated compounds (most active ones are depicted in red). The test concentration was 50 µg/mL.

To overcome the issue of solubility experienced with the tanshinone compounds, two synthetic derivatives from *S. miltiorrhiza* were prepared (also refer to section 2.2). Moreover, the assays which measure the % of exon inclusion/exclusion in the gene coding for insulin receptor (INSR) and cardiac troponin (TNNT2), that are commonly miss-spliced by the lack of functional MBNL1 in the DM1 disease were prepared at the Neurobiology Department, University of Basel. Utilising these assays, both synthetic derivatives of *S. miltiorrhiza*, three isolated active compounds (i.e., harmine, 1,2-dihydrotanshinquinone I, and methylenetanshinquinone) as well as a collection of selected in-house alkaloid compounds were tested. The structures of the collected alkaloids and the above assay test results are shown in Fig. 2.9 and Fig. 2.10, respectively.

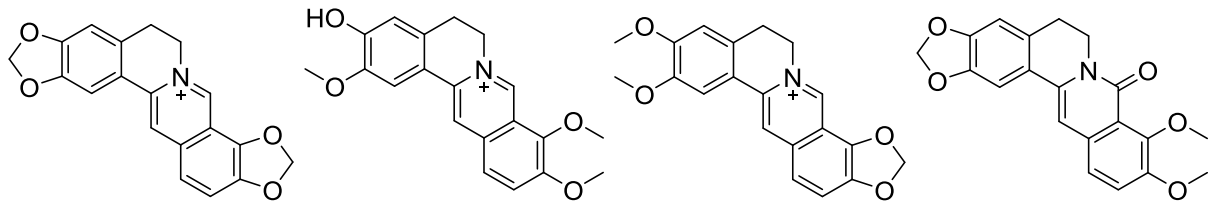

coptisine jatrorrhizine epiberberine 8-oxoberberine

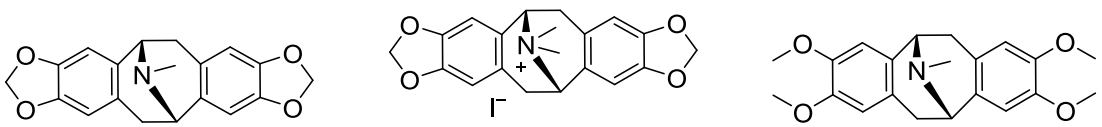

(-)-eschscholtzine (-)-californidine iodide (-)-argemonine

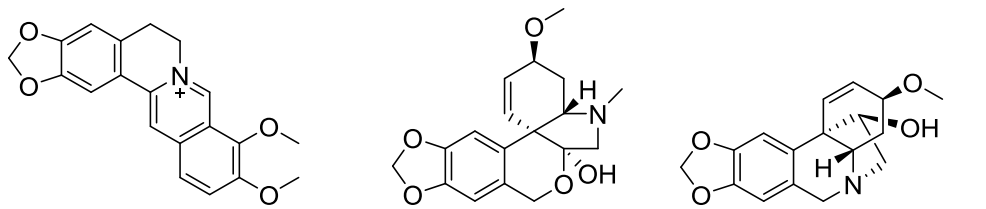

berberine (+)-tazettine (+)-haemanthamine

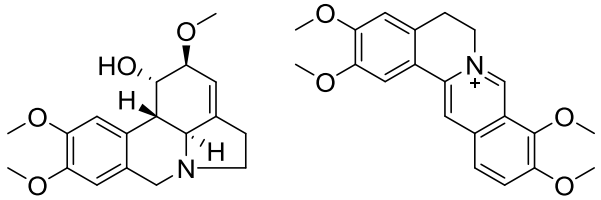

(-)-galanthine palmatine

Figure 2.9: Structures of selected alkaloid compounds which are chosen based on the active scaffold of harmine.

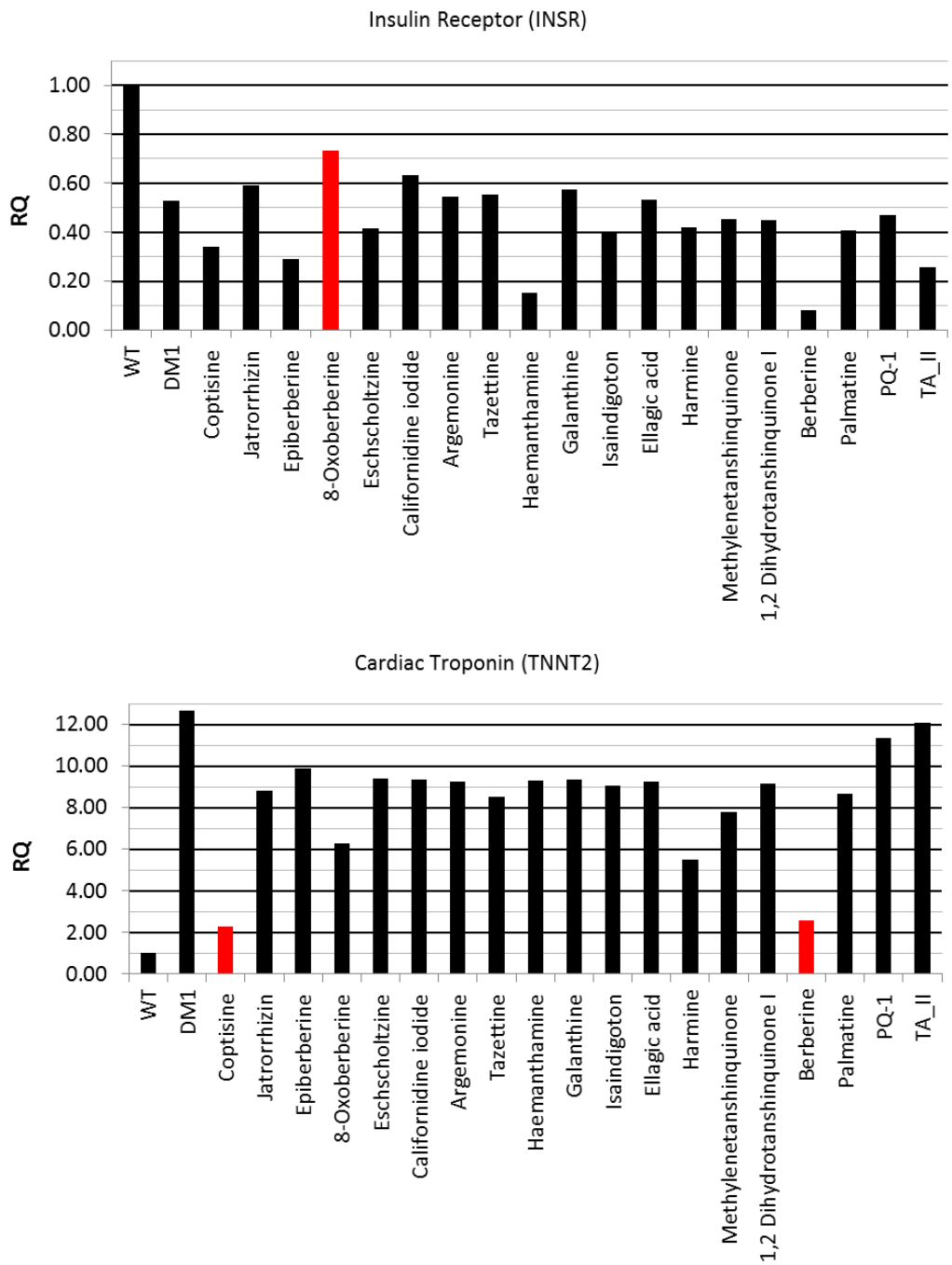

Figure 2.10: Test results for alkaloid collection, three isolated active compounds (i.e., harmine, 1,2-dihydrotanshinquinone I, and methylenetanshinquinone) and two synthetic derivatives of *S. miltiorrhiza*, in terms of – % of exon inclusion/exclusion for insulin receptor (INSR) and cardiac troponin (TNNT2) (the most active ones are depicted in red). RQ represents the relative quantification by qPCR. The test concentration for all experiments was 40 µM.

2.5 Discussion and conclusions

Myotonic dystrophy type 1 (DM1) is a genetically inherited muscle disorder that is characterised by progressive muscle wasting and weakening, cataracts, and cardiac conduction defects. At present there is no cure or effective treatment for this disabling disease. In this context, a collection of about 2100 extracts from different plant and fungal strains were screened with a novel DM1-based biochemical assay for their ability to inhibit the formation of the pathogenic complex formed between (CUG)n-RNA and the splicing-factor muscleblind-like 1 (MBNL1). From the ten extracts that were prioritised, 7 of them could be excluded due to false positives caused by interaction of tannins with protein based screens. Tannins are known to form non-specific interactions with protein-based screens, via reversible (ionic or H-bonding interactions) or irreversible (oxidative coupling) interactions. The remaining active extracts were from *Lamium album*, *Salvia miltiorrhiza*, and *Peganum harmala*. Auroside (La-peak-1) was identified from *L. album*. The compounds methyltanshinoate (Sm-peak-1), cryptotanshinone (Sm-peak-2), tanshinone I (Sm-peak-3), 1,2-dihydrotanshinquinone I (Sm-peak-4), methylenetanshinquinone (Sm-peak-5), dehydromiltirone (Sm-peak-6), and tanshinone IIA (Sm-peak-7) were isolated from *S. miltiorrhiza*. From *P. harmala* vasicine (Ph-peak-1), harmine (Ph-peak-3), and vasicinone (Ph-peak-4) were isolated from a previous study and were already available in-house, while harmol (Ph-peak-2) was identified via dereplication of data.

The results of the complex inhibition assay showed that harmine, 1,2-dihydrotanshinquinone I, and methylenetanshinquinone were the most active compounds. Quantification of the results also showed that harmine had an IC_{50} at 135.5 ± 9.3 µM and a toxicity-IC_{50} at 123.3 ± 4.6 µM, while 1,2-dihydrotanshinquinone and methylenetanshinquinone had solubility issues but both of them displayed $IC_{50} > 200$ µM. To increase the solubility of these tanshinone compounds, two derivatives starting from 9,10-phenanthrenquinone and tanshinone IIA were synthesised (namely PQ-1 and TA-II) and tested. Additionally, based on the active scaffold of harmine, planar-nitrogen-based compounds (such as protoberberine alkaloids) were hypothesised to possess higher activity. Given that the target is a RNA hairpin loop, selected alkaloids from the in-house library were tested in assays which measure the % of exon inclusion/exclusion in the gene coding for INSR and TNNT2. The results from these experiments showed that the most active compounds were 8-oxoberberine for INSR, and coptisine and berberine for TNNT2 (see Fig. 2.10). Further study on berberine displayed that it had the most potent activity in the

complex inhibition assay with an IC_{50} of 86.3 ± 5.8 µM and 212.1 ± 18.3 µM toxicity-IC_{50}, and it was able to restore splicing in TNNT2 by 75.1 ± 2.8%. Harmine was able to restore TNNT2 splicing by 76.8 ± 1.6%. Even though the IC_{50} and toxicity-IC_{50} values are relatively close for both alkaloids, the compounds were effective for alternative splicing at concentrations significantly lower than their respective IC_{50} and toxicity-IC_{50} values[199]. Besides these results, the compound screening showed that 1,2-dihydrotanshinquinone I, and methylenetanshinquinone had weaker activity in both INSR and TNNT2 assays than alkaloids, this might be due to poor solubility. The tanshinone-derivatives showed increased solubility but also increased toxicity and as a result their activities in restoring MBNL1 function were weaker. Accordingly, further medicinal chemistry optimisation of diterpenes is warranted.

Overall, the identified alkaloids (i.e., harmine and berberine) were able to ameliorate certain aspects of the DM1 pathology, whereas the compounds from *Salvia* species (i.e., *S. miltiorrhiza*) exhibit certain activities which need further investigation. Notably, the main findings of this study exhibit that compounds with planar scaffolds which contained mostly nitrogen are more active. Given the planar nature of the active molecules and the target being RNA, it is speculated that compound activity is due to reversible intercalation to the RNA hairpin loop via electrostatic interactions, thereby blocking the binding of MBNL1 and allowing it to carry out its normal function. Considering the fact that most drugs derived from natural products being alkaloids or related compounds, thus the lead compounds found in this study may have the potential for drug discovery in RNA-mediated diseases. This study represents the first screening of natural products for DM1 targeted drug discovery efforts. In addition, this work has been presented at the Society for Medicinal Plant and Natural Product Research (GA) conference (Faleschini, *et al.,* 2015) as well as parts of this study were published in Journal of Biological Chemistry (Herrendorff, *et al.*, 2016)[199].

Chapter 3

3. Results and Discussion: Tuberculosis

As stated in section 1.5, the TB project aims to identify small molecules of natural origin which have the ability to inhibit the expression of coronin-1 protein that has an essential role for the survival of *Mycobacterium tuberculosis* (MTB) within macrophages in the human body. In the following sections, extract library screening and hit prioritisation, the results of prioritised extracts: ethyl acetate extract of *Dorstenia contrajerva* and methanol extract of *Pancratium littorale* are presented. Lastly, summarised discussion on TB project and concluding remarks are given.

3.1 Extract library screening and hit prioritisation

A library containing approximately 2100 plant and fungal extracts, selected based on their chemotaxonomy and/or traditional uses were screened in the promoter based assay at 20 µg/mL for 72 hours. The results were analysed for their Green Fluorescence Protein (GFP) and Red Fluorescence Protein (RFP) readouts. A decrease in GFP represents a molecule interacting with the promoter region of murine coronin-1, thus inhibiting/activating the expression thereof and resulting in a decreased/increased GFP readout respectively (on the analysis of this study a decrease in GFP signifies coronin-1 inhibition and thus an active substance). Whereas RFP represents non-specific interaction with the promoter region of cytomegalovirus (CMV), thus inhibiting/activating the expression thereof and resulting in a decreased/increased RFP readout, respectively (on the analysis of this study a decrease in RFP signifies a toxic substance). Extracts that showed a significant decrease in GFP and an insignificant decrease or no decrease in RFP at 20 µg/mL after 72 hours, were prioritised for further investigation. As depicted in Fig. 3.1 (a) and (b), the ethyl acetate extract of *Dorstenia contrajerva* L. (Moraceae) displayed a 40% decrease in GFP and no decrease in RFP at 20 µg/mL, after 72 hours. Additionally, as showed in Fig. 3.1 (c) and (d), the methanol extract of *Pancratium littorale* Jacq. (Amaryllidaceae) significantly down regulated coronin-1 expression after 72 hours with ≥ 80% inhibition at 20 µg/mL.

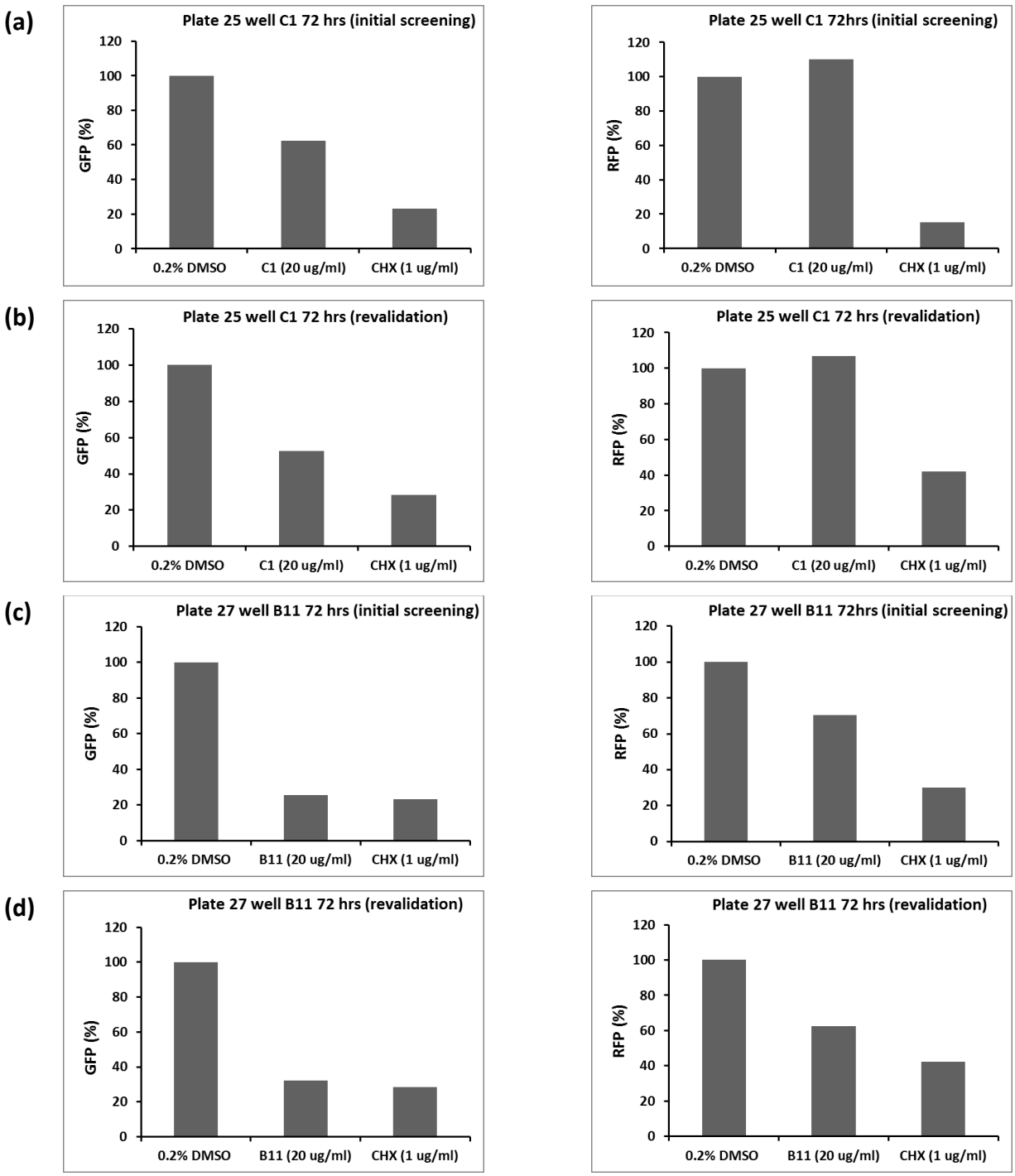

Figure 3.1: (**a**) GFP and RFP readouts (%) for *Dorstenia contrajerva* (Plate 25 well C1) at 20 µg/mL after 72 hours, with 0.2% DMSO as a blank control and cycloheximide (1 µg/mL, CHX) as a negative control; and the re-evaluation is given on row (**b**). (**c**) GFP and RFP readouts (%) for *Pancratium littorale* (Plate 27 well B11) at 20 µg/mL after 72 hours, with 0.2% DMSO as a blank control and CHX (1 µg/mL) as a negative control; and its re-evaluation is given on row (**d**).

3.2 *Dorstenia contrajerva* (Moraceae)

Following a validated procedure[60,62], HPLC-based activity profiling was carried out on the extract library sample of *D. contrajerva*. This allows the correlation of spectroscopic data recorded online (PDA scanning from 210-400 nm) and offline (MS scanning from 160-1500 *m/z*), with the biological information that are obtained from a time-based micro-fractionation and subsequent bioassay[60,62]. As shown in Fig. 3.2, the most prominent region of activity in the HPLC-UV chromatogram at 254 nm was seen at fraction 22 which corresponds to minute 21 – 22 (on the HPLC profile); with a reduction by about 40% in GFP and less than 15% in RFP. This activity could be correlated with one major UV active peak eluting in fraction 22. In fractions 9 and 10 (corresponding to minutes 8 to 10) the slight decrease in GFP (by about 15 to 20%: see Fig. 3.2) was assigned to minor constituents that were not identified. Additionally, increased toxicity of fractions 28 to 31 (minutes 27 to 31) was observed (which have RFP reduction above 25%).

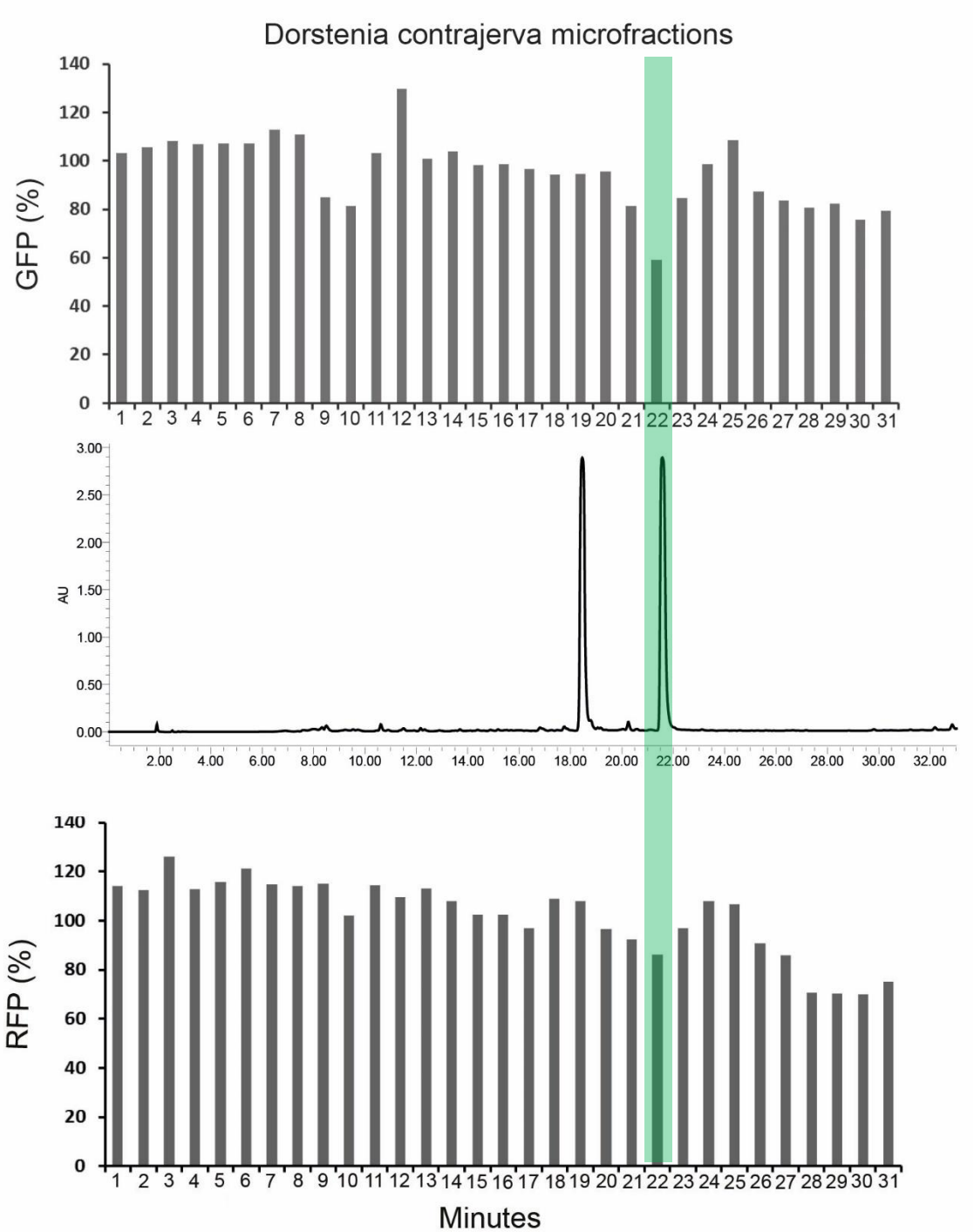

Figure 3.2: HPLC-based activity profiling for *D. contrajerva* on a C18 Sunfire column (3.0 x 150 mm; 3.5µm; Waters), with a 5 to 100% B gradient in 30 minutes, and 5 minute 100% B isocratic, using a flowrate of 0.4 mL/min. Solvent composition was (A): H_2O + 0.1% formic acid and (B): MeCN + 0.1% formic acid. Collection was 1 minute fractions starting from 0.00 to 31.00 minutes. The micro-fraction results: %GFP (top panel), UV chromatogram at 254 nm (middle panel), and %RFP (lower panel).

Online spectroscopic information, database searches and offline NMR analysis were used for dereplication of the known compounds. The main compounds were identified to be two major furanocoumarins that have been previously isolated from *D. contrajerva*[200]. Bergapten[201] was present in fraction 19 and another rather unusual furanocoumarin (also known as dorstenin[200]) was found to be the dominant compound in fraction 22, corresponding to the prominent activity shown during the HPLC-based activity profiling (see Fig. 3.2). Separation conditions were optimised for peak-based semi-preparative HPLC-UV collection and subsequent off-line microprobe NMR analysis (see Fig. 3.3). The two known compounds, bergapten and dorstenin were isolated (98% pure) and their structures were confirmed using NMR analysis. As previously described dorstenin was obtained as a racemic mixture of enantiomers[200]. ECD measurements were performed to determine the enantiomer obtained. No significant cotton effects were observed, thus confirming that dorstenin was obtained as a racemic mixture – as previously described.

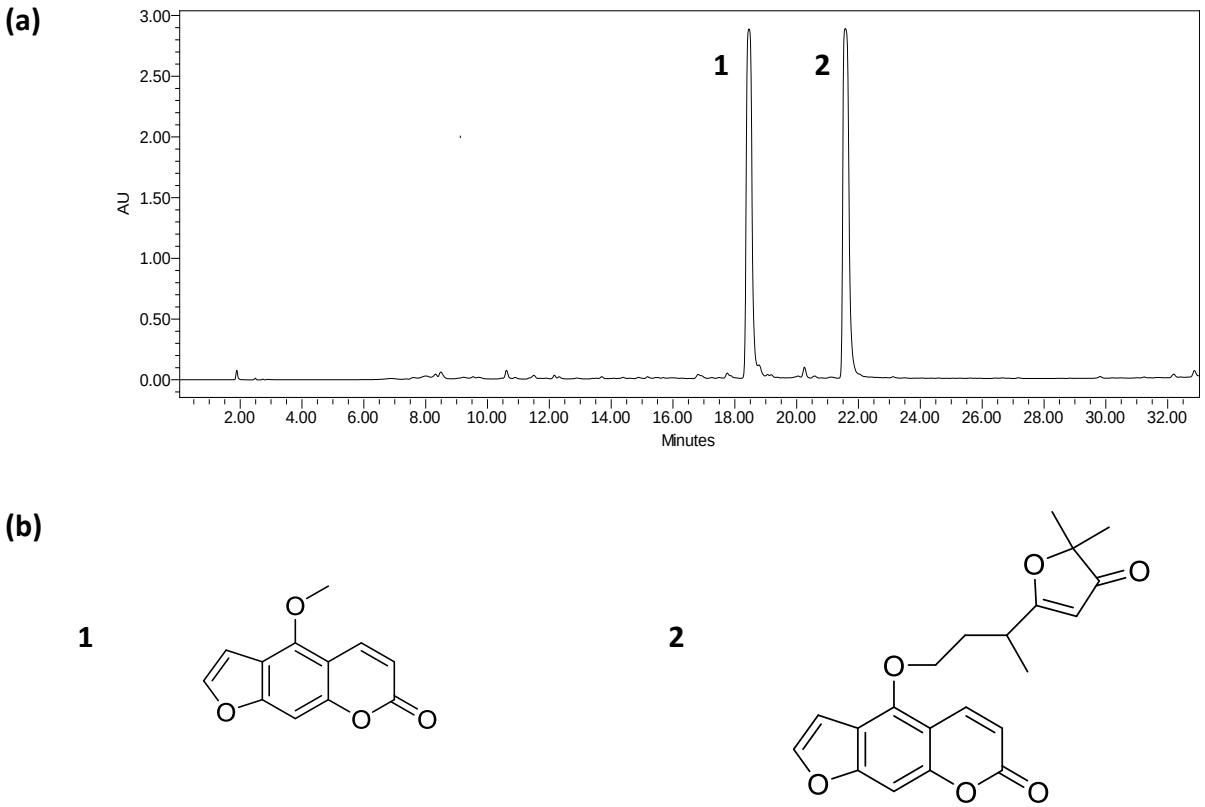

Figure 3.3: (**a**) UV chromatogram at 254 nm showing retention times; (**b**) structures of two furanocoumarins that are isolated from *D. contrajerva*: **peak-1:** bergapten and **peak-2:** dorstenin.

Dorstenin (the main active compound) was tested at various concentrations (20, 10, 5, and 2.5 µg/mL) for GFP and RFP readouts (see Fig. 3.4). However, even at these concentrations, activity of the pure compound could not be confirmed. Dorstenin only started to show a slight decrease in GFP at 20 µg/mL. Thus the main activity observed in fraction 22 could be either the presence of minor, potent compounds, or the high quantity of dorstenin present in fraction 22.

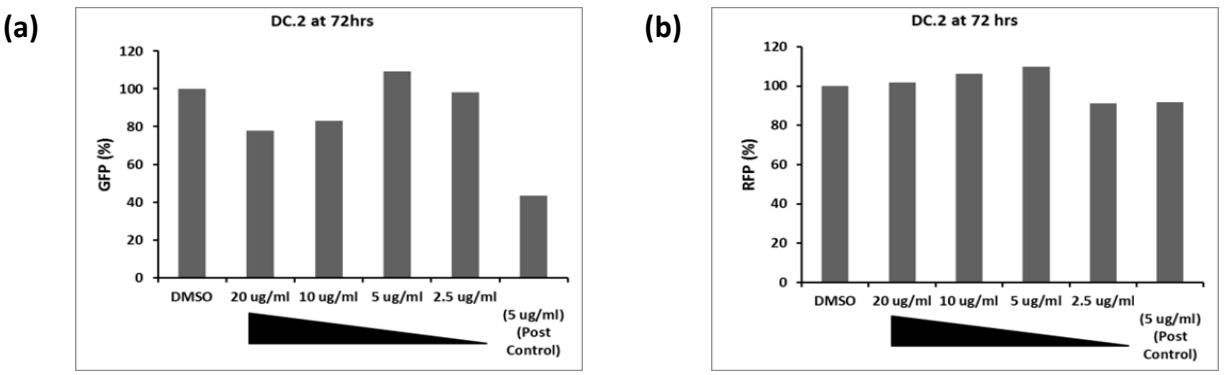

Figure 3.4: (**a**) GFP and (**b**) RFP results of dorstenin after 72 hours at 20, 10, 5, and 2.5 µg/mL. DMSO was used as a blank control and a lead compound as a positive control (Post Control).

During redissolution of the micro-fractions, the solvent type and volume required is a critical issue. Usually DMSO is used due its compatibility with biological assays and its solubilising properties. The volume for re-dissolution of the fractions should be half of the injection volume used during the fractionation, to enable the concentration of an active compound to be similar to that of the extract[60]. This is an arbitrary volume and is based on experience with setting up assays using the miniaturised HPLC-based activity profiling approach[60]. Since the distribution of the extract is unknown, the micro-fractions are taken up into the same volume; hence they are treated as if there is an equal distribution of the extract throughout the separation. Accordingly, the high activity found in fraction 22 (40% GFP reduction) was speculated to be one of two reasons, (1) presence of other minor compounds in fraction 22 that were not detected by UV, or (2) relative to other compounds, higher amount of dorstenin present in fraction 22, thus fraction 22 of the extract tested may have higher concentration of dorstenin. To identify the reason why the high activity was found in fraction 22, the above two speculations are independently examined.

Investigation of fraction 22 using TLC and NMR showed that the fraction did not contain additional minor or undetected compounds that could give rise to the potent activity which is

seen during the micro-fractionation (see Fig. 3.5). Also, for comparison purposes fraction 19 (which contains bergapten) was investigated, utilising TLC and NMR (see Fig. 3.5).

(a)

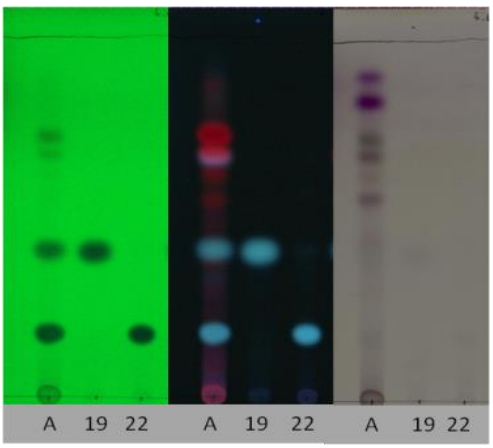

(b)

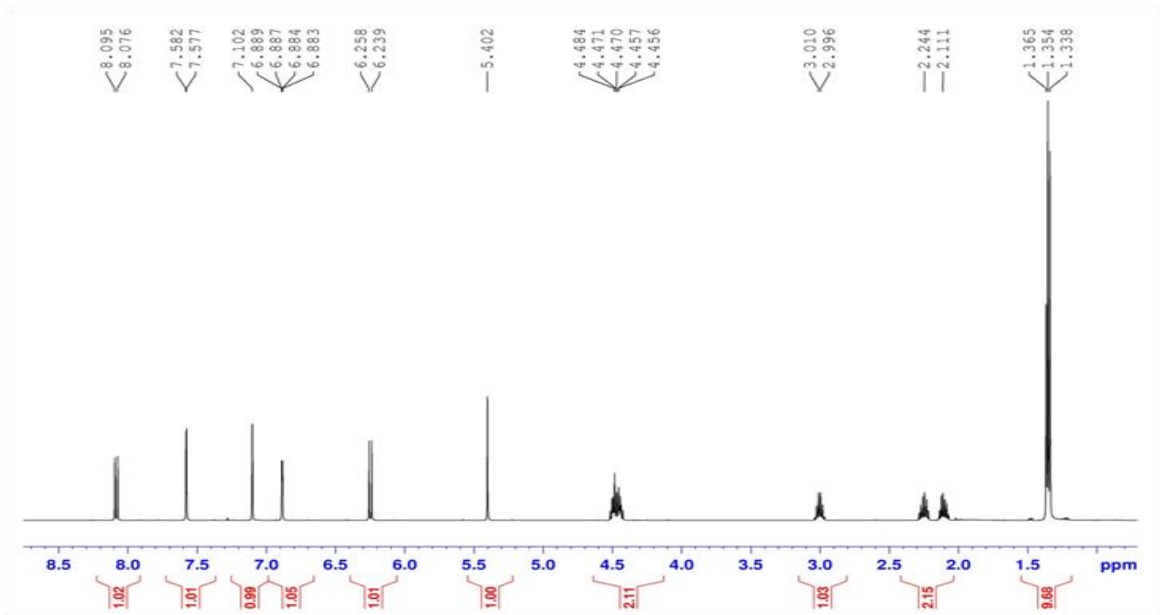

Figure 3.5: (**a**) TLC at 254 nm (green), 366 nm (black) and sprayed with Godin's reagent (grey) for the extract (abbreviated as "A" on the plate), fraction 19 (abbreviated as "19" on the plate), and fraction 22 (abbreviated as "22" on the plate) are given. (**b**) The ^{1}H-NMR of fraction 22 showing dorstenin > 95% pure.

The first speculation given above, which is the presence of minor active compounds, could be excluded as a possible reason for the activity in fraction 22. On the other hand, micro-fractionation is performed on a miniaturised scale and determining the weight of each fraction is not possible, therefore, micro-fractions are resuspended in the exact same amount and treated in the same way. If a compound happens to be present in a higher amount than other substances in an extract (which may be the case when working with nature), a higher weight

will be present in the well – resulting in this fraction being tested at a much higher concentration, since re-dissolution of the fractions are treated equally. Subsequent quantification of the pure compounds should be followed up to determine the relative concentration that the compounds were tested at. In this context, to examine the second speculation which states about the amount of dorstenin in fraction 22, bergapten and dorstenin concentration present in the library sample were quantified using UV and ^{1}H-NMR. This would allow the calculation of the concentration that fraction 22 may have been tested during the micro-fractionation, and provide a possible reason for the observed activity seen in Fig. 3.2.

Quantification of the two furanocoumarins was done via UV detection at a λ_{max} of 310 nm. The calibration curve for bergapten (with mean coefficient of determination, R^2: 0.994), and dorstenin (with R^2: 0.999) is shown in Fig. 3.6. Using the calibration curve for bergapten and dorstenin, it was calculated that the extract library contains these compounds with 4.6% and 12.4%, respectively.

(a)

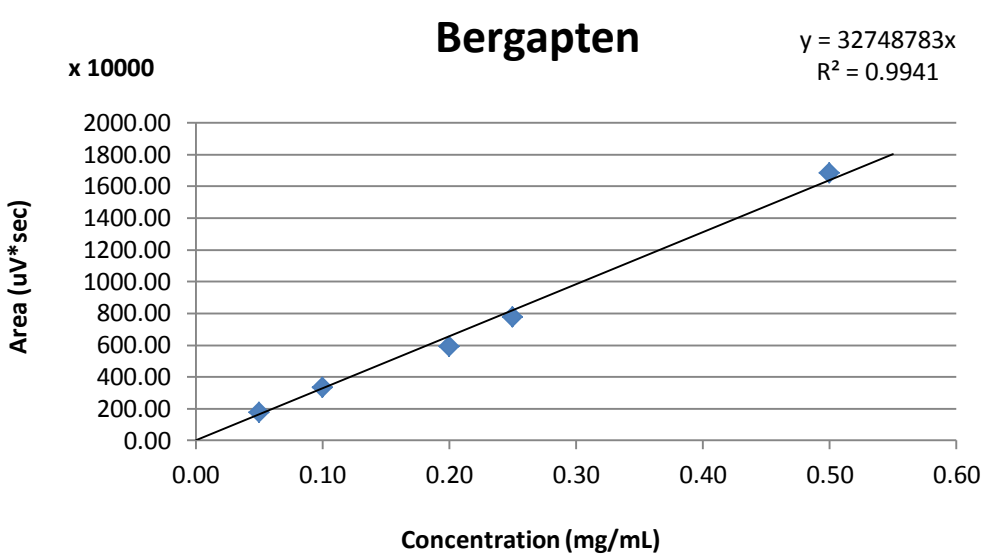

(b)

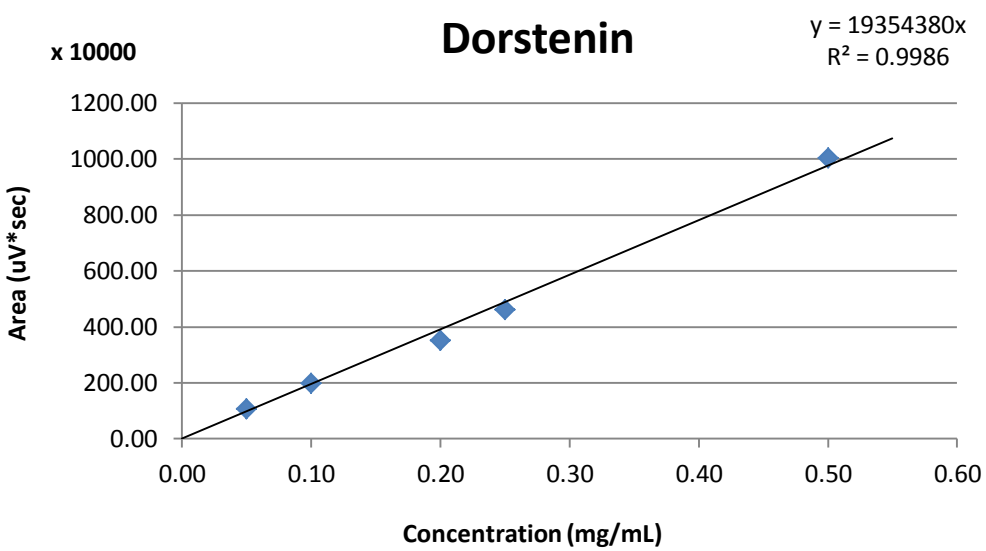

Figure 3.6: Calibration curves for (**a**) bergapten, and (**b**) dorstenin, with their mean coefficients of determination.

The second quantification (using ^{1}H-NMR) was done for comparison purposes with that of the UV quantification. Reference signals for integration were δ = 7.32 (bergapten), δ = 6.09 (Internal Standard: IS), and δ = 5.54 (dorstenin). The amount of the two compounds was calculated, using the equation below:

$$\text{If } \frac{Ix}{Iy} = \frac{Nx}{Ny} \text{ therefore } Nx = \frac{Ix \times Ny}{Iy \times Nx} \times Number\ of\ mmol\ from\ IS$$

The equation above allows the calculation of the number of moles of compound x. Where Ix is the integration of proton signal of compound x, Ny is the number of protons giving rise to the IS proton signal, Iy is the integration of proton signal of IS, and Nx is the number of protons giving rise to compound x proton signal. Thereafter, the number of moles of compound x can be used to calculate the weight of the compound and thus the % present in the sample[91]. An example of the signals used for integration is shown in Fig. 3.7.

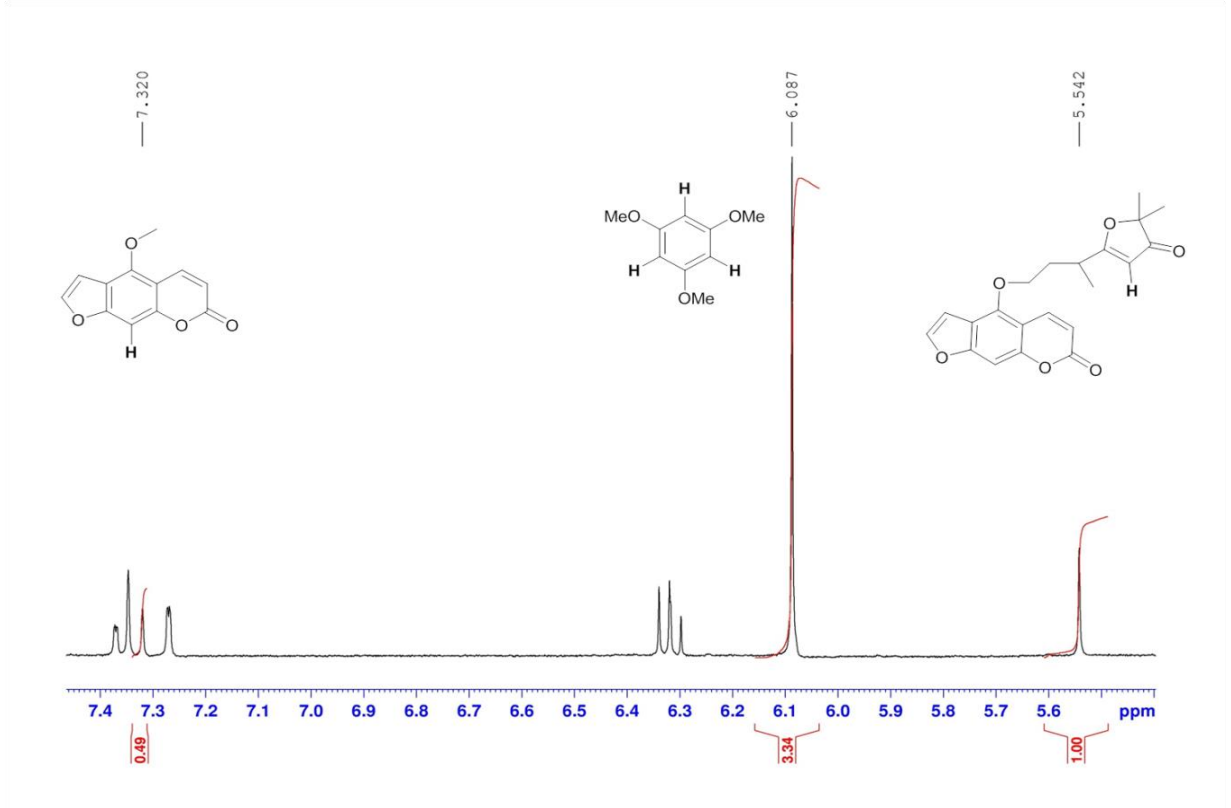

Figure 3.7: ^{1}H spectrum of *D. contrajerva* extract library sample (0.5 mg) with 1,3,5-trimethoxybenzene (0.03 mg) as IS, showing representative ^{1}H signals used for quantification of bergapten and dorstenin.

From the calculations of the three ^{1}H-NMR quantification samples, the amounts of bergapten and dorstenin present in the extract library sample were 3.4% and 11.6%, respectively. Possibly due to analytical error, these values are slightly lower than the quantification by UV however their averages are in a similar range of about 4.0% and 12.0% for each compound. These quantification analyses on the library sample allow the calculation of bergapten and dorstenin concentration that are present in fraction 19 and fraction 22.

Using the above mass contribution analysis, bergapten and dorstenin contributions on fraction 19 and fraction 22 were found to be 41.2 µg, and 112.0 µg, respectively. Taking into consideration the re-dissolution and dilutions used for the assay, during the HPLC profiling, fraction 19 was tested at 20.6 µg/mL and fraction 22 was tested at 56 µg/mL. At this concentration (56 µg/mL) fraction 22 was active. However, the extract library sample was initially tested at 20 µg/mL, this means based on the above mass contribution quantification – bergapten concentration is 0.92 µg/mL and dorstenin concentration is 2.5 µg/mL. These

concentrations are much lower than the testing that had been done during the HPLC profiling, accordingly as seen in Fig. 3.4 dorstenin is not active.

These results corroborate that fraction 22 only possessed a high activity due to the high amount of dorstenin in the extract. It should be taken into consideration that HPLC-based activity profiling is a qualitative analysis used to track bioactivity and lead investigators towards the potentially active compounds. It is crucial to follow up with testing of the pure compounds after identification to determine the concentration at which they are active. Additionally, the observed collective activity of the extract could be due to synergistic interactions of all the substances together. This can be corroborated with the slight increase in activity (decrease in GFP) seen in fractions 9 and 10, also the affect of the late eluting compounds (fractions 30-35) that show a decrease in GFP. Collectively they contribute to the overall activity (20% decrease in GFP) observed with the extract. Therefore, it is not always possible to isolate a single active substance that contributes to the overall potency observed with the whole extract.

An additional way to overcome the issue of varying abundance of compounds in an extract is to perform a larger fractionation (using semi-preparative quantities, i.e. macro-fractionation) and subsequently weighing the resulting fractions. This allows all fractions to be tested at the same concentration since the weight of each fraction is known. As shown in Fig. 3.8 one minute fractions were collected on a semi-preparative basis and resulting weights were obtained. All fractions were then tested at the same concentration (10 µg/mL, Fig. 3.8), and correlated to online UV data. Fig. 3.8 now shows the lack of activity for compound dorstenin (now in fraction 21) and the overall minor activity spread over all fractions. The activity of the extract therefore possibly comes from a synergetic effect of all constituents present in the extract as observed during the micro-fractionation (Fig. 3.2, the slight decrease of GFP in fractions 9 and 10, and also in the later eluting fractions that showed a decrease in GFP and RFP). Overall, the mass contribution analyses as well as the results shown in Fig. 3.8 confirm that the high activity of dorstenin observed in Fig. 3.2 was due to the high amount of the compound present.

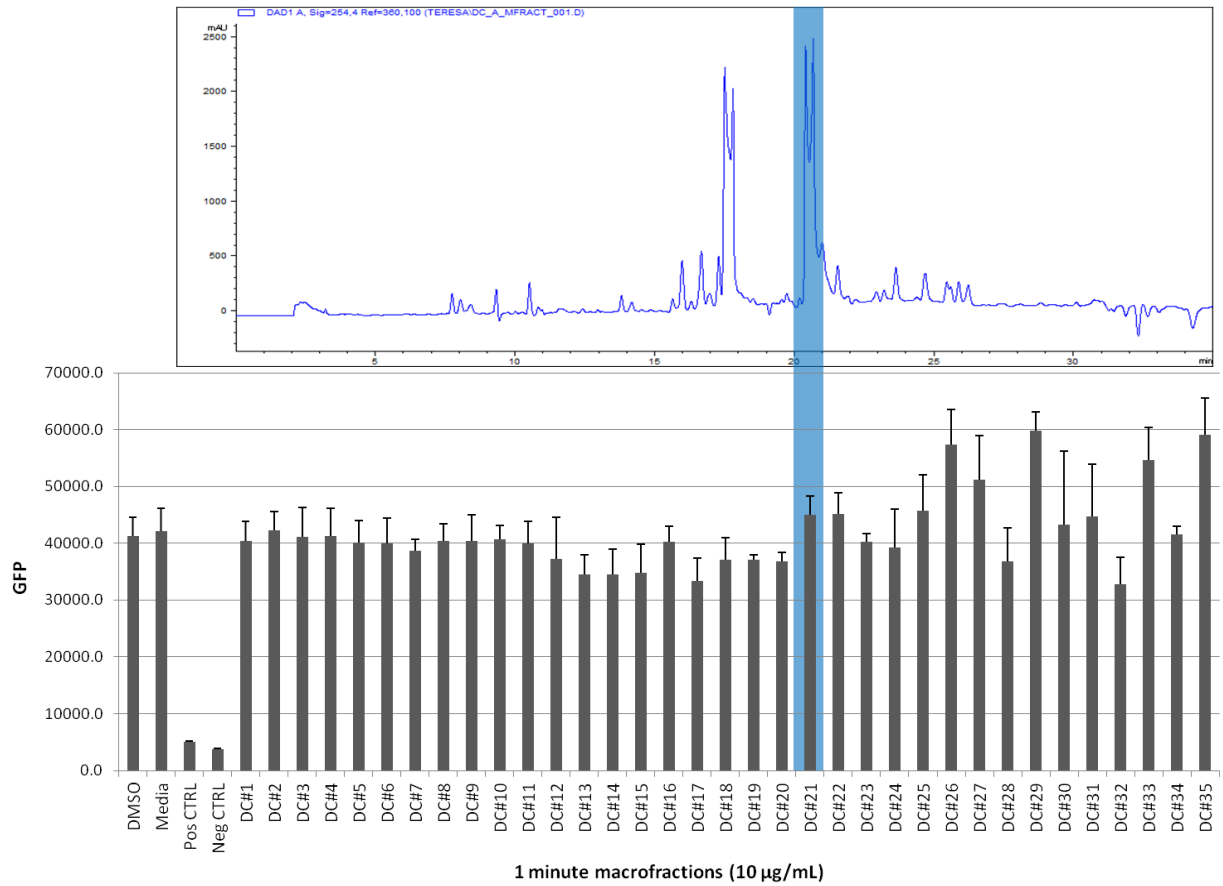

Figure 3.8: Semi-preparative HPLC-UV for *D. contrajerva*. Collection was 1 minute fractions starting from 0.00 to 35.00 minutes. The UV chromatogram at 254 nm (top panel) and GFP (lower panel) of the resulting fractions are given. All fractions were tested at 10 µg/mL.

3.3 *Pancratium littorale* (Amaryllidaceae)

HPLC-based activity profiling was carried out on the extract library sample of *P. littorale* and results are depicted in Fig. 3.9 and 3.10 below. This profiling was performed twice using different columns and conditions adapted for the separation of the more polar compounds since the highest GFP reduction was observed in the early eluting fractions from the first round of activity profiling (fractions 8 – 10, approximately 27-37% MeCN). During the second round of activity profiling, distinct active (fractions 14 – 16, approximately 28.2-33.6% MeCN) and toxic (fractions 21 – 24, 40.7-47.9% MeCN) regions could be distinguished. Further detailed investigation into the region of activity (using ESIMS and NMR data collected offline) led to the identification of alkaloids as the active constituents. It was speculated that under acidic conditions (the use of formic acid in the mobile phase), the alkaloidal compounds are charged and thus less retained on the C18 stationary phase and found in the early eluting fractions.

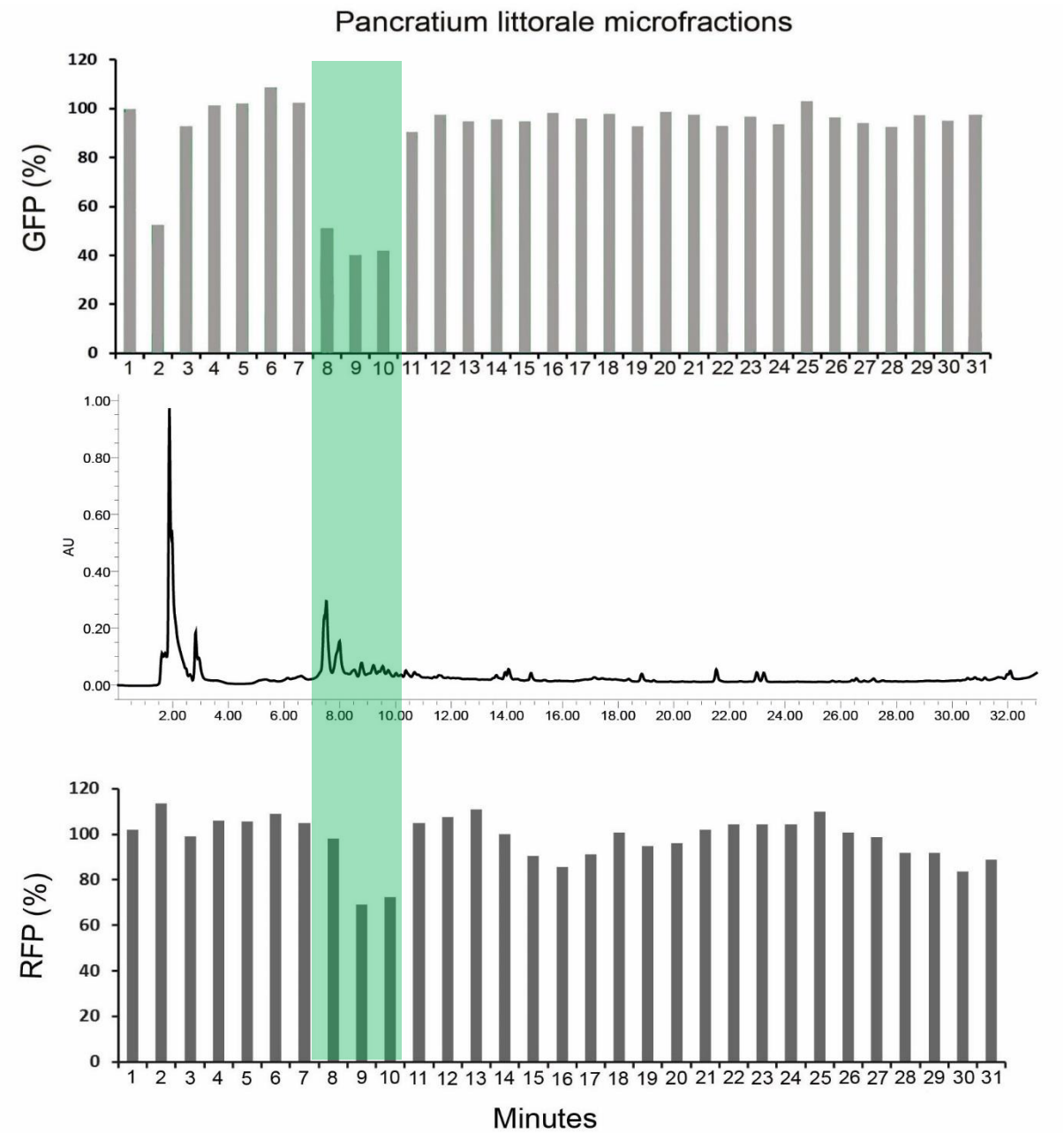

Figure 3.9: HPLC-based activity profiling for *P. littorale* on a C18 SunFire column (3.0 x 150 mm; 3.5µm; Waters), with a 5 to 100% B gradient in 30 minutes, and 5 minute 100% B isocratic, using a flowrate of 0.4 mL/min. Solvent composition was (A): H_2O + 0.1% formic acid and (B): MeCN + 0.1% formic acid. Collection was 1 minute fractions starting from 0.00 to 31.00 minutes. The micro-fraction results: %GFP (top panel), UV chromatogram at 254 nm (middle panel), and %RFP (lower panel).

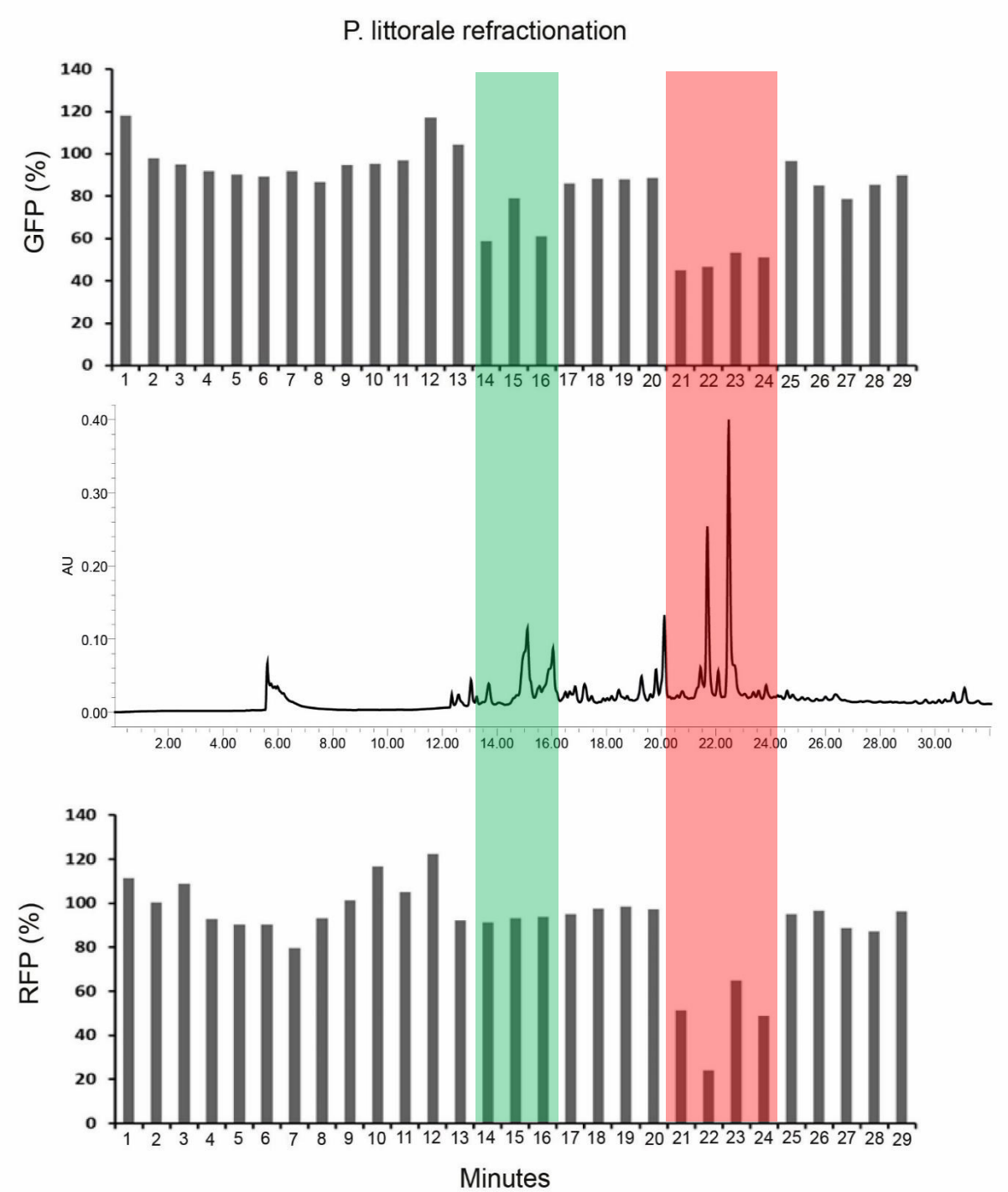

Figure 3.10: HPLC-based activity profiling for *P. littorale* on an Aqua C18 column (4.60 x 250 mm; 5µm; Phenomenex), with a 5 to 50% B gradient in 30 minutes, using a flowrate of 0.4 mL/min. Solvent composition was (A): H_2O + 0.1% formic acid and (B): MeCN + 0.1% formic acid. Collection was 1 minute fractions starting from 1.00 to 30.00 minutes. The micro-fraction results: %GFP (top panel), UV chromatogram at 254 nm (middle panel), and %RFP (lower panel).

The methanolic extract was further processed to remove the sugars and enrich the alkaloidal compounds using diaion and liquid-liquid extraction, respectively. Thereafter, the enriched alkaloid fraction was separated on a diol cartridge. Finally, separation conditions of fractions from the diol column were optimised on a RP column regulated at pH 9.0 (see chapter 6). After each enrichment step, the activity was assessed to make sure that GFP reduction was maintained (not lost during each process) with stable RFP [see Fig. 3.11 (a) and (b)].

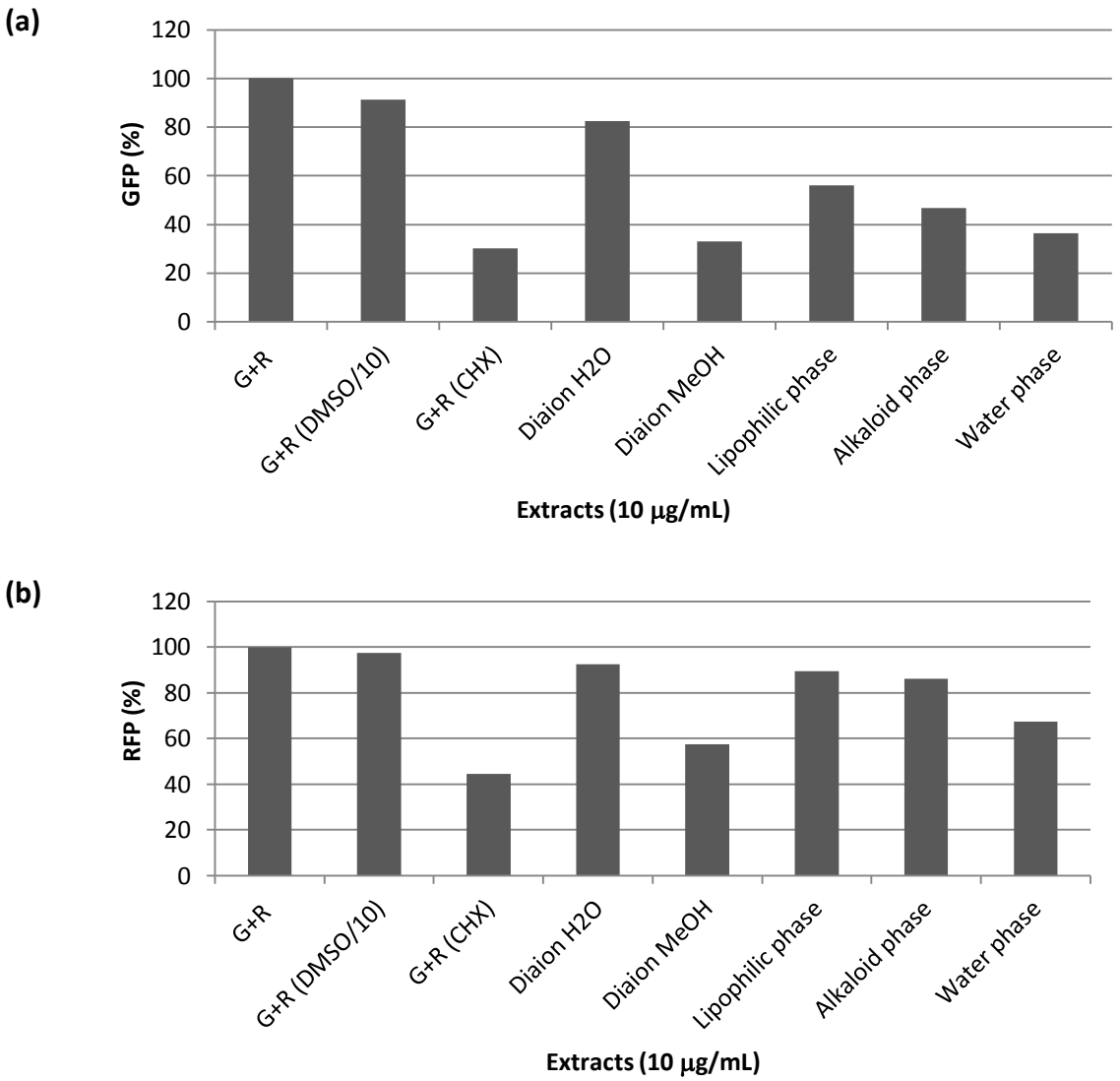

Figure 3.11: (**a**) GFP and (**b**) RFP results after each separation step. G+R: background green and red fluorescence of untreated cells, G+R (DMSO/10): DMSO control, CHX: cycloheximide as negative control, diaion H_2O: sugar containing portion, diaion MeOH: extract without sugar part which was subjected to alkaloid extraction: Lipophilic, alkaloid and water phases are from the alkaloid enrichment step.

After semi-preparative isolation, 15 isoquinoline alkaloids including three new congeners were structurally characterised. Their corresponding retention times are shown in the UV chromatogram at 254 nm (Fig. 3.12).

(a)

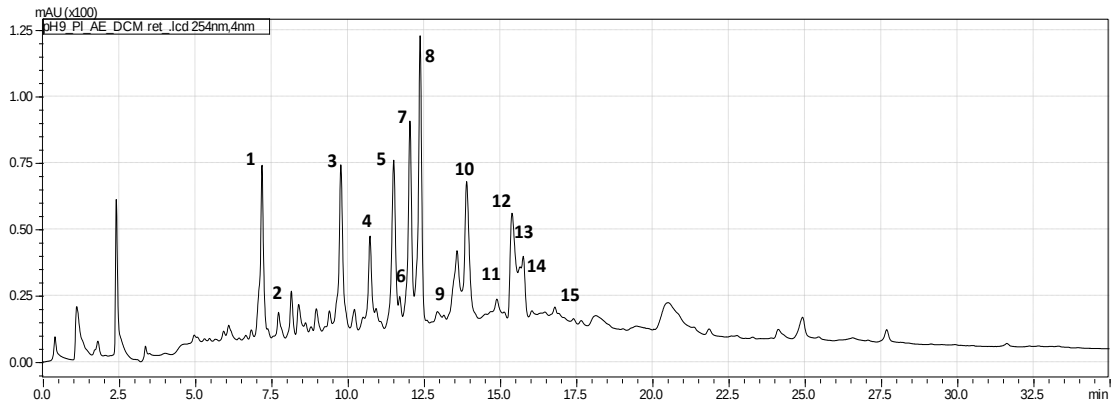

(b)

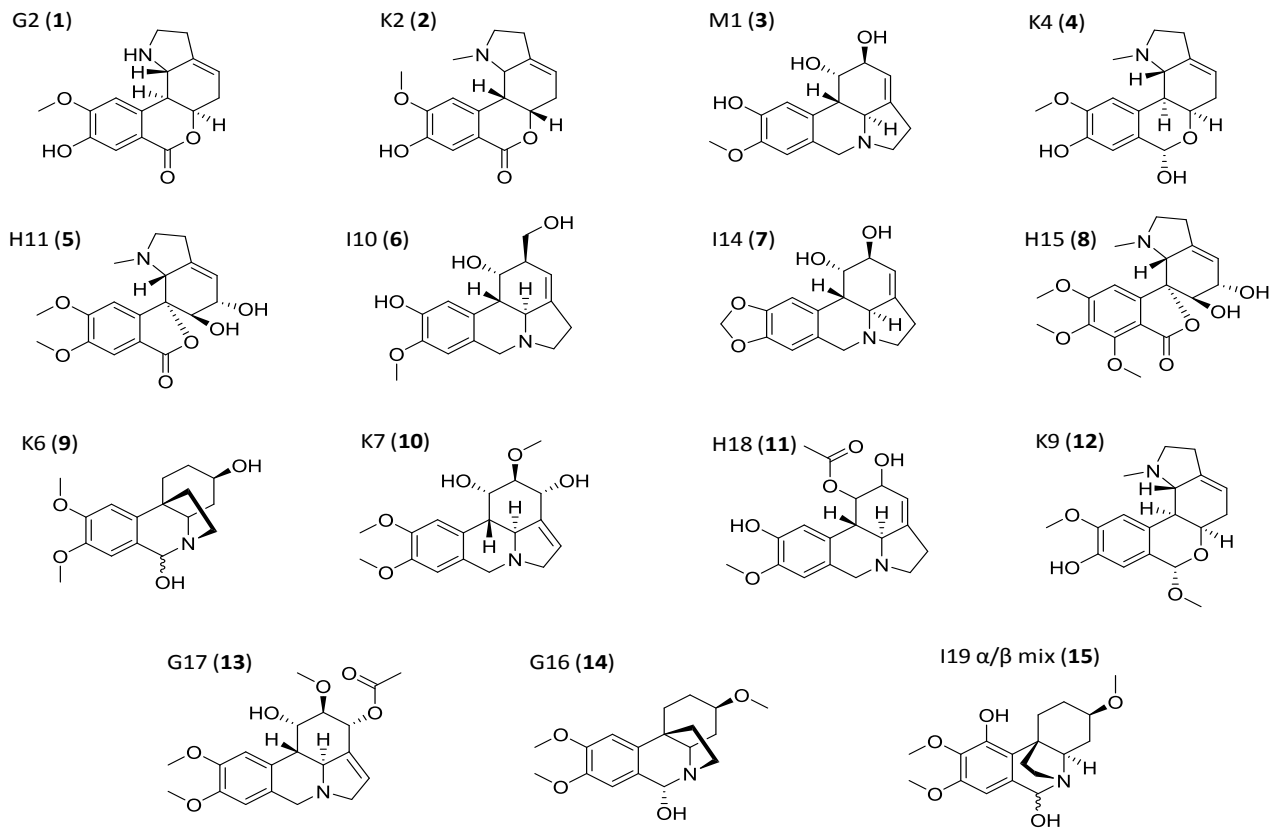

Figure 3.12: (**a**) HPLC-UV chromatogram at 254 nm of the alkaloid-enriched fraction with retention times of compounds isolated (the numbers in black indicate the spectrum-peak number), and (**b**) structures of isolated compounds with their codes and peak number. Separation condition was performed using a gradient of 2 to 100% B in 30 minutes, and 5 min at 100% B on the Reprosil-Pur Basic-C18 column. Solvent composition was (A): H_2O + 0.1% NH_3 solution, and (B): MeCN + IPA + 0.1% NH_3 solution (8:1:1) using a flowrate of 0.4 mL/min.

The isolated compounds are (**1**) 8-demethoxy-lycoranine F, (**2**) 8-*O*-demethyl-homolycorine, (**3**) pseudo-lycorine, (**4**) 8-*O*-demethyl-lycorenine, (**5**) 7-demethoxy-10-*O*-methyl-hostasine, (**6**) carinatine, (**7**) lycorine, (**8**) 10-*O*-methyl-hostasine, (**9**) 10-deoxy-3-hydroxy-6-hydroxy-hippeastidine, (**10**) narcissidine, (**11**) 1-*O*-acetyl-pseudo-lycorine, (**12**) 8-*O*-demethyl-6-*O*-methyl-lycorenine, (**13**) 3-*O*-acetyl-narcissidine, (**14**) 10-deoxy-6(α)-hydroxy-hippeastidine, and (**15**) 6-hydroxy-hippeastidine[202].

The structure elucidation, NMR correlations of the three new compounds (compounds **9**, **4**, and **1** on Fig. 3.12), and biosynthetic pathway of the isolated alkaloids from *P. littorale* are described next. Of the 15 compounds, three new congeners as well as 12 already known alkaloids were isolated. The known alkaloids were identified by comparison with published spectroscopic and physical data as (**2**) 8-*O*-demethyl-homolycorine[203], (**3**) pseudo-lycorine[204], (**5**) 8-demethyoxy-10-*O*-methyl-hostasine[205], (**6**) carinatine[206], (**7**) lycorine[206], (**8**) 10-*O*-methyl-hostasine[205], (**10**) narcissidine[207], (**11**) 1-*O*-acetyl-pseudolycorine[204], (**12**) 8-*O*-demethyl-6-*O*-methyl-lycorenine[205], (**13**) 3-*O*-acetyl-narcissidine[208], (**14**) 10-deoxy-6(α)-hydroxy-hippeastidine[209], and (**15**) 6-hydroxy-hippeastidine[209].

Compound **9** (K6, 0.50 mg) was isolated as an amorphous, yellow solid with a pseudomolecular ion at 306.1706 $[M+H]^+$ on HRESIMS consistent with the molecular formula of $C_{17}H_{23}NO_4$ (calculated for $C_{17}H_{24}NO_4^+$: 306.1700) and a positive optical rotation ($[\alpha]_D$ +25.7, *c* 0.05, $CHCl_3$). Preliminary data showed that compound **9** was related to 10-deoxy-6(α)-hydroxy-hippeastidine (compound **14**) with one major difference, the demethylation of the methoxy at position 3 resulting in a hydroxyl function. The ^{1}H-NMR spectrum exhibited two aromatic singlets at δ6.73 and δ6.68 assigned to protons H-7 and H-10. Two singlet proton signals at δ3.70 and δ3.73 indicating two methoxy groups were assigned to positions 13 and 14 by HMBC correlations with C-8 and C-9 and NOESY with H-7 and H-10, respectively (Fig. 3.13). The methoxy groups were assigned by HMBC correlations to the quaternary carbons C-8 and C-9 and also NOE correlations between H-13 to H-7, and H-14 to H-10. The quinoline nucleus was established as follows: an oxygenated proton singlet at δ4.82, with the respective carbon signal at δ88.3 was assigned to position 6, through its HMBC correlation to the aromatic ring (HMBC with C-10a) and NOESY with H-7 and to a protonated carbon (C-4a). It was noted that H-6 had correlations with (α)- and (β)-orientations, thus suggesting a mixture of diastereomers. The remaining signals to complete the structure were two pairs of methylene groups, H-11 (δ1.39, δ2.07) and

H-12 (δ2.59, δ3.14), that connected the nitrogen and the bridgehead quaternary carbon C-10a. An aliphatic proton signal at δ3.06 was assigned to H-4a. The latter proton (H-4a) was part of an 8 proton spin system (H-1–H-4a) consisting of 3 diastereotopic methylene groups H-1 (δ1.58, δ2.39), H-2 (δ1.44, δ1.83), H-4 (δ1.14, δ1.67), and an oxygenated methyne resonating at δ3.40 and located at position 3 by COSY. The relative configuration of the molecule was assigned as follows: the *J* couplings of H-3 δ3.40 dddd (11.2, 9.5, 4.0, 3.6) and H-4a δ3.06 dd (12.0, 5.1) and their NOESY correlations indicated their 1,3 diaxial relationship and cofacial orientation. The main differences of the ^{1}H NMR spectrum of **9** compared to hydroxy-hippeastidine (**15**) were the presence of the aliphatic proton signal at δ3.40 (H-3) suggesting the presence of a hydroxy group instead of a methoxy as in the case of hydroxy-hippeastidine; and the deoxygenation of the hydroxyl at H-10 resulting in an aromatic singlet signal instead of no proton signal; and the additional hydroxy at position H-6 with a singlet signal. The NOE correlation between H-4a and H-3 suggests the β-orientation for the hydroxy group at C-3 (since both protons are in the α-position). On the other hand, H-6 showed NOESY contacts with H-12 but no dipolar coupling to H-4a, thus suggesting the relative configuration of compound **9** as depicted in Fig. 3.13. Significant NMR correlations as well as ^{1}H and ^{13}C spectroscopic data for compound **9** are shown in Fig. 3.13, and Table 3.1, respectively.

Two singlet sp^{3} hybridized carbons at chemical shifts δ55.1 and δ55.3 indicating two methoxy groups at positions C-13 and C-14. HMBC correlations to the quaternary carbons C-8 and C-9 at δ147.6 and δ148.9 were assigned. Additional three quaternary carbons were assigned at positions C-6a, C-10a and C-10b with δ127.8, δ141.3 and δ41.3 chemical shifts, respectively. The carbons directly attached to the tertiary nitrogen C-4a, C-6 and C-12 experience a slight downfield shift compared to their aliphatic counterparts however not more deshielded than their oxygenated version. The pairs of alkaloids with a hydroxy substituent at C-6 appear as a mixture of diastereoisomers and are not separable by HPLC[210]. Closer inspection of the NMR spectra showed that the molecule was not pure. In particular, an oxygenated proton signal at δ5.45 with the corresponding carbon at δ86.0 indicated the presence of approx. 24% of the epimer at C-6 bearing the hydroxy function in beta configuration. The chemical instability of the emiaminal proton C-6, that is in equilibrium with the corresponding open form, can explain the coexistance of the two epimers. A similar case has been observed by Shitara *et al.* (2014) for 10-deoxy-6α-hydroxyhippeastidine[209].

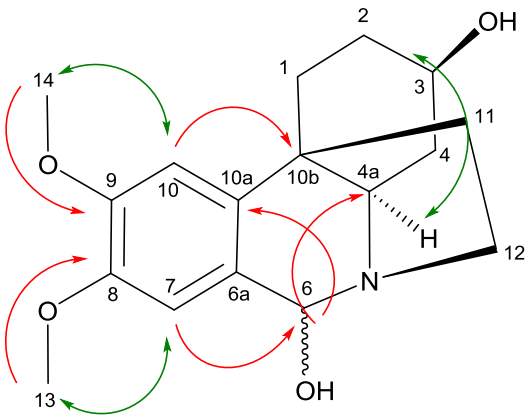

Figure 3.13: Significant NMR correlations and atom numbers of compound **9**. HMBC correlations are shown in red and NOE correlations are shown in green.

Table 3.1: ^{1}H and ^{13}C spectroscopic data for 3-*O*-demethyl-10-deoxy-6-hydroxy-hippeastidine (compound **9**) from *Pancratium littorale*, (DMSO-*d6*; 500 MHz for ^{1}H and ^{13}C extracted from ^{1}H-^{13}C 2D inverse detected experiments; δ in ppm)

	Compound 9 (K6)	
Position	**δ_H mult (*J* in Hz)**	**δ_C, type (from HSQC, HMBC)**
1	1.58 ddd (13.6, 12.5, 4.2) 2.39 ddd (13.6, 3.0, 3.3)	25.6, CH_2
2	1.44 m 1.83 m	30.5, CH_2
3	3.40 dddd (11.2, 9.5, 4.0, 3.6)	67.0, CH
4	1.14 ddd (12, 12, 12) 1.67 ddd (12, 5.1, 4.01)	35.9, CH_2
4a	3.06 dd (12.2, 5.1)	58.9, CH
6	4.82 s	88.3, CH
6a	-	127.8, qC
7	6.73 s	112.1, CH
8	-	147.6, qC
9	-	148.9, qC
10	6.68 s	105.5, CH
10a	-	141.3, qC
10b	-	41.3, qC
11	1.39 m 2.07 m	33.7, CH_2
12	2.59 ddd (13.3, 9.0, 6.0) 3.14 dddd (13.3, 10.0, 6.0, 3.7)	46.1, CH_2
8-MeO (13)	3.70 s	55.1, O-CH_3
9-MeO (14)	3.73 s	55.3, O-CH_3

For ^{13}C shifts, data was extrapolated by HSQC and HMBC contours.

Compound **4** (K4, 1.15 mg) was isolated as an amorphous, yellow solid with a positive optical rotation ($[\alpha]_D$ +82.4, *c* 0.11, $CHCl_3$). Compound **4** had a molecular formula of $C_{17}H_{21}NO_4$, based on HRESIMS (*m/z* 304.1547 $[M+H]^+$; calculated for $C_{17}H_{22}NO_4^+$: 304.1543). By comparing the ^1H NMR spectrum to that of known lycorenine type alkaloids, compound **4** was assigned to this scaffold. Key characteristics of the ^1H NMR spectrum are the two singlets for the *para*-oriented aromatic protons at δ6.71 and δ6.72 (H-7 and H-10). A singlet resonating at δ5.70 with the corresponding carbon at δ89.9 characteristic for a hemiacetal proton was attributed to H-6 by HMBC correlation H6/H10 and H7/H6. Two singlets integrating for 3 protons each suggested the presence of two methyl groups, one more deshielded at δ3.74 and the other at δ1.97. The CH_3 signal at δ3.74 is a methoxy and attached to C-9, according to lycorenine type HMBC correlations to the quaternary C-9 and NOE correlation between H-10 and H-14. The other singlet is an N-CH_3 and is part of the D-ring, according to HMBC correlations to C-4a and C-12 and NOE correlations to H-4a. Due to the absence of an additional methoxy singlet at C-8 a hydroxy substituent was assigned. Hemiacetal alkaloids always show the substituent at C-6 in α-disposition[210] therefore H-6β appears as a singlet at δ5.70. The majority of compounds belong to a single enantiomeric series containing a *cis* B/C ring junction[210], which is corroborated by the small coupling constant $J_{1\text{-}10b}$ (approx. 1.2-1.5). Ring C contains a vinylic proton H-3 at δ5.37 and diastereotopic protons (δ2.12, δ2.56) attached to a CH_2 at position C-2. The two protons attached to C-2 exhibit NOE correlations with H-1. Quaternary carbons were assigned to positions C-4, C-6a, C-8, C-9 and C-10a based on HMBC correlations. This compound was named 8-*O*-demethyl-lycorenine. NMR correlations as well as ^1H and ^{13}C spectroscopic data for compound **4** are shown in Fig. 3.14, and Table 3.2, respectively. Using the NOE correlations, relative configuration was established for the hydroxy position at C-6 in α-disposition (a strong correlation was seen between H-6 and H-4a).

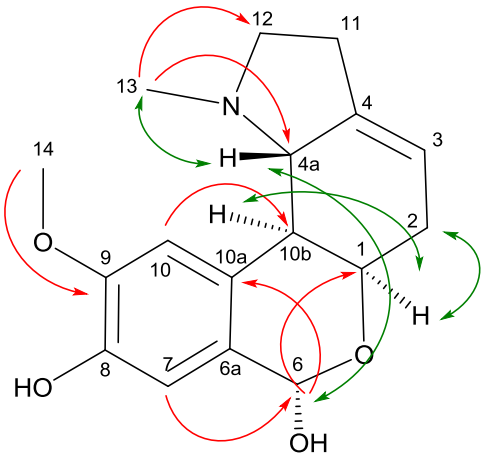

Figure 3.14: Significant NMR correlations and atom numbers of compound **4**. HMBC correlations are shown in red and NOE correlations are shown in green.

Table 3.2: ^{1}H and ^{13}C spectroscopic data for 8-*O*-demethyl-lycorenine (compound **4**) from *Pancratium littorale*, (DMSO-*d6*; 500 MHz for ^{1}H and ^{13}C extracted from ^{1}H-^{13}C 2D inverse detected experiments; δ in ppm)

	Compound 4 (K4)	
Position	**δ_H mult (*J* in Hz)**	**δ_C, type (from HSQC)**
1	4.21 dd (6.0, 1.5)	64.9, CH
2	2.12 ov	30.8, CH_2
	2.56 ov	
3	5.37 br m	114.4, CH
4	-	140.0, qC
4a	2.55 ov	66.4, CH
6	5.70 s	89.9, CH
6a	-	113.4, qC
7	6.71 s	113.7, CH
8	-	144.7, qC
9	-	145.8, qC
10	6.72 s	112.8, CH
10a	-	127.7, qC
10b	2.23 dd (9.5, 1.2)	43.2, CH
11	2.31 m	27.4, CH_2
	2.38 m	
12	2.13 ov	55.7, CH_2
	3.00 ov	
13	1.97 s	43.4, N-CH_3
9-MeO (14)	3.74 s	55.4, O-CH_3

For ^{13}C shifts, data was extrapolated by HSQC and HMBC contours.

Compound **1** (G2, 0.69 mg) was isolated as an amorphous, yellow solid with a positive optical rotation ($[\alpha]_D$ +47.0, *c* 0.06, CH_3OH) and a molecular formula of $C_{16}H_{17}NO_4$, based on HRESIMS (*m/z* 288.1237 $[M+H]^+$; calculated for $C_{16}H_{18}NO_4^+$: 288.1230). Compound **1** showed similar

signals as compound **4** on H-11, -12, -4, -3, -2, and -1. The lack of the singlet signal at H-6 and the replacement with a quaternary carbon at C-6 corroborated with HMBC correlations of H-7 to C-6, suggested the oxidation of the hemiacetal to a lactone ring. Additionally compound **1** lost the methyl substituent attached to the nitrogen in ring D, thus resulting in the presence of a secondary amine. Compound **1** is similar to the homolycorine core structure and thus was named 8-*O*-demethyl-lycoranine F. Noteworthy NMR correlations as well as ^{1}H and ^{13}C spectroscopic data for compound **1** are shown in Fig. 3.15, and Table 3.3, respectively.

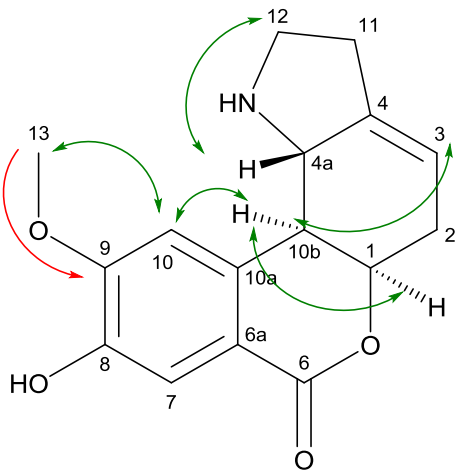

Figure 3.15: Significant NMR correlations and atom numbers of compound **1**. HMBC correlations are shown in red and NOE correlations are shown in green.

Table 3.3: ^{1}H and ^{13}C spectroscopic data for 8-*O*-demethyl-lycoranine F (compound **1**) from *Pancratium littorale*, (DMSO-*d6*; 500 MHz for ^{1}H and ^{13}C extracted from ^{1}H-^{13}C 2D inverse detected experiments; δ in ppm)

	Compound 1 (G2)	
Position	**δ_H mult (*J* in Hz)**	**δ_C, type (from HSQC)**
1	4.84 dd (4.8, 2.0)	75.1, CH
2	2.38 m	30.6, CH_2
	2.63 m	
3	5.50 br m	114.1, CH
4	-	140.0, qC
4a	3.13 br d (10.0)	58.5, CH
6	-	164.6, qC
6a	-	115.2, qC
7	7.33 s	115.2, CH
8	-	146.2, qC
9	-	152.2, qC
10	7.00 s	110.5, qC
10a	-	135.9, qC
10b	2.67 dd (10.0, 2.0)	40.8, CH

11	2.38-2.48 m	29.3, CH
12	2.79 ddd (10.2, 8.5, 8.3) 3.02 m	43.2, CH_2
13-MeO	3.86 s	55.5, O-CH_3

For ^{13}C shifts, data was extrapolated by HSQC and HMBC contours.

Utilising the NOE correlations as depicted in Fig. 3.15, relative configuration was established and ECD was measured to determine the absolute configuration. The measured ECD spectrum was compared to calculated spectra of the compound called lycoranine F in Ang *et al.*, (2015)[211] and thus the absolute configuration was confirmed as 1*R*,4a*S*,10b*S* (see Fig. 3.16).

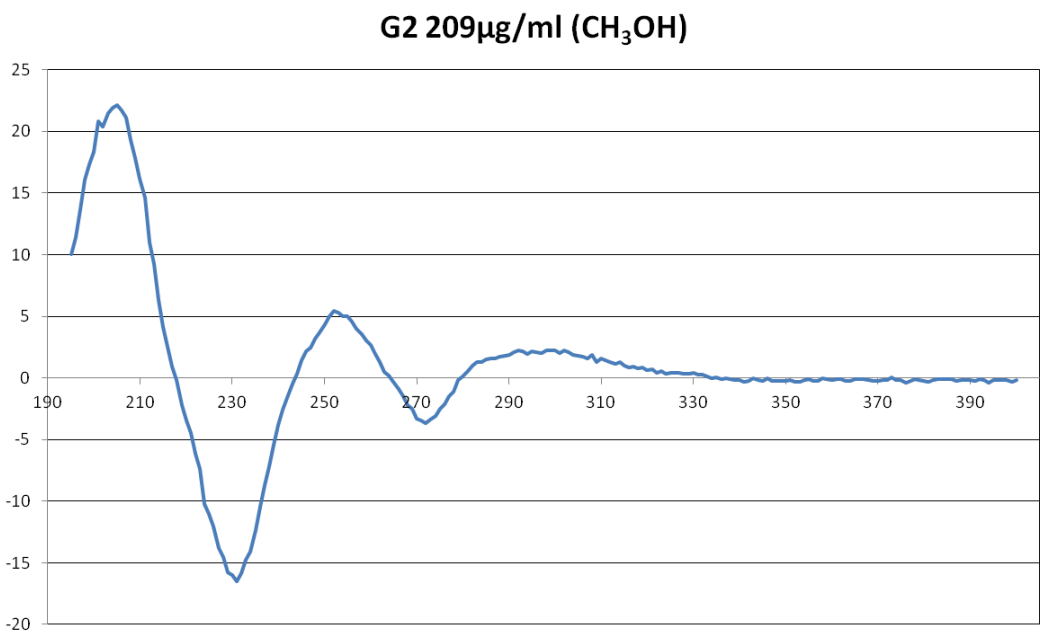

Figure 3.16: Measured ECD spectrum (experimental) from 190 to 400 nm showing positive and negative cotton effects.

Biosynthesis of Amaryllidaceae alkaloids is the result of several intramolecular oxidative couplings of precursors related to norbelladine. Norbelladine is formed through combination of 3,4-dihydroxy-benzaldehyde with tyramine. Methylation of norbelladine results in 4'-*O*-methylnorbelladine – which undergoes three types of oxidative couplings: *ortho-para'*, *para-para'*, and *para-ortho'*[202] (see Fig. 3.17).

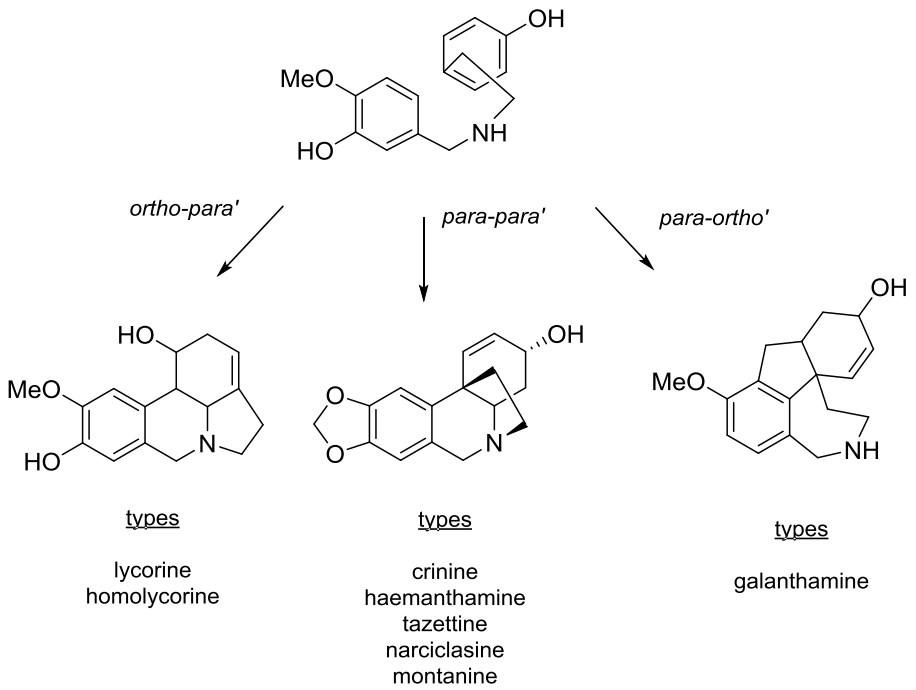

Figure 3.17: 4-*O*-methylnorbelladine and the three oxidative coupling reactions namely *ortho-para'*, *para-para'*, *and para-ortho'*, adapted from[202,212].

The formation of compounds **1** and **4** result from lycorenine scaffold (also known as homolycorine scaffold when a lactone ring is present instead of a hemiacetal), with demethylation in position C-8 (for both compounds **1** and **4**) resulting in a hydroxy group. Compound **1** arises due to oxidation of the hydroxyl group at C-6 resulting in a lactone ring, and demethylation of the N-CH_3 resulting in a secondary nitrogen (NH). The formation of lycorenine scaffold results from norpluviine – a precursor of lycorine. Norpluviine is oxidised at the benzylic position to yield a cyclic hemi-aminal group. The rotation of C-10a–C-10b bond of the amino aldehyde intermediate, followed by hemiacetal formation and methylation[202,213](see Fig. 3.18). Compound **9** is classified as a crinine skeleton, which is formed through a *para-para'* coupling of 4'-*O*-methylnorbelladine. Compound **9** differs from crinine at positions C-8 and C-9 with the opening of the methylenedioxy ring and oxidation at position C-6 resulting in a hydroxy substituent[202,212] (see Fig. 3.19). Haemanthamine is the enantiomeric skeleton of crinine. Haemanthamine is the precursor for tazettine, montanine and narciclasine skeletons.

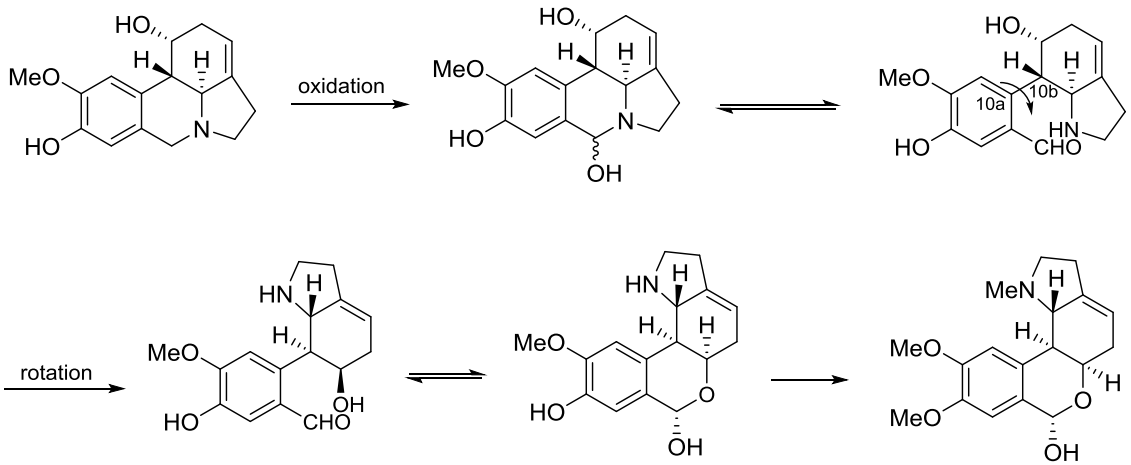

Figure 3.18: Biosynthetic pathway from norpluviine to lycorenine scaffold for compounds **1** and **4**[202].

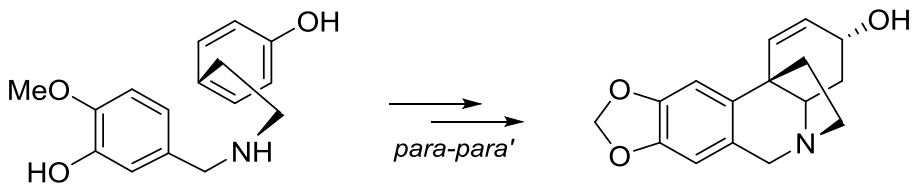

Figure 3.19: Biosynthetic pathway from norpluviine to crinine scaffold for compound **9**[202].

All the above mentioned isolated compounds (**1** – **15**), along with galanthine, tazettine and haemanthamine (from the in-house compound library) were tested at 5 and 10 µg/mL for 48 and 72 hours in the promoter-based assay (GFP/RFP). The GFP and RFP readout for each compound after 72 hours at 5 µg/mL are shown in Fig. 3.20.

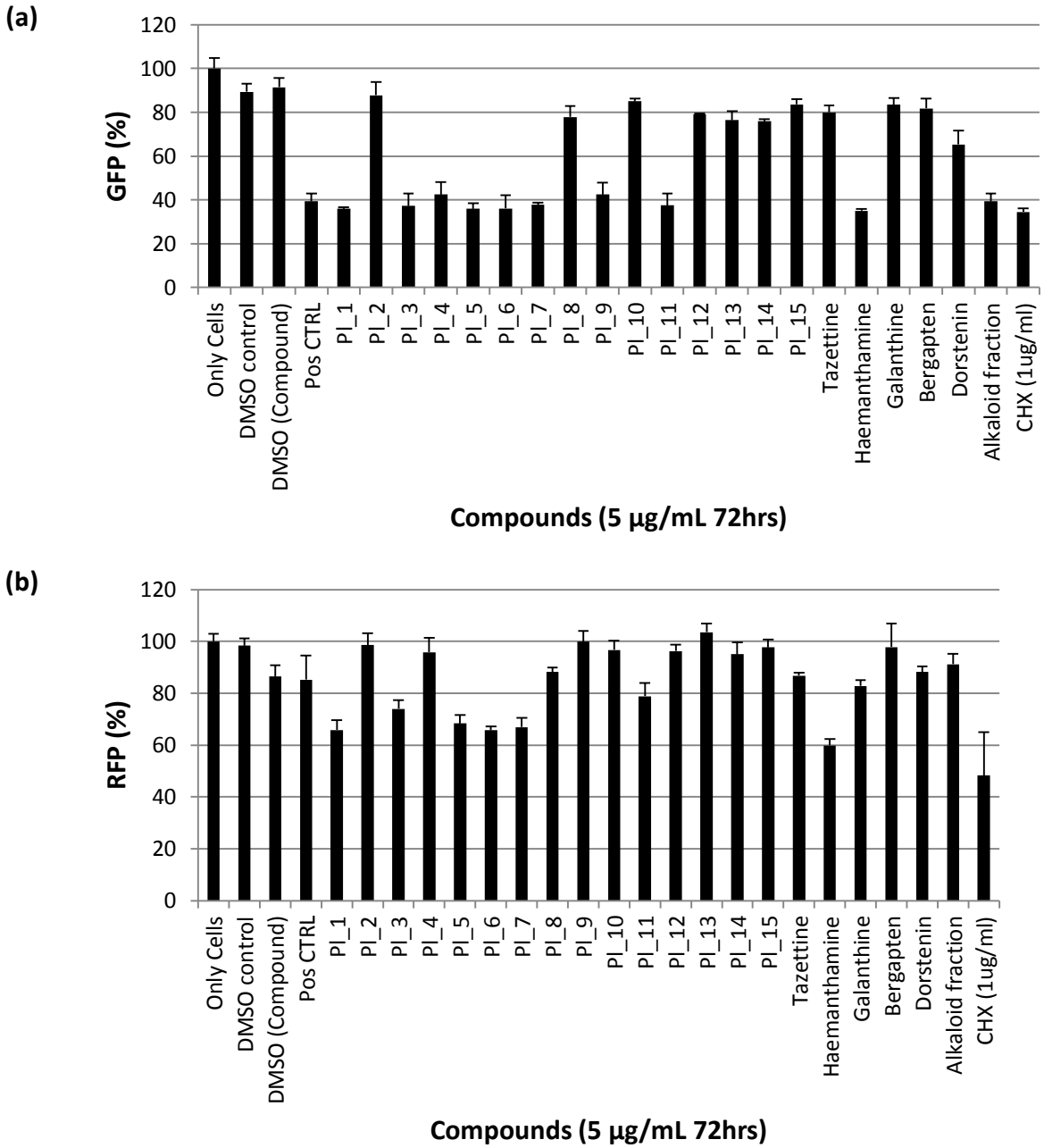

Figure 3.20: (**a**) GFP and (**b**) RFP results for *P. littorale* compounds, along with galanthine, tazettine and haemanthamine at 5 µg/mL for 72 hours.

In Fig. 3.21, the three most active and the four most toxic compounds with their structures are shown. The compounds in the graph display a significant decrease of GFP. Here the distinguishing factor is by how much RFP is decreased causing toxicity or activity. Compounds H18 (**11**), K4 (**4**) and K6 (**9**) after 72 hours show only a slight RFP reduction (approximately 0 to 20%), while G2 (**1**), I10 (**6**), I14 (**7**) and haemanthamine all showed increased RFP reduction (between 30 to 40%).

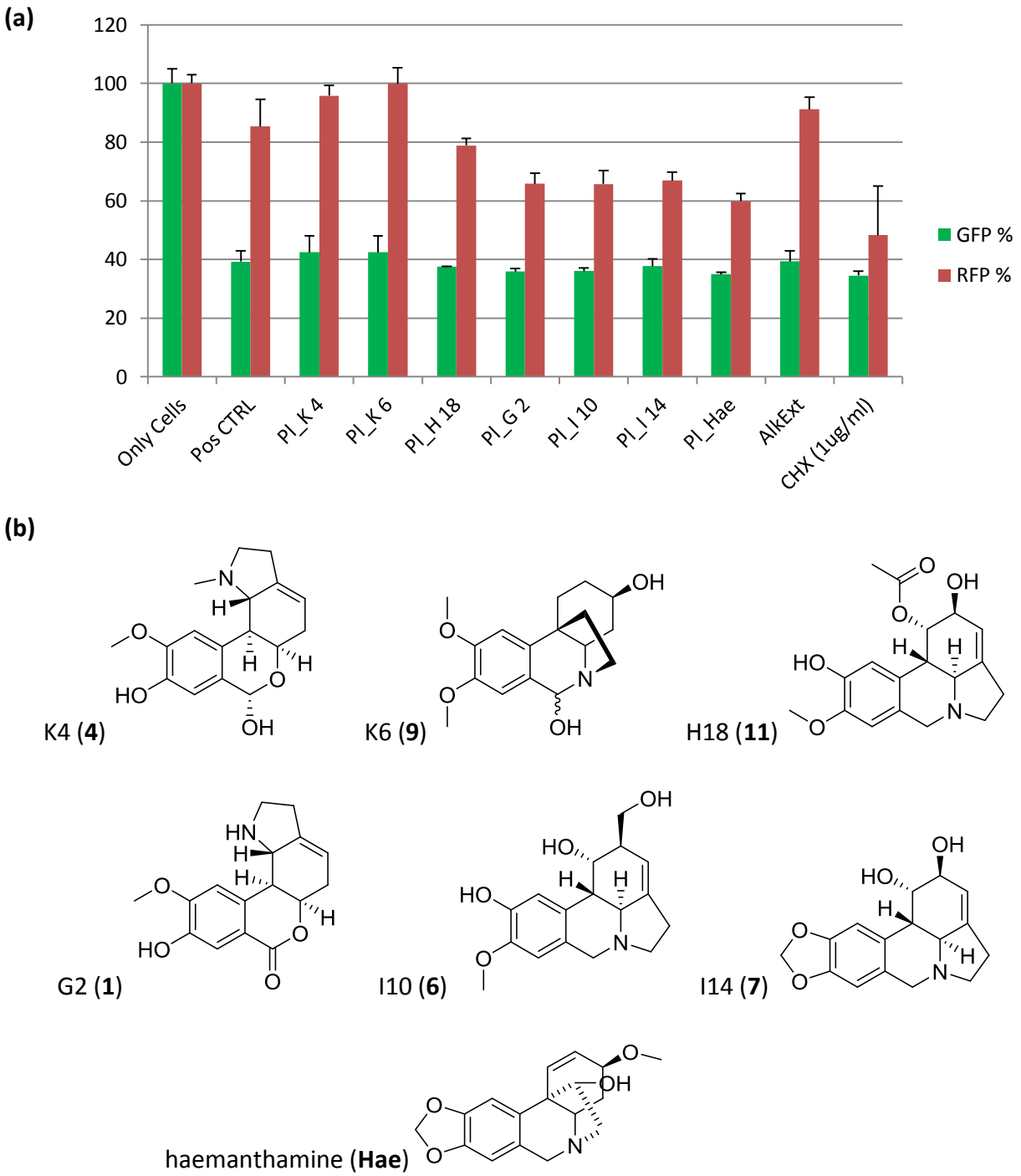

Figure 3.21: (**a**) GFP and RFP results for most active (**4**, **9**, **11**) and most toxic (**1**, **6**, **7**, **Hae**) compounds at 5 µg/mL for 72 hours. Cycloheximide (CHX) was used as a negative control and a lead compound for the positive control. (**b**) Structures of the compounds with their codes and peak numbers.

Based on the GFP/RFP results, preliminary structure-activity estimations can be established from the observations of key structural features between the different scaffolds. In Fig. 3.22 to

Fig. 3.26, the compounds are classified based on their scaffolds and structural features are presented.

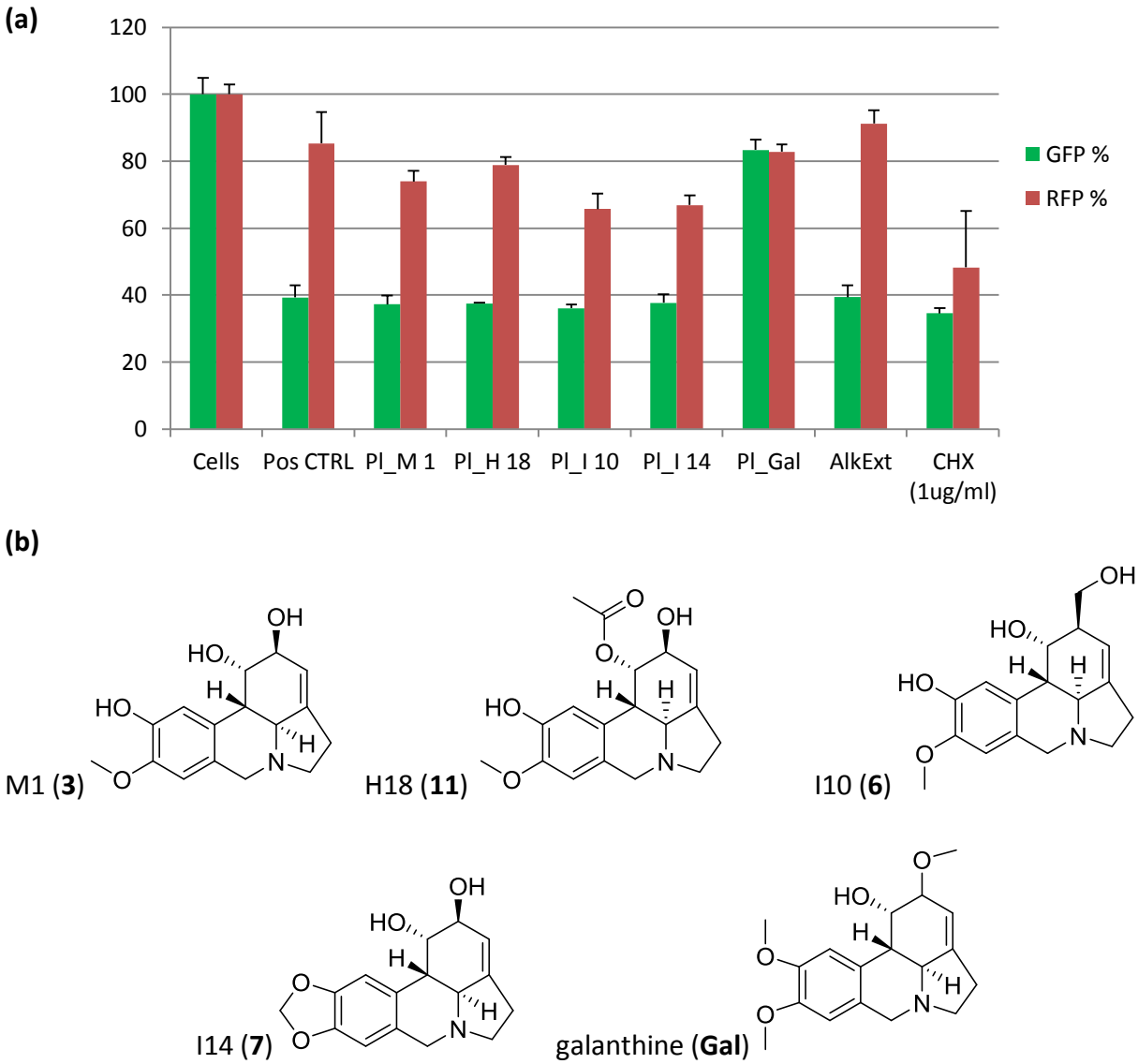

Figure 3.22: (**a**) GFP and RFP results of compounds with lycorine skeleton, compounds **3**, **6**, **7**, **11** and galanthine at 5 µg/mL for 72 hours. (**b**) Structures of the compounds with their codes and peak numbers.

In Fig. 3.22, GFP and RFP results of compounds with the lycorine skeleton, namely **3**, **6**, **7**, **11**, and galanthine (**Gal**) with their corresponding structures are shown. The methylenedioxy group at C-8 and C-9 on lycorine (**7**) and the presence of the hydroxy group on position 1 on ring C contribute to toxicity (in compounds **3**, **6**, and **7**); while acetylation of the hydroxyl group on C-1 resulted in a slight reduction of toxicity (**11**). Furthermore, the opening of the methylenedioxy

ring, resulting in two methoxy groups at C-8 and C-9 lead to a generally inactive compound (e.g. **Gal**) with a very minor decrease in GFP and RFP.

GFP and RFP results of compounds with the narcissidine skeleton, namely **10**, and **13** with their corresponding structures are shown in Fig. 3.23. These compounds possess a low activity (minor GFP reduction around 25%) which may be due to the opening of the methylenedioxy ring. Acetylation of the hydroxyl function at position C-3 in compound **13** displayed a slight increase of activity (approximately 25% GFP reduction) compared to compound **10** (with only 20% GFP reduction).

(a)

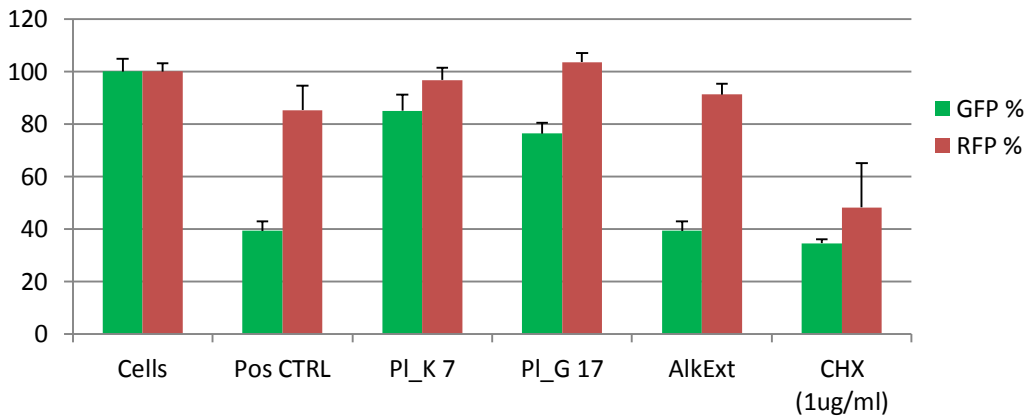

(b)

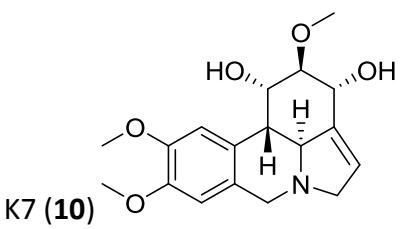

K7 (**10**)

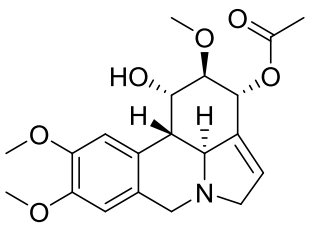

G17 (**13**)

Figure 3.23: (**a**) GFP and RFP results of compounds with narcissidine skeleton, compounds **10** and **13** at 5 µg/mL for 72 hours. (**b**) Structures of the compounds with their codes and peak numbers.

In Fig. 3.24, GFP and RFP results of compounds with lycorenine skeleton, namely **1**, **2**, **4**, and **12** with their corresponding structures are illustrated. In the lycorenine skeleton, the presence of a secondary nitrogen (compound **1**) showed increased toxicity. Reduction of the lactone ring (compound **2**) to a hemiacetal predominantly increased activity (compound **4**) and methylation of the hydroxy substituent of the hemiacetal group resulted in a decrease of activity (compound **12**).

(a)

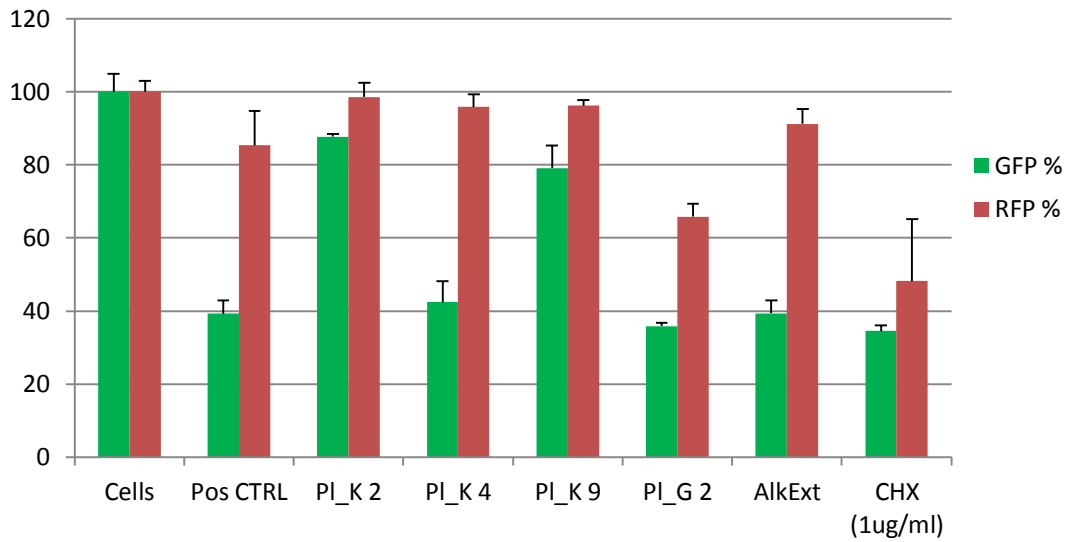

(b)

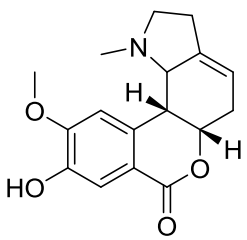

K2 (**2**)

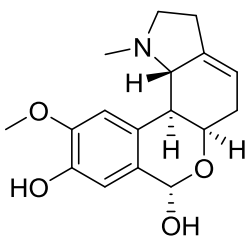

K4 (**4**)

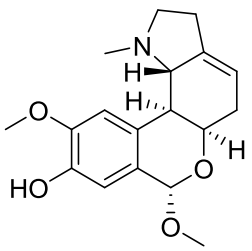

K9 (**12**)

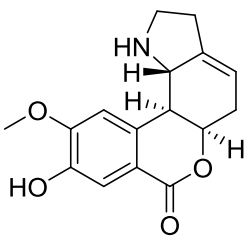

G2 (**1**)

Figure 3.24: (**a**) GFP and RFP results of compounds with lycorenine skeleton, compounds **1**, **2**, **4** and **12** at 5 µg/mL for 72 hours. (**b**) Structures of the compounds with their codes and peak numbers.

GFP and RFP results of compounds with crinine skeleton, namely **9**, **14**, **15**, and haemanthamine (**Hae**) with their corresponding structures are shown in Fig. 3.25. In crinine skeleton, the presence of the hydroxy function at C-3 improved activity significantly (compound **9**), while the presence of the methylenedioxy ring showed increased toxicity (**Hae**).

(a)

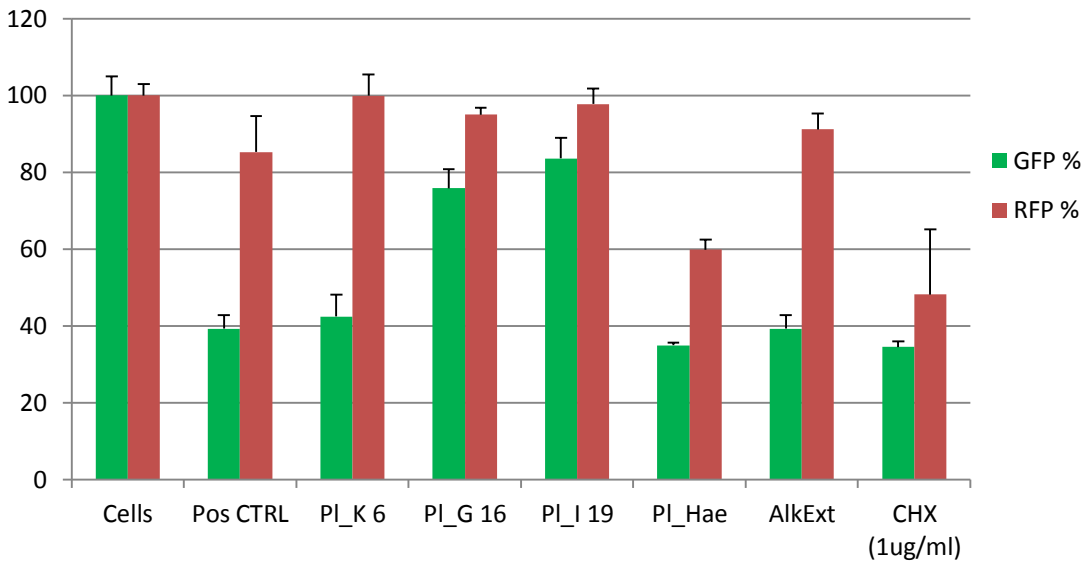

(b)

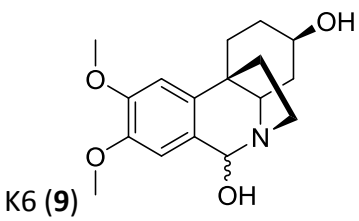

K6 (**9**)

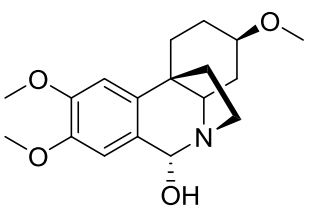

G16 (**14**)

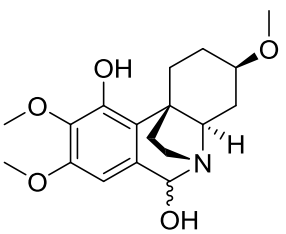

I19 (**15**)

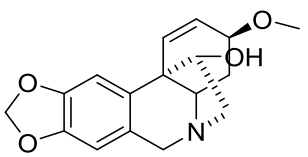

haemanthamine (**Hae**)

Figure 3.25: (**a**) GFP and RFP results of compounds with crinine skeleton, compounds **9**, **14**, **15** and **Hae** at 5 µg/mL for 72 hours. (**b**) Structures of the compounds with their codes and peak numbers.

The last skeleton of the isolated compounds is hostasine (compounds **5** and **8**). GFP and RFP results of these compounds with their corresponding structures are shown in Fig. 3.26. The removal of the methoxy group at C-7 on compound **5** lead to increased toxicity (RFP reduction was 15% more than compound **8**).

(a)

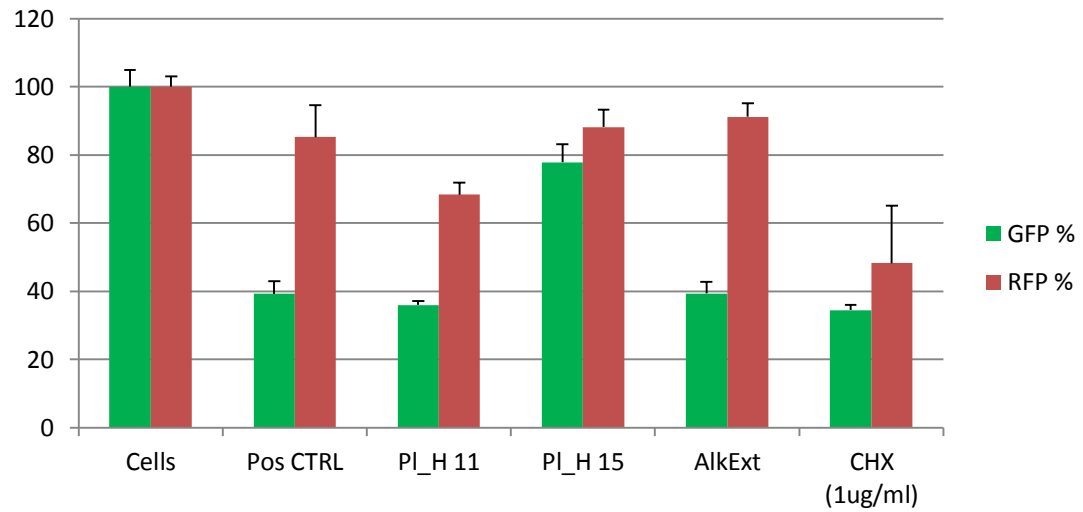

(b)

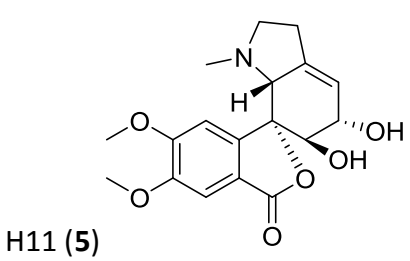

H11 (**5**)

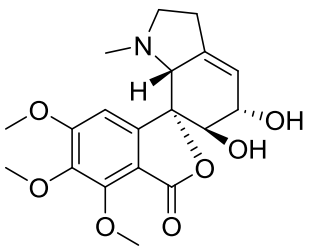

H15 (**8**)

Figure 3.26: (**a**) GFP and RFP results of compounds with hostasine skeleton, compounds **5** and **8** at 5 µg/mL for 72 hours. (**b**) Structures of the compounds with their codes and peak numbers.

The next step is to confirm the activity seen in the GFP/RFP assay with western blotting, which quantifies the amount of coronin-1 protein present, when treated with the compounds. This allows us to see by how much the compounds are down-regulating coronin-1 on the protein level. The three most active compounds (**4**, **9**, and **11**), some of the toxic compounds (**5**, **6** and **7**), and the enriched alkaloid fraction were all examined in the western blot (see Fig. 3.27). These preliminary results revealed that the three most active compounds (**4**, **9**, and **11**) and toxic/alkaloid fraction were found to not interact with the down-regulation of coronin-1 on the protein level but rather by unexplained mechanisms might be directly interacting with GFP as quenching agents. The compounds seem to interfere directly with GFP fluorescence and thus mislead the results as coronin-1 inhibitors. Moreover, on an assay with western blotting, compound **4** no longer displayed its initial activity seen in the first round of 72 hour testing.

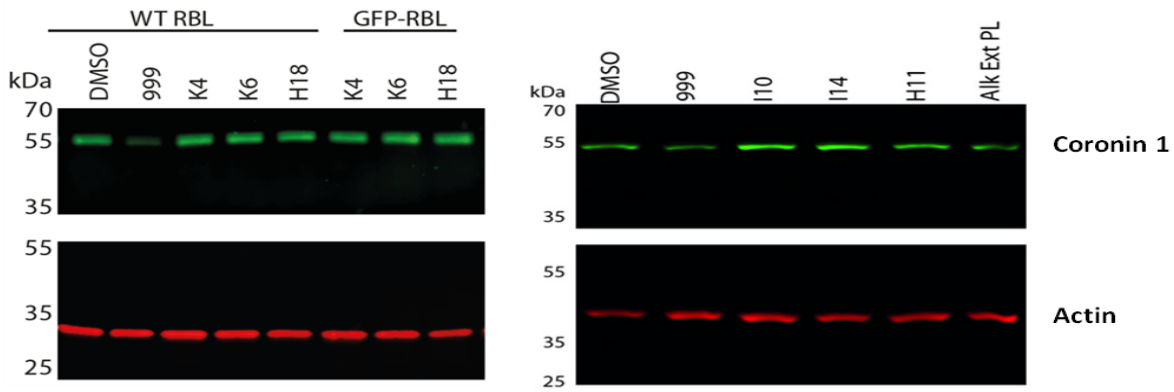

Figure 3.27: Western blot for coronin 1 (green) and actin (red) controls from the total lysate of GFP-RBL cells incubated with various compounds mentioned (K4/**4**, K6/**9**, H18/**11**, H11/**5**, I10/**6** and I14/**7**) as well as the alkaloid fraction (Alk Ext) in comparison with positive control 999. Actin serves as the loading control. Licor imaging system was used to develop the results and coronin1/actin ratio analysed using Image Studio Lite Software.

The samples tested were also viewed by electron microscopy to visualise the state of the cells after incubation with test samples and GFP/RFP readout. As seen in Fig. 3.28, the cells seem to decrease in number and some are apoptotic. Therefore, the compounds might be cytostatic at the concentrations tested and cause cell proliferation to decrease.

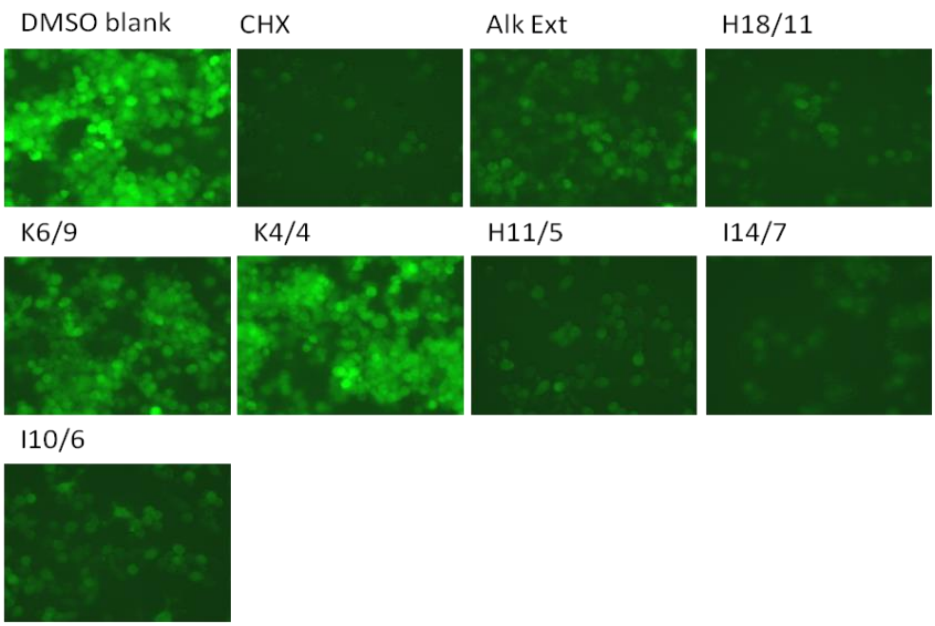

Figure 3.28: Cells viewed with electron microscope after addition of compounds mentioned (K4/**4**, K6/**9**, H18/**11**, H11/**5**, I10/**6** and I14/**7**) and the alkaloid fraction (Alk Ext) in comparison with cycloheximide (CHX: toxic) and DMSO blank.

3.4 Discussion and conclusions

Tuberculosis is a widespread infectious disease caused by MTB transmitted through droplets of air. Globally, in 2015, about 1.4 million people died from the disease[115]. Combating the pathogen is problematic since multidrug resistant strains have emerged. A coat protein known as coronin-1 was found to be essential for the survival of MTB within macrophages in the human body[137,138]. In this context, an assay based on coronin-1 downregulation in model cell lines was established and used to screen an in-house library of plant and fungal extracts. Among various extracts, the ethyl acetate extract of *Dorstenia contrajerva* L. (Moraceae) displayed a 40% decrease in GFP and no decrease in RFP at 20 µg/mL, after 72 hours. In addition, a methanol extract from the bulbs of *Pancratium littorale* Jacq., (Amaryllidaceae) significantly decreased GFP after 72 hours (≥ 80% inhibition at 20 µg/mL). Bioactivity tracking by HPLC-based activity profiling, a miniaturised approach which combines bioactivity data with structural information from online HPLC-UV and offline HPLC-MS, microprobe NMR analyses, led to the identification of active constituents: alkaloids from *P. littorale* and furanocoumarins from *D. contrajerva*.

The furanocoumarin dorstenin was only active during the micro-fractionation due to its high amount in the extract, as quantified using UV and ^{1}H-NMR. Thus, the overall activity of *D. contrajerva* extract could possibly come from a synergetic effect of all constituents present. After preparative isolation of *P. littorale*, 15 alkaloids including three new congeners were structurally characterised and tested in the GFP/RFP assay. Three compounds, 8-*O*-demethyl-lycorenine (**4**), 3-*O*-demethyl-10-deoxy-6-hydroxy-hippeastidine (**9**), and 1-*O*-acetyl-pseudolycorine (**11**) showed the most potent activity (decreases higher than 50% in GFP at 5 µg/mL) as compared to the other isolated alkaloids. These activities were comparable with the positive control which exhibited 60.7% decrease in GFP. On the other hand, 9-demethoxy-lycoranine F (**1**), 8-demethoxy-10-*O*-methylhostasine (**5**), carinatine (**6**), lycorine (**7**), pseudolycorine (**3**), and haemanthamine (**hae**) demonstrated toxicity. Based on these results, structure-activity relationship cannot be established; however it is possible to extrapolate some general rules. For example, the presence of a secondary nitrogen and methylenedioxy group consistently displayed increased toxicity, while a hemiacetal ring and acetylation of some hydroxy functions were more active. Besides these, further biochemical investigations showed that the three most active compounds mentioned above (**4**, **9**, and **11**) are not active in

downregulating coronin-1 at the protein level determined by western blotting. This exhibits that these compounds were not active in inhibiting coronin-1 expression. This may open a question through which mechanism they are able to induce GFP reduction, currently this is not fully understood but it might be through direct interaction with GFP via acting as quenching agents. Furthermore, this study examined coronin-1 inhibiting capabilities of some of the compounds which exhibited toxicity (in RFP) as well as the alkaloid fraction via western blot. These test results showed that even the toxic compounds were not active in inhibiting coronin-1 expression.

Compounds examined in this study may provide useful tools for chemical biology aspects as future chemical probes. However, considering the GFP assay and western blotting contradictory results, this study would like to remark the importance of re-evaluating the GFP assay usage for coronin-1 inhibition test. Accordingly, to better understand the interactions of compounds from natural origins with that of GFP, the compounds ability to interfere with GFP fluorescence and other GFP-expressing promoter constructs, more specific tests are ongoing. Besides these, to confirm coronin-1 expression on a genetic level when treated with the compounds, this study recommends the need of RT-PCR tests.

Chapter 4

4. Results and Discussion: Lymphangiogenesis

As highlighted in section 1.5, the Lymphatic project aims to assess the potential of plant secondary metabolites in promoting lymphatic vessel growth. In the following sections, extract library screening and hit prioritisation, prioritised extract (dichloromethane extract of *Daphne giraldii*) test results, projected analysis, and characterisations are presented. Lastly, summarised discussion on Lymphatic project and concluding remarks are given.

4.1 Extract library screening and hit prioritisation

To identify potential inducers of lymphatic vessel growth [i.e., which have the ability to induce sprouting of Lymphatic Endothelial Cells (LECs)], a phenotypic screening for 1952 plant and fungal extracts was carried out, via a 3D sprouting assay. The screening results shows that extracts that are prepared from root bark of *Daphne giraldii* via DCM, EtOAc, and MeOH as well as *Patrinia scabiosifolia* MeOH extract were more active (see Fig. 4.1). However, due to issues of reproducibility, *Patrinia scabiosifolia* extract was dropped from the prioritisation, and the study proceeded with *Daphne giraldii* extracts.

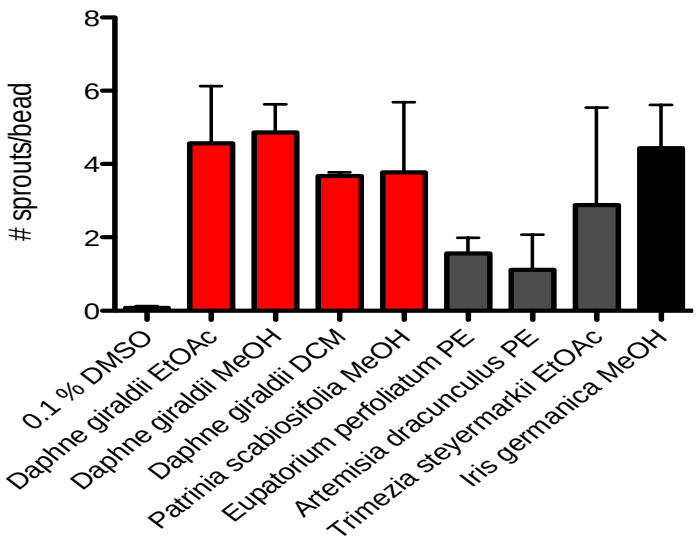

Figure 4.1: Sprouting results (n = 2) of extract library screening showing seven active extracts from five plant species (at 10 µg/mL), with 0.1% DMSO as negative control and *I. germanica* MeOH extract as positive control.

4.2 *Daphne giraldii* (Thymelaeaceae)

Among active extracts shown in Fig. 4.1, *Daphne giraldii* MeOH extract displayed the highest activity; accordingly it was further subjected to HPLC-based activity profiling (see Fig. 4.2). The profiling results exhibit varying degrees of an increase in sprouting on fractions 22 to 29 corresponding to minutes 23.00 – 30.00. Since no compounds possessing UV absorbance were identified in fractions 22 to 29, based on the UV chromatogram, it becomes challenging to assign activity to compounds eluting in this region. The activity of *Daphne giraldii* MeOH extract on lipophilic region of the chromatogram lead to the reasoning that these lipophilic compounds might be present in dichloromethane extract (i.e., DCM extract) in higher quantities. Therefore, further investigations were undertaken on the DCM extract.

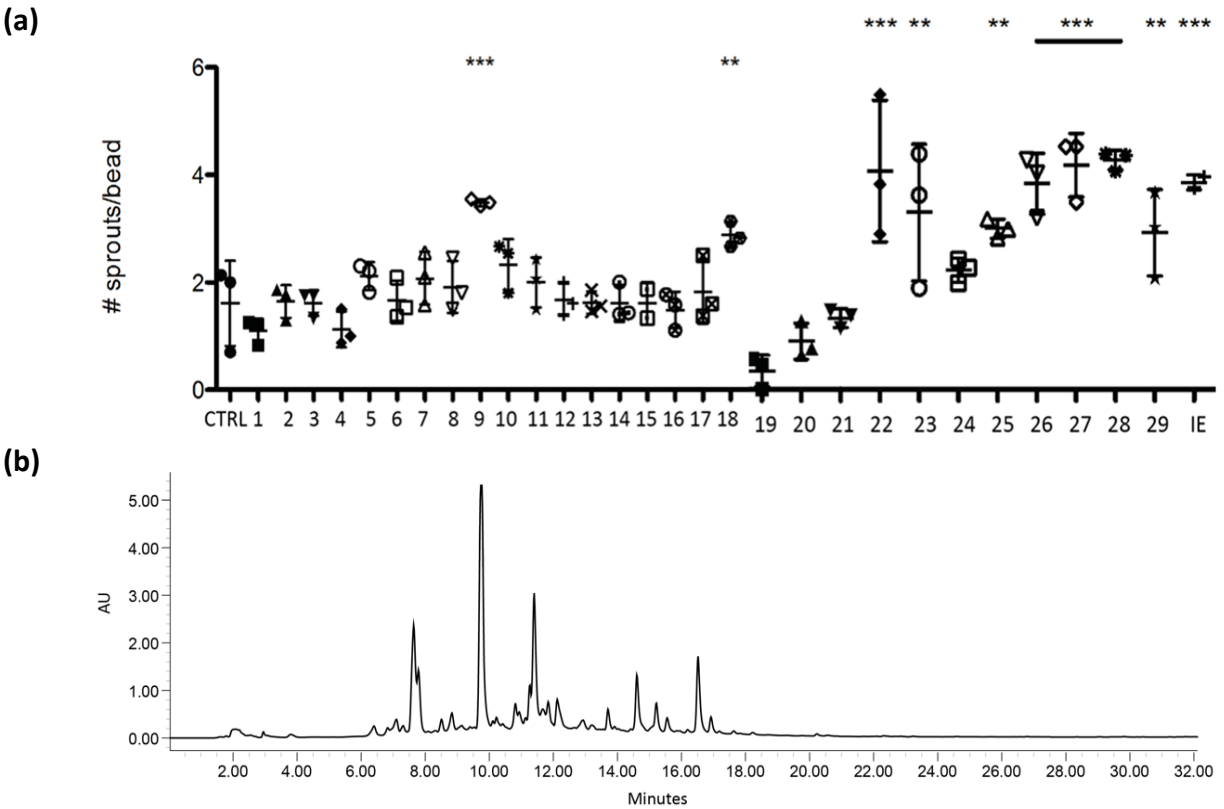

Figure 4.2: (**a**) Number of sprouts per bead of each micro-fraction (n = 3) with a DMSO blank (CTRL) and *I. germanica* extract (IE: positive control, at 10 µg/mL). (**b**) HPLC-UV profile (at 254 nm) for *D. giraldii* MeOH extract. This was performed using a C18 SunFire column (3.0 x 150 mm; 3.5µm; Waters), with a 5 to 100% B gradient in 30 minutes, and 5 minute 100% B isocratic, using a flowrate of 0.4 mL/min. Solvent composition was (A): H_2O + 0.1% formic acid and (B): MeCN + 0.1% formic acid. Collection was 1 minute fractions starting from 1.00 to 30.00 minutes (29 fractions).

Large scale extraction and fractionation of DCM extract was followed up. For dereplication, a macro-fractionation of the DCM extract was done with a combination of time- and peak-based collection, these fractions were tested, and their activity was found distributed throughout the fractions. At this point, identification of the compounds responsible for the activity was not possible. Thus starting with normal phase flash chromatography, a follow up separation scheme was employed. Using the separation scheme (which employed a normal phase silica gel cartridge) 8 fractions (Dgi-A to Dgi-H) were collected and tested in the sprouting assay. The results on Fig. 4.3 show that fractions E to H (Dgi-E, Dgi-F, Dgi-G, Dgi-H) were most active.

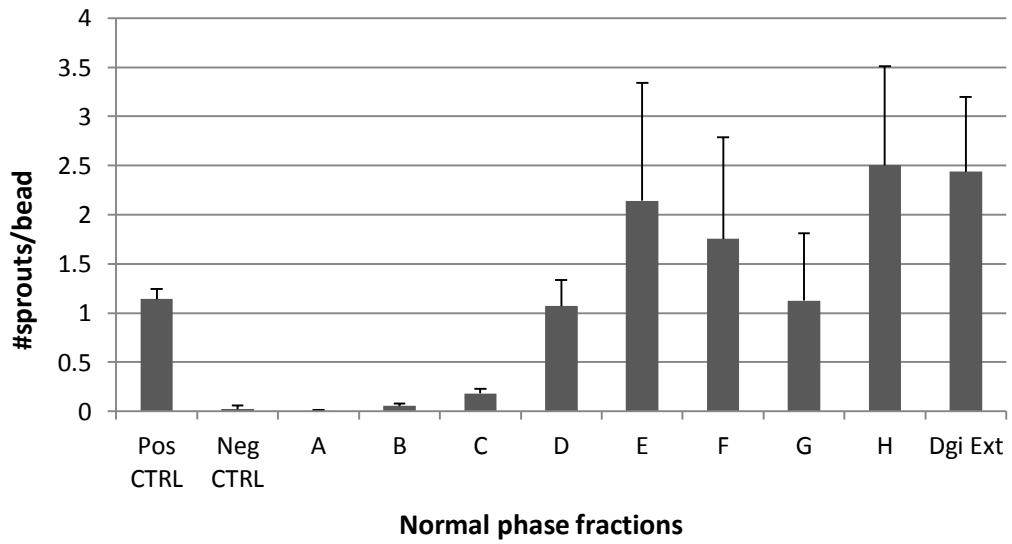

Figure 4.3: Sprouting results (n = 3) of normal phase fractions A to H, and the DCM extract of *D. giraldii* (Dgi Ext), with positive and negative controls.

To trace activity of each fraction and identify the types of compounds present, HPLC-based activity profiling was carried out (see Fig. 4.4 a – h). Also to dilute out the activity and further pinpoint the major active regions, two dilution factors were applied to the micro-fractions (1x and 10x dilutions). The trend observed on activity profiles of fractions E, F, G and H indicates that more major compounds with higher UV absorbance and generally more polar in nature did not show any significant stimulation of LECs. However, the more non-polar region with compounds possessing a weaker chromophore (low UV absorbance) and possibly much lower in quantity were higher inducers of sprouting in LECs. This in overall indicates that activity is generally observed in the region with minor, non-polar compounds.

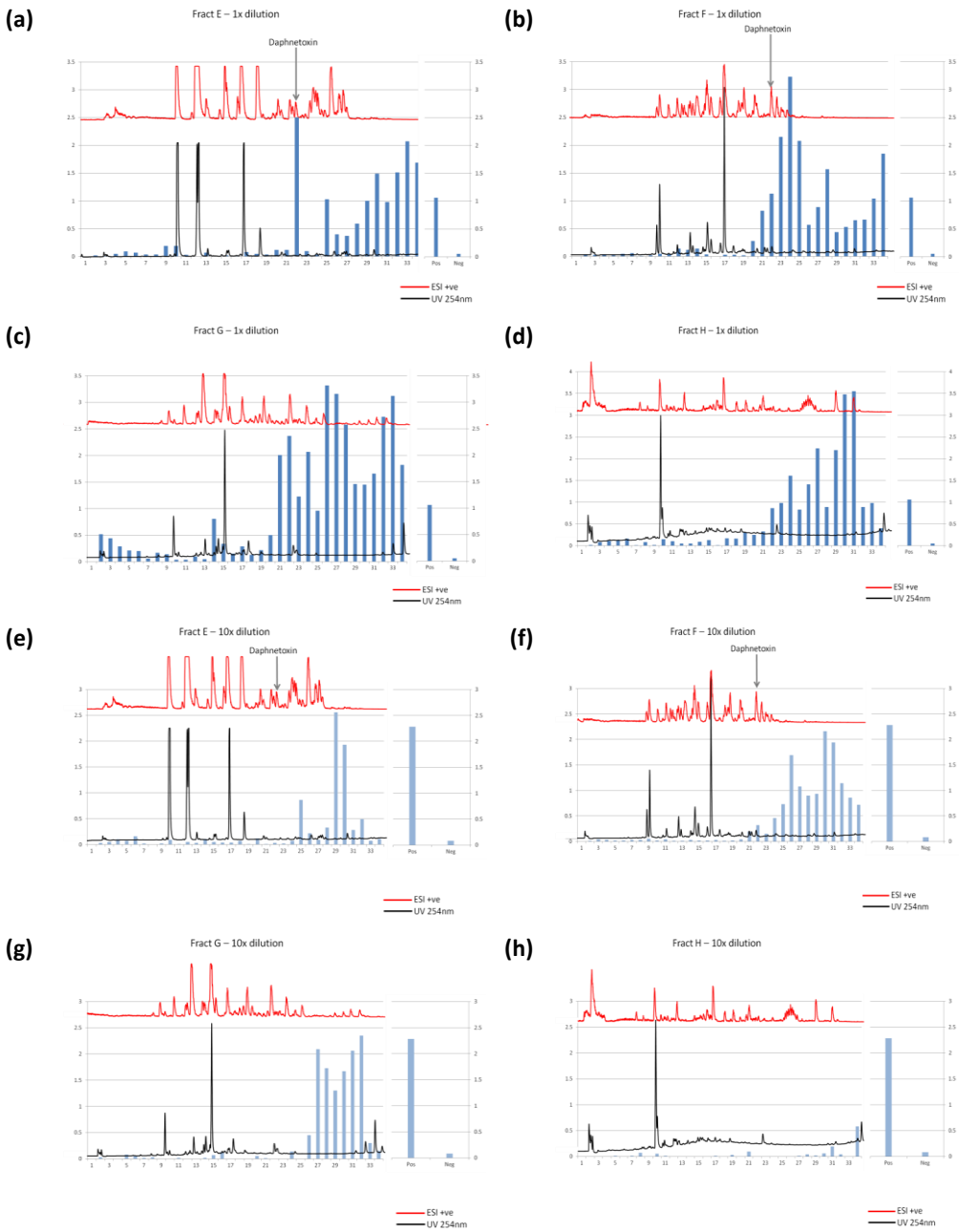

Figure 4.4: HPLC-based activity profiles of normal phase fractions E, F, G, and H, with positive and negative controls. HPLC-UV trace at 254 nm in black and HPLC-ESIMS trace in positive mode shown in red. Dark blue activity bars represent sprouting activity for the 1 time dilution, while light blue activity bars represent sprouting activity for the 10 times dilution factor. (**a**) Fraction E (1x dilution), (**b**) Fraction F (1x dilution), (**c**) Fraction G (1x dilution), (**d**) Fraction H (1x dilution), (**e**) Fraction E (10x dilution), (**f**) Fraction F (10x dilution), (**g**) Fraction G (10x dilution), (**h**) Fraction H (10x dilution).

On the other hand, based on a previously reported study[214] as well as our results shown in Fig. 4.5, a daphnane type orthoester diterpene called daphnetoxin, which was isolated from another *Daphne* species (*D. gnidium*), is active in inducing lymphatic vessel growth. Thus to compare the activity of the fractions (E, F, G, and H) this compound was used as a reference. The retention time of daphnetoxin in the HPLC-MS chromatogram is t_R 22.5 minutes; this corresponds to the activity of micro-fraction 22 in samples E and F, which implies that the activity on micro-fraction 22 (E and F) is due to the presence of daphnetoxin.

(a)

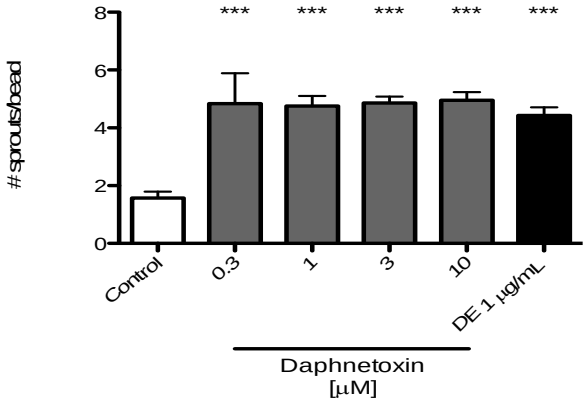

(b)

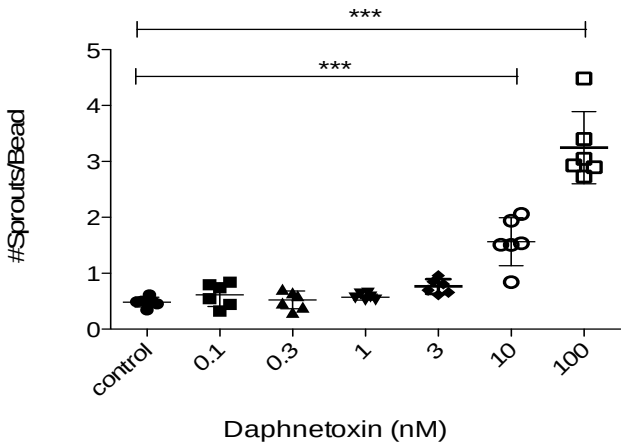

Figure 4.5: Daphnetoxin activity on LEC sprouting in (**a**) µM range from 0.3 to 10, and (**b**) range of 0.1 to 100 nM.

The profiling of DCM extract with their elution time on the HPLC separation as well as peak numbers representing isolated compounds on the HPLC-UV-MS-ELSD chromatograms are shown in Fig. 4.6 (a). Fig. 4.6 (b) exhibits the structures of daphnetoxin and all isolated compounds from the DCM extract.

(a)

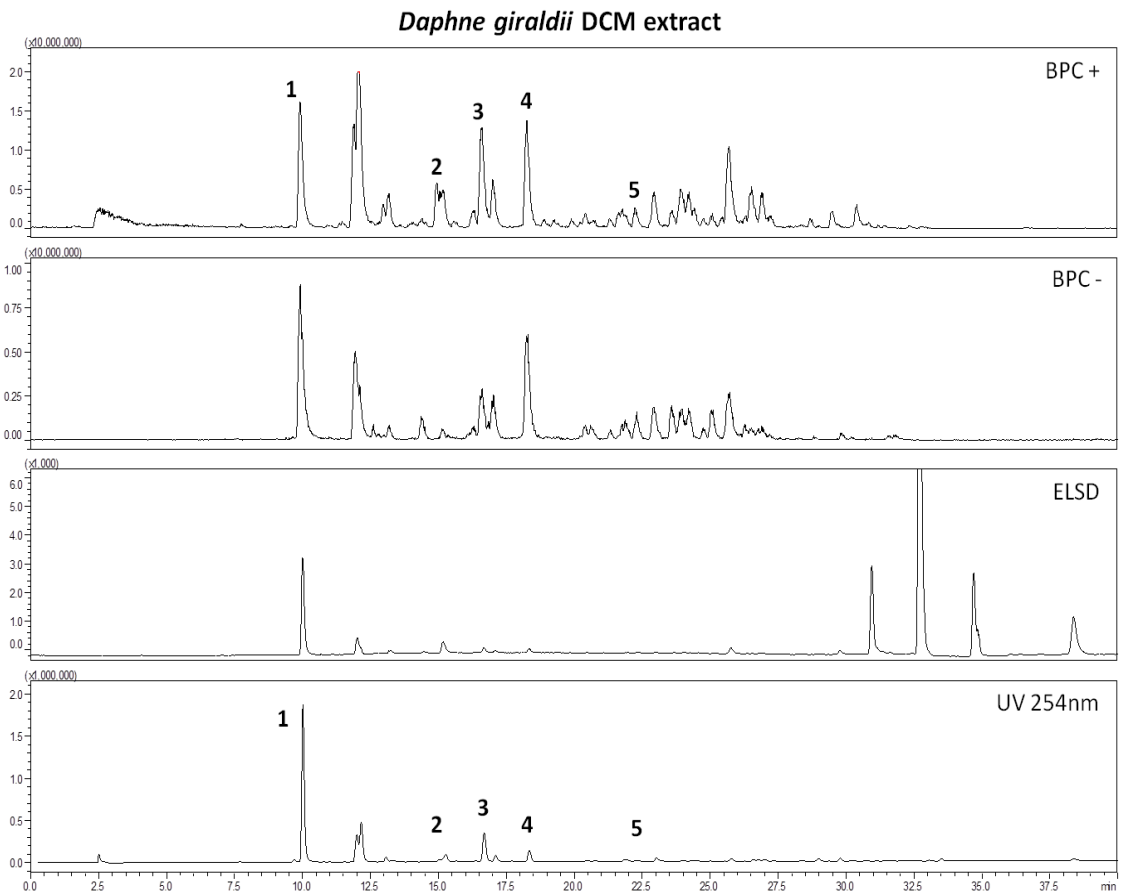

(b)

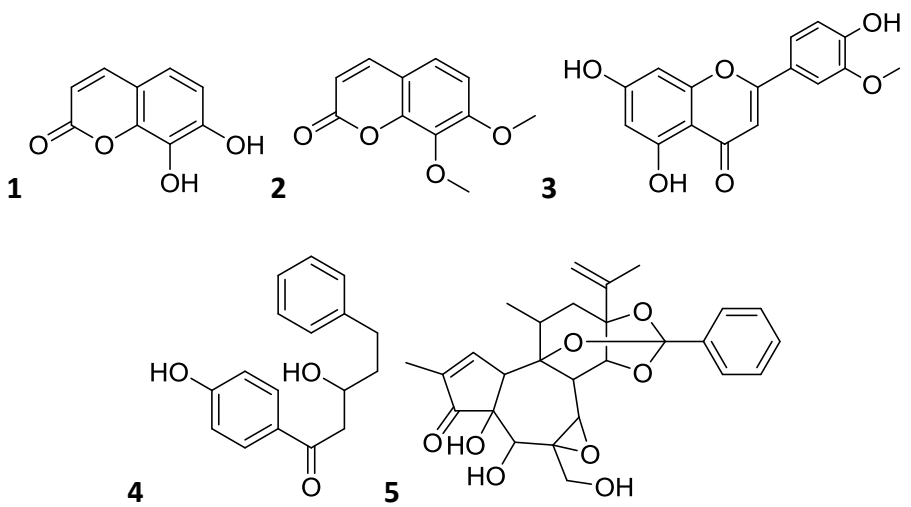

Figure 4.6: (**a**) HPLC chromatograms (ESI+, ESI-, ELSD, and UV at 254 nm) of *Daphne giraldii* DCM extract with their elution time on the HPLC separation and peak numbers representing isolated compounds. (**b**) Structures of daphnetoxin and all isolated compounds from the DCM extract: (**peak-1**) daphnetin, (**peak-2**) daphnetin dimethyl ether, (**peak-3**) chrysoeriol, (**peak-4**) daphneolone, and (**peak-5**) daphnetoxin.

With the exception of daphnetoxin, compounds managed to be isolated in this study (from DCM extract) are not from the regions that exhibited activity on Fig. 4.4. Besides these, several literature reports exhibited that plants which belong to the family Thymelaeaceae are well-known to contain numerous derivatives of phorbol esters (tigliane family of diterpenes). Thus correlating literature and our results which exhibited a-polar nature and lower UV absorbance properties – it was speculated that the main molecules giving rise to the observed activity were due to daphnetoxin-related compounds.

Based on the results discussed so far, the region of interest becomes a-polar compounds. Thus to work on a-polar compounds and reduce the complexity of the fractions, the next step is to try to remove major interfering compounds (higher UV absorbing and more polar) from each of the main fractions Dgi-E, -F, -G, -H. Separation on RP-HPLC usually results in a large loss of sample and its optimisation is not always optimal to obtain pure compounds in a single run; thus, for enrichment of the a-polar compounds (which have low UV absorbing nature), Centrifugal Partition Chromatography (CPC) was used. CPC is a series of channels linked in cascade by ducts, and aligned in disks in a circle around a rotor. This setup is submitted to a constant centrifugal field by setting the rotor in motion[215]. The main advantage of this technique is the complete recovery of the injected sample since the phases are made up of immiscible liquids. Sample Dgi-E, -F, -G, and -H were separated on CPC. Subsequently, based on similarity analysis via HPLC-UV-MS, the resulting fractions were combined (Dgi-E-a to -i, Dgi-F-a to -i, Dgi-G-a to -j, and Dgi-H-a to -k) and tested for sprouting of LECs (see Fig. 4.7). The results on Fig. 4.7 show that – with the exception of E-a and E-b – all fractions significantly induced sprouting on LECs. This might be due to insufficient phase separation of the CPC run which allowed the distribution of trace amounts of potent compounds throughout all fractions. The most active CPC fractions were G-b, G-a, E-d, and H-j (with 2.9, 2.2, 2.1, and 2.0 sprouts/bead, respectively) as well as their weights were 3.8, 23.3, 45.9, and 21.4 mg, respectively.

(a)

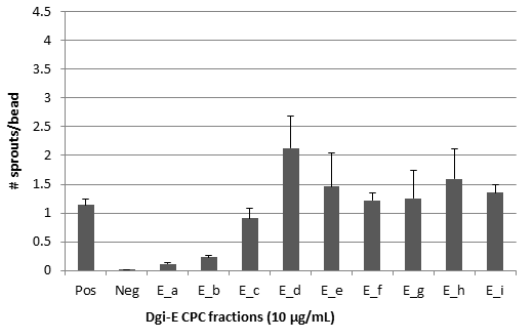

Sample name	Weight (mg)
Dgi_E_a	463.4
Dgi_E_b	150.7
Dgi_E_c	3.4
Dgi_E_d	45.9
Dgi_E_e	15.8
Dgi_E_f	561.9
Dgi_E_g	97.9
Dgi_E_h	21.3
Dgi_E_i	45.0

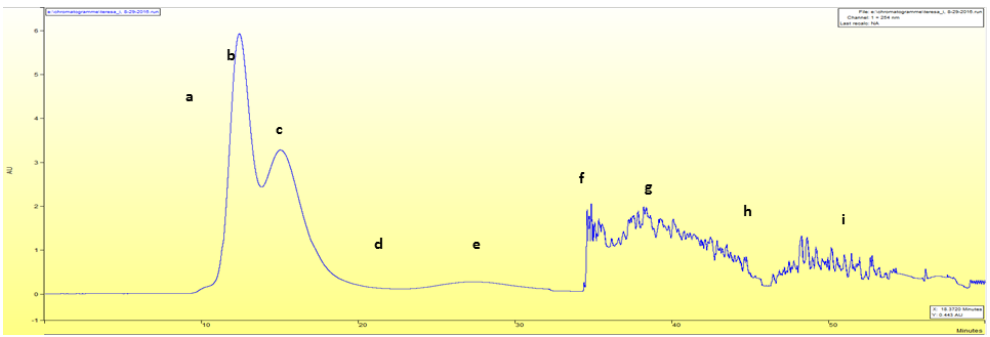

(b)

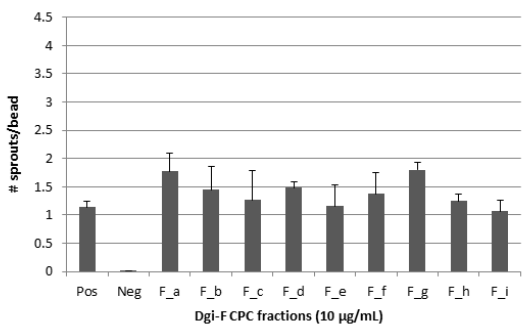

Sample name	Weight (mg)
Dgi_F_a	96.3
Dgi_F_b	39.1
Dgi_F_c	27.2
Dgi_F_d	311.5
Dgi_F_e	17.1
Dgi_F_f	18.2
Dgi_F_g	5.5
Dgi_F_h	7.3
Dgi_F_i	13.4

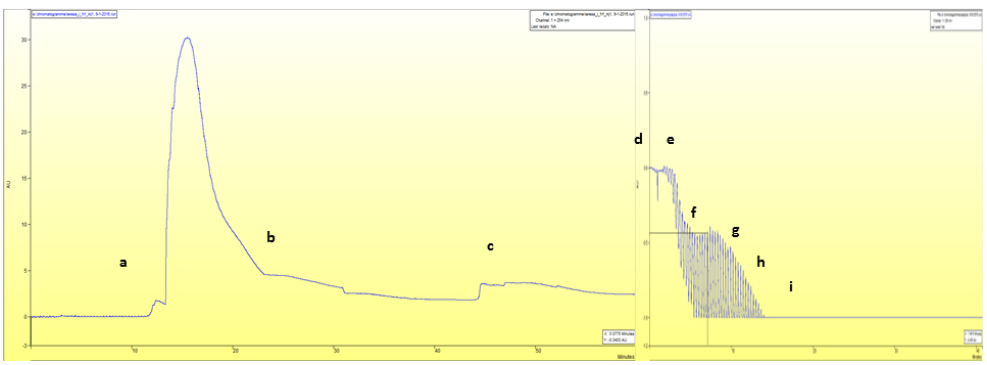

(c)

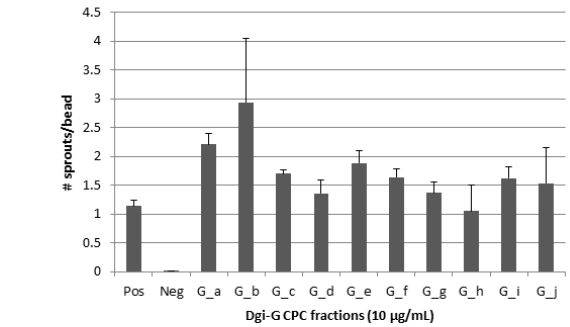

Sample name	Weight (mg)
Dgi_G_a	23.3
Dgi_G_b	3.8
Dgi_G_c	2.1
Dgi_G_d	4.2
Dgi_G_e	1.2
Dgi_G_f	21.2
Dgi_G_g	3.3
Dgi_G_h	3.4
Dgi_G_i	3.0
Dgi_G_j	11.9

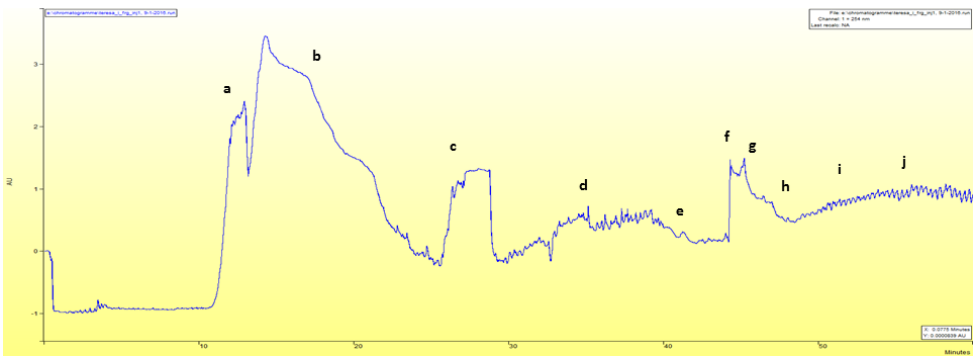

(d)

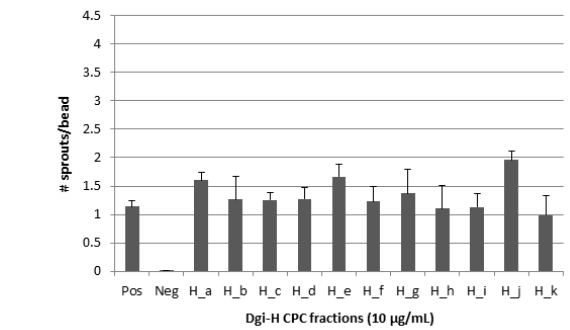

Sample name	Weight (mg)
Dgi_H_a	584.8
Dgi_H_b	35.3
Dgi_H_c	14.7
Dgi_H_d	20.9
Dgi_H_e	18.4
Dgi_H_f	422.2
Dgi_H_g	68.9
Dgi_H_h	27.9
Dgi_H_i	31.2
Dgi_H_j	21.4
Dgi_H_k	6.8

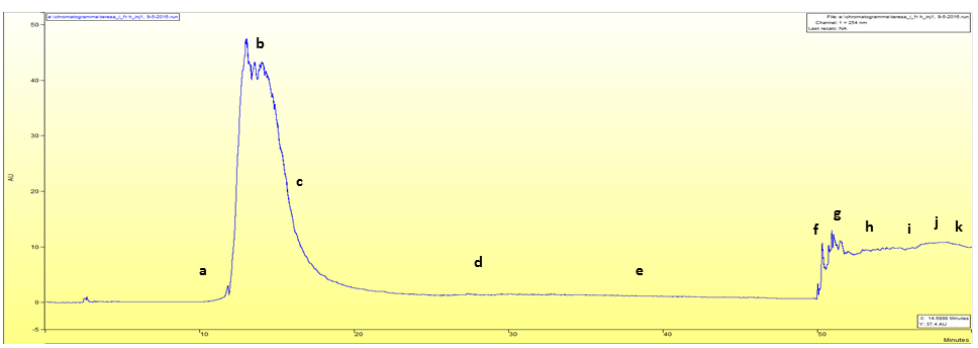

Figure 4.7: Sprouting results (10 µg/mL; n = 3) of CPC fractions from (**a**) E, (**b**) F, (**c**) G, and (**d**) H, with respective weights obtained and CPC profiles with estimation of fraction elution times.

As aforementioned, even while employing CPC, trace amounts of potent compounds were distributed throughout all fractions; this created a challenge for the determination of similarities/differences among CPC fractions, via analysing HPLC-UV-MS-ELSD and ^{1}H-NMR. Due

to these circumstances, the fraction analysis of this study focused on one CPC fraction that met the criteria of (a) enough yield, (b) less complex, and (c) higher activity. Fig. 4.8 exhibits an overlay of ^{1}H-NMR spectra from the three most active CPC fractions (E-d, H-j, and G-b), as well as an overlay of HPLC-MS-ELSD-UV profiles of the four most active CPC fractions (E-d, H-j, G-b and G-a). From this figure, it can be seen that CPC fraction E-d is the least complex sample. Considering this and other criteria mentioned above, the chosen CPC fraction was E-d, which had 45.9 mg yield, sprouting of LECs ≥ 2, as well as one major compound (via HPLC-UV-MS-ELSD and ^{1}H-NMR analysis).

(a)

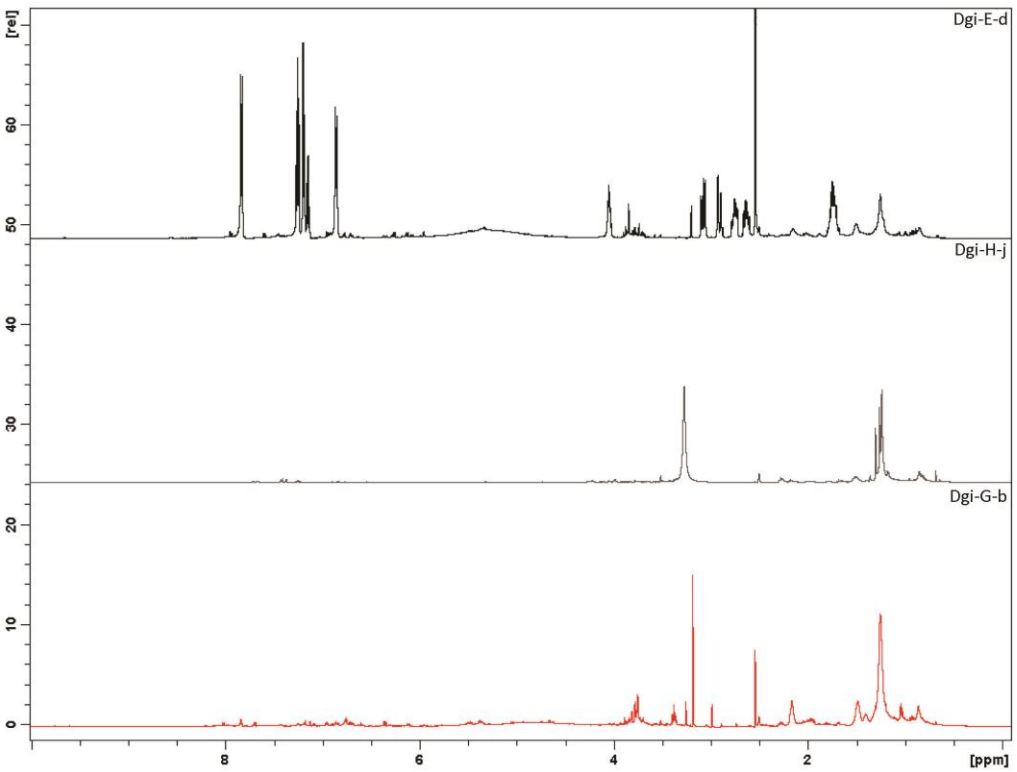

(b)

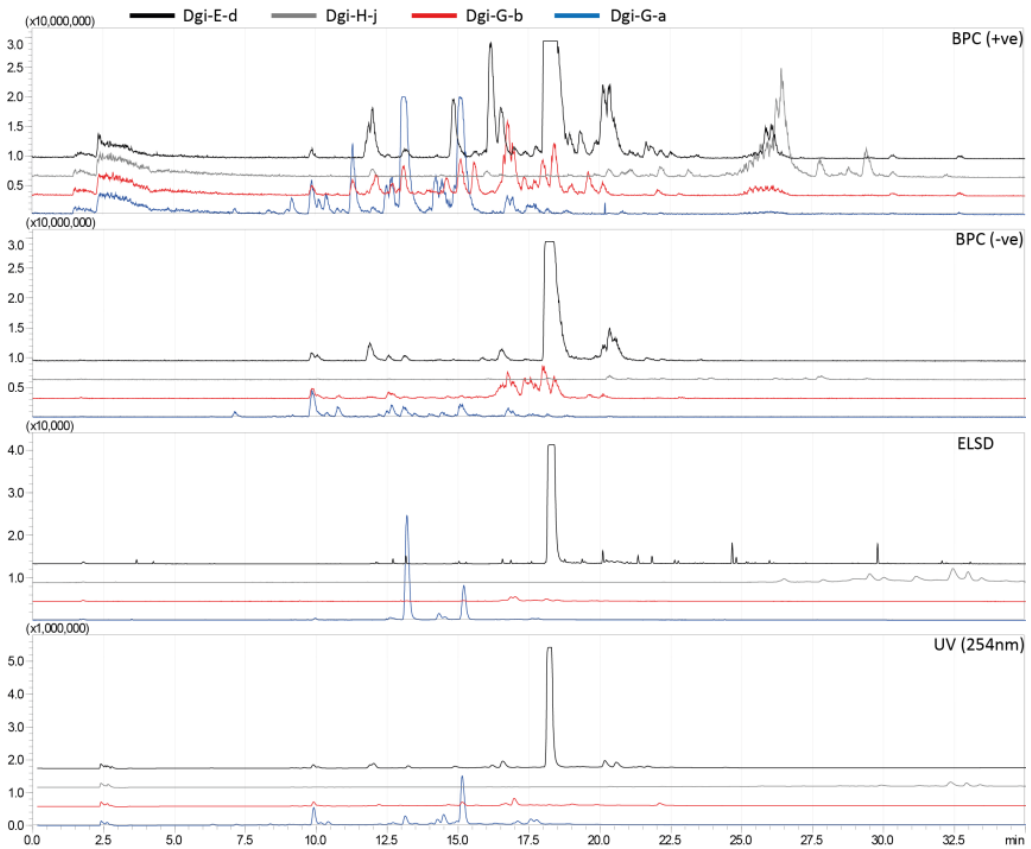

Figure 4.8: (**a**) Overlay of ^{1}H-NMR spectra of E-d, H-j, and G-b, and (**b**) overlay of HPLC-MS-ELSD-UV profiles of E-d, H-j, G-b and G-a.

To narrow down the activity, E-d was fractionated by a combination of time- and peak-based HPLC-UV chromatography into a further 11 fractions (E-d-1 to E-d-11, see Fig. 4.9 a). These fractions were tested at three concentrations 10, 1.0, and 0.1 µg/mL (see Fig. 4.9 b, c, d). Activity was consistently located in the a-polar region of the separation. Fractions E-d-9, E-d-10, and E-d-11 were the most active at 10 µg/mL, while E-d-11 still showed potent activity at 1.0 µg/mL. Moreover, each fraction from E-d (E-d-1 to -11) was analysed by HPLC-UV-ELSD-MS and ^{1}H-NMR. The 2D-NMR analysis showed that the main compound present in fraction E-d-5 (which was marginally active, sprouting ≈ 2 at 10 µg/mL) is 7,8-dimethoxy-coumarin (or daphnetin dimethyl ether). On the other hand, the structural analysis illustrated that the major compound present in fraction E-d (especially in E-d-8) was daphneolone (an oxidised chalcone), which was not the active constituent (see Fig. 4.9 b, c, d). Due to the presence of more than two compounds, low signal-to-noise (S/N) ratio (≤ 100 S/N) from ^{1}H-NMR, and low yield of fractions (≤ 1.0 mg), further structural elucidation from E-d fractions (E-d-9, -10, -11) was not possible. As shown in Fig. 4.6 (b), daphnetin and chrysoeriol were isolated from DCM extract.

These compounds are also found in CPC fraction E-a (which is inactive fraction) however they were not present in any of the E-d sub-fractions.

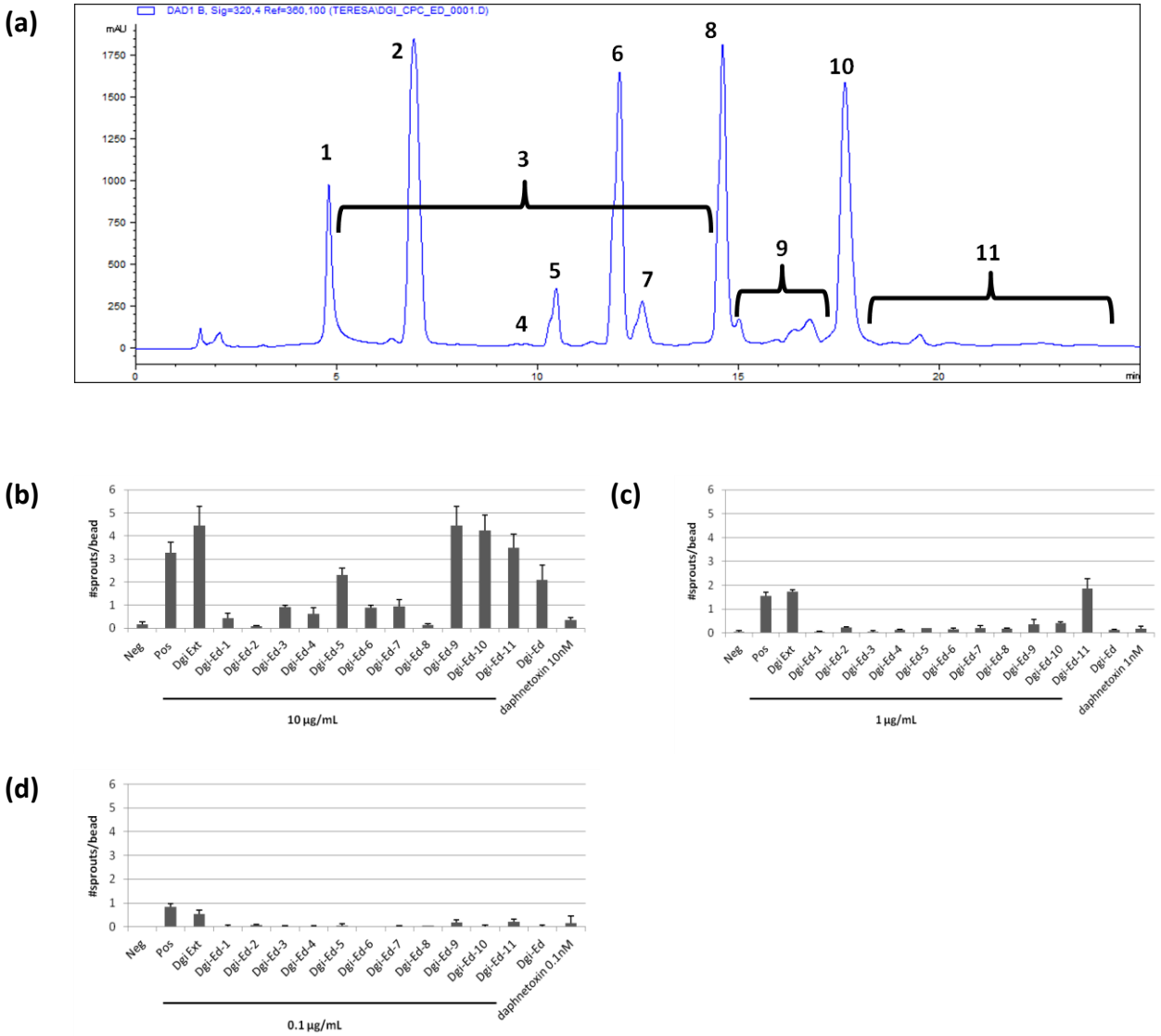

Figure 4.9: (**a**) E-d semi-preparative HPLC-UV separation on a RP C18 column at 320 nm and sprouting results tested at (**b**) 10, (**c**) 1.0, and (**d**) 0.1 µg/mL with 0.1% DMSO as negative control and Iris extract (10 µg/mL) as positive control.

In HPLC-MS, the main peaks observed in E-d-9 to E-d-11 had *m/z* ratios lower than that of tigliane diterpenes (*m/z* 365 $[M+H]^+$), and daphnane diterpenes (*m/z* 315 $[M+H]^+$) core structures; thus, these main compounds might not be diterpene derivatives, as well as at this point their activity cannot be defined. Therefore, to further fractionate active E-d fractions (E-d-9, -10, -11), based on time- and peak-based separation (see Fig. 4.10 a, b, c), semi-preparative HPLC-UV methods were optimised. Particularly these fractions were tracked via their UV

signatures at different wavelengths: E-d-9 was tracked by 254, 205, and 280 nm; for E-d-10 270, 205, and 320 nm were used and for E-d-11 254, 290, and 320 nm were used. All the sub-fractions of E-d active fractions (i.e., E-d-9-1 to -10; E-d-10-1 to -6; E-d-11-1 to -9) were tested at 10 and 1.0 µg/mL (Fig. 4.10 d, e). The most active sub-fractions were E-d-9-10, E-d-10-6, and E-d-11-9 which were the 100% B region from each separation. Additional sub-fractions from E-d-11 were also active namely -4, -5, -7, and -8 at 10 µg/mL as well as E-d-11-6, -7, -8, and -9 were still active at 1.0 µg/mL. Major activity was again consistently observed in the lipophilic region of the separation.

(a)

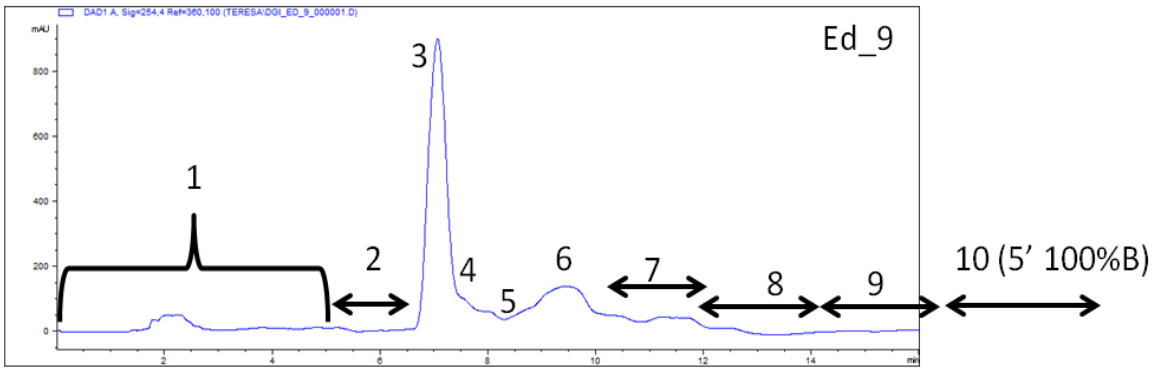

(b)

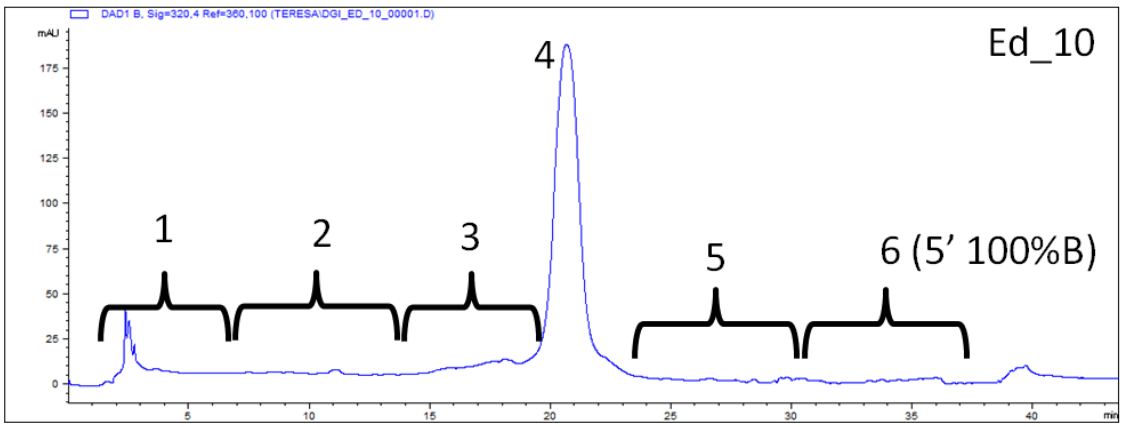

(c)

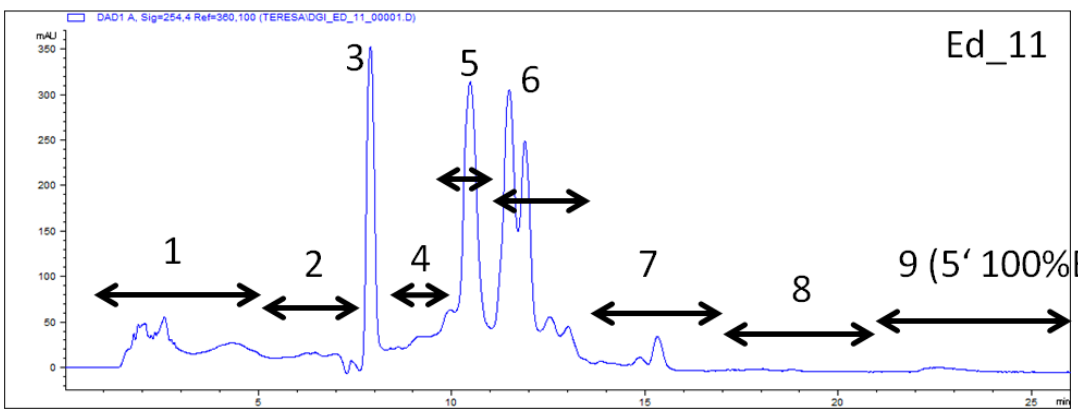

(d)

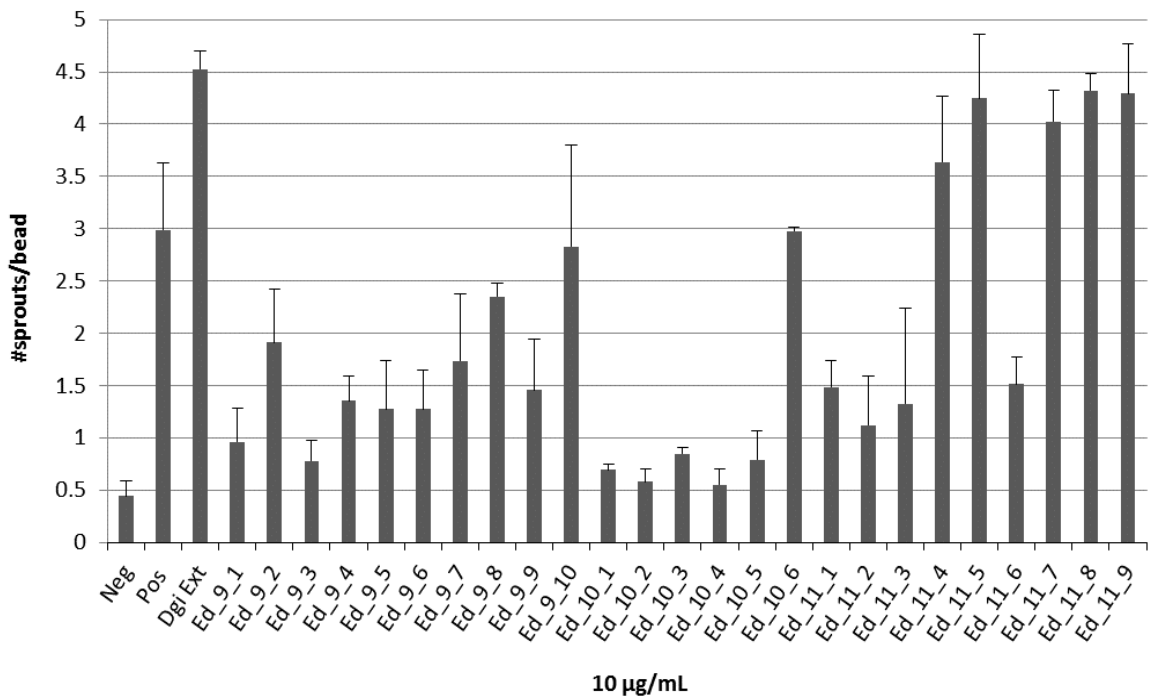

(e)

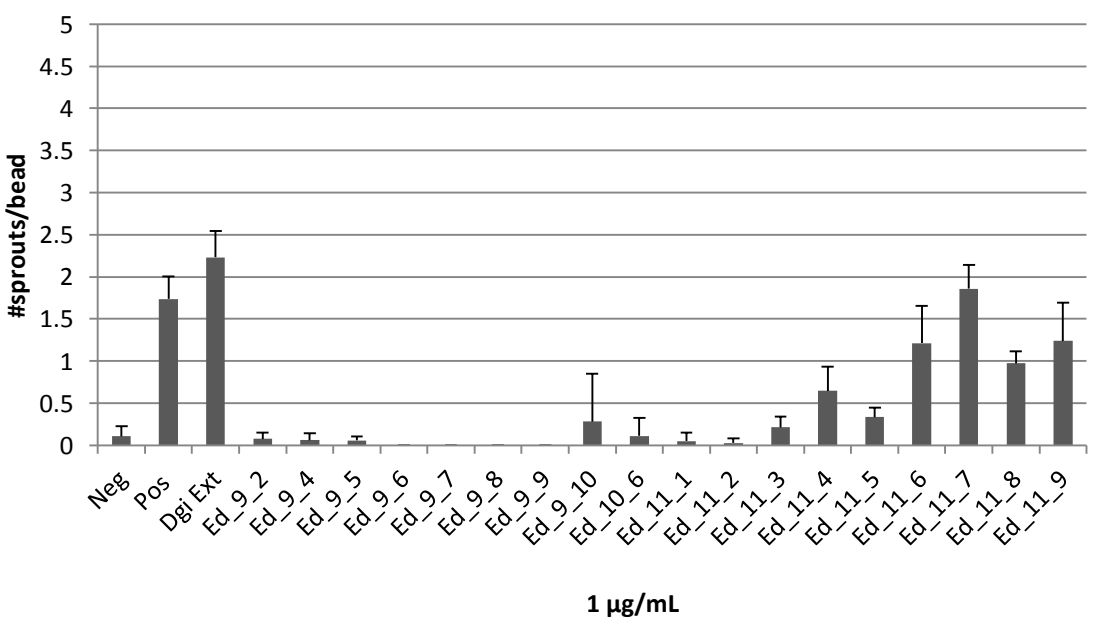

Figure 4.10: Semi-preparative HPLC-UV sub-fractionation of (**a**) E-d-9, (**b**) E-d-10, and (**c**) E-d-11 at 254 nm and sprouting results of each sub-fraction tested at (**d**) 10, and (**e**) 1.0 µg/mL with 0.1% DMSO as negative control and Iris extract (10 µg/mL) as positive control.

The sub-fraction E-d-10 contained three unresolved peaks each with a different λ_{max} namely, at 320 nm (1st peak, *m/z* 307 $[M+H]^+$), 270 nm (2nd peak, *m/z* 311 $[M+H]^+$), and 205 nm (3rd peak, *m/z* 313 $[M+H]^+$). All sub-fractions were analysed using ^{1}H-NMR, which showed that all sub-

fractions from E-d-9 to E-d-11 were a mixture of compounds (i.e., no pure compounds were obtained). This was due to insufficient separation possibilities given the low amounts of each fraction and the close-elution of the compounds. Common pseudo-molecular masses found in these fractions were 307 $[M+H]^+$, 311 $[M+H]^+$, and 313 $[M+H]^+$ and were speculated to be the active compounds. Nevertheless they were found to be inactive in sub-fractions E-d-9-7 and E-d-10-4 which contained these masses at the same retention times in a higher quantity (see Fig. 4.11). This implies that on sub-fractions E-d-10-4, E-d-11-3, and E-d-9-7 these masses are also not active. This means that these common peaks could be excluded from the activity found in 10-6, 11-4, and 11-5.

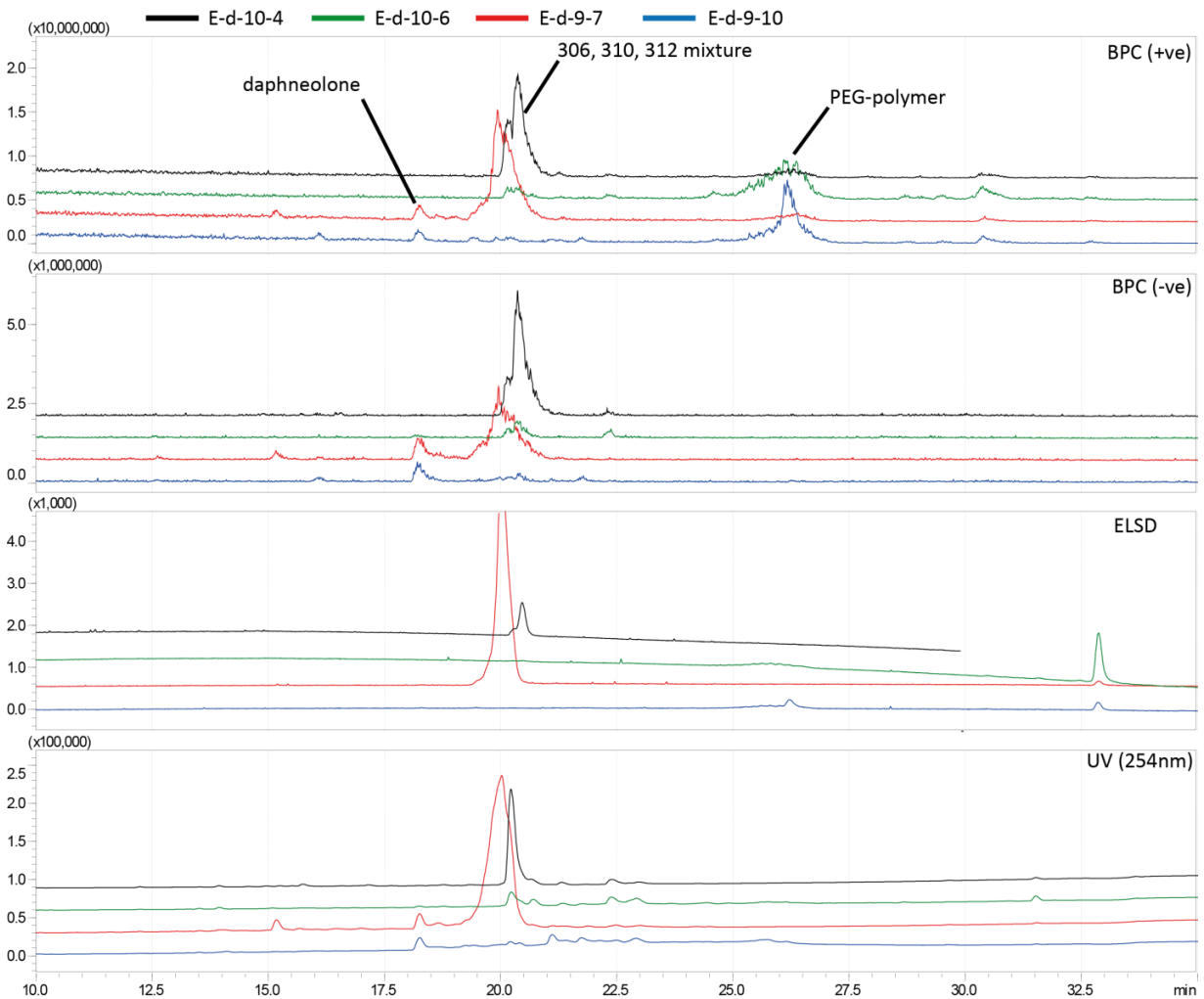

Figure 4.11: HPLC-UV-ELSD-MS chromatograms of sub-fractions E-d -10-4, -10-6, -9-7, and -9-10.

4.2.1 Projected analysis on composition of *Daphne giraldii* active micro-fractions

Based on the discussion given so far, identifying pure active compounds was challenging, mainly due to low amounts of active fractions and quite close-elution of the compounds. Therefore in this section the study presents different projected analysis on the composition of *D. giraldii* active micro-fractions. APCI-MS analysis did not provide further insight, thus as an alternative technique for detection of the active and inactive common metabolites present on *D. giraldii* micro-fractions, GC-MS analysis was used. GC-MS analysis indicates that benezenepropanol was present in both active and inactive micro-fractions, thus this common metabolite could not be responsible for activity.

Analysis using in-house developed clustering scripts[216] showed the presence of daphnetoxin in all of the active micro-fractions (E-d-9-10, 10-6, 11-6, 11-7, 11-8, 11-9) as well as in two inactive micro-fractions (E-d-9-1, -9-3) (Fig. 4.12 b). Micro-fraction E-d-11-6 contains a higher intensity of daphnetoxin shown in the Bayesian plot which can be corroborated by MS data (extracted m/z 483 $[M+H]^+$ of daphnetoxin in 11-6). The presence of daphnetoxin in inactive -9-1 and -9-3 samples is rather low and cannot be seen by visual inspection of MS data. It should be taken into consideration that this clustering method of data representation has only recently been developed and there are still certain aspects that need optimisation, e.g. the normalisation of data with reference to an internal standard. In this context, the presence of daphnetoxin in these inactive micro-fractions might be due to the lack of optimisation in the clustering scripts, in any case this needs further insight. Utilising clustering scripts, some commonalities among active micro-fractions and inactive micro-fractions were made (see Fig. 4.12 a and b). Basically, active micro-fractions showed commonality due to the presence of the polymer PEG classified by characteristic 'mountain' pattern with *m/z* signals in increments of 44 (as seen in Fig. 4.11). However, inactive micro-fractions showed commonality by the presence of the main UV absorbing and MS ionising compounds (*m/z* 307, 311, 313 $[M+H]^+$).

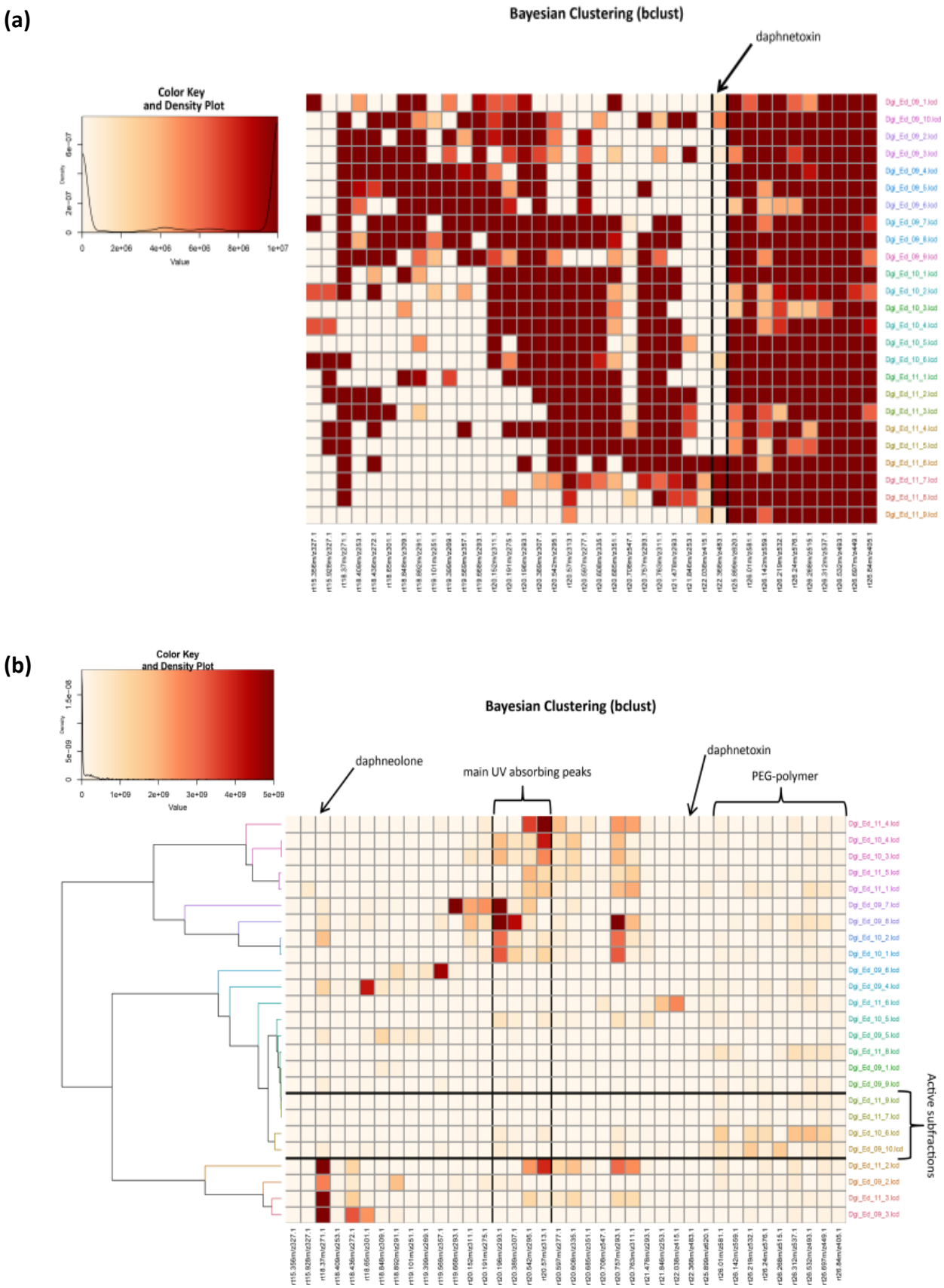

Figure 4.12: (**a**) Bayesian clustering zoomed in to 1 x 10^7 of all micro-fractions; (**b**) Bayesian clustering plot with grouped micro-fractions.

Utilising NMR instruments with strong magnets (such as with 800 MHz), full structure elucidation can be achieved for samples which have approximately 1-2 µg amounts. However this study uses 500 MHz NMR instrument, thus below 100 µg is too low for full structure elucidation. For instance, to assess the detection capabilities of the NMR used in this study, 1.0 µg and 1.0 mg of pure daphnetoxin were prepared and run in 1-mm NMR tube, then using standard measuring times (128 scans) ^{1}H-NMR were acquired. The ^{1}H-NMR spectra for 1.0 µg and 1.0 mg experiments were shown in Fig. 4.13. As shown in Fig. 4.13 the signals for 1.0 mg-^{1}H-spectrum were clear, however for 1.0 µg experiments the instrument can barely detect daphnetoxin signals. Though the active micro-fractions found in this study contain trace amounts of daphnane derivatives, these NMR experimental results illustrated that structure elucidation and quantifying trace amounts of daphnetoxin (and its derivatives) via 500 MHz NMR from the active micro-fractions is challenging; nonetheless to a certain degree their presence can be traced. For example, Fig. 4.14 exhibits the overlay of ^{1}H-NMR spectra of daphnetoxin, E-d-11-6, and E-d-11-7. In line with the outcome of clustering analysis, the results in Fig. 4.14 illustrated that even with the low S/N ratio of the spectra; some signals of daphnetoxin can be identified in 11-6 and 11-7.

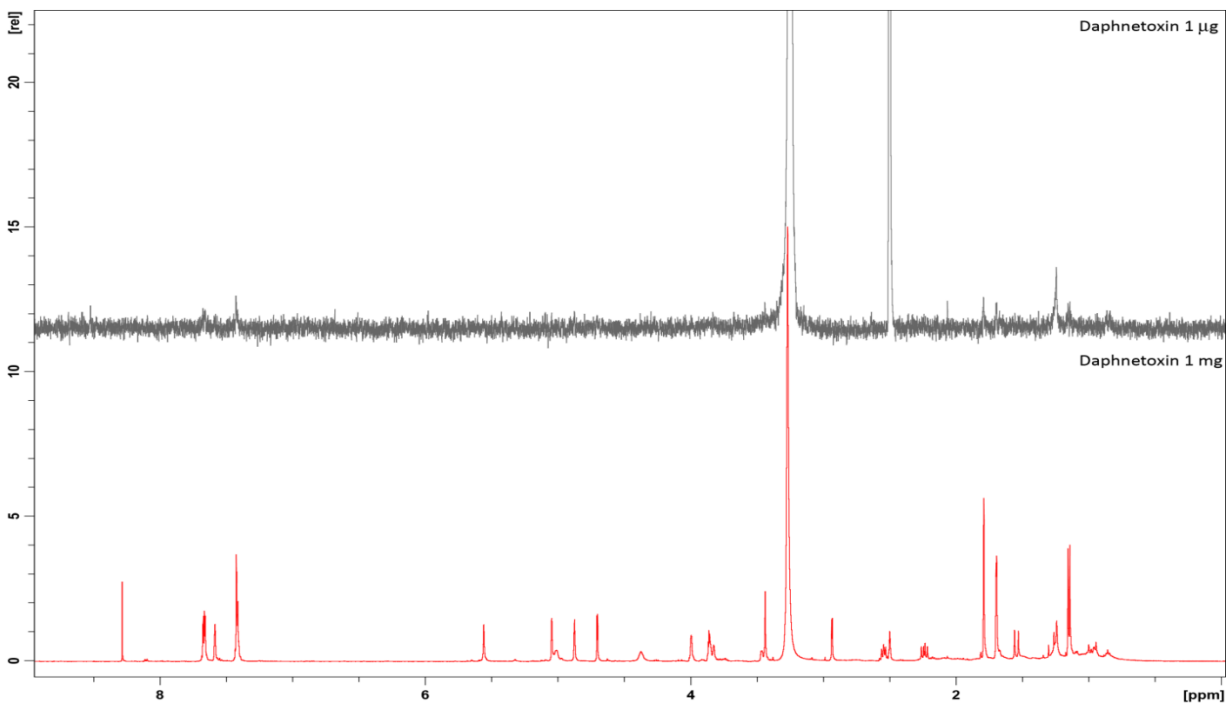

Figure 4.13: Overlay of ^{1}H-NMR spectra of 1 µg (grey) versus 1 mg (red) of daphnetoxin in a 1-mm NMR tube measured in DMSO-*d6*.

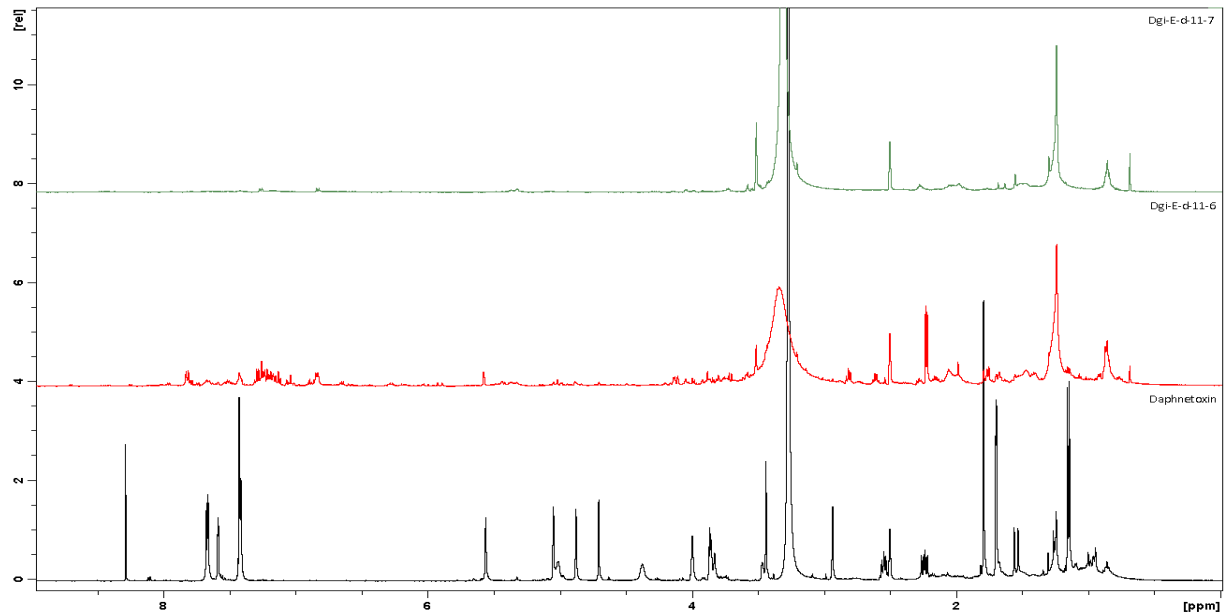

Figure 4.14: Overlay of ^{1}H-NMR spectra for daphnetoxin (black), E-d-11-6 (red), and E-d-11-7 (green) in DMSO-*d6*.

As mentioned previously daphnetoxin is active in inducing lymphatic vessel growth and it was used as a reference for comparing with the activities of *D. giraldii* fractions. Added to this, the clustering analysis (given above) exhibited the presence of daphnetoxin in all *D. giraldii* active micro-fractions (E-d-9-10, -10-6, -11-6, -11-7, -11-8, -11-9). However the concentration of daphnetoxin in these active micro-fractions was small. These circumstances raise a question that are these micro-fractions active because they contain trace amounts of daphnetoxin? In order to answer this, it is important to determine a minimum effective concentration (min EC) of daphnetoxin. This is also crucial to make an evidence-based speculation on which type of compound(s) were responsible for activities seen in micro-fractions E-d-9-10, E-d-10-6, E-d-11-6, E-d-11-7, E-d-11-8 and E-d-11-9. To determine min EC of daphnetoxin, LECs sprouting was conducted with varying concentrations of daphnetoxin (see Fig. 4.15). The results in Fig. 4.15 illustrated that the min EC for daphnetoxin was 10 nM, which is 4.82 ng/mL. Also, the EC_{50} values for daphnetoxin as well as for more active micro-fractions (i.e., E-d-11-7, and E-d-11-9: see Fig. 4.10 d, e) were calculated. As shown in Fig. 4.15 (a–e), the EC_{50} values for daphnetoxin, E-d-11-7, and E-d-11-9 were found to be 11.67 nM (5.77 ng/mL), 0.6092 µg/mL (609.2 ng/mL), and 1.345 µg/mL (1345.0 ng/mL), respectively. The EC_{50} values for daphnetoxin implies that, in terms of daphnetoxin, an EC_{50} of 0.6092 µg/mL is equivalent to 1.4 µg in 152.0 µg of the sample. Based on these min EC and EC_{50} results and analyses, this study speculated that trace

amounts of daphnetoxin present on *Daphne giraldii* active micro-fractions could be (or at least one of) the main contributing factors for activities seen on Fig. 4.10 d, e.

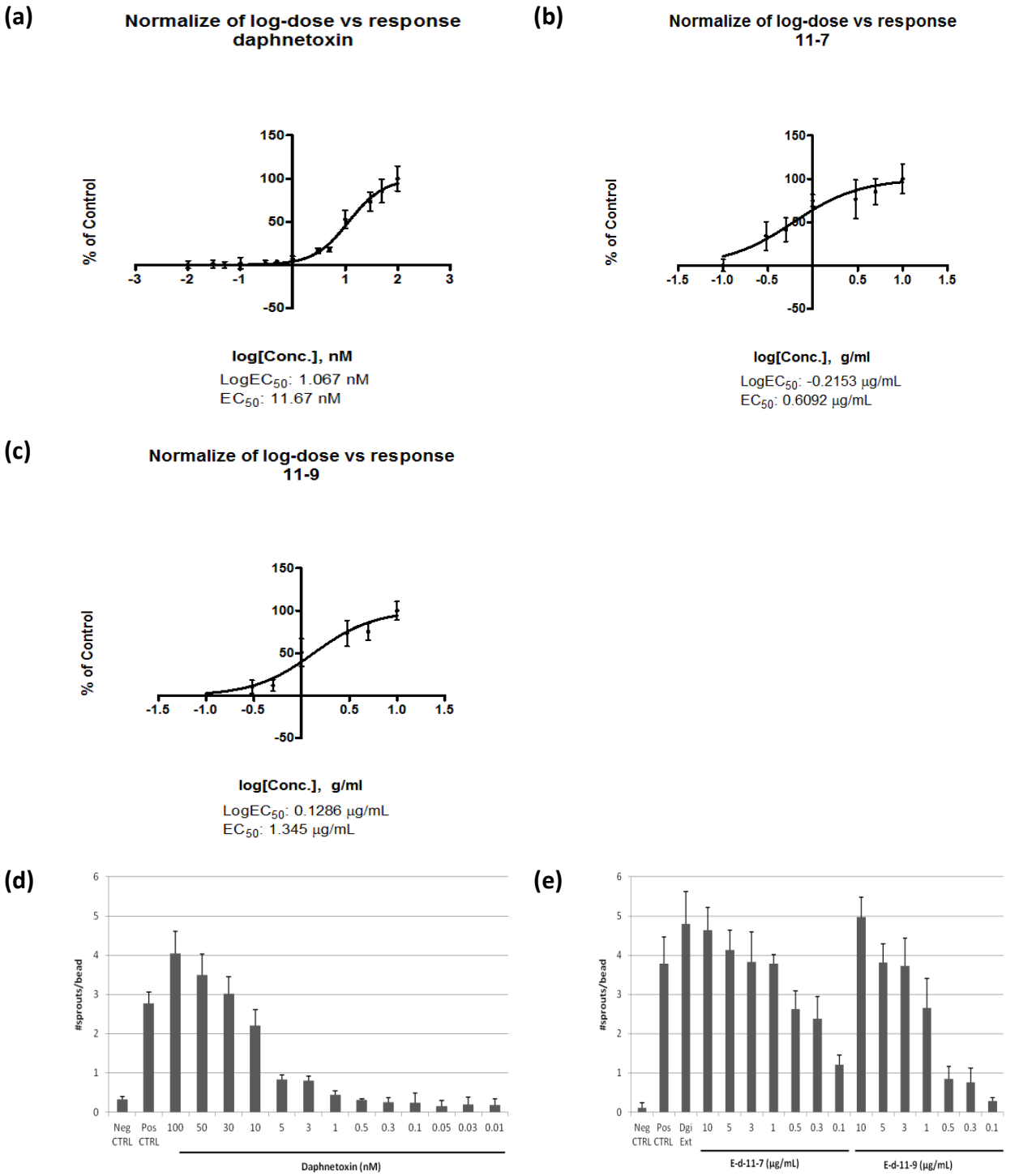

Figure 4.15: Calculated EC_{50} values for (**a**) daphnetoxin, and micro-fractions (**b**) E-d-11-7 and (**c**) E-d-11-9. (**d**) Actual values of sprouting used in the calculation of EC_{50} for daphnetoxin (positive control at 10 µg/mL), and (**e**) for micro-fractions E-d-11-7 and E-d-11-9 (positive control and *D. giraldii* extract at 1.0 µg/mL).

Besides daphnetoxin (and its derivatives), relating the results of this study with that of literature and other databases, it is also possible to make inclusion/exclusion projections on the composition of *D. giraldii* active micro-fraction components. Based on the results found so far and literature reviews, it is rational to exclude compounds of high UV absorbing, polar in nature, coumarins, and chalcones as contributors for the observed activities; but it is not possible to exclude diterpene derivatives or fatty acids. For instance, Fig. 4.16 shows an overlay of ^{1}H-NMR spectra for a fatty acid, daphnetoxin, and active micro-fraction E-d-10-6. The figure exhibits the presence of fatty acid signals in E-d-10-6 which has high sprouting activity. Considering the fact that common fatty acids are present in many a-polar extracts of plants, if the activity on Fig. 4.10 comes from fatty acid, it would have to be a less common fatty acid and/or unique to *D. giraldii*.

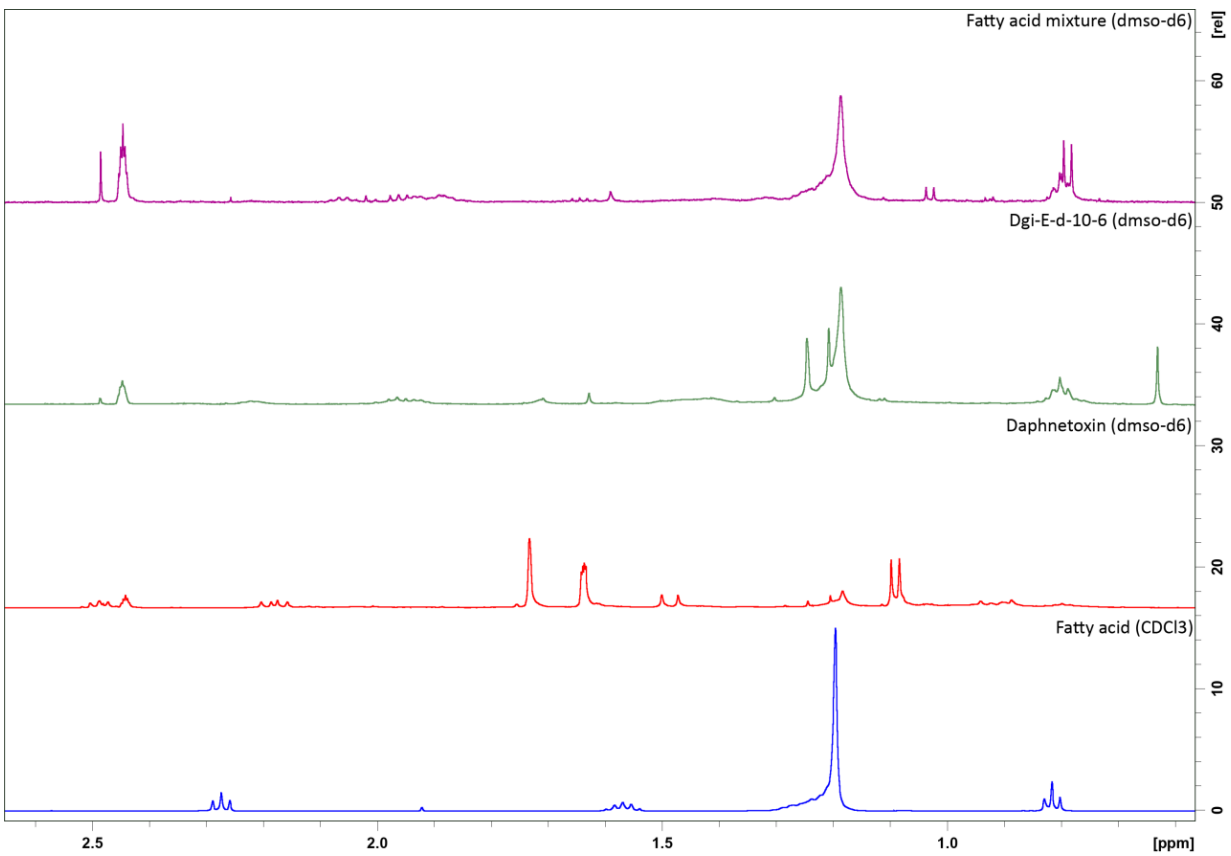

Figure 4.16: Overlay of ^{1}H-NMR spectra for a fatty acid mixture, E-d-10-6, daphnetoxin, and a pure fatty acid (palmitic acid).

4.3 Discussion and conclusions

To identify natural molecules that have a potential to induce lymphatic vessel growth, a phenotypic screening (3D sprouting assay) was conducted on an extract library which comprised 1952 plant and fungal extracts. Of all the extracts that were tested, the DCM, EtOAc, and MeOH extracts from *Daphne giraldii* were identified as potent inducers of LEC sprouting. Among these three, more activity was noted on MeOH extract; accordingly further HPLC-based activity profiling was carried out on this extract. During the micro-fractionation of the MeOH extract, activity was localised in the lipophilic region of the HPLC separation. This lead to the reasoning that these lipophilic compounds might be present in DCM extract at higher quantities, thus the study was carried out based on DCM. With the DCM extract, separation on normal phase silica gel was used to obtain eight fractions, of which, four were active (namely fractions: E, F, G, H). To refine the regions of activity on these fractions, further HPLC-based activity profiling and tests on the 3D sprouting assay were carried out. This profiling consistently exhibited that prominent sprouting of LECs are located in the a-polar regions of the micro-fractions. Accordingly to enrich the a-polar and low UV absorbing compounds from the silica gel-fractions (i.e., E, F, G, H), CPC was used and the resulting CPC sub-fractions were tested. The test results show sprouting activities were spread throughout all CPC sub-fractions. This might be due to insufficient phase separation in the CPC chambers which lead to leaking of minute amounts of potent, a-polar compounds in each of the CPC sub-fractions. Unlocalised activities found on CPC sub-fractions became a challenge for selecting any of the CPC sub-fractions for isolation of the active compounds. As a result various other factors had to be employed for selection, such as higher yield, less complex, and higher activity. The CPC sub-fraction which is named as E-d, met the above selection criteria and step-by-step this sub-fraction underwent a series of assaying and time-peak-based HPLC-UV semi-preparative-fractionations, until the micro-fractions weighed ≤ 100 µg. Since activities were localised in a-polar and low UV absorbing regions, following the test results in each round of HPLC-fractionations, the E-d micro-fractions which possessed compounds with UV absorbing properties and MS ionisation were excluded from the list of targeted micro-fractions. Similar to the sub-fractions, activity was consistently found in the late eluting micro-fractions (lipophilic regions). Thus polar compounds can be excluded as the constituents responsible for activity.

Compounds such as daphnetin dimethyl ether and daphneolone were isolated from E-d micro-fractions, however these compounds eluted outside the lipophilic regions, thus they were found to be constituents not responsible for activity. Overall, after all HPLC-UV-fractionation steps that E-d micro-fractions went through, it remained challenging to identify pure a-polar compounds that are responsible for observed activities. This is mainly due to two reasons, (a) minor concentrations of complex micro-fractions that results setbacks on their detectable signatures such as via NMR, and (b) presence of a wide array of minor metabolites structurally related to each other, thereby it becomes difficult to separate the NMR signature of individual constituents without interference; as well as to isolate them on semi-preparative RP-HPLC. Generally, if a fraction is ≤ 2.0 mg then separation of the compounds should be done on analytical scale and not semi-preparative. This has its drawbacks since many injections have to be done so as to not overload the column and loss of sample has to be taken into consideration. However, when the compounds are closely related, the separation would be better on an analytical HPLC column. Additionally, microprobe NMR analysis has a significant advantage for detecting small amounts of compounds, however is has instrument dependent minimum limitations. Considering the sensitivity of the NMR instrument used in this study (500 MHz) and minor sample amounts it became difficult to analyse compounds responsible for activity. In order to identify trace amounts of constituents via improving S/N ratios in NMR, more sensitive instruments should be employed; for example NMR which have increased magnetic field strength (such as 800 MHz instead of 500 MHz), enhanced coil quality and that can operate at lower temperatures (such as 0.3-mm microprobe or 1.7-mm cryoprobe)[217].

Though, for aforementioned reasons, the study could not certainly identify and provide the structure of active constituent(s) which are responsible for observed activity; it provides a projected analysis on composition of *D. giraldii* active micro-fractions. Generally, *D. giraldii* belongs to the family Thymelaeaceae, which is well known to contain daphnetoxin and other daphnane type orthoester diterpenes. Particularly, various activities of daphnetoxin are well documented[214] thereby activities observed in this study could possibly be related to the presence of these compounds. Daphnetoxin which was previously isolated in another study was used as a reference compound in this study. It displayed potent sprouting activity. Although daphnetoxin concentration in active micro-fractions was small, it might at least be one of the compounds responsible for observed activity. In order to support this, the minimum effective concentration (min EC) and EC_{50} of daphnetoxin was determined. Additionally, to correlate the

EC_{50} of daphnetoxin with that of daphnetoxin presence in the micro-fractions, EC_{50} for micro-fractions E-d-11-7 and -11-9 were determined. The results of these experiments support a projection that trace amounts of daphnetoxin present in *D. giraldii* active micro-fractions could be (at least one of) the main contributing factors for observed activities. Furthermore, analysis of ^{1}H-NMR spectra for a fatty acid, daphnetoxin, and active micro-fraction showed the presence of fatty acid signals in active micro-fractions. Studies such as, Wong *et al.,* (2016) have described the essential role of fatty acid β-oxidation (FAO) in endothelial cells to generate acetyl-CoA for histone acetylation that is required for lymphangiogenesis[162]. LECs use FAO to proliferate and for regulation of lymphatic marker expression during differentiation. Dietary modulation of fatty acids or supplementation with metabolites could be used to promote lymphangiogenesis in pathological conditions such as lymphedema[162]. Typical fatty acid signals could be seen in some active micro-fractions. However, if ubiquitous fatty acids were contributors to the observed activity, then more lipophilic extracts would have been active during the extract library screening. Based on this hypothesis, ubiquitous fatty acids would probably not be the main contributors of activity. However, unique fatty acids present in *D. giraldii* which have not yet been identified may play a role in the overall observed activity of the fractions and extract.

An extract may show an activity which might be due to: (1) one active metabolite present with large quantities; or (2) a number of moderately active constituents at reasonable concentrations which act together; or (3) a number of constituents present in minor concentrations but are potent in inducing active responses[70]. The study on *D. giraldii* for inducers of LEC sprouting can be classified into the third case, where minor compounds with potent activity are present. In such cases, to identify compounds that are responsible for activity, large amounts of optimally prepared extracts are needed. This will allow bioassay-guided refined separations to end up with suitable amounts of pure compounds for identification. While using large amounts of extracts, this study recommends the use of partition chromatography (such as CCC and CPC) for making the initial fractionations. These chromatographic techniques can reduce time needed for isolation of active metabolites and provide different advantages such as lack of irreversible adsorption to a stationary phase and loss-free fractionations[70,88].

Chapter 5

5. Results and Discussion: Chronic Heart Failure

As stated in section 1.5, the CHF project focuses on characterising secondary metabolites present in active sub-fractions of *Crataegus* species, which contribute to the further use of *Crataegus* in the treatment of mild forms of CHF. In the following sections, *Crataegus* fraction test results in a Fura-2 calcium imaging cell assay are presented. Lastly, a brief discussion and concluding remarks are given.

5.1 *Crataegus* extract WS 1442

Crataegus (hawthorn) extract (Dr. Willmar Schwabe's Hawthorn Extract WS® 1442) is widely used as an adjuvant treatment for mild forms of CHF according to the New York Heart Association functional class II[191]. Its mechanism of action was recently investigated and *Crataegus* was shown to reduce endothelial hyperpermeability via two pathways, (1) inhibition of thrombin-induced [Ca^{2+}] influx, and (2) cortactin activation. It was also previously shown that the *Crataegus* special WS 1442 extract significantly reduced thrombin-evoked macromolecular permeability[196]. This study aims to characterise *Crataegus* extract WS 1442 active constituents that interact with the underlying molecular mode of action. The study was conducted in collaboration with the Goethe University, Frankfurt, Germany. The *Crataegus* special extract WS 1442 was provided by Dr. Willmar Schwabe Gmbh & Co. KG (Karlsruhe, Germany). It is a dry extract from hawthorn leaves with flowers using ethanol as the extraction solvent[197].

In a previously reported study[218], to determine the exact constituents that gave rise to this observed effect, the WS 1442 extract was separated into four fractions using Sephadex (LH-20), namely: [1] water (fraction A), [2] ethanol (fraction B), [3] methanol (fraction C) and [4] acetone (fraction D). Bauhart (2013)[218] subsequently tested these fractions for their ability to prevent vascular leakage and edema formation[197]. On test results of Bauhart (2013) fraction B was shown to block the thrombin-induced [Ca^{2+}] influx pathway, while fraction C was shown to protect against endothelial barrier dysfunction via cortactin activation[218]. Moreover, Bauhart (2013) partitioned the *Crataegus* ethanolic extract in H_2O and EtOAc in a separating funnel. Then after, the EtOAc portion was evaporated and nine fractions from a silica gel open column were obtained and tested (Fractions E-1 to E-9)[218]. In addition, Bauhart (2013) isolated 4

triterpenes from E-3 fraction (namely: corosolic acid, pomolic acid, oleanolic acid, and ursolic acid). These isolated compounds were tested and found to be inactive[218].

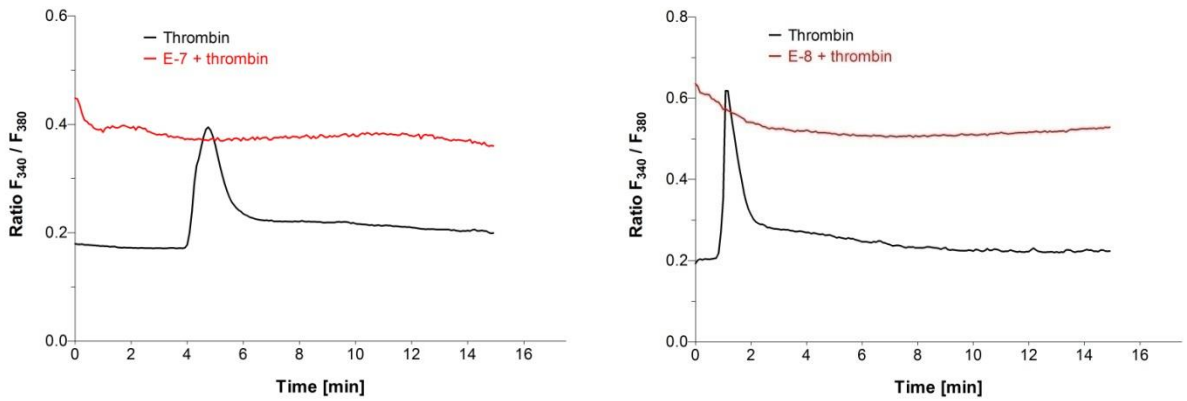

Figure 5.1: Changes in $[Ca^{2+}]_i$ detected by fluorescence microscopy using Fura-2-AM (2 µM) in a static tempered system, with thrombin addition (1 U/mL) at time point 1.0 min after experiment initiation and treatment with fractions E-7 and E-8 (10 µg/mL) for 30.0 min. One representative experiment out of 3 independently performed experiments (n = 3) is depicted[197].

The current study is basically a follow up of Bauhart (2013)[218]. Thus, this study tested the activity of these fractions from the silica gel open column (E-1 to E-9) and only two fractions (E-7 and E-8) were found to be active (sees Fig. 5.1). Thereby these fractions were further separated by semi-preparative HPLC-UV, with a combination of peak- and time-based fractionation. Peak- and time-based fractionation of these two fractions (i.e., resulting sub-fractions from E-7 and E-8) is shown in Fig. 5.2. The sub-fractions were tested and it was found that only E-8-4, E-8-5 and E-8-6 were active (see Fig. 5.3), whereas sub-fractions from E-7 did not possess any activity.

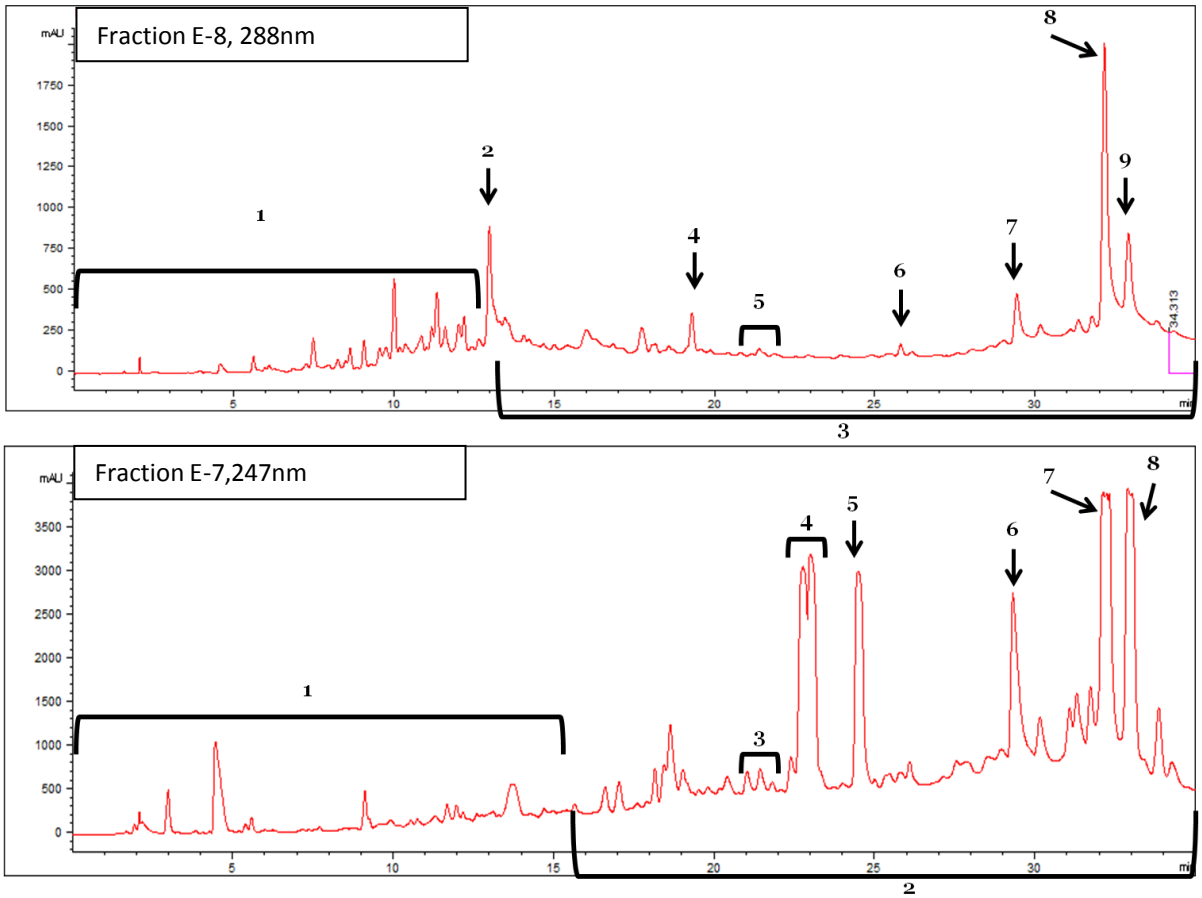

Figure 5.2: HPLC-UV chromatograms for active fractions E-8 (at 288 nm) and E-7 (at 247 nm) and resulting fractions based on peak- and time-based fractionation.

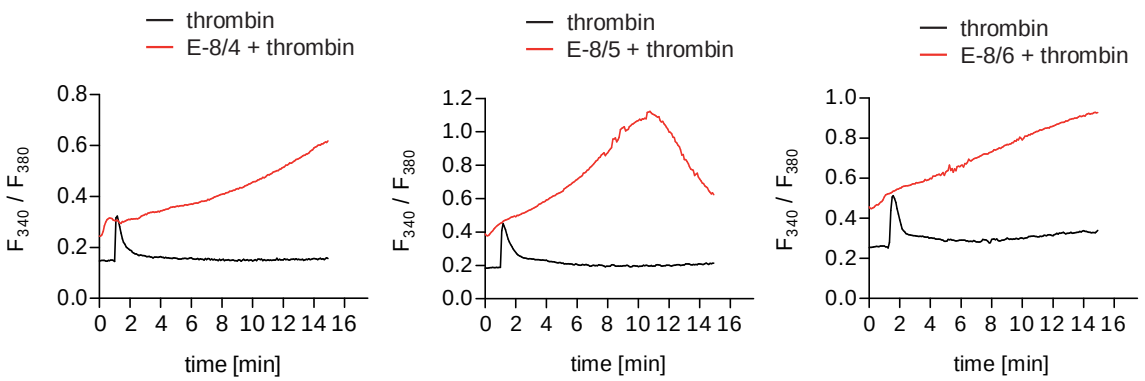

Figure 5.3: Changes in $[Ca^{2+}]_i$ detected by fluorescence microscopy using Fura-2-AM (2 µM) in a static tempered system, with thrombin addition (1 U/mL) at time point 1.0 min after experiment initiation and treatment with fractions E-8-4, E-8-5 and E-8-6 (10 µg/mL) for 30.0 min. One representative experiment out of 3 independently performed experiments (n = 3) is depicted[197]. Only active sub-fractions are shown.

5.2 Discussion and conclusions

In most literature, hawthorn (*Crataegus*) extract is recommended as an oral treatment option for chronic heart failure[219]. Extracts of different *Crataegus* species are used as an adjuvant therapy for patients with CHF. The *Crataegus* WS 1442 extract is approved for treatment in patients with NYHA class II symptoms[191]. Based on positive inotropic, antiarrhythmic, vasodilating, and cardioprotective properties[193,219,220], the efficacy of the extract WS 1442 has been shown in various clinical trials[192,221]. In a previously reported study (Bauhart, 2013)[218], *Crataegus* ethanolic extract was partitioned in H_2O and EtOAc, subsequently, the EtOAc portion was evaporated and nine fractions from a silica gel open column were obtained (Fractions E-1 to E-9). Following Bauhart (2013), this study tested the activity of these fractions and the results exhibited that only E-7 and E-8 were active. Due to the limited amount of these active fractions (E-7 and E-8), only semi-preparative separations were done. Fraction E-7 was separated into 8 sub-fractions, while E-8 was separated into 9 sub-fractions which were all submitted for testing. Sub-fractions from E-7 did not show any activity, while sub-fractions E-8-4, E-8-5 and E-8-6 were active (see Fig. 5.3). Further purification of constituents could not be achieved due to the small amounts of sub-fractions obtained. Thus, to characterise the compounds present in these 3 active sub-fractions, HPLC-MS, GC-MS and NMR (^{1}H and 2D) analyses were carried out. These integrated analyses indicated that E-8-4, -5, and -6 main constituents were fatty acids and triterpenes. Particularly, in all active sub-fractions, fatty acids (stearic acid and palmitic acid) were detected; while triterpene (hyptatic acid A) was detected in E-8-5. This discussion would like to remark that on Bauhart (2013) 4 triterpenes were isolated from fraction E-3 (namely: corosolic acid, pomolic acid, oleanolic acid, and ursolic acid); however the test results on these pure compounds exhibited that they are inactive. Furthermore, based on NMR and GC-MS analysis, this study finds that active sub-fraction E-8-5 is composed of 50% hyptatic acid A and 40% fatty acids (stearic acid and palmitic acid)[197]. This study obtained stearic acid and palmitic acid as references, as well as through collaboration with a Chinese colleague a pure form of hyptatic acid A was acquired. All these pure compounds were tested and found to be inactive. Considering the fact that constituents which comprise almost 90% of active sub-fraction E-8-5 were not active in their pure form, the observed activity strongly relies on the 10% E-8-5 constituents. Although the main active constituents remain to be identified, the findings of this study evidently exhibits that unidentified minor constituent with potent activity or minor constituents with moderate activity which act synergistically, were the main reasons for

observed activity. To certainly identify the molecule(s) responsible for observed activity and to assess their biological interactions, this study recommends the need of further studies on large amounts of optimally prepared *Crataegus* extracts which allows the researcher to end up with suitable amounts of fractions after refined separations. This work has been published in Journal of Planta Medica (Fuchs, *et al.*, 2017)[197].

Chapter 6

6. Materials & Methods

6.1 General approach

Accelerated Solvent Extraction (ASE): Extracts for library screening and HPLC-based activity profiling were prepared with an ASE 200 extraction system with solvent module (Dionex) by extraction with ethyl acetate and methanol, sequentially or petroleum ether, dichloromethane and methanol sequentially. Extraction was performed following a validated method[222]. Approximately 3.00 g of ground plant material was weighed out and mixed with approx. 2.00 g silaceous earth (depending on the plant material size and stickiness). This was packed into an ASE cell with filter at the bottom of the cell. The solvent extraction method was setup according to which sequential extraction was needed. Parameters used were preheat for 1.00 min, heat for 5.00 min, static for 5.00 min, flush with 100% solvent, and purge for 120 sec. The pressure was set at 120 bar, temperature was 70 °C, and three cycles of extraction was done with each solvent. Solvents that were used include petroleum ether, ethyl acetate (EtOAc), methanol (MeOH), and dichloromethane (DCM). Sequential extractions were setup with solvents of increasing polarity.

High Performance Liquid Chromatography (HPLC)-based activity profiling: The in-house extract library samples were submitted to HPLC-based activity profiling for further characterisation of the active compounds. HPLC-based activity profiling was performed on a Waters 2695 Alliance Separation Module equipped with a Waters 996 Photodiode Array Detector and a C18 SunFire column (3.0 x 150 mm; 3.5 µm; Waters). The mobile phase consisted of H_2O (A) and MeCN (B), both with the addition of 0.1% formic acid. A gradient of 5-100% B in 30 min, with 5 min 100% B was applied. The flowrate was 0.4 mL/min. 900 µg of extract were injected in three portions (10 mg/mL, 3 x 30 µL injections) and time-based micro-fractions were collected into a deep well 96-well microtiter plate with a fraction collector Gilson FC204. The microtiter plate was dried in a Genevac EZ-2 evaporating system at 35 °C overnight.

Scale-up for Isolation: Percolation of between 200-300 g of ground plant material was packed into a glass column and saturated with the first solvent of extraction (usually EtOAc), this was left for 1 hour to extract and then the column was eluted for about 3 hours and thereafter left

overnight to extract. Extraction with the first solvent was done for about 24 hours, then the column was left to dry until the next solvent (usually MeOH) was poured into the column for extraction and left for 1 hour before eluting the solvent through. The second round of extraction was usually done for 48 hours. Each extract was evaporated to dryness on the rotatory evaporator (Büchi). Each extract that was active (100 mg/mL; 10 mg/inj x 5) was then separated by HPLC-UV on a semi-preparative scale using an Agilent 1100 Series HPLC system equipped with Diode Array Detector (DAD) and SunFire prep C18 column (10 x 150 mm; 5 µm; Waters). Other columns used were an Atlantis dC18 (10 x 150 mm; 5 µm; Waters), and an Aqua C18 (10 x 250 mm; 5 µm; 125A; Phenomenex). Peak-based fractionation using an optimised method for each extract was done and resulting fractions were evaporated. TLC, HPLC-UV-MS, and microprobe NMR data was collected on the resulting fractions to determine the class of compounds that are responsible for the activity. Using database searches (such as the Dictionary of Natural Products, DNP) and the data collected from various analyses, the class of compounds and sometimes the active compounds could already be identified.

Nuclear Magnetic Resonance (NMR): ^{1}H-NMR and 2D (HSQC, HMBC, COSY and NOESY) spectra of compounds were recorded on a 500 MHz Avance III spectrometer (Bruker BioSpin) equipped with a 1-mm TXI microprobe at 18 °C. Around 0.5 to 1.0 mg of sample is dissolved in 5 to 10 µL of deuterated solvent and centrifuged into a 1.0 mm NMR tube (1.0 x 103.5 mm SampleJet tube, Bruker), which is then capped and labelled. Deuterated solvents are from Armar chemicals. ^{1}H-NMR standard measuring time is 128 scans (± 10.00 min) and depending on S/N ratio, 2D measurements are setup with appropriate number of scans. Standard pulse sequences of the software package Topspin 3.0 were used. For measurements of ^{13}C-NMR spectra, a 5-mm BBO probe is used at 23 °C, with 5.0 or 3.0 mm NMR tubes (depending on sample amount; e.g. for 5mm tubes: ≥ 10 mg in ca. 500 µL solvent, and 3 mm tubes: ≤ 10 mg in 100 µL solvent).

HPLC – Ultraviolet (UV) – Mass Spectrometry (MS) – Evaporative Light Scattering Detector (ELSD): A Shimadzu HPLC system (LC-20 AD) equipped with DAD (SDP-M20A module), triple quadrupole mass spectrometer (LCMS-8030) and ELSD (Alltech 3300) detectors was used for recording the UV, ESIMS and ELSD traces of each sample. Generally, extracts at 10 mg/mL (5-10 µL/injection), fractions at 5 mg/mL (5 µL/injection) and compounds at 1 mg/mL (3-5 µL/injection) are prepared. Spectra are recorded with UV scanning from 190 – 400 nm, MS +/- switching scanning from 160 – 1500 *m/z*, capillary voltage: 4.0 V (3.0 V in negative mode), scan

speed: 6000 u/sec, event time: 0.150 seconds, nebulising gas flow 3 L/min, DL temperature 350 °C, heat block temperature 400 °C, and drying gas flow 15 L/min. ELSD was operated at 2.5 L/min nitrogen flow, 55 °C temperature, and 8 detector gain.

High resolution mass spectra were recorded on a Bruker micrOTOF time-of-flight mass spectrometer with ESI interface (Bruker Daltonics) connected to an 1100 series HPLC Agilent system (HPLC-TOF-ESIMS). A reference solution consisting of sodium formate 0.1% (m/v) in isopropanol:H_2O (1:1) containing 5 mM NaOH was used for calibration. Data acquisition and processing was performed using HyStar 3.0.

Electronic Circular Dichroism (ECD) + optical rotation (α_D): For ECD, an Applied Photophysics Chirascan CD spectrometer with Pro-Data V2.4 software at the Biophysics facility (Biozentrum, University of Basel) was used for measurements. HPLC grade solvents (Scharlau) such as MeOH, or MeCN (cut-off wavelength ≤ 205 nm) were used for dissolving compounds. Blank measurement for background with solvent was done before and auto-subtracted from measurements with compounds. Concentration used is specific to the compound and depends on the UV absorbance. Wavelength range can be setup according to each compound (generally, 205 – 400 nm), with 1 nm bandwidth. For optical rotation measurements, a Jasco P-2000 polarimeter (BrechBühler) with Spectra Manager software and temperature control (BrechBühler) was used with HPLC grade solvents (MeOH or $CHCl_3$, Scharlau). Blank measurements for background with solvent was done before and automatically subtracted from the measurements with compounds. Generally, 1.2 mg of compound is dissolved in 1.2 mL of solvent and carefully added to the cell without the addition of bubbles. Measurements were performed at room temperature (24 to 25.5°C).

6.2 DM1 project

Plant material: 10 plant extracts were prioritised and analysed for their activity in the DM1 project, namely MeOH extract of roots from *Peganum harmala* (Zygophyllaceae), EtOAc extract of roots from *Salvia miltiorrhiza* (Lamiaceae), MeOH extract of leaves from *Bathysa veraguensis* (Rubiaceae), EtOAc extract of leaves from *Lamium album* (Lamiaceae), MeOH extract of the herb from *Pistacia lentiscus* (Anacardiaceae), MeOH extract of stems from *Henriettella tuberculosa* (Melastomataceae), MeOH extract of the leaves from *Henriettella tuberculosa* (Melastomataceae), MeOH extract of leaves from *Casearia arborea* (Flacourtiaceae), MeOH

extract of leaves from *Coccoloba* spp. (Polygonaceae), and MeOH extract of aerial parts from *Struthanthus orbicularis* (Loranthaceae).

Micro-fractionation for activity profiling: For all 10 prioritised extracts a first round of micro-fractionation was performed as described above using the extract library sample. Fractions (60 s each) were collected from 1.00 to 30.00 min with a Gilson FC204. A second round of micro-fractionation for *P. lentiscus*, *H. tuberculosa* (leaves and stems), *Coccoloba* spp., and *S. orbicularis*was performed using an Atlantis dC18 column (5 µm; 4.6 x 150 mm; Waters). The mobile phase consisted of H_2O (A) and MeCN (B), both with the addition of 0.1% formic acid. A gradient of 0-40% B in 30 minutes with a flowrate of 0.5 mL/min was applied. Fractions (60 s each) were collected from 0.00 to 30.00 min and dried on the Genevac overnight. The dried fractions were taken up in 16 µL of DMSO and 2 µL of this was used in the CUG_{78}-MBNL1 inhibition assay.

Polyamide filtration: For filtration over polyamide, ASE extracts of *P. lentiscus*, *C. arborea*, *B. veraguensis*, *H. tuberculosa* (leaves and stems), *Coccoloba* spp., and *S. orbicularis* (approx. 25-50 mg each) were suspended in 2.00 mL 1:1 H_2O:MeOH and eluted through an activated polyamide cartridge (Chromabond, 6 mL / 1000 mg) using a vacuum chamber. Samples were eluted with 20 mL 1:1 H_2O:MeOH and again with 20 mL MeOH through the cartridge, combined and evaporated to dryness.

***Lamium album* semi-preparative isolation:** Methanol ASE extract of *L. album* (Lamiaceae) leaves was dissolved in DMSO (50 mg in 500 µL, 6 mg/inj). Semi-preparative purification of the main UV active peak was collected using an Agilent 1100 Series HPLC system equipped with Diode Array Detector (DAD) and SunFire prep C18 column (10 x 150 mm; 5 µm; Waters). The mobile phases were H_2O (A) and MeCN (B). An isocratic method at 10% B in 20 min was used with UV detection at 233 nm. The fraction was dried under vacuum using a rotavap (Büchi), and freeze dried after organic solvent was removed. The compound in the fraction was identified as aureoside (3.74 mg).

***Salvia miltiorrhiza* extraction:** *S. miltiorrhiza* radix (Lamiaceae) was obtained from China (voucher specimen number: 289). A percolation of EtOAc on ground plant material (406.26 g) was done for 48 hours and resulting extract (4.61 g) was dried under reduced pressure on the rotatory evaporator (see Fig. 6.1).

***S. miltiorrhiza* normal phase open column:** 4.30 g of the EtOAc extract was loaded onto an open silica gel column (6.5 x 60 cm) with starting conditions 95:5 hexane:EtOAc. The column was run isocratic for 3 column volumes, and then sequential portions of hexane:EtOAc 90:10, 50:50, 10:90, and finally with the introduction of MeOH in portions of 90:10 and 0:100 (EtOAc:MeOH). Fractions were combined based on TLC profiles and evaporated to dryness resulting in 17 fractions (A to Q). Fraction H (192.0 mg) crystallised in MeOH to give tanshinone IIA (100 mg), while fraction J (32.1 mg) crystallised in MeOH to give a mixture of the positional isomers – 1,2-dihydrotanshinquinone I and methylenetanshinquinone (20 mg).

***S. miltiorrhiza* semi-preparative purification of compounds:** Fractions F, L, N and O were optimised for separation. Fraction F (12.3 mg) was separated on a semi-preparative scale using a SunFire prep C18 column (10 x 150 mm; 5 µm; Waters) on an Agilent 1100 Series HPLC system equipped with Diode Array Detector (DAD). The mobile phase consisted of H_2O (A) and MeCN (B) and the flowrate was set at 4.0 mL/min. An isocratic method of 75% B in 15 min was applied; UV detection was recorded at 254 nm. The peak eluting at 9.25 min was elucidated as dehydromiltirone (3.1 mg). Fraction L (8.4 mg) was separated using an isocratic method at 70% B for 15 min, the peak eluting at t_R 9.1 min was identified as tanshinone I (2.69 mg). The compound methyltanshinoate (t_R 10.8 min; 1.1 mg) was separated from fraction N (42.7 mg) using an isocratic method at 60% B in 20.00 min. Cryptotanshinone (t_R 12.3 min; 2.37 mg) was separated from fraction O (30 mg/mL) using an isocratic method of 63% B in 15 min.

Separation of positional isomers: The separation of the positional isomers (1,2-dihydrotanshinquinone I and methylenetanshinquinone) was obtained using a Nucleodur 100-5 NH_2 column (4 x 250 mm; 5 µm; Macherey-Nagel; analytical scale) in normal phase with solvents C:D (hexane:IPA). The optimised separation was achieved with isocratic 100% C in 10 min. Compounds eluted at t_R 1.95 and 2.67 minutes. For preparative scale separation a Nucleodur 100-5 NH_2 (21 x 250 mm; 5 µm; Macherey-Nagel) was used in normal phase.

Synthetic tanshinone IIA derivatives: The dicarbonilic group of tanshinone II A, isolated in large amount from *S. miltiorrhiza*, and of the commercially available 9,10-phenanthrenquinone were transformed into oxazole and methyl-imidazole groups, respectively, by reductive amination with methyl amine[198]. Resulting synthetic compounds were coded as TA-II and PQ-1 respectively.

CUG_{78}-MBNL1 inhibition assay: Test plates were prepared according to a validated procedure[199] and is briefly described here. Test substances were added at appropriate concentrations to 45 µL incubation buffer. Wells were washed with anti-HIS antibody and plates were incubated for 1 hour. Various wash steps preceded the incubation time and the colorimetric reaction was performed at 30 °C and 700 rpm for 5 min and stopped with 70 µL of 0.15 M H_2SO_4/well. The optical density was read at λ_{max} 450 nm with a plate reader.

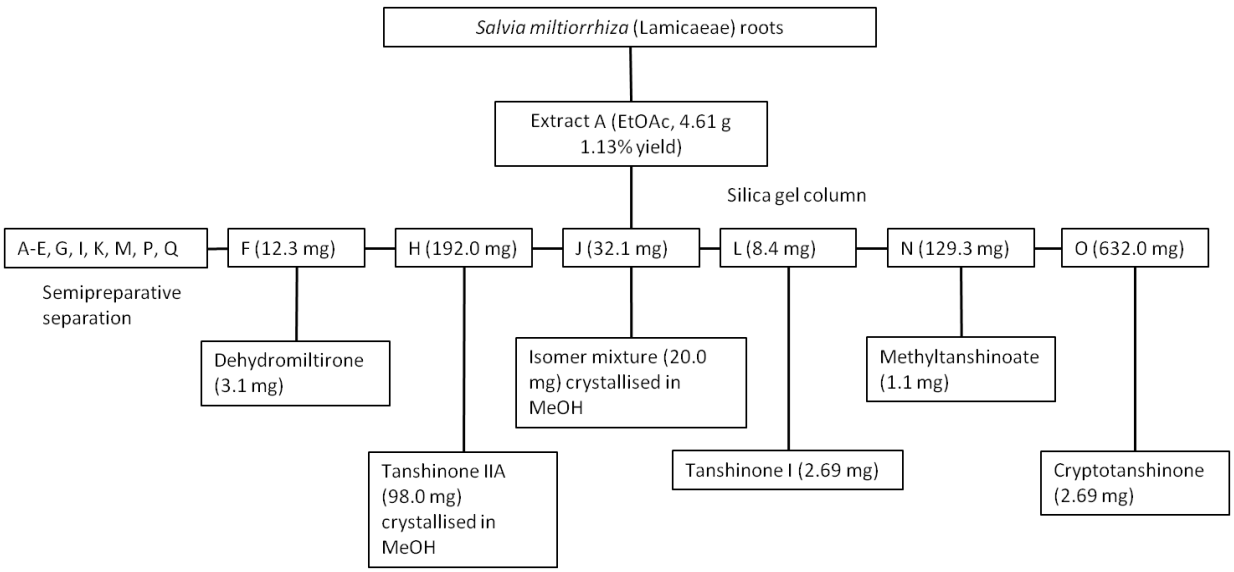

Figure 6.1: Isolation scheme for *Salvia miltiorrhiza* and resulting compounds.

Compound data:

Auroside[223] (La_1): yellow, amorphous solid; $[\alpha]_D$ = -99.7 (*c*, 0.1 in CH_3OH)[224]. ^1H NMR data, see Table A1 in Appendix; ESIMS *m/z* 429.0 $[M + Na]^+$; t_R: 7.9 min.

Methyltanshinoate (Sm_N2): orange, amorphous solid; $[\alpha]_D$ = -91.5 (*c*, 0.02 in $CHCl_3$). ^1H NMR data, see Table A2 in Appendix; ESIMS *m/z* 339.2 $[M + H]^+$; t_R: 23.8 min.

Cryptotanshinone (Sm_O2): yellow-orange, fine needles; $[\alpha]_D$ = -35.6 (*c*, 0.06 in $CHCl_3$). ^1H NMR data, see Table A2 in Appendix; ESIMS *m/z* 297.2 $[M + H]^+$; t_R: 25.4 min.

Tanshinone I (Sm_L2): red-yellow, fine needles; $[\alpha]_D$ = -1319.6 (*c*, 0.13 in $CHCl_3$). ^1H NMR data, see Table A2 in Appendix; ESIMS *m/z* 277.1 $[M + H]^+$; t_R: 25.8 min.

1,2-dihydrotanshinquinone I (Sm_J_XTL): purple, fine crystalline powder; $[\alpha]_D$ = -1989.0 (*c*, 0.1 in $CHCl_3$). ESIMS *m/z* 279.1 $[M + H]^+$; t_R: 26.7 min.

Methylenetanshinquinone (Sm_J_XTL): purple, fine crystalline powder; $[\alpha]_D$ = -5050.5 (*c*, 0.1 in $CHCl_3$). ESIMS *m/z* 279.1 $[M + H]^+$; t_R: 26.7 min.

Dehydromiltirone (Sm_F1): red, amorphous solid; $[\alpha]_D$ = -6.62 (*c*, 0.08 in $CHCl_3$). ^1H NMR data, see Table A2 in Appendix; ESIMS *m/z* 281.2 $[M + H]^+$; t_R: 27.7 min.

Tanshinone IIA (Sm_H_XTL): red-orange, amorphous solid; $[\alpha]_D$ = -12.3 (*c*, 0.09 in $CHCl_3$). ^1H NMR data, see Table A2 in Appendix; ESIMS *m/z* 295.2 $[M + H]^+$; t_R: 28.4 min.

6.3 TB project

Plant material: Dried roots of *Dorstenia contrajerva* L. (Moraceae) was obtained from Parque Nacional Soberania, camino de Plantacion, Panama (Florpan No. 5683). Dried bulbs of *Pancratium littorale* Jacq. (Amaryllidaceae) were obtained from Costa Arriba, Cuango, Colón, Panama (Florpan No. 5518). A voucher specimen for each plant was deposited in the Pharmaceutical Biology Division at the University of Basel (plant number 837 and 836, respectively).

Extraction: For *D. contrajerva*, 158.3 g of the plant material was powdered by cryomilling, mixed with quartz sand and extracted by percolation at room temperature sequentially with EtOAc (extracted over the duration of 48 hours with 5 L of solvent) and methanol (allowed to extract overnight and percolated the day after with 5 L of solvent). The extracts were evaporated to dryness under reduced pressure to yield 3.23 g (2.04% yield) and 3.31 g (2.10% yield), respectively.

For *P. littorale*, 301.5 g of the plant material was powdered by cryomilling, mixed with quartz sand and extracted by percolation at room temperature sequentially with ethyl acetate (extracted over the duration of 48 hours) and methanol (extracted over the duration of 48 hours). The extracts were evaporated to dryness under reduced pressure to yield 3.34 g (1.1% yield) and 45.05 g (14.9% yield), respectively.

Micro-fractionation for activity profiling: For both extracts the first round of micro-fractionation was followed as described above with collection of 31 fractions of 60 s each, starting from min 0.00 until 31.00 with a Gilson FC204. The dried fractions were taken up in 4 µL of DMSO, and diluted into 16 µL media (1:5 dilution) which was used in the promoter based screening assay. For the micro-fractions – where the weight is not known – each well was

treated in the same way, 2 µL of the 5x diluted solutions were added to 198 µL cell suspension, which made up a total volume of 200 µL. Therefore the micro-fractions were further diluted by 1:100 times for their final concentration.

A second round of micro-fractionation for *P. littorale* was performed using an Aqua C18 column (250 x 4.60 mm; 5µm; Phenomenex). The mobile phase consisted of H_2O (A) and MeCN (B), both with the addition of 0.1% formic acid. A gradient of 0-50% B in 30 minutes with a flowrate of 0.6 mL/min was applied.

Isolation of furanocoumarins: 100 mg of the ethyl acetate extract of *D. contrajerva* was dissolved in 1.0 mL of MeOH. This solution was prefiltered through a small C18 cartridge (under vacuum) to remove very lipophilic compounds. The remaining extract was dried under nitrogen flow and redissolved in DMSO (at 25 mg/mL). Semi-preparative purification of the two main UV active peaks were collected using an Agilent 1100 Series HPLC system equipped with Diode Array Detector (DAD) and SunFire prep C18 column (10 x 150 mm; 5 µm; Waters). The mobile phases were H_2O (A) and MeCN (B). A gradient of 5-100% B in 30 min with a 5 min 100% B, UV detection was done at 254 and 310 nm. Fractions were dried under vacuum using a rotavap (Büchi), and freeze dried after organic solvent was removed. The two compounds (bergapten and dorstenin) crystallised out of solution and NMR data were recorded at 500 MHz with a 1-mm TXI probe for structure elucidation.

Quantification of bergapten and dorstenin by UV: for the UV quantification of the two major furanocoumarins in *D. contrajerva*, the Alliance 2695 system coupled with a DAD 996 was used. Wavelength was 310 nm and calibrators (0.05, 0.1, 0.2, 0.25 and 0.5 mg/mL) were prepared from the pure compounds previously isolated as described above. All calibrators and samples were injected in triplicates and mean ± SD was calculated (acceptable range of SD was ± 15%).

Quantification by ^{1}H-NMR: ^{1}H NMR spectra were recorded at 18 °C in DMSO-*d6* (Armar Chemicals, Switzerland) on a Bruker Avance III^{TM} 500 MHz NMR spectrometer equipped with a 1-mm TXI probe. Data were processed with Topspin 3.2 software (Bruker). For quantification of the two *Dorstenia* compounds, 1,3,5-trimethoxybenzene (>99 pure, Sigma-Aldrich) was used as internal standard. Quantitative ^{1}H NMR was carried out using the pulse program zg30 (Bruker) with a recycle delay of 20 sec (>5xT1). Two dummy scans, 128 scans, and a sweep width of 11 ppm, covering 64 K data points, provided the FID. Processing of the spectra included zero filling

(x1) and multiplication of the FID by an exponential decay apodization function of 0.3 Hz prior to Fourier transformation. A digital filter (baseopt; Bruker) improved the automatic baseline correction, which was performed before signal integration. Reference signals for integration were δ = 7.32 (bergapten), δ = 6.09 (IS) and δ = 5.54 (dorstenin).

The sample was prepared and measured in triplicate as follows.

50 µL (0.5 mg) of the extract library sample (10 mg/mL) was transferred into an HPLC vial and lyophilised over night on the freeze dryer, this was prepared in triplicate. A stock solution of the internal standard, 1,3,5-trimethoxybenzene (in DMSO-*d6*, 10 mg/mL) was prepared. The dried extract samples were then taken up in 9.7 µL DMSO-*d6*. 3 µL of the internal standard ($1.78x10^{-4}$ mmol/L) was added as a reference to each sample to make a total volume of 10 µL and transferred into an NMR tube for measurement.

Macro-fractionation for *D. contrajerva* activity profiling: 47.5 mg of extract was dissolved in DMSO at a concentration of 25 mg/mL and centrifuged for 15 min at 14.5 rpm. Supernatant was removed and injected onto a semi-preparative SunFire prep C18 column (10 x 150 mm; 5 µm; Waters) using an Agilent 1100 Series HPLC system equipped with Diode Array Detector (DAD). The mobile phase consisted of H_2O (A) and MeCN (B). A gradient of 5-100% B in 30 min with 5 min isocratic at 100% B, UV detection was recorded at 254 and 310 nm. Flowrate used was 4.0 mL/minute. Two injections of 400 µl (25 mg) and time-based fractions (1.00 minute/fraction) were collected into 6 mL test tubes (rack 21) from 0.00 to 35.00 minutes (35 fractions) using a Gilson FC204. Test tubes were directly dried in the Genevac EZ-2 evaporating system at 27 °C overnight and transferred into small vials for exact weights. The dried fractions were dissolved at a concentration of 10 mg/mL and tested in the promoter based screening assay at 10 and 5 µg/mL on the cells.

Diaion filtration of *P. littorale* extract: 45.05 g of the extract was suspended in 800 mL H_2O (pH 3.0) and loaded onto column packed with diaion (HP-20). Extract was eluted slowly to allow adsorption onto beads. Column was then eluted with 3 volumes (about 4 L) of H_2O (pH 3.0) to wash out sugar portion. Methanol was used thereafter as eluent to collect the remaining extract and acetone was used to wash the diaion column after use (see Fig. 6.2).

Alkaloid extraction: Using 3.09 g of the remaining methanol extract after diaion, enrichment of alkaloids was done in two portions (1.31 g first round and 1.78 g second round). Briefly, the

extract was suspended in 200 mL of 0.25 M H_2SO_4 solution (pH 3.0) and partitioned in a separating funnel with $CHCl_3$ (200 mL x 3) to remove the lipophilic compounds. The aqueous portion was then basified to pH 10.0 with NH_3 solution (about 2-3 mL). The alkaline aqueous solution was then partitioned with DCM (200 mL x 3, NaCl was added to break the foamy layer formed in between) to collect the enriched alkaloid portion. The remaining aqueous portion was neutralised before freeze drying.

Diol cartridge of alkaloid portion: The alkaloid portion (261.1 mg) was loaded (in 3.0 mL starting conditions) onto a Sepacore diol cartridge (40-63 µm; 40 g; 16 bar; Büchi) using the PuriFlash system (Interchim PuriFlash 4100 module). Normal phase chromatography was used with a solvent system of MeOH (B), DCM (C), and IPA (D) following the elution gradient starting at 0:99:1 (B:C:D) to 0:80:20 (B:C:D) in 100 min, then 0:0:100 (B:C:D) for 60 min, and held for 5 min, thereafter 10:90:0 (B:C:D) in 5 min, and 20:80:0 (B:C:D) in 25 min, and finally 50:50:0 (B:C:D) for 45 min to elute remaining compounds out. A flowrate of 5 mL/min was setup and collection volume was 6 mL/tube. Fractions were combined based on TLC profiles and evaporated to dryness on the rotavap (Resulting in 13 diol fractions).

Semi-preparative HPLC-UV-MS for isolation of alkaloid compounds: For each resulting diol fraction separation conditions were optimised on a reverse phase analytical column (Reprosil-Pur Basic-C18; 3.0 µm; 150 x 3.0 mm; Dr Maisch) under basic conditions (pH 9.0). Separation was performed on a semi-preparative scale with the column Reprosil-Pur 100 Basic-C18 (5.0 µm; 150 x 10.0 mm with pre-column 30.0 x 10.0 mm; Dr Maisch) on an Agilent 1100 Series equipped with DAD (scanning 190-400 nm) and MSD (scanning 150-1500 m/z). Solvent system was made up of H_2O adjusted to pH 9.0 with NH_3 solution (A) and 8:1:1 of MeCN:IPA:solution A (B) and the flowrate was set to 4.0 mL/min.

Diol fractions G to I, K, and M were optimised for separation. A gradient of 5-32% B in 17.00 min, 32% B isocratic for 10.00 min and 100% B for 5.00 min was applied for the separation of fraction G (27.85 mg in 500 µL DMSO, 5 mg/inj). For fraction H (31.51 mg in 600 µL, 5 mg/inj), a method of 5-20% B for 5.00 min, 20-24% B until 21.00 min, 24-38% B for 1.00 min, 38-42% B in 2.00 min and 100% B for 5.00 min was used. A separation method of 2-9% B in 5.00 min, 9% B isocratic for 5.00 min, 9-15% B in 1.00 min, 15-42% B for 16.00 min and 100% B for 5.00 min was applied for fraction I (16.46 mg in 400 µL DMSO, 2 mg/inj). The separation method for fraction K (41.86 mg in 700 µL DMSO, 6 mg/inj) was 2-46% B in 14.00 min, 46-52% B in 1.00

min, 52% B isocratic for 5.00 min, and 100% B for 5.00 min. Detection for fraction K, and M was only UV at λ_{max} 254 and 290 nm. Fraction M (15.3 mg in 400 µL DMSO, 4 mg/inj) was separated using a method of 2-15% B for 5.00 min, 15-18% B in 4.00 min, 18-19% B in 2.00 min, 19-22% B in 3.00 min, 22-23% B in 3.00 min, 23-31% B in 5.00 min, 31-32% B in 1.00 min, 32-35% B in 1.00 min, and 100% B for 5.00 min.

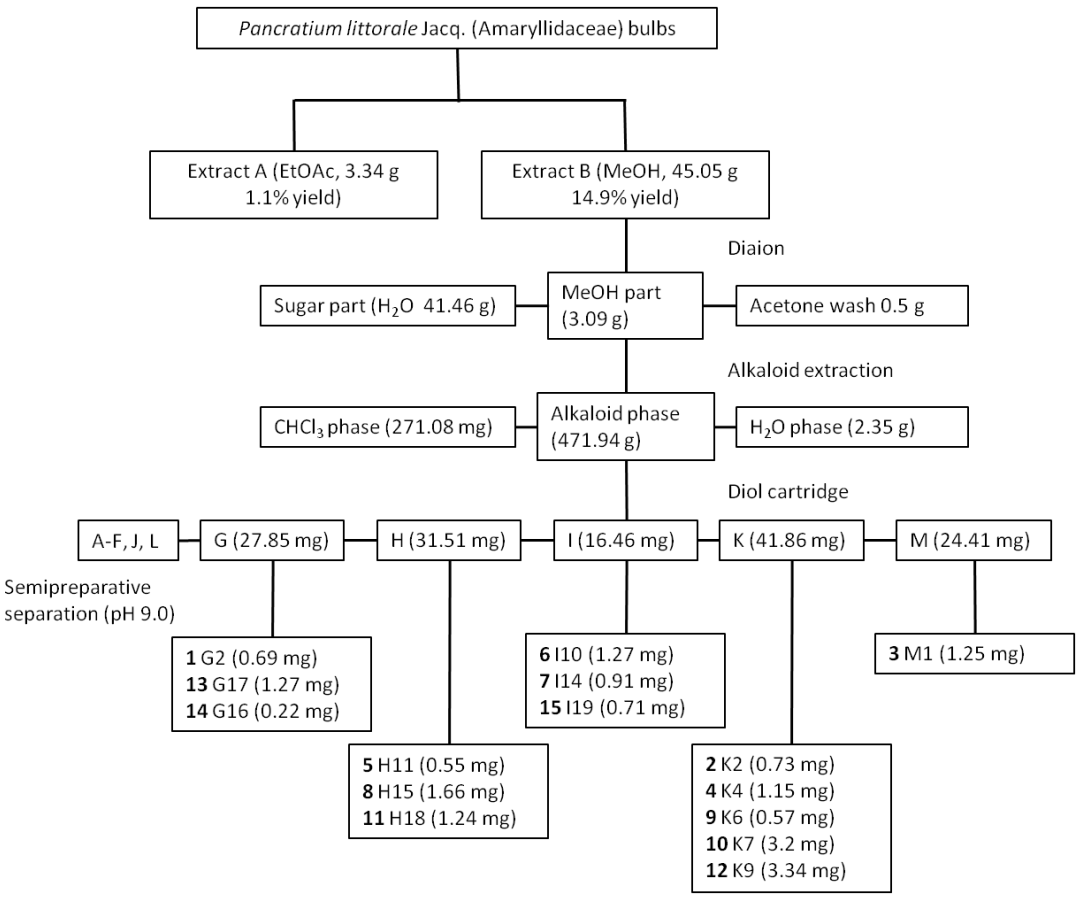

Figure 6.2: Isolation scheme for *Pancratium littorale* and resulting compound codes and numbers.

RBL GFP (Coronin-1 promoter) and RBL RFP (CMV promoter) cells: Stably transfected Rat Basophil Leukemia (RBL) with Green Fluorescence Protein (GFP) expression under control of coronin-1 promoter was generated by transfecting a promoterless plasmid containing the essential 1.5 kb promoter element of coronin-1 upstream of destabilised GFP (Clonetech). Likewise, a promoterless plasmid with an early cytomegaloviral (CMV) promoter driving the expression of Red Fluorescent Protein (RFP) served as internal control for non-specific promoter inhibition and toxicity during the screening. The promoter sequences were verified by sequencing (Microsynth).

Western blotting: RBL-GFP cells were seeded at a density of 50'000 cells/well on a 96 well plate in a volume of 200 µl of phenol red free RPMI media supplemented with 8% fetal bovine serum and penicillin (100 U/ml), streptomycin (100 mg/ml) and L-glutamine (2 mM) along with compounds and vehicle controls. The cells were incubated in a humidified incubator at 37 ^{o}C for 72 hrs and later they were replenished with freshly prepared compounds and further incubated for another 48 to 72 h. Subsequently, the cells were washed in Phosphate Buffered Saline (PBS) and lysed in RIPA lysis buffer (0.1% SDS, 50 mM Tris, 1% NP-40, 0.5% sodium deoxycholate, 1mM $MgCl_2$, 100 mM NaCl, 1mM EDTA) with protease and phosphatase inhibitors (Roche). Protein amounts were estimated using a BCA kit (Thermo) and equal protein amounts (15 µg per lane) were loaded onto a 12.5% SDS-PAGE and run under denaturing condition, transferred onto a nitrocellulose membrane and immunoblotted with rabbit anti-coronin-1 antibody (Serum 320, 1:5000, in-house generated) and mouse anti-actin antibody (mAB H1501, 1:5000, Merck Millipore) followed by Infrared dye-tagged secondary antibodies (LI-COR) and imaged using an Odyssey CLx system (LI-COR). Coronin-1/actin ratiometric analysis of Western blot data was performed using Image Studio Lite Software.

Synergy plate reader: RBL-GFP cells were seeded at a density of 50'000 cells/well on a 96 well plate in a volume of 200 ml of phenol red free RPMI media supplemented with 8% fetal bovine serum and penicillin (100 U/ml), streptomycin (100 mg/ml) and L-glutamine (2 mM) along with compounds and vehicle controls. The cells were incubated in a humidified incubator at 37 ^{o}C and at indicated time points, the GFP fluorescence intensity was measured using a Synergy H4 hybrid microplate reader system (Biotek).

Compound data:

Bergapten (DcA1): white, fine needles; $[\alpha]_D$ = +0.03 (*c*, 0.04 in $CHCl_3$). ^{1}H NMR data, see Table A3 in Appendix; ESIMS *m/z* 217.0 $[M + H]^+$; t_R: 18.45 min.

Dorstenin (DcA2): yellow, amorphous solid; $[\alpha]_D$ = -7.76 (*c*, 0.09 in $CHCl_3$). ^{1}H NMR data, see Table A3 in Appendix; ESIMS *m/z* 369.2 $[M + H]^+$; t_R: 21.5 min.

8-demethoxy-lycoranine F (Pl_G2, **1**): yellow, amorphous solid; $[\alpha]_D$ = +47.0 (*c*, 0.06, CH_3OH). ^{1}H NMR data, see chapter 4; HRESIMS (*m/z* 288.1237 $[M+H]^+$; calculated for $C_{16}H_{18}NO_4^+$: 288.1230); t_R: 7.2 min.

8-*O*-demethyl-homolycorine (Pl_K2, **2**): yellow, amorphous solid; $[\alpha]_D$ = +43.71 (*c*, 0.05, $CHCl_3$). ^1H NMR data, see Table A4 in Appendix; ESIMS *m/z* 301.9 $[M+H]^+$; t_R: 7.7 min.

pseudo-lycorine (Pl_M1, **3**): yellow, amorphous solid; $[\alpha]_D$ = +2.38 (*c*, 0.09, CH_3OH). ^1H NMR data, see Table A6 in Appendix; ESIMS *m/z* 289.8 $[M+H]^+$; t_R: 10.1 min.

8-*O*-demethyl-lycorenine (Pl_K4, **4**): yellow, amorphous solid; $[\alpha]_D$ = +82.4 (*c*, 0.11, $CHCl_3$). ^1H NMR data, see chapter 4; HRESIMS (*m/z* 304.1547 $[M+H]^+$; calculated for $C_{17}H_{22}NO_4^+$: 304.1543); t_R: 10.8 min.

7-demethoxy-10-*O*-methyl-hostasine (Pl_H11, **5**): white, amorphous solid; $[\alpha]_D$ = -38.28 (*c*, 0.05, $CHCl_3$). ^1H NMR data, see Table A5 in Appendix; ESIMS *m/z* 347.9 $[M+H]^+$; t_R: 11.5 min.

Carinatine (Pl_I10, **6**): white, amorphous solid; $[\alpha]_D$ = -28.56 (*c*, 0.02, $CHCl_3$). ^1H NMR data, see Table A6 in Appendix; ESIMS *m/z* 303.8 $[M+H]^+$; t_R: 11.7 min.

Lycorine (Pl_I14, **7**): white, solid precipitate; $[\alpha]_D$ = -9.07 (*c*, 0.07, $CHCl_3$). ^1H NMR data, see Table A6 in Appendix; ESIMS *m/z* 287.9 $[M+H]^+$; t_R: 12.0 min.

10-*O*-methyl-hostasine (Pl_H15, **8**): yellow, amorphous solid; $[\alpha]_D$ = -70.52 (*c*, 0.08, $CHCl_3$). ^1H NMR data, see Table A5 in Appendix; ESIMS *m/z* 377.9 $[M+H]^+$; t_R: 12.5 min.

10-deoxy-3-hydroxy-6-hydroxy-hippeastidine (Pl_K6, **9**): yellow, amorphous solid; $[\alpha]_D$ = +25.7 (*c*, 0.05, $CHCl_3$). ^1H NMR data, see chapter 4; HRESIMS (*m/z* 306.1706 $[M+H]^+$; calculated for $C_{17}H_{24}NO_4^+$: 306.1700); t_R: 13.0 min.

Narcissidine (Pl_K7, **10**): dark yellow, amorphous solid; $[\alpha]_D$ = -49.65 (*c*, 0.1, $CHCl_3$). ^1H NMR data, see Table A7 in Appendix; ESIMS *m/z* 333.9 $[M+H]^+$; t_R: 14.1 min.

1-*O*-acetyl-pseudo-lycorine (Pl_H18, **11**): yellow, amorphous solid; $[\alpha]_D$ = -60.0 (*c*, 0.06, $CHCl_3$). ^1H NMR data, see Table A6 in Appendix; ESIMS *m/z* 331.8 $[M+H]^+$; t_R: 15.0 min.

8-*O*-demethyl-6-*O*-methyl-lycorenine (Pl_K9, **12**): dark yellow, amorphous solid; $[\alpha]_D$ = +130.8 (*c*, 0.11, $CHCl_3$). ^1H NMR data, see Table A4 in Appendix; ESIMS *m/z* 317.8 $[M+H]^+$; t_R: 15.5 min.

3-*O*-acetyl-narcissidine (Pl_G17, **13**): yellow, amorphous solid; $[\alpha]_D$ = -146.16 (*c*, 0.05, $CHCl_3$). ^1H NMR data, see Table A7 in Appendix; ESIMS *m/z* 375.9 $[M+H]^+$; t_R: 15.8 min.

10-deoxy-6(α)-hydroxy-hippeastidine (Pl_G16, **14**): yellow, amorphous solid; $[\alpha]_D$ = +6.44 (*c*, 0.027, $CHCl_3$). ^1H NMR data, see Table A8 in Appendix; ESIMS *m/z* 319.8 $[M+H]^+$; t_R: 16.0 min.

6-hydroxy-hippeastidine (Pl_I19, **15**): white, amorphous solid; $[\alpha]_D$ = +19.3 (*c*, 0.014, $CHCl_3$). ^1H NMR data, see Table A8 in Appendix; ESIMS *m/z* 335.9 $[M+H]^+$; t_R: 16.2 min.

6.4 Lymphatic project

Plant material: Dried root bark of *Daphne giraldii* (Thymelaceae) was obtained (500 g) from Bozhou herbal market in Bozhou city, Anhui, China. A voucher specimen for the plant was deposited in the Pharmaceutical Biology Division at the University of Basel (plant number 351).

Extraction: For *D. giraldii*, 474.61 g of plant material was powdered by cryomilling before extraction by percolation at room temperature sequentially with DCM (extracted over 48 hours with 4 L of solvent), EtOAc (extracted over 48 hours with 4 L of solvent) and MeOH (extracted with 4 L of solvent over 48 hours). The extracts were evaporated to dryness under reduced pressure to yield 13.34 g (2.8% yield), 8.23 g (1.7% yield), and approximately 60 g (approx. 12% yield), respectively (see Fig. 6.3).

Micro-fractionation for activity profiling: For *D. giraldii* extract, the first round of micro-fractionation was followed as described above with collection of 29 fractions of 60 s each, starting from min 1.00 until 30.00 with a Gilson FC204. The dried fractions were taken up in 50 µL of DMSO and diluted 1:100 times with the medium. All test samples were further diluted (1:10 times) and tested in the 3D sprouting assay (total volume per well is 160 µL).

Micro-fractionation on the 4 active normal phase fractions (Dgi-E, Dgi-F, Dgi-G, Dgi-H) from the silica column was performed to localize the region of activity in each. This was performed using a C18 SunFire column (3.0 x 150 mm; 3.5 µm; Waters) on a Shimadzu HPLC system equipped with DAD (SPD-M20A, Shimadzu), ELSD (3300, Alltech), and ESIMS (LCMS-8030, Shimadzu). The mobile phase consisted of H_2O (A) and MeCN (B), both with the addition of 0.1% formic acid. A gradient of 5-100% B in 30 min, with 10.00 min 100% B isocratic was applied. The flowrate of 0.4 mL/min was applied. Fractions were collected time-based starting from 2.00 until 35.00 min (33 fractions of 60 s each). UV trace was tracked online, while ELSD and ESIMS was recorded offline after fractions were collected. The dried fractions were tested at a 1x and a 10x dilution in the 3D sprouting assay.

Normal phase column chromatography: The DCM extract was dry loaded (adsorbed to silica) onto a pre-packed silica cartridge (Si-HP, 30 µm, 120 g, 20 bar, Interchim PuriFlash) using the PuriFlash system (Interchim PuriFlash 4100 module). A solvent system of MeOH (B), Hexane (C), and EtOAc (D) following the elution gradient in Table 6.1. A flowrate of 30 mL/min was setup and collection volume was 15 mL/tube (30 sec). UV was recorded at 254 nm and scanning from 220 to 600 nm. Fractions were combined based on TLC profiles and evaporated to dryness on the rotavap (resulting in 8 fractions, A to H). This process was repeated four times with 0.99 g (run 1), 1.35 g (run 2), 4.52 g (run 3), and 3.13 g (run 4) of the extract.

Table 6.1: Elution steps for gradient of the DCM extract from *D. giraldii*.

Time	%B	%C	%D
00 s	00	95	05
38 s	00	94	06
04:21	00	94	06
04:24	00	93	07
04:47	00	93	07
04:57	00	92	08
05:03	00	92	08
05:41	00	90	10
10:23	00	90	10
13:47	00	79	21
18:48	00	79	21
43:47	00	00	100
44:47	50	00	50
48:47	50	00	50
49:47	100	00	00
53:47	100	00	00
01:02:14	100	00	00

Speed-Centrifugal-Partition-Chromatography (SCPC) on Dgi-E, -F, -G, and -H: The SCPC system (AlphaCrom SCPC-250) was kindly borrowed from AlphaCrom (Dr. Thomas Pfeiffer). Components of the system include AlphaCrom SCPC-250 (sample size up to 5 g, rotor volume 250 mL), diode array detector 335 (190 – 950 nm, flowrate into flow cell up to 1 000 mL/min), sample loading loop (10 mL volume), Pump 210 (flow 0.01-100 mL/min, low pulsation), and a fraction collector (FC 701). An appropriate liquid phase system was selected based on the distribution of compounds in the upper and lower phases monitored by TLC and HPLC-UV-MS. Solvent system selected for all four fractions was hexane:EtOAc:MeOH:H_2O 1:1:1:1. The upper phase (hexane:EtOAC) was used as a stationary phase (SP) while the lower phase (MeOH:H_2O) was used as the mobile phase (MP). Solvents were mixed in a separating funnel by shaking

thoroughly. The flowrate for loading of the solvent systems was set at 20 mL/min with the rotor at 500 rpm (or acceleration of 21 G), and the run time flowrate was set at 5 mL/min with 2 000 rpm (or 332 G). UV was monitored at 254 nm. Once stationary and mobile phases were equilibrated into the system, the sample was taken up into 10 mL of 1:1 ratio of the two phases (volume depends on size of injection loop) and injected into the rotor (column). Instrument was run in DSC mode (descending) while MP was passed through; thereafter the instrument was switched to ASC mode (ascending) to push the SP out. Fractions were collected every 2.00 min (10 mL/tube) and the pressure was maintained at 54 bar.

Fraction E was loaded into four parts (100 mg in 1.0 mL, 500 mg in 10 mL, 500 mg in 10 mL, and 1.5 g in 10 mL). MP was run for 30, 60, 40 and 40 min, respectively while SP was run for 30 min each time. Fraction F was loaded one time (680.68 mg in 10 mL) with MP run for 44 min and SP for 30 min. Fraction G was also loaded one time (89.15 mg in 10 mL) with MP runtime of 39 min and SP runtime of 28 min. Fraction H was loaded in two parts (1.0 g in 10 mL, and 0.6 g in 10 mL) with MP runtime of 50 and 41 min, respectively, while SP runtime was 30 min each time. Fractions were monitored by HPLC-UV-MS and combined based on their similarities to give fractions E-a to E-i (9 fractions), F-a to F-i (9 fractions), G-a to G-j (10 fractions) and H-a to H-k (11 fractions). All CPC fractions were tested at 10 µg/mL.

CPC fraction Ed semi-preparative sub-fractionation: 45.9 mg of Ed was dissolved in 230 µL of DMSO and separated by semi-preparative HPLC-UV on a C18 SunFire HPLC column (10.0 x 150 mm; 5 µm; Waters). The mobile phase consisted of H_2O (A) and MeCN (B) with a gradient of 20 to 70% B in 25 min. The flowrate was 4.0 mL/min. Detection was set at UV 210, and 320 nm. Aliquots of 50 µL (3 times) and 75 µL (2 times) were injected. Eleven fractions were obtained (fractions Ed-1 to Ed-11), by using a combination of peak-based and time-based collection. Sub-fractions were tested at 10, 1 and 0.1 µg/mL. ^{1}H-NMR spectra of active fractions were recorded on an Avance III spectrometer (Bruker) equipped with a 1-mmTXI microprobe. Fraction Ed-8 was elucidated to be daphneolone.

Semi-preparative micro-fractionation of Ed-9, -10, and -11: Ed-9, Ed-10 and Ed-11 were further separated by semi-preparative HPLC-UV, using the same column and solvent system as above just with optimised conditions for each. For Ed-9 (1.89 mg in 200 µL DMSO), two injections of 100 µL each were separated with 45% B isocratic for 16 min and a 5 min 100% B wash fraction was collected at the end. Detection was set at UV 254, 205 and, 320 nm. For Ed-10 (1.09 mg in

200 µL DMSO), 2 injections of 100 µL each were separated with a gradient of 38 to 40% B in 35 min, 40% B isocratic for 1 min followed by 5 min of 100% B. Detection was set at UV 205, 320 and, 270 nm. For Ed-11 (1.95 mg in 200 µL DMSO), 2 injections of 100 µL each were separated with a gradient of 35 to 85% B in 20 min, followed by 5 min of 100% B. Detection was set at UV 254, and 320 nm.

A total of 35 micro-fractions were obtained (fractions Ed-9-1 to Ed-9-10; Ed-10-1 to Ed-10-6; and Ed-11-1 to Ed-11-9), by using a combination of peak-based and time-based collection. ^{1}H-NMR spectra and HPLC-UV-MS-ELSD data of all micro-fractions were recorded before sending an aliquot of each for testing. Micro-fractions were tested at 10, and 1 µg/mL.

Semi-preparative isolation of compounds from CPC fraction Ea: 86 mg were dissolved in 430 µL DMSO (200 mg/mL concentration). Aliquots of 100 µL each were injected and separated by semi-preparative HPLC-UV on a C18 SunFire HPLC column (10.0 x 150 mm; 5 µm; Waters). The mobile phase consisted of H_2O (A) and MeCN (B). A gradient of 10-50% B in 20 min, with a 5 min 100% B wash was applied. The flowrate was 4.0 mL/min. Detection was set at UV 254, and 277 nm. Twelve fractions were obtained (fractions Ea-1 to Ea-12), by using a combination of peak-based and time-based collection. Fractions Ea-4 and Ea-12 crystallised upon drying under nitrogen flow. Crystals from these samples were cleaned up with cold MeOH and elucidated to be daphnetin and chrysoeriol, respectively.

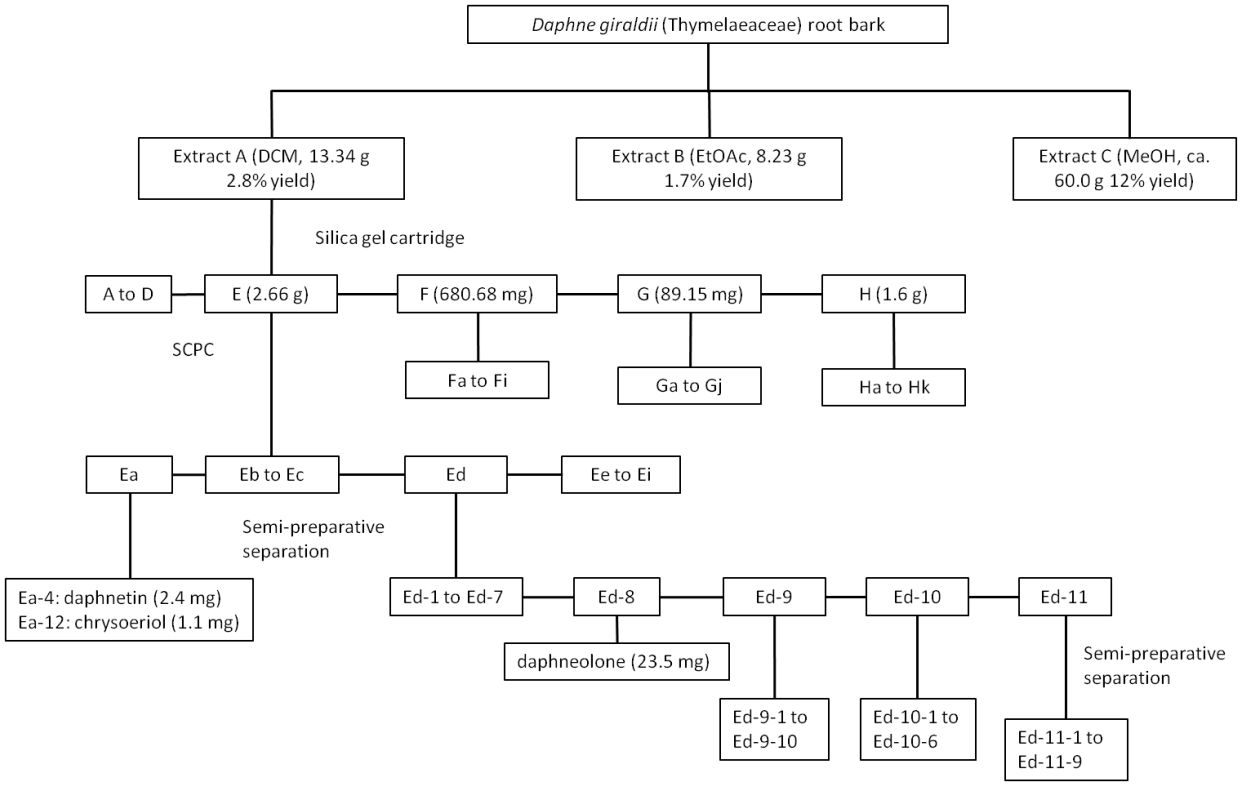

Figure 6.3: Isolation scheme for *Daphne giraldii* and resulting compounds, fractions, sub-fractions and micro-fractions.

3D sprouting assay: The assay was developed at the ETH Zürich. It is a phenotypic screening of novel inducers of lymphatic vessel growth in a 3D sprouting assay. Human dermal microvascular lymphatic endothelial cells (LECs) were coated onto gelatin-covered cytodextran microcarrier beads (Sigma) and labelled with cell tracker green (CTG, Invitrogen). Fully LEC-covered beads were embedded into collagen type I hydrogels in black clear-bottom 96-well plates. Plates are incubated at 37 °C with / without the addition of test samples for 24 hours and afterwards fixed with 1% paraformaldehyde. Extracts from the library were tested at 10 µg/mL, with 0.1% DMSO as a negative control and 10 µg/mL *Iris germanica* extract as a positive control. Automated imaging and analysis of number of sprouts / bead was used as a readout for positive inducers of LEC growth[154].

Compound data:

Daphnetin (Dgi_Ea_4_XTL): white, amorphous solid; $[\alpha]_D$ = +0.92 (*c*, 0.1, CH_3OH). ^1H NMR data, see Table A9 in Appendix; ESIMS *m/z* 178.7 $[M+H]^+$; t_R: 10.2 min.

Chrysoeriol (Dgi_Ea_12_XTL): yellow, amorphous solid; $[\alpha]_D$ = +0.89 (*c*, 0.1, CH_3OH). ^1H NMR data, see Table A9 in Appendix; ESIMS *m/z* 300.8 $[M+H]^+$; t_R: 16.8 min.

Daphneolone (Dgi_Ed_8): yellow, oil; $[\alpha]_D$ = +57.05 (*c*, 0.1, $CHCl_3$). ^1H NMR data, see Table A9 in Appendix; ESIMS *m/z* 270.8 $[M+H]^+$; t_R: 18.5 min.

6.5 CHF project

***Crataegus* extract semi-preparative isolation:** From an ongoing project, two fractions were found active (fractions E-7 and E-8) and further separated by semi-preparative HPLC-UV. Fraction E-8 (92 mg) was dissolved in DMSO-THF 1:1 at a concentration of 100 mg/mL, and separated by semi-preparative HPLC on a C18 SunFire HPLC column (10.0 x 150 mm; 5 µm; Waters). The mobile phase consisted of H_2O (A) and MeCN (B). A gradient of 5-100% B in 30 min, with a 5 min 100% B wash was applied. The flowrate was 4.0 mL/min. Detection was set at UV 288 nm. Aliquots of 100 µL each were injected. Nine fractions were obtained (fractions E-8/1 to E-8/9), by using a combination of peak-based and time-based collection. Fraction E-7 (141 mg) was separated following the same chromatographic conditions as for fraction E-8, but with detection at UV 247 nm resulting in 8 fractions (E-7/1 to E-7/8). ^1H-NMR spectra of active fractions and the reference compound hyptatic acid were recorded on a 500 MHz Avance III spectrometer (Bruker) equipped with a 1-mmTXI microprobe (see Fig. 6.4).

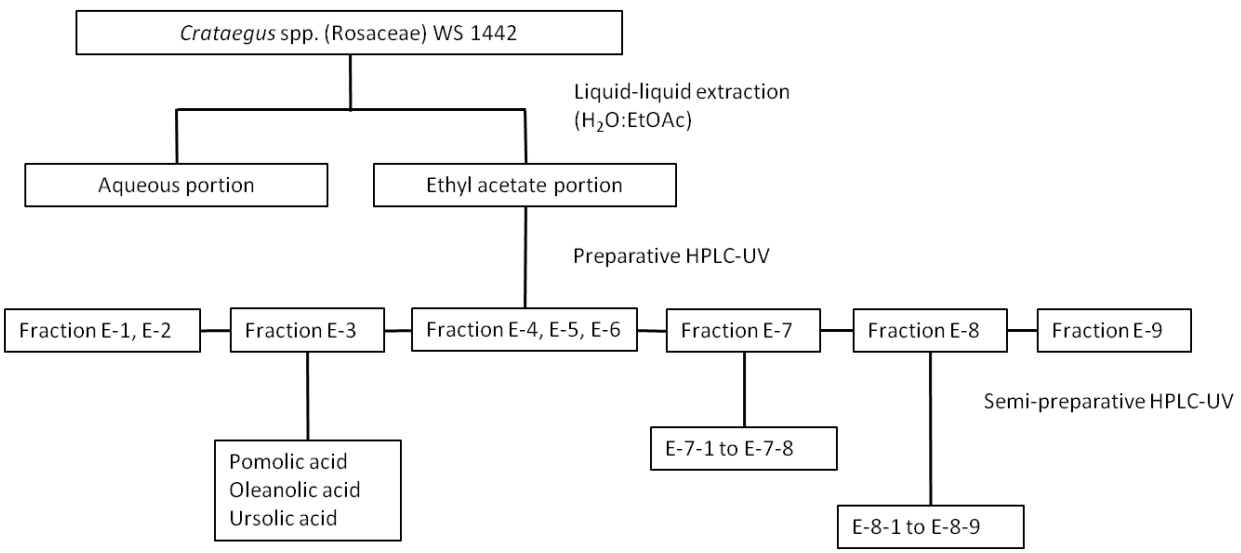

Figure 6.4: Isolation scheme for *Crataegus* WS 1442 extract and resulting compounds (isolated by M. Bauhart) and fractions.

Bioassay for *Crataegus* samples: Testing of the samples was done on edema-preventing mechanisms which include interference with calcium signalling induced by thrombin and activation of cortactin. A detailed explanation of the process followed with the biological assays can be found in the article by Fuchs *et al.*, 2017[197]. Briefly, the fraction worked on by our group was shown to inhibit the influx of calcium induced by thrombin. Changes in cytosolic calcium levels were detected by fluorescence microscopy using Fura-2-AM in a static tempered system at 37 °C. Thrombin was added at time point t = 1 min after initiation of experiment. Experiments were independently performed three times (n = 3) as expressed as a %.

Chapter 7

7. Conclusions and Future Perspectives

Natural products have contributed approximately 50% of new chemical entity approvals in 2010 and still possess a large amount of unexplored chemical diversity. It is estimated that from approximately 300 000 plant species, only about 6% of higher plants, very few marine sources, as well as less than 1% of microbial species have been pharmacologically investigated so far[79]. Their structural and molecular diversity allow natural products to continue to play a fundamental role in the discovery of novel bioactive molecules. Following technological advances on instruments that are used for characterisation of natural products as well as in extraction and screening methods, the field of natural products is growing fast and making significant contributions in areas of biochemistry and drug discovery[79]. On the other hand, progress in genetics and molecular biology swiftly improve the target-based drug discovery approach; as a result it enhances the pharmaceutical values of natural products. For example between 1999 and 2013, 113 drugs were approved by the FDA[225]; of which 69% were discovered through target-based research approaches[225]. The target-based approach is hypothesis driven with the goal to modulate a specific component within a biological system[226]. As part of the target identification process, understanding the molecular mechanisms of a biological system is of fundamental importance to increase the confidence in target selection[226].

At the Neurobiology Department, University of Basel, the inhibition of pathogenic complex formation between CUGn-RNA and MBNL1 was identified to be an important target for the treatment of Myotonic Dystrophy type 1. A protein called coronin-1 was found to be essential for the survival of pathogenic *Mycobacterium tuberculosis* (MTB) in the human host[138]. Thus at the Biozentrum, University of Basel, an assay which enables us to measure the effectiveness of a molecule in inhibiting the expression of coronin-1 was developed (referred as GFP and RFP assay). Promoting Lymphatic Endothelial Cell (LEC) growth plays an essential role in treating lymphedema[149]; accordingly, at the Pharmacogenomics group, ETH Zürich, an assay which allows us to test the efficiency of a molecule in promoting lymphatic vessel growth was developed. The underlying mechanism through which *Crataegus* extracts treats Chronic Heart Failure (CHF) was found to be via inhibiting thrombin-induced [Ca^{2+}] influx which leads to a

reduction in endothelial hyperpermeability[186,197]. Therefore, to assess various aspects of *Crataegus* extracts that are related with CHF, at the Institute of Pharmaceutical Biology, Goethe University, an assay was developed.

The aforementioned emerging biological targets are very crucial for various research activities which intend to discover molecules that have the ability to interact with these respective biological targets. Given the fact that natural products are a major source of complex and highly structurally diverse chemical compounds, they need to be tested on these emerging biological targets, via processing them and analysing their results with modern technologies such as HPLC and NMR. In this context, the main aims of this study were: (a) to test the activity of various plant and fungal extracts on aforementioned biological targets (assays), and (b) to characterise the active extracts and to distinguish the molecules which are possibly responsible for observed biological activities on each of these biological targets (assays). With these main objectives, this study was divided into four projects; namely: (1) DM1 project which focuses on Myotonic Dystrophy type 1 and natural products; (2) TB project which focuses on Tuberculosis and natural products; (3) Lymphatic project which focuses on lymphedema and natural products; and (4) CHF project which focuses on Chronic Heart Failure and *Crataegus* extracts. The main findings, concluding remarks and future perspectives for each of these projects are given as follows:

[1] After testing and analysing over 2100 plant and fungal extracts, harmine (from *Peganum harmala*) as well as 1,2-dihydrotanshinquinone I and methylenetanshinquinone (from *Salvia miltiorrhiza*) were identified as the most active compounds in inhibiting CUGn-RNA and MBNL1 complex formation. Based on the identification of active scaffold of harmine, planar-nitrogen-based compounds (such as protoberberine alkaloids) were hypothesised to possess higher activity. Thus selected alkaloids from a compound library were tested in assays which measure the % of exon inclusion/exclusion in the gene coding for INSR and TNNT2. These test results exhibited that the most active compounds were 8-oxoberberine (in INSR assay), and coptisine and berberine (in TNNT2 assay). The IC_{50} and toxicity-IC_{50} test results for berberine and harmine showed that they were effective in restoring MBNL1 function at a concentration much lower than their respective IC_{50} and toxicity-IC_{50} values. Whereas, relative to the alkaloids, 1,2-dihydrotanshinquinone I, and methylenetanshinquinone

were found to be weaker in both INSR and TNNT2 assays, this might be due to their poor solubility. The identified alkaloids (i.e., harmine and berberine) were able to ameliorate certain aspects of the DM1 pathology, whereas the compounds from *Salvia* species (i.e., *S. miltiorrhiza*) exhibit some activities with certain degrees of toxicity, thus these compounds need further investigation. Remarkably, the main findings of this study exhibit that compounds with planar scaffolds which contained mostly nitrogen are more active in inhibiting CUGn-RNA–MBNL1 complex formation and restoring MBNL1 function. Given the planar nature of the active molecules and the target being RNA, it is projected that the observed activities occurred due to bioactive molecules induced reversible intercalation into the RNA hairpin loop via electrostatic interactions, thereby blocking the binding of MBNL1 and allowing it to carry out its normal function. Overall the hit compounds found in this study may have the potential for drug discovery in RNA-mediated diseases.

[2] The TB project finds that among various plant and fungal extracts, the ethyl acetate extract from *Dorstenia contrajerva* and methanol extract from *Pancratium littorale* significantly decreased GFP after 72 hours (indicating they were active). Bioactivity tracking on active extracts (via HPLC-based activity profiling) led to the identification of constituents (class of compounds) that are possibly responsible for observed activities: alkaloids (from *P. littorale*) and furanocoumarins (from *D. contrajerva*). A compound dorstenin was isolated from *D. contrajerva* EtOAc extract and it was found that the molecule is active only at a higher concentration. This implies that dorstenin was not the major contributor for activity observed from *D. contrajerva* EtOAc extract. Moreover, 15 alkaloids were isolated from *P. littorale* MeOH extract and it was found that in GFP assay three of them were the most active while four of them were more toxic in RFP assay. Also through activity correlated structural analysis of these isolated compounds this study found that molecules which contain secondary nitrogen and methylenedioxy group had higher toxicity, whereas the active molecules contain a hemiacetal ring and acetylation of some hydroxy functions. Moreover, through further tests using western blotting, this study found that the above three compounds which exhibited activity in GFP assay were not active in downregulating coronin-1 at the protein level (i.e., they were not active in inhibiting coronin-1 expression). These contrasting results found from the two different test methods (i.e., GFP assay and western blotting) open a question

that through which mechanism the active molecules can be able to induce GFP reduction? Currently this study did not come across a definite answer to this question but it might be through direct interaction with GFP via acting as quenching agents. Also considering the GFP assay and western blotting contradictory results, this study would like to remark that (a) it is crucial to confirm coronin-1 expression on a genetic level when treated with the compounds, such as via RT-PCR tests; and (b) it is important to re-evaluate the utilisation of GFP assay for coronin-1 inhibition test, this may include the need of conducting further investigation on understanding the interaction mechanism of compounds with GFP and its responses.

[3] The extract library screening results showed that DCM, EtOAc, and MeOH extracts from *Daphne giraldii* were potent inducers of LEC sprouting. The HPLC-activity profiling of the MeOH extract illustrated that activities were localised in the lipophilic (a-polar) regions; therefore, further studies of this project focused on DCM extract which was considered to contain lipophilic compounds in higher quantities. Based on criteria such as higher yield, less complex, and higher activity, this study selected a CPC sub-fraction of DCM extract (named as E-d) for further investigation. The results of time-peak-based HPLC-UV semi-preparative-fractionations of sub-fraction E-d (until micro-fractions weighed ≤ 100 µg) and a series of assaying showed that the activity is consistently localised in a-polar regions. Thus this study excluded polar compounds from the list of compounds that are responsible for observed activity. Also due to the lower amount of E-d complex micro-fractions as well as presence of a wide array of structurally related minor metabolites in them, the identification of pure a-polar compounds that are responsible for observed activities remains challenging. However using daphnetoxin (which displayed potent sprouting activity) as a reference, this study conducted projected analysis on composition of E-d micro-fractions and it was found that trace amounts of daphnetoxin present in *D. giraldii* active micro-fractions could be (at least one of) the main contributing factors for observed activities. This projected remark was found through correlative analysis of E-d micro-fractions and daphnetoxin minimum effective concentration. Furthermore, this study found the presence of fatty acid signals in active E-d micro-fractions, this lead to the projection that a specific type of fatty acid present in *D. giraldii* may play a role in the overall observed activity. However to certainly identify this and other constituents of E-d micro-fractions, this study

recommends the need of working with large amounts of optimally prepared extracts. This will allow bioassay-guided refined separations to end up with suitable amounts of pure compounds for identification. Overall, the findings of this study showed that even if the active constituents of *D. giraldii* DCM extract were minor in terms of concentrations, they were potent in inducing LEC sprouting. This suggests that *D. giraldii* is crucial for future research activities that are focused on lymphedema.

[4] On CHF project, *Crataegus* WS 1442 extract was separated into 9 fractions (namely: E-1 to E-9) and their activities were tested in the calcium imaging assay. The results exhibited that only E-7 and E-8 were active in inhibiting thrombin-induced [Ca2+] influx which leads to a reduction in endothelial hyperpermeability. Through further fractionations of E-7 and E-8 (via semi-preparative HPLC-UV chromatography), this study found that activities are only located in sub-fractions E-8-4, E-8-5 and E-8-6. Further analysis on composition of active sub-fractions showed that all of them contain fatty acids and triterpenes; particularly E-8-5 consisted of 40% fatty acids (stearic acid and palmitic acid) and 50% triterpene (hyptatic acid A). The test results for these compounds (in their pure form) displayed that they were inactive in inhibiting thrombin-induced calcium influx. Overall the test results showed that constituents which comprise almost 90% of E-8-5 active sub-fraction were not active in their pure form, therefore it was evident that observed activities were instigated by unidentified minor compounds which comprise about 10% of E-8-5 constituents. This suggests that the activities of *Crataegus* WS 1442 extracts were induced by: (a) a minor constituent with potent activity; or (b) minor constituents with moderate activity which act synergistically. Finally this study recommends that to certainly identify the molecule(s) responsible for observed activity and to assess their biological interactions, further studies on large amounts of optimally prepared *Crataegus* extracts is needed. This will allow the researcher to end up with suitable amounts of fractions after refined separations.

Overall each of the studies presented in this thesis (the four projects provided above) were one of the first to employ natural products in assessing their interactions or abilities to interact with four emerging biological targets. Therefore, the results presented in this thesis make a significant contribution in fields of pharmacological studies through the use of natural products, via providing: (a) new hit compounds; (b) possible constituents of potently active fractions; (c)

activity correlated structural analysis and extract characterisation; (d) opportunities for understanding interactions among natural products and biochemical assays; as well as (e) in identifying challenges and providing possible recommendations. Moreover, besides presenting the findings on different conferences, parts of the studies presented in this thesis have been published:

1) From the DM1 project:

Herrendorff, R., **Faleschini, M. T.**, Stiefvater, A., Erne, B., Wiktorowicz, T., Kern, F., Hamburger, M., Potterat, O., Kinter, J., and Sinnreich, M. (2016) Identification of Plant-derived Alkaloids with Therapeutic Potential for Myotonic Dystrophy Type I. *J. Biol. Chem.* 291, 17165–17177

2) From the CHF project:

Fuchs, S., Bischoff, I., Willer, E. A., Bräutigam, J., Bubik, M. F., Erdelmeier, C. A., Koch, E., **Faleschini, M. T.**, De Mieri, M., Bauhart, M., Zahler, S., Hensel, A., Hamburger, M., Potterat, O., and Fürst, R. (2017) The Dual Edema-Preventing Molecular Mechanism of the *Crataegus* Extract WS 1442 Can Be Assigned to Distinct Phytochemical Fractions. *Planta Med.* 83, 1–8

References

(1) Alinio, J. Importance Of Medicine In Our Daily Lives http://ezinearticles.com/?Importance-Of-Medicine-In-Our-Daily-Lives&id=480726 (accessed May 2, 2017).

(2) Gualtieri, F. Medicinal Chemistry. In *Organic and Biomolecular Chemistry*; EOLSS Publications: Oxford: United Kingdom, 2009; Vol. II, p 434.

(3) Rick Mullin. Cost to Develop New Pharmaceutical Drug Now Exceeds $2.5B http://www.scientificamerican.com/article/cost-to-develop-new-pharmaceutical-drug-now-exceeds-2-5b/ (accessed Jun 16, 2016).

(4) Hughes, J.; Rees, S.; Kalindjian, S.; Philpott, K. Principles of Early Drug Discovery. *Br. J. Pharmacol.* **2011**, *162* (6), 1239–1249.

(5) Sneader, W. E. *Drug Discovery (The History)*; Wiley Online Library, 2005.

(6) Takenaka, T. Classical vs Reverse Pharmacology in Drug Discovery. *BJU Int.* **2001**, *88* (s2), 7–10.

(7) Swinney, D. C.; Anthony, J. How Were New Medicines Discovered? *Nat. Rev. Drug Discov.* **2011**, *10* (7), 507–519.

(8) Lee, J. A.; Uhlik, M. T.; Moxham, C. M.; Tomandl, D.; Sall, D. J. Modern Phenotypic Drug Discovery Is a Viable, Neoclassic Pharma Strategy. *J. Med. Chem.* **2012**, *55* (10), 4527–4538.

(9) Wittlin, S. & Rottmann, M. (2015, October 9) Two successful malaria drug discovery projects at Swiss TPH. Lecture notes.

(10) Terstappen, G. C.; Schlüpen, C.; Raggiaschi, R.; Gaviraghi, G. Target Deconvolution Strategies in Drug Discovery. *Nat. Rev. Drug Discov.* **2007**, *6* (11), 891–903.

(11) Balunas, M. J.; Kinghorn, A. D. Drug Discovery from Medicinal Plants. *Life Sci.* **2005**, *78* (5), 431–441.

(12) Lahlou, M. The Success of Natural Products in Drug Discovery. *Pharmacol. Amp Pharm.* **2013**, *04* (03), 17–31.

(13) Azwanida, N. N. A Review on the Extraction Methods Use in Medicinal Plants, Principle, Strength and Limitation. *Med Aromat Plants* **2015**, *4* (196), 2167–0412.1000196.

(14) Ashburn, T. T.; Thor, K. B. Drug Repositioning: Identifying and Developing New Uses for Existing Drugs. *Nat. Rev. Drug Discov.* **2004**, *3* (8), 673–683.

(15) Partners in BioPharma Consulting, LLC http://partnersinbpc.com/ (accessed Mar 28, 2017).

(16) Feher, M.; Schmidt, J. M. Property Distributions: Differences between Drugs, Natural Products, and Molecules from Combinatorial Chemistry. *J. Chem. Inf. Comput. Sci.* **2003**, *43* (1), 218–227.

(17) Pascolutti, M.; Campitelli, M.; Nguyen, B.; Pham, N.; Gorse, A.-D.; Quinn, R. J. Capturing Nature's Diversity. *PLoS ONE* **2015**, *10* (4), e0120942.

(18) Scripps Institute. Why Natural Products? http://www.scripps.edu/shen/NPLI/whynaturalproducts.html (accessed Jun 12, 2016).

(19) Pascolutti, M.; Quinn, R. J. Natural Products as Lead Structures: Chemical Transformations to Create Lead-like Libraries. *Drug Discov. Today* **2014**, *19* (3), 215–221.

(20) Dias, D. A.; Urban, S.; Roessner, U. A Historical Overview of Natural Products in Drug Discovery. *Metabolites* **2012**, *2* (4), 303–336.

(21) Newman, D. J.; Cragg, G. M. Natural Products as Drugs and Leads to Drugs: The Historical Perspective. In *Natural Product Chemistry for Drug Discovery*; Buss, A. D., Ed.; Royal Society of Chemistry: Cambridge, 2009; pp 3–27.

(22) Magendie, F.; Pelletier, P. J. *Recherches Chimiques et Physiologiques Sur l'ipécacuanha*; L. Colas, 1817.

(23) Ladenburg, A. Die Natürlich Vorkommenden Mydriatisch Wirkenden Alkaloide. *Justus Liebigs Ann. Chem.* **1881**, *206* (3), 274–307.

(24) Rosenkranz, V.; Wink, M. Alkaloids Induce Programmed Cell Death in Bloodstream Forms of Trypanosomes (Trypanosoma b. Brucei). *Molecules* **2008**, *13* (10), 2462–2473.

(25) Carlson, E. E. Natural Products as Chemical Probes. *ACS Chem. Biol.* **2010**, *5* (7), 639–653.

(26) Ortega, A.; Blount, J. F.; Manchand, P. S. Salvinorin, a New Trans-Neoclerodane Diterpene from Salvia Divinorum(Labiatae). *J. Chem. Soc. [Perkin 1]* **1982**, No. 0, 2505–2508.

(27) Roth, B. L.; Baner, K.; Westkaemper, R.; Siebert, D.; Rice, K. C.; Steinberg, S.; Ernsberger, P.; Rothman, R. B. Salvinorin A: A Potent Naturally Occurring Nonnitrogenous κ Opioid Selective Agonist. *Proc. Natl. Acad. Sci. U. S. A.* **2002**, *99* (18), 11934–11939.

(28) Newman, D. J.; Cragg, G. M. Natural Products as Sources of New Drugs from 1981 to 2014. *J. Nat. Prod.* **2016**.

(29) Clardy, J.; Walsh, C. Lessons from Natural Molecules. *Nature* **2004**, *432* (7019), 829–837.

(30) Piggott, A. M.; Karuso, P. Quality, Not Quantity: The Role of Natural Products and Chemical Proteomics in Modern Drug Discovery. *Comb. Chem. High Throughput Screen.* **2004**, *7* (7), 607–630.

(31) Pucheault, M. Natural Products: Chemical Instruments to Apprehend Biological Symphony. *Org. Biomol. Chem.* **2008**, *6* (3), 424–432.

(32) Crews, C. M.; Splittgerber, U. Chemical Genetics: Exploring and Controlling Cellular Processes with Chemical Probes. *Trends Biochem. Sci.* **1999**, *24* (8), 317–320.

(33) Vera, M. D.; Joullié, M. M. Natural Products as Probes of Cell Biology: 20 Years of Didemnin Research: DIDEMNIN RESEARCH. *Med. Res. Rev.* **2002**, *22* (2), 102–145.

(34) Rosen, M. K.; Schreiber, S. L. Natural Products as Probes of Cellular Function: Studies of Immunophilins. *Angew. Chem. Int. Ed. Engl.* **1992**, *31*, 384–400.

(35) Hung, D. T.; Jamison, T. F.; Schreiber, S. L. Understanding and Controlling the Cell Cycle with Natural Products. *Chem. Biol.* **1996**, *3* (8), 623–639.

(36) Newman, D. J.; Cragg, G. M.; Holbeck, S.; Sausville, E. A. Natural Products and Derivatives as Leads to Cell Cycle Pathway Targets in Cancer Chemotherapy. *Curr. Cancer Drug Targets* **2002**, *2* (4), 279–308.

(37) Itazaki, H.; Nagashima, K.; Sugita, K.; Yoshida, H.; Kawamura, Y.; Yasuda, Y.; Matsumoto, K.; Ishii, K.; Uotani, N.; Nakai, H. Isolation and Structural Elucidation of New Cyclotetrapeptides, Trapoxins A and B, Having Detransformation Activities as Antitumor Agents. *J. Antibiot. (Tokyo)* **1990**, *43* (12), 1524–1532.

(38) Tsuji, N.; Kobayashi, M.; Nagashima, K.; Wakisaka, Y.; Koizumi, K. A New Antifungal Antibiotic, Trichostatin. *J. Antibiot. (Tokyo)* **1976**, *29* (1), 1–6.

(39) Taunton, J.; Collins, J. L.; Schreiber, S. L. Synthesis of Natural and Modified Trapoxins, Useful Reagents for Exploring Histone Deacetylase Function. *J. Am. Chem. Soc.* **1996**, *118* (43), 10412–10422.

(40) Abraham, R. T. Mammalian Target of Rapamycin: Immunosuppressive Drugs Uncover a Novel Pathway of Cytokine Receptor Signaling. *Curr. Opin. Immunol.* **1998**, *10* (3), 330–336.

(41) Crespo, J. L.; Hall, M. N. Elucidating TOR Signaling and Rapamycin Action: Lessons from Saccharomyces Cerevisiae. *Microbiol. Mol. Biol. Rev.* **2002**, *66* (4), 579–591.

(42) Hall, M. N. MTOR Signalling in Growth and Metabolism, 2016.

(43) Gibbons, J. J.; Abraham, R. T.; Yu, K. Mammalian Target of Rapamycin: Discovery of Rapamycin Reveals a Signaling Pathway Important for Normal and Cancer Cell Growth. In *Seminars in oncology*; Elsevier, 2009; Vol. 36, pp S3–S17.

(44) Moore, D. Origin of drugs in current use: the cyclosporine story (contributed by Harriet Upton, 2001) http://www.davidmoore.org.uk/Sec04_01.htm (accessed Jul 25, 2016).

(45) Voets, T.; Talavera, K.; Owsianik, G.; Nilius, B. Sensing with TRP Channels. *Nat. Chem. Biol.* **2005**, *1* (2), 85–92.

(46) Caterina, M. J.; Schumacher, M. A.; Tominaga, M.; Rosen, T. A.; Levine, J. D.; Julius, D. The Capsaicin Receptor: A Heat-Activated Ion Channel in the Pain Pathway. *Nature* **1997**, *389* (6653), 816–824.

(47) McKemy, D. D.; Neuhausser, W. M.; Julius, D. Identification of a Cold Receptor Reveals a General Role for TRP Channels in Thermosensation. *Nature* **2002**, *416* (6876), 52–58.

(48) Hui, K.; Guo, Y.; Feng, Z.-P. Biophysical Properties of Menthol-Activated Cold Receptor TRPM8 Channels. *Biochem. Biophys. Res. Commun.* **2005**, *333* (2), 374–382.

(49) Peterson, J. R.; Mitchison, T. J. Small Molecules, Big Impact: A History of Chemical Inhibitors and the Cytoskeleton. *Chem. Biol.* **2002**, *9* (12), 1275–1285.

(50) Barbosa, W. L. R.; do Nascimento, M. S.; do Nascimento Pinto, L.; Maia, F. L. C.; Sousa, A. J. A.; Júnior, J. O. C. S.; Monteiro, M. M.; de Oliveira, D. R. Selecting Medicinal Plants for Development of Phytomedicine and Use in Primary Health Care. In *Bioactive Compounds in Phytomedicine*; InTech, 2012.

(51) Potterat, O.; Hamburger, M. Drug Discovery and Development with Plant-Derived Compounds. In *Natural Compounds as Drugs Volume I*; Springer, 2008; pp 45–118.

(52) Soejarto, D. D.; Gyllenhaal, C.; Fong, H. H. S.; Xuan, L. T.; Hiep, N. T.; Hung, N. V.; Bich, T. Q.; Southavong, B.; Sydara, K.; Pezzuto, J. M. The UIC ICBG (University of Illinois at Chicago International Cooperative Biodiversity Group) Memorandum of Agreement: A Model of Benefit-Sharing Arrangement in Natural Products Drug Discovery and Development ⊥. *J. Nat. Prod.* **2004**, *67* (2), 294–299.

(53) Iwu, M. M. Implementing the Biodiversity Treaty: How to Make International Co-Operative Agreements Work. *Trends Biotechnol.* **1996**, *14* (3), 78–83.

(54) David, B.; Wolfender, J.-L.; Dias, D. A. The Pharmaceutical Industry and Natural Products: Historical Status and New Trends. *Phytochem. Rev.* **2015**, *14* (2), 299–315.

(55) Handa, S. S. *Extraction Technologies for Medicinal and Aromatic Plants*; International Centre for Science and High Technology, 2008.

(56) Rahmalia, W.; Fabre, J.-F.; Mouloungui, Z. Effects of Cyclohexane/Acetone Ratio on Bixin Extraction Yield by Accelerated Solvent Extraction Method. *Procedia Chem.* **2015**, *14*, 455–464.

(57) Trusheva, B.; Trunkova, D.; Bankova, V. Different Extraction Methods of Biologically Active Components from Propolis: A Preliminary Study. *Chem. Cent. J.* **2007**, *1* (1), 13.

(58) Dhanani, T.; Shah, S.; Gajbhiye, N. A.; Kumar, S. Effect of Extraction Methods on Yield, Phytochemical Constituents and Antioxidant Activity of Withania Somnifera. *Arab. J. Chem.* **2013**.

(59) Sasidharan, S.; Chen, Y.; Saravanan, D.; Sundram, K. M.; Latha, L. Y. Extraction, Isolation and Characterization of Bioactive Compounds from Plants' Extracts. *Afr. J. Tradit. Complement. Altern. Med.* **2011**, *8* (1).

(60) Potterat, O.; Hamburger, M. Combined Use of Extract Libraries and HPLC-Based Activity Profiling for Lead Discovery: Potential, Challenges, and Practical Considerations. *Planta Med.* **2014**, *80* (14), 1171–1181.

(61) Moore, K.; Rees, S. Cell-Based versus Isolated Target Screening: How Lucky Do You Feel? *J. Biomol. Screen.* **2001**, *6* (2), 69–74.

(62) Potterat, O.; Hamburger, M. Concepts and Technologies for Tracking Bioactive Compounds in Natural Product Extracts: Generation of Libraries, and Hyphenation of Analytical Processes with Bioassays. *Nat. Prod. Rep.* **2013**, *30* (4), 546.

(63) Bucar, F.; Wube, A.; Schmid, M. Natural Product Isolation–how to Get from Biological Material to Pure Compounds. *Nat. Prod. Rep.* **2013**, *30* (4), 525–545.

(64) Sarker, S. D.; Nahar, L. An Introduction to Natural Products Isolation. *Nat. Prod. Isol.* **2012**, 1–25.

(65) Taylor, T. Important Aspects of UV Detection for HPLC | LCGC http://www.chromatographyonline.com/important-aspects-uv-detection-hplc (accessed May 2, 2017).

(66) Wolfender, J.-L. HPLC in Natural Product Analysis: The Detection Issue. *Planta Med.* **2009**, *75* (07), 719–734.

(67) Potterat, O.; Hamburger, M. Natural Products in Drug Discovery - Concepts and Approaches for Tracking Bioactivity. *Curr. Org. Chem.* **2006**, *10* (8), 899–920.

(68) Wolfender, J.-L.; Marti, G.; Thomas, A.; Bertrand, S. Current Approaches and Challenges for the Metabolite Profiling of Complex Natural Extracts. *J. Chromatogr. A* **2015**, *1382*, 136–164.

(69) Kingston, D. G. I. Modern Natural Products Drug Discovery and Its Relevance to Biodiversity Conservation. *J. Nat. Prod.* **2011**, *74* (3), 496–511.

(70) Pauli, G. F.; Case, R. J.; Inui, T.; Wang, Y.; Cho, S.; Fischer, N. H.; Franzblau, S. G. New Perspectives on Natural Products in TB Drug Research. *Life Sci.* **2005**, *78* (5), 485–494.

(71) Burdine, L.; Kodadek, T. Target Identification in Chemical Genetics: The (Often) Missing Link. *Chem. Biol.* **2004**, *11* (5), 593–597.

(72) Böttcher, T.; Pitscheider, M.; Sieber, S. A. Natural Products and Their Biological Targets: Proteomic and Metabolomic Labeling Strategies. *Angew. Chem. Int. Ed.* **2010**, *49* (15), 2680–2698.

(73) Cheng, K.-W.; Wong, C.-C.; Wang, M.; He, Q.-Y.; Chen, F. Identification and Characterization of Molecular Targets of Natural Products by Mass Spectrometry. *Mass Spectrom. Rev.* **2010**, *29* (1), 126–155.

(74) Newman, D. J.; Cragg, G. M. Natural Products as Sources of New Drugs over the 30 Years from 1981 to 2010. *J. Nat. Prod.* **2012**, *75* (3), 311–335.

(75) Harvey, A. Strategies for Discovering Drugs from Previously Unexplored Natural Products. *Drug Discov. Today* **2000**, *5* (7), 294–300.

(76) Henkel, T.; Brunne, R. M.; Müller, H.; Reichel, F. Statistical Investigation into the Structural Complementarity of Natural Products and Synthetic Compounds. *Angew. Chem. Int. Ed.* **1999**, *38* (5), 643–647.

(77) Tasdemir, D. Natural Products as Source of Drugs, 2014.

(78) Borman, S. The Many Faces of Combinatorial Chemistry. *Chem. Eng. News* **2003**, *81* (43), 45–56.

(79) Cragg, G. M.; Newman, D. J. Natural Products: A Continuing Source of Novel Drug Leads. *Biochim. Biophys. Acta BBA-Gen. Subj.* **2013**, *1830* (6), 3670–3695.

(80) Koehn, F. E.; Carter, G. T. The Evolving Role of Natural Products in Drug Discovery. *Nat. Rev. Drug Discov.* **2005**, *4* (3), 206–220.

(81) Harvey, A. L. Natural Products as a Screening Resource. *Curr. Opin. Chem. Biol.* **2007**, *11* (5), 480–484.

(82) Baker, D. D.; Chu, M.; Oza, U.; Rajgarhia, V. The Value of Natural Products to Future Pharmaceutical Discovery. *Nat. Prod. Rep.* **2007**, *24* (6), 1225.

(83) Hamburger, M.; Hostettmann, K. 7. Bioactivity in Plants: The Link between Phytochemistry and Medicine. *Phytochemistry* **1991**, *30* (12), 3864–3874.

(84) Wolfender, J.-L.; Queiroz, E. F.; Hostettmann, K. Phytochemistry in the Microgram Domain—a LC–NMR Perspective. *Magn. Reson. Chem.* **2005**, *43* (9), 697–709.

(85) Füllbeck, M.; Michalsky, E.; Dunkel, M.; Preissner, R. Natural Products: Sources and Databases. *Nat. Prod. Rep.* **2006**, *23* (3), 347–356.

(86) Harborne, A. J. *Phytochemical Methods a Guide to Modern Techniques of Plant Analysis*; springer science & business media, 1998.

(87) Hostettmann, K.; Marston, A. Countercurrent Chromatography in the Preparative Separation of Plant-Derived Natural Products. *J. Liq. Chromatogr. Relat. Technol.* **2001**, *24* (11–12), 1711–1721.

(88) Pauli, G. F.; Pro, S. M.; Friesen, J. B. Countercurrent Separation of Natural Products. *J. Nat. Prod.* **2008**, *71* (8), 1489–1508.

(89) Berthold, A. Countercurrent Chromatography: The Support-Free Liquid Stationary Phase. In *Comprehensive Analytical Chemistry*; Barcelo, D., Ed.; Elsevier Science: Amsterdam: Netherlands, 2002; Vol. XXXVIII, p 397.

(90) Reynolds, W. F.; Enríquez, R. G. Choosing the Best Pulse Sequences, Acquisition Parameters, Postacquisition Processing Strategies, and Probes for Natural Product Structure Elucidation by NMR Spectroscopy. *J. Nat. Prod.* **2002**, *65* (2), 221–244.

(91) Pauli, G. F.; Jaki, B. U.; Lankin, D. C. Quantitative 1H NMR: Development and Potential of a Method for Natural Products Analysis. *J. Nat. Prod.* **2005**, *68* (1), 133–149.

(92) Li, X.-C.; Ferreira, D.; Ding, Y. Determination of Absolute Configuration of Natural Products: Theoretical Calculation of Electronic Circular Dichroism as a Tool. *Curr. Org. Chem.* **2010**, *14* (16), 1678–1697.

(93) Felippe, L. G.; Batista Jr, J. M.; Baldoqui, D. C.; Nascimento, I. R.; Kato, M. J.; He, Y.; Nafie, L. A.; Furlan, M. VCD to Determine Absolute Configuration of Natural Product Molecules: Secolignans from Peperomia Blanda. *Org. Biomol. Chem.* **2012**, *10* (21), 4208–4214.

(94) Freedman, T. B.; Cao, X.; Dukor, R. K.; Nafie, L. A. Absolute Configuration Determination of Chiral Molecules in the Solution State Using Vibrational Circular Dichroism. *Chirality* **2003**, *15* (9), 743–758.

(95) Harper, P. S. Myotonic Dystrophy 2nd Ed. *Lond. Saunders* **1989**.

(96) Korf, B. R.; Irons, M. B. *Human Genetics and Genomics*; John Wiley & Sons, 2012.

(97) Kinter, J.; Sinnreich, M. Molecular Targets to Treat Muscular Dystrophies. *Swiss Med. Wkly.* **2014**.

(98) Brook, J. D.; McCurrach, M. E.; Harley, H. G.; Buckler, A. J.; Church, D.; Aburatani, H.; Hunter, K.; Stanton, V. P.; Thirion, J.-P.; Hudson, T. Molecular Basis of Myotonic Dystrophy: Expansion of a Trinucleotide (CTG) Repeat at the 3′ End of a Transcript Encoding a Protein Kinase Family Member. *Cell* **1992**, *68* (4), 799–808.

(99) Yuan, Y.; Compton, S. A.; Sobczak, K.; Stenberg, M. G.; Thornton, C. A.; Griffith, J. D.; Swanson, M. S. Muscleblind-like 1 Interacts with RNA Hairpins in Splicing Target and Pathogenic RNAs. *Nucleic Acids Res.* **2007**, *35* (16), 5474–5486.

(100) Charlet-B, N.; Savkur, R. S.; Singh, G.; Philips, A. V.; Grice, E. A.; Cooper, T. A. Loss of the Muscle-Specific Chloride Channel in Type 1 Myotonic Dystrophy Due to Misregulated Alternative Splicing. *Mol. Cell* **2002**, *10* (1), 45–53.

(101) Savkur, R. S.; Philips, A. V.; Cooper, T. A. Aberrant Regulation of Insulin Receptor Alternative Splicing Is Associated with Insulin Resistance in Myotonic Dystrophy. *Nat. Genet.* **2001**, *29* (1), 40–47.

(102) Hino, S.; Kondo, S.; Sekiya, H.; Saito, A.; Kanemoto, S.; Murakami, T.; Chihara, K.; Aoki, Y.; Nakamori, M.; Takahashi, M. P. Molecular Mechanisms Responsible for Aberrant Splicing of SERCA1 in Myotonic Dystrophy Type 1. *Hum. Mol. Genet.* **2007**, *16* (23), 2834–2843.

(103) Ho, T. H.; Charlet-B, N.; Poulos, M. G.; Singh, G.; Swanson, M. S.; Cooper, T. A. Muscleblind Proteins Regulate Alternative Splicing. *EMBO J.* **2004**, *23* (15), 3103–3112.

(104) Emery, A. E. The Muscular Dystrophies. *The Lancet* **2002**, *359* (9307), 687–695.

(105) Krzyzosiak, W. J.; Sobczak, K.; Wojciechowska, M.; Fiszer, A.; Mykowska, A.; Kozlowski, P. Triplet Repeat RNA Structure and Its Role as Pathogenic Agent and Therapeutic Target. *Nucleic Acids Res.* **2011**, gkr729.

(106) Lee, J. E.; Bennett, C. F.; Cooper, T. A. RNase H-Mediated Degradation of Toxic RNA in Myotonic Dystrophy Type 1. *Proc. Natl. Acad. Sci.* **2012**, *109* (11), 4221–4226.

(107) Kanadia, R. N.; Shin, J.; Yuan, Y.; Beattie, S. G.; Wheeler, T. M.; Thornton, C. A.; Swanson, M. S. Reversal of RNA Missplicing and Myotonia after Muscleblind Overexpression in a Mouse Poly (CUG) Model for Myotonic Dystrophy. *Proc. Natl. Acad. Sci.* **2006**, *103* (31), 11748–11753.

(108) Langlois, M.-A.; Boniface, C.; Wang, G.; Alluin, J.; Salvaterra, P. M.; Puymirat, J.; Rossi, J. J.; Lee, N. S. Cytoplasmic and Nuclear Retained DMPK MRNAs Are Targets for RNA Interference in Myotonic Dystrophy Cells. *J. Biol. Chem.* **2005**, *280* (17), 16949–16954.

(109) Langlois, M.-A.; Lee, N. S.; Rossi, J. J.; Puymirat, J. Hammerhead Ribozyme-Mediated Destruction of Nuclear Foci in Myotonic Dystrophy Myoblasts. *Mol. Ther.* **2003**, *7* (5), 670–680.

(110) García-López, A.; Llamusí, B.; Orzáez, M.; Pérez-Payá, E.; Artero, R. D. In Vivo Discovery of a Peptide That Prevents CUG–RNA Hairpin Formation and Reverses RNA Toxicity in Myotonic Dystrophy Models. *Proc. Natl. Acad. Sci.* **2011**, *108* (29), 11866–11871.

(111) Childs-Disney, J. L.; Hoskins, J.; Rzuczek, S. G.; Thornton, C. A.; Disney, M. D. Rationally Designed Small Molecules Targeting the RNA That Causes Myotonic Dystrophy Type 1 Are Potently Bioactive. *ACS Chem. Biol.* **2012**, *7* (5), 856–862.

(112) Warf, M. B.; Nakamori, M.; Matthys, C. M.; Thornton, C. A.; Berglund, J. A. Pentamidine Reverses the Splicing Defects Associated with Myotonic Dystrophy. *Proc. Natl. Acad. Sci.* **2009**, *106* (44), 18551–18556.

(113) Coonrod, L. A.; Nakamori, M.; Wang, W.; Carrell, S.; Hilton, C. L.; Bodner, M. J.; Siboni, R. B.; Docter, A. G.; Haley, M. M.; Thornton, C. A. Reducing Levels of Toxic RNA with Small Molecules. *ACS Chem. Biol.* **2013**, *8* (11), 2528.

(114) Hoskins, J. W.; Ofori, L. O.; Chen, C. Z.; Kumar, A.; Sobczak, K.; Nakamori, M.; Southall, N.; Patnaik, S.; Marugan, J. J.; Zheng, W. Lomofungin and Dilomofungin: Inhibitors of MBNL1-CUG RNA Binding with Distinct Cellular Effects. *Nucleic Acids Res.* **2014**, 6591–6602.

(115) World Health Organization. *Global Tuberculosis Report 2016*; 2016.

(116) Organisation mondiale de la santé. *Global Tuberculosis Report 2015*, 20th Edition.; World Health Organization: Geneva, 2015.

(117) Tuberculosis. *Wikipedia, the free encyclopedia*; 2016.

(118) Daffé, M.; Draper, P. The Envelope Layers of Mycobacteria with Reference to Their Pathogenicity. *Adv. Microb. Physiol.* **1998**, *39*, 131–203.

(119) Pieters, J. Entry and Survival of Pathogenic Mycobacteriain Macrophages. *Microbes Infect.* **2001**, *3* (3), 249–255.

(120) Nguyen, L.; Pieters, J. The Trojan Horse: Survival Tactics of Pathogenic Mycobacteria in Macrophages. *Trends Cell Biol.* **2005**, *15* (5), 269–276.

(121) Ernst, J. D. The Immunological Life Cycle of Tuberculosis. *Nat. Rev. Immunol.* **2012**, *12* (8), 581–591.

(122) Barry, C. E. Tuberculosis: Drug Discovery Goes Au Naturel. *Nature* **2014**, *506* (7489), 436–437.

(123) Blondiaux, N.; Moune, M.; Desroses, M.; Frita, R.; Flipo, M.; Mathys, V.; Soetaert, K.; Kiass, M.; Delorme, V.; Djaout, K.; Trebosc, V.; Kemmer, C.; Wintjens, R.; Wohlkönig, A.; Antoine, R.; Huot, L.; Hot, D.; Coscolla, M.; Feldmann, J.; Gagneux, S.; Locht, C.; Brodin, P.; Gitzinger, M.; Déprez, B.; Willand, N.; Baulard, A. R. Reversion of Antibiotic Resistance in Mycobacterium Tuberculosis by Spiroisoxazoline SMARt-420. *Science* **2017**, *355* (6330), 1206–1211.

(124) TB Drugs | First & Second Line, Drug Names, Regimens. *TB Facts.org*.

(125) Stop TB Partnership | "Stop TB Partnership's Global Drug Facility jumpstarts access to new drugs for MDR-TB with innovative public-private partnerships http://www.stoptb.org/news/stories/2016/ns16_005.asp (accessed Mar 24, 2017).

(126) Nath, H.; Ryoo, S. First– and Second–Line Drugs and Drug Resistance. In *Tuberculosis - Current Issues in Diagnosis and Management*; Mahboub, B., Ed.; InTech, 2013.

(127) Lee, R. E.; Hurdle, J. G.; Liu, J.; Bruhn, D. F.; Matt, T.; Scherman, M. S.; Vaddady, P. K.; Zheng, Z.; Qi, J.; Akbergenov, R. Spectinamides: A New Class of Semisynthetic Antituberculosis Agents That Overcome Native Drug Efflux. *Nat. Med.* **2014**, *20* (2), 152–158.

(128) Nguta, J. M.; Appiah-Opong, R.; Nyarko, A. K.; Yeboah-Manu, D.; Addo, P. G. A. Current Perspectives in Drug Discovery against Tuberculosis from Natural Products. *Int. J. Mycobacteriology* **2015**, *4* (3), 165–183.

(129) Kling, A.; Lukat, P.; Almeida, D. V.; Bauer, A.; Fontaine, E.; Sordello, S.; Zaburannyi, N.; Herrmann, J.; Wenzel, S. C.; König, C.; others. Targeting DnaN for Tuberculosis Therapy Using Novel Griselimycins. *Science* **2015**, *348* (6239), 1106–1112.

(130) Pieters, J. Mycobacterium Tuberculosis and the Macrophage: Maintaining a Balance. *Cell Host Microbe* **2008**, *3* (6), 399–407.

(131) Armstrong, J. A.; Hart, P. Response of Cultured Macrophages to Mycobacterium Tuberculosis, with Observations on Fusion of Lysosomes with Phagosomes. *J. Exp. Med.* **1971**, *134* (3), 713–740.

(132) Armstrong, J. A.; Hart, P. Phagosome-Lysosome Interactions in Cultured Macrophages Infected with Virulent Tubercle Bacilli. Reversal of the Usual Nonfusion Pattern and Observations on Bacterial Survival. *J. Exp. Med.* **1975**, *142* (1), 1–16.

(133) Stossel, T. P. The Early History of Phagocytosis. In *Phagocytosis: The Host*; Jai Press: Greenwich, Connecticut, 1999; Vol. 5, pp 3–18.

(134) Pieters, J. Processing and Presentation of Phagocytosed Antigens to the Immune System. In *Phagocytosis: The Host*; Jai Press: Greenwich, Connecticut, 1999; Vol. 5, pp 379–406.

(135) Gatfield, J.; Pieters, J. Essential Role for Cholesterol in Entry of Mycobacteria into Macrophages. *Science* **2000**, *288* (5471), 1647–1651.

(136) Jayachandran, R.; Pieters, J. Regulation of Immune Cell Homeostasis and Function by Coronin 1. *Int. Immunopharmacol.* **2015**, *28* (2), 825–828.

(137) Ferrari, G.; Langen, H.; Naito, M.; Pieters, J. A Coat Protein on Phagosomes Involved in the Intracellular Survival of Mycobacteria. *Cell* **1999**, *97* (4), 435–447.

(138) Jayachandran, R.; Sundaramurthy, V.; Combaluzier, B.; Mueller, P.; Korf, H.; Huygen, K.; Miyazaki, T.; Albrecht, I.; Massner, J.; Pieters, J. Survival of Mycobacteria in Macrophages Is Mediated by Coronin 1-Dependent Activation of Calcineurin. *Cell* **2007**, *130* (1), 37–50.

(139) BoseDasgupta, S.; Pieters, J. Coronin 1 Trimerization Is Essential to Protect Pathogenic Mycobacteria within Macrophages from Lysosomal Delivery. *FEBS Lett.* **2014**, *588* (21), 3898–3905.

(140) BoseDasgupta, S.; Pieters, J. Inflammatory Stimuli Reprogram Macrophage Phagocytosis to Macropinocytosis for the Rapid Elimination of Pathogens. *PLoS Pathog.* **2014**, *10* (1), e1003879.

(141) BoseDasgupta, S.; Pieters, J. Striking the Right Balance Determines TB or Not TB. *Front. Immunol.* **2014**, *5*, 455.

(142) Pieters, J.; Gatfield, J. Hijacking the Host: Survival of Pathogenic Mycobacteria inside Macrophages. *Trends Microbiol.* **2002**, *10* (3), 142–146.

(143) BoseDasgupta, S.; Pieters, J. How to Clear a Pathogen during Inflammation: Switching from Phagocytosis to Macropinocytosis through Coronin 1 Phosphorylation. *Inflamm. Cell Signal.* **2014**, *1* (2).

(144) Hartkoorn, R. C.; Sala, C.; Neres, J.; Pojer, F.; Magnet, S.; Mukherjee, R.; Uplekar, S.; Boy-Röttger, S.; Altmann, K.-H.; Cole, S. T. Towards a New Tuberculosis Drug: Pyridomycin - Nature's Isoniazid: Pyridomycin Targets InhA. *EMBO Mol. Med.* **2012**, *4* (10), 1032–1042.

(145) Wright, G. D. Back to the Future: A New 'Old'Lead for Tuberculosis. *EMBO Mol. Med.* **2012**, *4* (10), 1029–1031.

(146) Noufflard-Guy-Loé, H.; Berteaux, S. Action Antituberculeuse Expérimentale d'une Nouvelle Substance Antibiotique: Le 11.072 RP. *Rev Tuberc PneumolParis* **1965**, *29*, 301–326.

(147) Holzgrabe, U. New Griselimycins for Treatment of Tuberculosis. *Chem. Biol.* **2015**, *22* (8), 981–982.

(148) Tran, A. T.; Watson, E. E.; Pujari, V.; Conroy, T.; Dowman, L. J.; Giltrap, A. M.; Pang, A.; Wong, W. R.; Linington, R. G.; Mahapatra, S.; Saunders, J.; Charman, S. A.; West, N. P.; Bugg, T. D. H.; Tod, J.; Dowson, C. G.; Roper, D. I.; Crick, D. C.; Britton, W. J.; Payne, R. J. Sansanmycin Natural Product Analogues as Potent and Selective Anti-Mycobacterials That Inhibit Lipid I Biosynthesis. *Nat. Commun.* **2017**, *8*, 14414.

(149) Cueni, L. N.; Detmar, M. The Lymphatic System in Health and Disease. *Lymphat. Res. Biol.* **2008**, *6* (3–4), 109–122.

(150) Kim, H.; Kataru, R. P.; Koh, G. Y. Regulation and Implications of Inflammatory Lymphangiogenesis. *Trends Immunol.* **2012**, *33* (7), 350–356.

(151) Karkkainen, M. J.; Haiko, P.; Sainio, K.; Partanen, J.; Taipale, J.; Petrova, T. V.; Jeltsch, M.; Jackson, D. G.; Talikka, M.; Rauvala, H. Vascular Endothelial Growth Factor C Is Required for Sprouting of the First Lymphatic Vessels from Embryonic Veins. *Nat. Immunol.* **2004**, *5* (1), 74–80.

(152) Alitalo, K. The Lymphatic Vasculature in Disease. *Nat. Med.* **2011**, *17* (11), 1371–1380.

(153) Zheng, W.; Tammela, T.; Yamamoto, M.; Anisimov, A.; Holopainen, T.; Kaijalainen, S.; Karpanen, T.; Lehti, K.; Ylä-Herttuala, S.; Alitalo, K. Notch Restricts Lymphatic Vessel Sprouting Induced by Vascular Endothelial Growth Factor. *Blood* **2011**, *118* (4), 1154–1162.

(154) Schulz, M. M. P.; Reisen, F.; Zgraggen, S.; Fischer, S.; Yuen, D.; Kang, G. J.; Chen, L.; Schneider, G.; Detmar, M. Phenotype-Based High-Content Chemical Library Screening Identifies Statins as Inhibitors of in Vivo Lymphangiogenesis. *Proc. Natl. Acad. Sci.* **2012**, *109* (40), E2665–E2674.

(155) Adams, R. H.; Alitalo, K. Molecular Regulation of Angiogenesis and Lymphangiogenesis. *Nat. Rev. Mol. Cell Biol.* **2007**, *8* (6), 464–478.

(156) Xu, Y.; Yuan, L.; Mak, J.; Pardanaud, L.; Caunt, M.; Kasman, I.; Larrivée, B.; del Toro, R.; Suchting, S.; Medvinsky, A. Neuropilin-2 Mediates VEGF-C–induced Lymphatic Sprouting Together with VEGFR3. *J. Cell Biol.* **2010**, *188* (1), 115–130.

(157) Mäkinen, T.; Adams, R. H.; Bailey, J.; Lu, Q.; Ziemiecki, A.; Alitalo, K.; Klein, R.; Wilkinson, G. A. PDZ Interaction Site in EphrinB2 Is Required for the Remodeling of Lymphatic Vasculature. *Genes Dev.* **2005**, *19* (3), 397–410.

(158) Niessen, K.; Zhang, G.; Ridgway, J. B.; Chen, H.; Kolumam, G.; Siebel, C. W.; Yan, M. The Notch1-Dll4 Signaling Pathway Regulates Mouse Postnatal Lymphatic Development. *Blood* **2011**, *118* (7), 1989–1997.

(159) Carmeliet, P. Angiogenesis in Health and Disease. *Nat. Med.* **2003**, *9* (6), 653.

(160) Huggenberger, R.; Detmar, M. The Cutaneous Vascular System in Chronic Skin Inflammation. In *Journal of Investigative Dermatology Symposium Proceedings*; Elsevier, 2011; Vol. 15, pp 24–32.

(161) Christiansen, A.; Detmar, M. Lymphangiogenesis and Cancer. *Genes Cancer* **2011**, *2* (12), 1146–1158.

(162) Wong, B. W.; Wang, X.; Zecchin, A.; Thienpont, B.; Cornelissen, I.; Kalucka, J.; García-Caballero, M.; Missiaen, R.; Huang, H.; Brüning, U.; Blacher, S.; Vinckier, S.; Goveia, J.; Knobloch, M.; Zhao, H.; Dierkes, C.; Shi, C.; Hägerling, R.; Moral-Dardé, V.; Wyns, S.; Lippens, M.; Jessberger, S.; Fendt, S.-M.; Luttun, A.; Noel, A.; Kiefer, F.; Ghesquière, B.; Moons, L.; Schoonjans, L.; Dewerchin, M.; Eelen, G.; Lambrechts, D.; Carmeliet, P. The Role of Fatty Acid β-Oxidation in Lymphangiogenesis. *Nature* **2016**, *542* (7639), 49–54.

(163) Gousopoulos, E.; Proulx, S. T.; Scholl, J.; Uecker, M.; Detmar, M. Prominent Lymphatic Vessel Hyperplasia with Progressive Dysfunction and Distinct Immune Cell Infiltration in Lymphedema. *Am. J. Pathol.* **2016**, *186* (8), 2193–2203.

(164) Baluk, P.; Tammela, T.; Ator, E.; Lyubynska, N.; Achen, M. G.; Hicklin, D. J.; Jeltsch, M.; Petrova, T. V.; Pytowski, B.; Stacker, S. A. Pathogenesis of Persistent Lymphatic Vessel Hyperplasia in Chronic Airway Inflammation. *J. Clin. Invest.* **2005**, *115* (2), 247–257.

(165) Mortimer, P. S.; Rockson, S. G. New Developments in Clinical Aspects of Lymphatic Disease. *J. Clin. Invest.* **2014**, *124* (3), 915–921.

(166) Kaipainen, A.; Korhonen, J.; Mustonen, T.; Van Hinsbergh, V. W.; Fang, G.-H.; Dumont, D.; Breitman, M.; Alitalo, K. Expression of the Fms-like Tyrosine Kinase 4 Gene Becomes Restricted to Lymphatic Endothelium during Development. *Proc. Natl. Acad. Sci.* **1995**, *92* (8), 3566–3570.

(167) Guo, R.; Zhou, Q.; Proulx, S. T.; Wood, R.; Ji, R.-C.; Ritchlin, C. T.; Pytowski, B.; Zhu, Z.; Wang, Y.-J.; Schwarz, E. M. Inhibition of Lymphangiogenesis and Lymphatic Drainage via Vascular Endothelial Growth Factor Receptor 3 Blockade Increases the Severity of Inflammation in a Mouse Model of Chronic Inflammatory Arthritis. *Arthritis Rheum.* **2009**, *60* (9), 2666–2676.

(168) Huggenberger, R.; Ullmann, S.; Proulx, S. T.; Pytowski, B.; Alitalo, K.; Detmar, M. Stimulation of Lymphangiogenesis via VEGFR-3 Inhibits Chronic Skin Inflammation. *J. Exp. Med.* **2010**, *207* (10), 2255–2269.

(169) Rockson, S. G. Lymphedema. *Am. J. Med.* **2001**, *110* (4), 288–295.

(170) Smeltzer, D. M.; Stickler, G. B.; Schirger, A. Primary Lymphedema in Children and Adolescents: A Follow-up Study and Review. *Pediatrics* **1985**, *76* (2), 206–218.

(171) Karkkainen, M. J.; Ferrell, R. E.; Lawrence, E. C.; Kimak, M. A.; Levinson, K. L.; McTigue, M. A.; Alitalo, K.; Finegold, D. N. Missense Mutations Interfere with VEGFR-3 Signalling in Primary Lymphoedema. *Nat. Genet.* **2000**, *25* (2), 153–159.

(172) Irrthum, A.; Karkkainen, M. J.; Devriendt, K.; Alitalo, K.; Vikkula, M. Congenital Hereditary Lymphedema Caused by a Mutation That Inactivates VEGFR3 Tyrosine Kinase. *Am. J. Hum. Genet.* **2000**, *67* (2), 295–301.

(173) Cormier, J. N.; Askew, R. L.; Mungovan, K. S.; Xing, Y.; Ross, M. I.; Armer, J. M. Lymphedema beyond Breast Cancer. *Cancer* **2010**, *116* (22), 5138–5149.

(174) McLaughlin, S. A.; Wright, M. J.; Morris, K. T.; Giron, G. L.; Sampson, M. R.; Brockway, J. P.; Hurley, K. E.; Riedel, E. R.; Van Zee, K. J. Prevalence of Lymphedema in Women with Breast Cancer 5 Years after Sentinel Lymph Node Biopsy or Axillary Dissection: Objective Measurements. *J. Clin. Oncol.* **2008**, *26* (32), 5213–5219.

(175) Frueh, F. S.; Gousopoulos, E.; Rezaeian, F.; Menger, M. D.; Lindenblatt, N.; Giovanoli, P. Animal Models in Surgical Lymphedema Research—a Systematic Review. *J. Surg. Res.* **2016**, *200* (1), 208–220.

(176) WHO | Lymphatic filariasis http://www.who.int/mediacentre/factsheets/fs102/en/ (accessed Mar 24, 2017).

(177) Casley-Smith, J. R.; Morgan, R. G.; Piller, N. B. Treatment of Lymphedema of the Arms and Legs with 5, 6-Benzo-[Alpha]-Pyrone. *N. Engl. J. Med.* **1993**, *329* (16), 1158–1163.

(178) Soria, P.; Cuesta, A.; Romero, H.; Martinez, F. J.; Sastre, A. Dietary Treatment of Lymphedema by Restriction of Long-Chain Triglycerides. *Angiology* **1994**, *45* (8), 703–707.

(179) Foundation, T. H. Chronic heart failure https://www.heartfoundation.org.au/for-professionals/clinical-information/chronic-heart-failure (accessed Feb 9, 2017).

(180) Mozaffarian, D.; Benjamin, E. J.; Go, A. S.; Arnett, D. K.; Blaha, M. J.; Cushman, M.; Das, S. R.; de Ferranti, S.; Després, J.-P.; Fullerton, H. J.; Howard, V. J.; Huffman, M. D.; Isasi, C. R.; Jiménez, M. C.; Judd, S. E.; Kissela, B. M.; Lichtman, J. H.; Lisabeth, L. D.; Liu, S.; Mackey, R. H.; Magid, D. J.; McGuire, D. K.; Mohler, E. R.; Moy, C. S.; Muntner, P.; Mussolino, M. E.; Nasir, K.; Neumar, R. W.; Nichol, G.; Palaniappan, L.; Pandey, D. K.; Reeves, M. J.; Rodriguez, C. J.; Rosamond, W.; Sorlie, P. D.; Stein, J.; Towfighi, A.; Turan, T. N.; Virani, S. S.; Woo, D.; Yeh, R. W.; Turner, M. B. Heart Disease and Stroke Statistics—2016 Update: A Report From the American Heart Association. *Circulation* **2016**, *133* (4), e38–e360.

(181) Alagiakrishnan, K.; Banach, M.; Jones, L. G.; Ahmed, A.; Aronow, W. S. Medication Management of Chronic Heart Failure in Older Adults. *Drugs Aging* **2013**, *30* (10), 765–782.

(182) Galley, H. F.; Webster, N. R. Physiology of the Endothelium. *Br. J. Anaesth.* **2004**, *93* (1), 105–113.

(183) Tran, Q.-K.; Watanabe, H. Calcium Signalling in the Endothelium. In *The Vascular Endothelium I*; Springer, 2006; pp 145–187.

(184) Tran, Q.-K.; Ohashi, K.; Watanabe, H. Calcium Signalling in Endothelial Cells. *Cardiovasc. Res.* **2000**, *48* (1), 13–22.

(185) Clapham, D. E. Calcium Signaling. *Cell* **2007**, *131* (6), 1047–1058.

(186) Willer, E. A.; Malli, R.; Bondarenko, A. I.; Zahler, S.; Vollmar, A. M.; Graier, W. F.; Fürst, R. The Vascular Barrier-Protecting Hawthorn Extract WS® 1442 Raises Endothelial Calcium Levels by Inhibition of SERCA and Activation of the IP 3 Pathway. *J. Mol. Cell. Cardiol.* **2012**, *53* (4), 567–577.

(187) Ahmmed, G. U.; Malik, A. B. Functional Role of TRPC Channels in the Regulation of Endothelial Permeability. *Pflüg. Arch.* **2005**, *451* (1), 131–142.

(188) Tassell, M.; Kingston, R.; Gilroy, D.; Lehane, M.; Furey, A. Hawthorn (Crataegus Spp.) in the Treatment of Cardiovascular Disease. *Pharmacogn. Rev.* **2010**, *4* (7), 32–41.

(189) Fong, H. H. S.; Bauman, J. L. Hawthorn. *J. Cardiovasc. Nurs.* **2002**, *16* (4), 1–8.

(190) Czygan, F. C. A Short Cultural History in Retrospect. Crataegus as a Cardiac Agent. *Pharm. Unserer Zeit* **2004**, *34* (1), 10–13.

(191) Tauchert, M. Efficacy and Safety of Crataegus Extract WS 1442 in Comparison with Placebo in Patients with Chronic Stable New York Heart Association Class-III Heart Failure. *Am. Heart J.* **2002**, *143* (5), 910–915.

(192) Zapfe, G. Clinical Efficacy of Crataegus Extract WS® 1442 in Congestive Heart Failure NYHA Class II. *Phytomedicine* **2001**, *8* (4), 262–266.

(193) Asher, G. N.; Viera, A. J.; Weaver, M. A.; Dominik, R.; Caughey, M.; Hinderliter, A. L. Effect of Hawthorn Standardized Extract on Flow Mediated Dilation in Prehypertensive and Mildly Hypertensive Adults: A Randomized, Controlled Cross-over Trial. *BMC Complement. Altern. Med.* **2012**, *12* (1), 26.

(194) Härtel, S.; Kutzner, C.; Westphal, E.; Limberger, M.; Burkart, M.; Ebner-Priemer, U.; Kohl-Bareis, M.; Bös, K. Effects of Endurance Exercise Training and Crataegus Extract WS® 1442 in Patients with Heart Failure with Preserved Ejection Fraction–A Randomized Controlled Trial. *Sports* **2014**, *2* (3), 59–75.

(195) Eggeling, T.; Regitz-Zagrosek, V.; Zimmermann, A.; Burkart, M. Baseline Severity but Not Gender Modulates Quantified Crataegus Extract Effects in Early Heart Failure–A Pooled Analysis of Clinical Trials. *Phytomedicine* **2011**, *18* (14), 1214–1219.

(196) Bubik, M. F.; Willer, E. A.; Bihari, P.; Jürgenliemk, G.; Ammer, H.; Krombach, F.; Zahler, S.; Vollmar, A. M.; Fürst, R. A Novel Approach to Prevent Endothelial Hyperpermeability: The Crataegus Extract WS® 1442 Targets the CAMP/Rap1 Pathway. *J. Mol. Cell. Cardiol.* **2012**, *52* (1), 196–205.

(197) Fuchs, S.; Bischoff, I.; Willer, E. A.; Bräutigam, J.; Bubik, M. F.; Erdelmeier, C. A.; Koch, E.; Faleschini, M. T.; De Mieri, M.; Bauhart, M.; Zahler, S.; Hensel, A.; Hamburger, M.; Potterat, O.; Fürst, R. The Dual Edema-Preventing Molecular Mechanism of the Crataegus Extract WS 1442 Can Be Assigned to Distinct Phytochemical Fractions. *Planta Med.* **2017**, *83*, 1–8.

(198) Barba, F.; Recio, J.; Batanero, B. Microwave-Assisted Conversion of Carbonyl Compounds into Formylated Secondary Amines: New Contribution to the Leuckart Reaction Mechanism in N-Methylformamide. *Tetrahedron Lett.* **2013**, *54* (14), 1835–1838.

(199) Herrendorff, R.; Faleschini, M. T.; Stiefvater, A.; Erne, B.; Wiktorowicz, T.; Kern, F.; Hamburger, M.; Potterat, O.; Kinter, J.; Sinnreich, M. Identification of Plant-Derived Alkaloids with Therapeutic Potential for Myotonic Dystrophy Type I. *J. Biol. Chem.* **2016**, *291* (33), 17165–17177.

(200) Terreaux, C.; Maillard, M.; Stoeckli-Evans, H.; Gupta, M. P.; Downum, K. R.; Quirke, J. M. E.; Hostettmann, K. Structure Revision of a Furanocoumarin from Dorstenia Contrajerva. *Phytochemistry* **1995**, *39* (3), 645–647.

(201) Kuster, R. M.; Bernardo, R. R.; Da Silva, A. J.; Parente, J. P.; Mors, W. B. Furocoumarins from the Rhizomes of Dorstenia Brasiliensis. *Phytochemistry* **1994**, *36* (1), 221–223.

(202) Cedrón, J. C.; Del Arco-Aguilar, M.; Estévez-Braun, A.; Ravelo, Á. G. Chemistry and Biology of Pancratium Alkaloids. *Alkaloids Chem. Biol.* **2010**, *68*, 1–37.

(203) Jeffs, P. W.; Abou-Donia, A.; Campau, D.; Staiger, D. Alkaloids of the Amaryllidaceae. 27. Structures of 9-O-Demethylhomolycorine and 5. Alpha.-Hydroxyhomolycorine. Alkaloids of Crinum Defixum, C. Scabrum, and C. Latifolium. Assignment of Aromatic Substitution Patterns from 1H-Coupled Carbon-13 Spectra. *J. Org. Chem.* **1985**, *50* (10), 1732–1737.

(204) Llabrés, J. M.; Viladomat, F.; Bastida, J.; Codina, C.; Serrano, M.; Rubiralta, M.; Feliz, M. Two Alkaloids from Narcissus Requienii. *Phytochemistry* **1986**, *25* (6), 1453–1459.

(205) Wang, Y.-H.; Zhang, Z.-K.; Yang, F.-M.; Sun, Q.-Y.; He, H.-P.; Di, Y.-T.; Mu, S.-Z.; Lu, Y.; Chang, Y.; Zheng, Q.-T. Benzylphenethylamine Alkaloids from Hosta Plantaginea with Inhibitory Activity against Tobacco Mosaic Virus and Acetylcholinesterase. *J. Nat. Prod.* **2007**, *70* (9), 1458–1461.

(206) Evidente, A.; Cicala, M. R.; Giudicianni, I.; Randazzo, G.; Riccio, R. 1H and 13C NMR Analysis of Lycorine and α-Dihydrolycorine. *Phytochemistry* **1983**, *22* (2), 581–584.

(207) Kihara, M.; Ozaki, T.; Kobayashi, S.; Shingu, T. Alkaloidal Constituents of Leucojum Autumnale L.(Amaryllidaceae). *Chem. Pharm. Bull. (Tokyo)* **1995**, *43* (2), 318–320.

(208) Santana, O.; Reina, M.; Anaya, A. L.; Hernández, F.; Izquierdo, M. E.; González-Coloma, A. 3-O-Acetyl-Narcissidine, a Bioactive Alkaloid from Hippeastrum Puniceum Lam.(Amaryllidaceae). *Z. Für Naturforschung C* **2008**, *63* (9–10), 639–643.

(209) Shitara, N.; Hirasawa, Y.; Hasumi, S.; Sasaki, T.; Matsumoto, M.; Wong, C. P.; Kaneda, T.; Asakawa, Y.; Morita, H. Four New Amaryllidaceae Alkaloids from Zephyranthes Candida. *J. Nat. Med.* **2014**, *68* (3), 610–614.

(210) Bastida, J.; Viladomat, F. Chapter 6: Alkaloids of Narcissus. In *Narcissus and daffodil: the genus narcissus*; Taylor & Francis: London and New York, 2002; Vol. 21, p 141.

(211) Ang, S.; Liu, X.-M.; Huang, X.-J.; Zhang, D.-M.; Zhang, W.; Wang, L.; Ye, W.-C. Four New Amaryllidaceae Alkaloids from Lycoris Radiata and Their Cytotoxicity. *Planta Med.* **2015**, *81* (18), 1712–1718.

(212) Bastida, J.; Lavilla, R.; Viladomat, F. Chapter 3 Chemical and Biological Aspects of Narcissus Alkaloids. In *The Alkaloids: Chemistry and Biology*; Elsevier, 2006; Vol. 63, pp 87–179.

(213) Harken, R. D.; Christensen, C. P.; Wildman, W. C. Interconversions in the Pluviine-Lycorenine Series. *J. Org. Chem.* **1976**, *41* (14), 2450–2454.

(214) Vidal, V.; Potterat, O.; Louvel, S.; Hamy, F.; Mojarrab, M.; Sanglier, J.-J.; Klimkait, T.; Hamburger, M. Library-Based Discovery and Characterization of Daphnane Diterpenes as Potent and Selective HIV Inhibitors in Daphne Gnidium. *J. Nat. Prod.* **2011**, *75* (3), 414–419.

(215) *Wilson and Wilson's Comprehensive Analytical Chemistry*; Alain Berthod, Ed.; Elsevier: Amsterdam, Netherlands, 2002; Vol. Volume 38.

(216) Bozicevic, A.; De Bie, H.; Dobrzynski, M.; Gafner, F.; Garo, E.; Hamburger, M. Automated LC-ESIMS Batch Processing Implemented in ACD/MS Workbook Suite and Supported by the External Data Clustering Platform FreeClust. *Anal. Chem.* **2017**, *Submitted*.

(217) Wolfender, J.-L.; Ndjoko, K.; Hostettmann, K. The Potential of LC-NMR in Phytochemical Analysis. *Phytochem. Anal.* **2001**, *12* (1), 2–22.

(218) Bauhart, M. Isolation and Identification of Vascular Barrier Protecting Constituents in Crataegus, University of Basel: Basel, 2013.

(219) Eaton, L. J. Hawthorn Extract Improves Chronic Heart Failure. *J. Fam. Pract.* **2003**, *52* (10).

(220) Schmidt, U.; Kuhn, U.; Ploch, M.; Hübner, W.-D. Efficacy of the Hawthorn (Crataegus) Preparation LI 132 in 78 Patients with Chronic Congestive Heart Failure Defined as NYHA Functional Class II. *Phytomedicine* **1994**, *1* (1), 17–24.

(221) Guo, R.; Pittler, M. H.; Ernst, E. Hawthorn Extract for Treating Chronic Heart Failure. *Cochrane Database Syst. Rev.* **2008**, No. 1.

(222) Mohn, T.; Cutting, B.; Ernst, B.; Hamburger, M. Extraction and Analysis of Intact Glucosinolates—A Validated Pressurized Liquid Extraction/Liquid Chromatography–mass Spectrometry Protocol for Isatis Tinctoria, and Qualitative Analysis of Other Cruciferous Plants. *J. Chromatogr. A* **2007**, *1166* (1), 142–151.

(223) Güvenalp, Z.; Özbek, H.; Ünsalar, T.; Kazaz, C.; DEMİREZER, L. Ö. Iridoid, Flavonoid, and Phenylethanoid Glycosides from Wiedemannia Orientalis. *Turk. J. Chem.* **2006**, *30* (3), 391–400.

(224) Maksudov, M. S.; Maksimov, E. S.; Umarova, R. U.; Saatov, Z.; Abdullaev, N. D. Phlomoside B-An Iridoid Glycoside FromPhlomis Regelii. *Chem. Nat. Compd.* **1996**, *32* (1), 36–38.

(225) Eder, J.; Sedrani, R.; Wiesmann, C. The Discovery of First-in-Class Drugs: Origins and Evolution. *Nat Rev Drug Discov* **2014**, *13* (8), 577–587.

(226) Willis, C. The 21st Century Gold Rush: Novel Molecular Targets http://stateofinnovation.com/the-21st-century-gold-rush-novel-molecular-targets (accessed Apr 7, 2017).

Appendices

Appendix A: NMR Tables and Structures of Isolated Compounds

Table A1: ^{1}H and ^{13}C spectroscopic data for auroside (La-1) from *Lamium album*, (CD_3OD; 500 MHz for ^{1}H and ^{13}C extracted from ^{1}H-^{13}C 2D inverse detected experiments; δ in ppm)

	auroside	
Position	**δ_H mult (*J* in Hz)**	**δ_C type**
1	5.76 d (1.7)	93.6 CH
3	7.40 s	151.7 CH
4	-	113.3
5	-	69.6 qC
6	2.10 dd (13.8, 6)	46.4 CH_3
	2.60 dd (13.8, 6)	
7	3.61 m	76.9 CH
8	2.30 m	42.0 CH
9	2.83 dd (10, 1.5)	49.9 CH
10	0.98 d (7.4)	12.9
11	-	166.1 qC
12	3.77 s	50.5 CH_3
1’	4.60 d (8.0)	99.4 CH
2’	3.24 dd (9.0, 8.0)	73.4 CH
3’	3.41 t (9.0)	76.0 CH
4’	3.33 m	70.4 CH
5’	3.37 m	76.6 CH
6’	3.70 dd (12.0, 6.0)	61.3 CH_2
	3.93 dd (12.0, 6.0)	

For ^{13}C shifts, data was extrapolated by HSQC and HMBC contours.

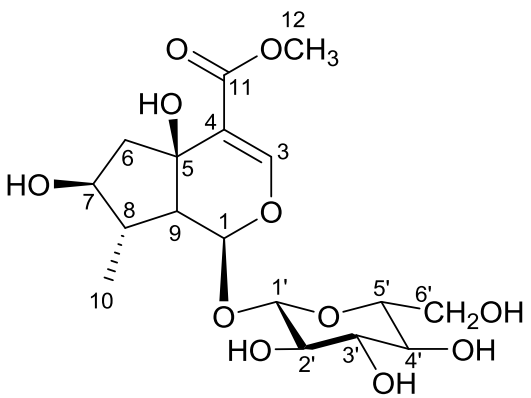

Structure of auroside with atom numbering

Table A2: ^{1}H and ^{13}C spectroscopic data for compounds methyltanshinoate (Sm-N2), cryptotanhinone (Sm-O2), tanshinone I (Sm-L2), dehydromiltirone (Sm-F1) and tanshinone IIA (Sm-H-xtl) from *Salvia miltiorrhiza*, ($CDCl_3$; 500 MHz for ^{1}H and ^{13}C extracted from ^{1}H-^{13}C 2D inverse detected experiments; δ in ppm)

	methyltanshinoate		**cryptotanshinone**		**tanshinone I**		**dehydromiltirone**		**tanshinone IIA**	
Position	**δ_H mult (*J* in Hz)**	**δ_C type**	**δ_H mult (*J* in Hz)**	**δ_C type**	**δ_H mult (*J* in Hz)**	**δ_C type**	**δ_H mult (*J* in Hz)**	**δ_C type**	**δ_H mult (*J* in Hz)**	**δ_C type**
1	3.23 m	28.9 CH_2	3.17 t (7.0)	29.3 CH_2	8.70 d (8.0)	118.7 CH	7.84 br dt (10.0)	122.5 CH	3.15 t (7.0)	29.5 CH_2
2	1.81 m	19.2 CH_2	1.75 m	19.0 CH_2	7.53 br dd (8.0, 6.0)	129.1 CH	6.28 br ddd (9.0, 7.1, 4.9)	132.1 CH	1.81 m	19.3 CH_2
3	1.75 m 2.27 m	34.1 CH_2	1.62 m	37.8 CH_2	7.32 d (6.0)	128.8 CH	2.24 br dd (4.5, 2.0)	35.9 CH_2	1.64 m	37.9 CH_2
4	-	47.3 qC	-	34.5 qC	-	134.8 qC	-	32.4 qC	-	34.5 qC
5	-	149.5 qC	-	150.0 qC	-	123.2 qC	-	146.2 qC	-	150.0 qC
6	7.55 d (8.0)	135.4 CH	7.58 d (8.0)	132.4 CH	7.98 d (8.0)	131.9 CH	7.45 br d (8.0)	128.4 CH	7.60 br d (8.0)	135.4 CH
7	7.47 d (8.0)	120.4 CH	7.44 d (8.0)	122.3 CH	8.05 d (8.0)	124.8 CH	7.20 d (8.0)	126.9 CH	7.50 br d (8.0)	120.4 CH
8	-	127.4 qC	-	127.4 qC	-	129.6 qC	-	132.4 qC	-	127.4 qC
9	-	128.3 qC	-	126.6 qC	-	126.9 qC	-	125.5 qC	-	126.2 qC
10	-	144.9 qC		144.3 qC	-	133.6 qC	-	136.2 qC	-	144.0 qC
11	-	183.1 qC		183.2 qC	-	183.4 qC	-	182.5 qC	-	183.1 qC
12	-	175.6 qC		175.6 qC	-	175.6 qC	-	180.0 qC	-	175.6 qC
13	-	121.2 qC		120.0 qC	-	121.0 qC	-	143.5 qC	-	121.1 qC
14	-	161.8 qC		161.4 qC	-	161.7 qC	7.06 s	137.7 CH	-	161.7 qC
15	-	141.8 qC	3.54 m	34.5 CH	-	120.9 qC	2.98 br spt (6.9)	24.81 CH	-	142.0 qC
16	7.22 br d (1.3)	141.3 CH	4.30 dd (9.0, 6.0) 4.84 t (9.0)	81.4 CH_2	7.27 d (1.5)	141.7 CH	1.13 d (6.9)	19.4 CH_3	7.20 br s	120.1 CH
17	2.25 s	8.7 CH_3	1.32 d (7.0)	18.5 CH_3	3.02 s	8.8 CH_3	1.13 d (6.9)	19.4 CH_3	2.24 br d (1.5)	8.6 CH_3
18	1.57 s	27.5 CH_3	1.27 br d (1.5)	31.9 CH_3	3.16 s	20.7 CH_3	1.25 s	26.2 CH_3	1.31 s	31.7 CH_3
19	-	176.9 qC	1.27 br d (1.5)	31.9 CH_3			1.25 s	26.2 CH_3	1.31 s	31.7 CH_3
20	3.66 s	52.3 CH_3								

For ^{13}C shifts, data was extrapolated by HSQC and HMBC contours.

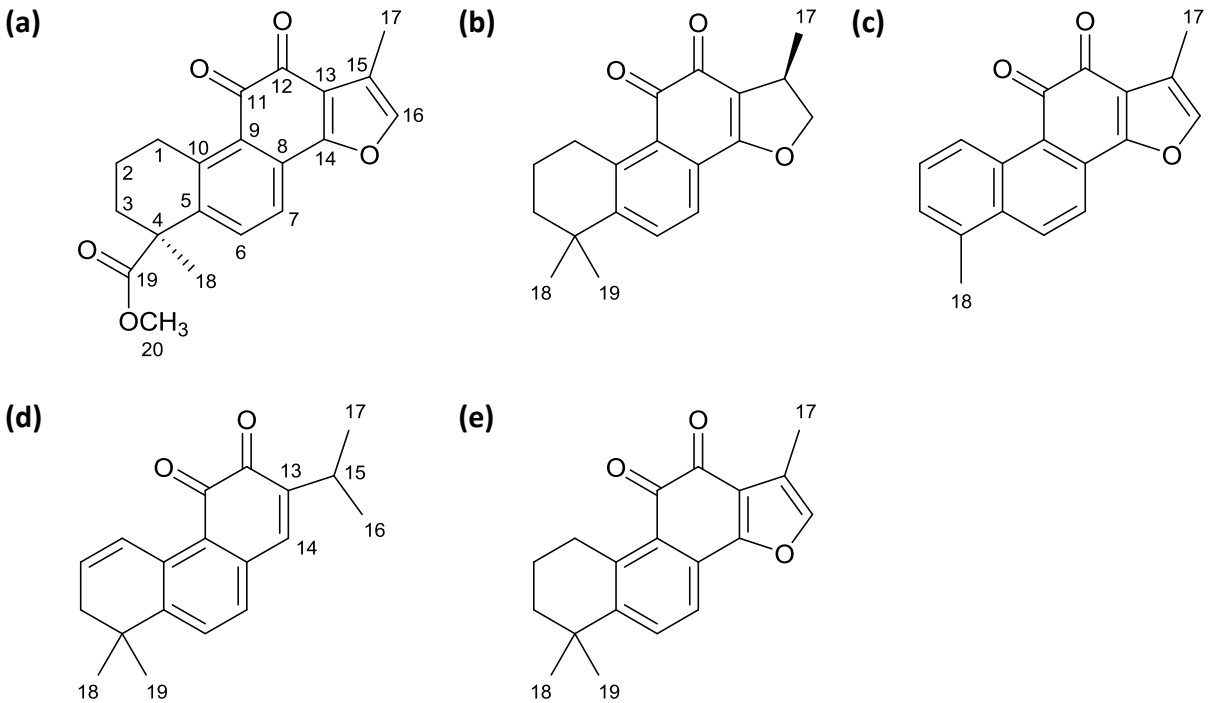

Structures of (**a**) methyltanshinoate, (**b**) cryptotanhinone, (**c**) tanshinone I, (**d**) dehydromiltirone, and (**e**) tanshinone IIA with atom numbering

Table A3: ^{1}H and ^{13}C spectroscopic data for bergapten and dorstenin (compounds Dc-A1 and Dc-A2) from *Dorstenia contrajerva*, ($CDCl_3$; 500 MHz for ^{1}H and ^{13}C extracted from ^{1}H-^{13}C 2D inverse detected experiments; δ in ppm)

	bergapten		dorstenin	
Position	**δ_H mult (*J* in Hz)**	**δ_C type**	**δ_H mult (*J* in Hz)**	**δ_C type**
2	-	161.1 qC	-	161.5 qC
3	6.19 d (9.9)	112.3 CH	6.30 d (9.7)	113.1 CH
4	8.06 d (9.9)	139.6 CH	8.13 d (9.7)	139.1 CH
4a	-	105.5 qC	-	107.1 qC
5	-	149.9 qC	-	148.7 qC
6	-	112.6 qC	-	113.8 qC
7	-	158.4 qC	-	158.5 qC
8	7.05 s	93.4 CH	7.17 s	94.6 CH
8a	-	151.3 qC	-	152.7 qC
2’	6.94 d (2.5)	146.2 CH	7.60 d (2.3)	145.1 CH
3’	7.51 d (2.5)	104.3 CH	7.07 m	104.9 CH
1’’	4.19 s	60.7 CH_3	4.49 m	70.49 CH_2
2’’			2.11 m	34.5 CH_2
			2.25 m	
3’’			3.00 m	32.7 CH
4’’			1.36 m	18.1 CH_3
2’’’			-	194.2 qC
3’’’			5.42 s	100.3 CH
4’’’			-	207.2 qC
5’’’			-	88.9 qC
6’’’			1.35 m	23.1 CH_3
7’’’			1.35 m	23.1 CH_3

For ^{13}C shifts, data was extrapolated by HSQC and HMBC contours.

(a)

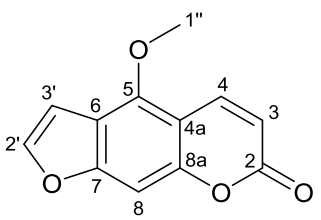

(b)

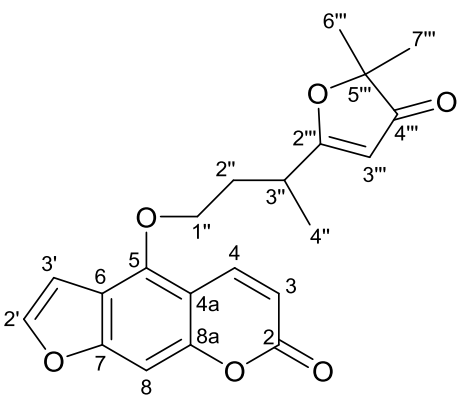

Structures of (**a**) bergapten, and (**b**) dorstenin with atom numbering

Table A4: ^{1}H and ^{13}C spectroscopic data for 8-*O*-demethyl-homolycorine and 8-*O*-demethyl-6-*O*-methyl-lycorenine (compounds Pl-K2 and Pl-K9) from *Pancratium littorale*, (DMSO-*d6*; 500 MHz for ^{1}H and ^{13}C extracted from ^{1}H-^{13}C 2D inverse detected experiments; δ in ppm)

	8-*O*-demethyl-homolycorine		**8-*O*-demethyl-6-*O*-methyl-lycorenine**	
Position	**δ_H mult (*J* in Hz)**	**δ_C type**	**δ_H mult (*J* in Hz)**	**δ_C type**
1	4,75 dd (5.0, 1.5)	76.3 CH	4.09 dd (5.8, 1.8)	65.9 CH
2	2.35 ov	30.2 CH_2	2.15 ov	31.0 CH_2
	2.61 ov		2.55 m	
3	5.45 m	114.2 CH	5.37 m	115.0 CH
4	-	140.3 qC	-	140.6 qC
4a	2.46 ov	65.8 CH	2.39 br d (9.0)	66.7 CH
6	-	163.9 qC	5.35 br s	97.3 CH
6a	-	116.0 qC	-	126.0 qC
7	7.32 s	115.0 CH	6.66 s	114.0 CH
8	-	146.0 qC	-	145.4 qC
9	-	151.2 qC	-	146.7 qC
10	7.01 s	111.2 CH	6.84 s	112.9 CH
10a	-	135.8 qC	-	128.4 qC
10b	2.62 dd (9.2, 1.5)	42.2 CH	2.28 dd (9.0, 1.8)	43.0 CH
11	2.35 m	27.2 CH_2	2.28 m	27.7 CH_2
	2.42 m		2.42 m	
12	2.12 dd (9.2, 8.9)	55.2 CH_2	2.13 ov	55.9 CH_2
	3.00 ddd (9.5, 8.0, 2.5)		3.00 ddd (8.8, 8.8, 3.0)	
MeN (13)	1.89 s	42.7 CH_3	1.95 s	43.7 N-CH_3
9-MeO (14)	3.85 s	55.4 CH_3	3.73 s	55.5 O-CH_3
6-MeO (15)			3.36 s	54.5 O-CH_3

For ^{13}C shifts, data was extrapolated by HSQC and HMBC contours.

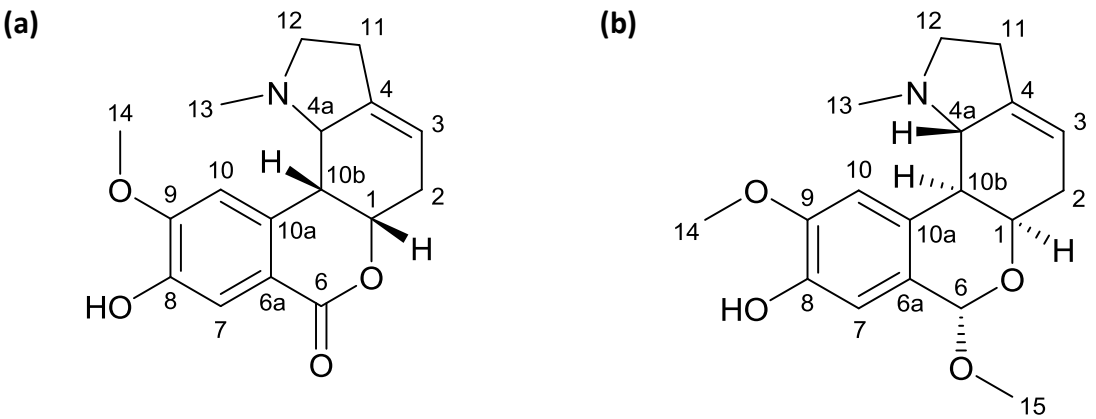

Structures of (**a**) 8-*O*-demethyl-homolycorine, and (**b**) 8-*O*-demethyl-6-*O*-methyl-lycorenine with atom numbering

Table A5: ^{1}H and ^{13}C spectroscopic data for 8-demethyoxy-10-*O*-methyl-hostasine and 10-*O*-methyl-hostasine (compounds Pl-H11 and Pl-H15) from *Pancratium littorale*, (DMSO-*d6*; 500 MHz for ^{1}H and ^{13}C extracted from ^{1}H-^{13}C 2D inverse detected experiments; δ in ppm)

	8-demethyoxy-10-*O*-methyl-hostasine		**10-*O*-methyl-hostasine**	
Position	**δ_H mult (*J* in Hz)**	**δ_C type**	**δ_H mult (*J* in Hz)**	**δ_C type**
1	3.51 br s	76.6 CH	3.53 br s	76.4 CH
2	4.05 br s	70.9 CH	4.04 br s	71.0 CH
3	5.53 br s	119.5 CH	5.53 br s	119.5 CH
4	-	145.5 qC	-	139.5 qC
4a	3.31 br s	65.5 CH	3.28 br s	65.8 CH
6	-	169.4 qC	-	170.1 qC
6a	-	117.8 qC	-	110.3 qC
7	7.24 s	105.7 CH	-	151.3 qC
8	-	150.6 qC	-	141.8 qC
9	-	153.5 qC	-	158.3 qC
10	7.26 s	106.8 CH	7.10 s	103.3 CH
10a	-	145.1 qC	-	148.6 qC
10b	-	83.8 qC	-	83.0 qC
11	2.33 m	27.7 CH_2	2.32 m	27.7 CH_2
	2.45 m		2.44 m	
12	2.20 q (8.8)	55.1 CH_2	2.21 q (8.8)	55.2 CH_2
	2.92 td (8.8, 3.0)		2.93 td (8.8, 3.1)	
MeN (13)	1.49 s	42.8 N-CH_3	1.55 s	42.9 N-CH_3
9-MeO (14)	3.88 s	55.9 O-CH_3	3.90 s	56.4 O-CH_3
6-MeO (15)	3.85 s	55.9 O-CH_3	3.76 s	60.9 O-CH_3
7-MeO (16)	3.85 s	55.9 O-CH_3	3.96 s	62.0 O-CH_3

For ^{13}C shifts, data was extrapolated by HSQC and HMBC contours.

(a)

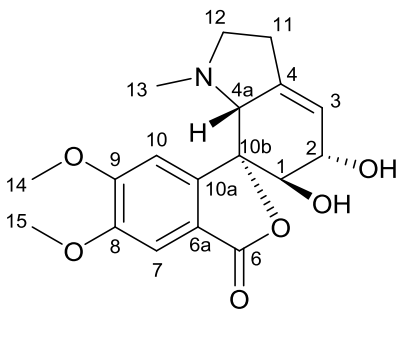

(b)

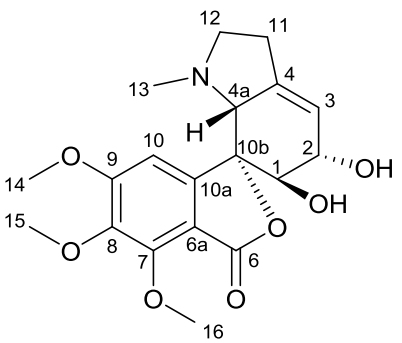

Structures of (**a**) 8-demethyoxy-10-*O*-methyl-hostasine, and (**b**) 10-*O*-methyl-hostasine with atom numbering

Table A6: ^{1}H and ^{13}C spectroscopic data for carinatine, lycorine, pseudolycorine, and 1-*O*-acetyl-pseudolycorine (compounds Pl-I10, Pl-I14, Pl-M1, and Pl-H18) from *Pancratium littorale*, (DMSO-*d6*; 500 MHz for ^{1}H and ^{13}C extracted from ^{1}H-^{13}C 2D inverse detected experiments; δ in ppm)

	carinatine		lycorine		pseudolycorine		1-*O*-acetyl-pseudolycorine	
Position	**δ_H mult (*J* in Hz)**	**δ_C type**	**δ_H mult (*J* in Hz)**	**δ_C type**	**δ_H mult (*J* in Hz)**	**δ_C type**	**δ_H mult (*J* in Hz)**	**δ_C type**
1	4.39 m	66.0 CH	4.29 m	69.5 CH	4.28 m	70.8 CH	5.50 br s	71.9 CH
2	3.65 m	81.2 CH	4.00 m	71.0 CH	4.04 m	72.0 CH	3.97 m	68.5 CH
3	5.46 m	115.0 CH	5.39 m	118.1 CH	5.41 br s	118.8 CH	5.41 m	117.9 CH
4	-	143.1 qC	-	140.6 qC	-	142.4 qC	-	142.2 qC
4a	2.64 br d (10.3)	60.3 CH	2.69 br d (10.5)	60.2 CH	2.66 br d (10.5)	61.4 CH	2.60 br d (10.5)	61.0 CH
6	3.35 d (14.0)	55.9 CH_2	3.41 d (13.0)	55.9 CH_2	3.37 br d (13.8)	56.9 CH_2	3.37 d (14.0)	55.6 CH_2
	4.00 d (14.0)		4.04 d (13.0)		4.05 br d (13.8)		4.04 d (14.0)	
6a	-	127.8 qC	-	129.2 qC	-	127.3 qC	-	126.5 qC
7	6.64 s	110.9 CH	6.68 s	106.5 CH	6.68 s	111.8 CH	6.66 s	111.3 CH
8	-	145.5 qC	-	146.0 qC	-	146.2 qC	-	145.0 qC
9	-	144.5 qC	-	145.8 qC	-	145.4 qC	-	145.9 qC
10	6.76 s	111.6 CH	6.81 s	104.6 CH	6.78 s	112.5 CH	6.59 s	111.1 CH
10a	-	126.2 qC	-	128.9 qC	-	129.0 qC	-	126.8 qC
10b	2.35 br d (10.3)	40.2 CH	2.54 m	39.6 CH	2.55 m	40.2 CH	2.75 br d (10.5)	38.4 CH
11	2.40-2.54 m	27.7 CH_2	2.40-2.50 m	27.8 CH_2	2.45-2.53 m	28.5 CH_2	2.47-2.53 m	27.8 CH_2
12	2.26 q (8.5)	52.8 CH_2	2.31 q (8.5)	52.8 CH_2	2.25 q (8.5)	53.8 CH_2	2.28 q (8.5)	53.1 CH_2
	3.21 td (8.8, 1.6)		3.19 td (8.5, 1.8)		3.26 br t (8.5)		3.23 br d (8.5)	
13	3.72 s	55.7 O-CH_3	5.94 br d (5.6)	100.0 CH_2	3.77 s	56.4 O-CH_3	3.72 s	55.5 O-CH_3
14							-	169.8 qC
15							1.85 s	20.7 O-CH_3

For ^{13}C shifts, data was extrapolated by HSQC and HMBC contours.

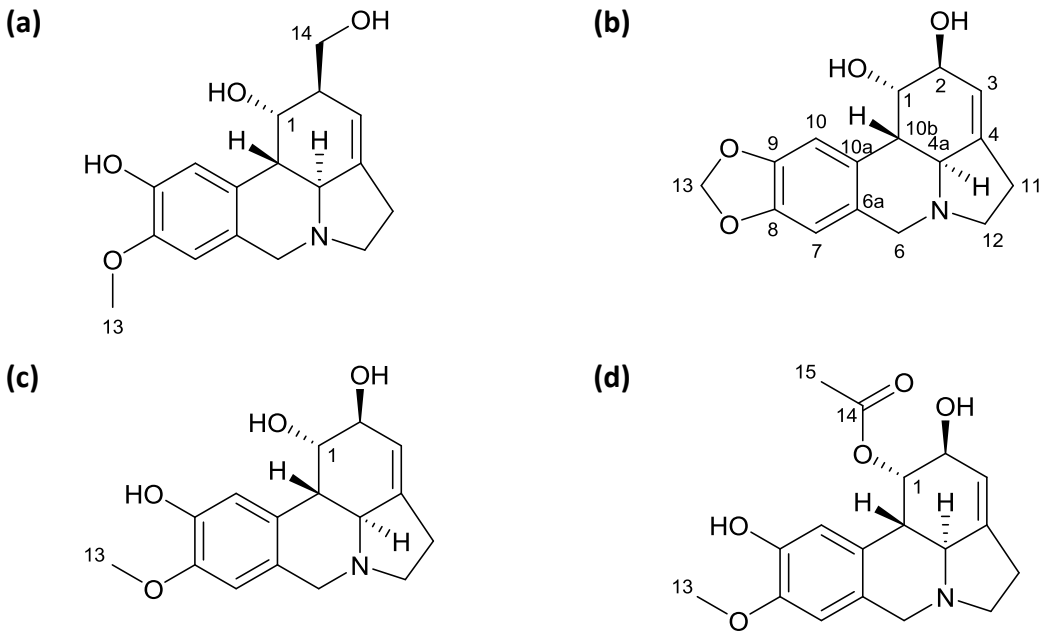

Structures of (**a**) carinatine, (**b**) lycorine, (**c**) pseudolycorine, and (**d**) 1-*O*-acetyl-pseudolycorine with atom numbering

Table A7: ^{1}H and ^{13}C spectroscopic data for narcissidine, and 3-*O*-acetyl-narcissidine (compounds Pl-K7, and Pl-G17) from *Pancratium littorale*, (DMSO-*d6*; 500 MHz for ^{1}H and ^{13}C extracted from ^{1}H-^{13}C 2D inverse detected experiments; δ in ppm)

	narcissidine		**3-*O*-acetyl-narcissidine**	
Position	**δ_H mult (*J* in Hz)**	**δ_C type**	**δ_H mult (*J* in Hz)**	**δ_C type**
1	4.67 br s	66.0 CH	4.58 br t(2.5)	65.8 CH
2	3.62 dd(3.5, 2.0)	80.7 CH	3.60 br t (2.3)	80.9 CH
3	4.50 d (2.0)	66.3 CH	5.51 br s	67.6 CH
4	-	140.4 qC	-	136.7 qC
4a	3.81 m	60.9 CH	3.77 ov	61.5 CH
6	3.55 d (13.0)	53.0 CH_2	3.57 br d (13.1)	53.7 CH_2
	4.01 d (13.0)		3.97 br d (13.1)	
6a	-	128.4 qC	-	129.5 qC
7	6.82 s	110.4 CH	6.79 s	111.0 CH
8	-	147.2 qC	-	142.2 qC
9	-	148.0 qC	-	147.1 qC
10	6.94 s	108.2 CH	6.95 s	109.2 CH
10a	-	129.2 qC	-	129.3 qC
10b	2.63 br d (11.0)	39.8 CH	2.57 br d (11.0)	40.1 CH
11	5.67 ddd (2.0, 2.0, 1.5)	120.1 CH	5.87 br q (1.8)	125.6 CH
12	3.49 ddd (14.0, 6.0, 2.0)	60.7 CH_2	3.51 br dd	60.9 CH_2
	3.89 ddd (14.0, 6.0, 2.0)		3,84 br dd	
8-MeO (13)	3.77 s	56.3 O-CH_3	3.73 s	55.5 O-CH_3
9-MeO (14)	3.80 s	56.2 O-CH_3	3.77 s	55.5 O-CH_3
2-MeO (15)	3.41 s	57.7 O-CH_3	3.40 s	57.2 O-CH_3
16			-	169.9 qC
17			1.95 s	20.7 CH_3

For ^{13}C shifts, data was extrapolated by HSQC and HMBC contours.

(a)

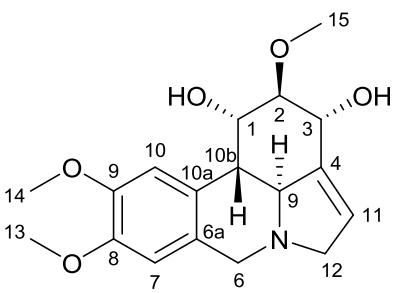

(b)

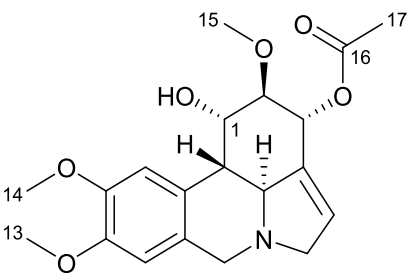

Structures of (**a**) narcissidine, and (**b**) 3-*O*-acetyl-narcissidine with atom numbering

Table A8: ^{1}H and ^{13}C spectroscopic data for 10-deoxy-6(α)-hydroxy-hippeastidine, and 6-hydroxy-hippeastidine (compounds PI-G16, and PI-I19) from *Pancratium littorale*, (DMSO-*d6*; 500 MHz for ^{1}H and ^{13}C extracted from ^{1}H-^{13}C 2D inverse detected experiments; δ in ppm)

	10-deoxy-6(α)-hydroxy-hippeastidine		6-hydroxy-hippeastidine	
Position	**δ_H mult (*J* in Hz)**	**δ_C type**	**δ_H mult (*J* in Hz)**	**δ_C type**
1	1.58 td (13.6, 4.4)	25.5 CH_2	1.62 ov	25.8 CH_2
	2.45 dt (13.6, 3.5, 3.5)		3.15 ov	
2	1.37 m	26.7 CH_2	1.34 ov	26.7 CH_2
	2.00 m		1.92 ov	
3	3.12 ov	77.0 CH	3.15 ov	76.5 CH
4	1.10 q (12.0)	32.2 CH_2	1.92 q (12.0)	31.8 CH_2
	1.85 m		1.14 q (12.0)	
4a	3.11 m	59.4 CH	3.34 m	60.0 CH
6	4.87 s	87.8 CH	5.02 s	87.9 CH
6a	-	127.6 qC	-	129.8 qC
7	6.74 br s	112.2 CH	6.38 s	103.7 CH
8	-	147.5 qC	-	150.8 qC
9	-	148.6 qC	-	136.1 qC
10	6.69 br s	106.0 CH	-	147.8 qC
10a	-	140.5 qC	-	125.6 qC
10b	-	42.2 qC	-	46.3 qC
11	1.40 m	33.9 CH_2	1.56 m	31.6 CH_2
	2.09 m		2.19 m	
12	2.61 m	46.2 CH_2	2.70 m	46.3 CH_2
	3.16 m		3.30 m	
8-MeO (13)	3.70 s	55.3 O-CH_3	3.73 s	55.3 O-CH_3
9-MeO (14)	3.73 s	55.6 O-CH_3	3.65 s	59.9 O-CH_3
3-MeO (15)	3.26 s	54.5 O-CH_3	3.25 s	54.7 O-CH_3

For ^{13}C shifts, data was extrapolated by HSQC and HMBC contours.

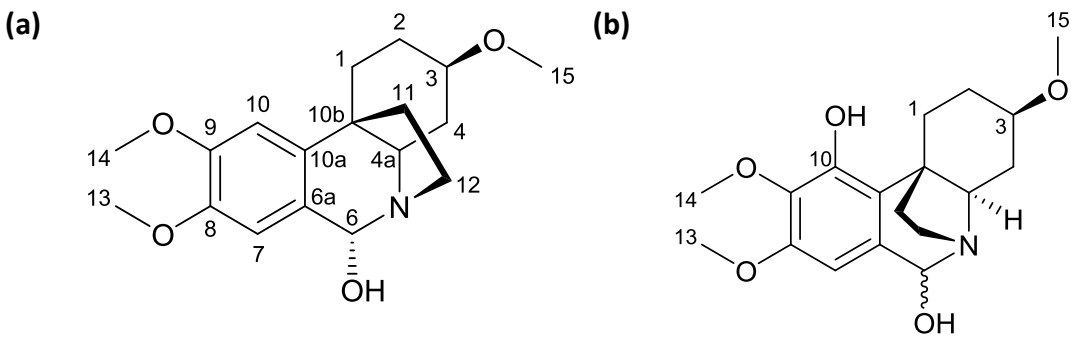

Structures of (**a**) 10-deoxy-6(α)-hydroxy-hippeastidine, and (**b**) 6-hydroxy-hippeastidine with atom numbering

Table A9: ^{1}H and ^{13}C spectroscopic data for daphnetin, chrysoeriol, and daphneolone (compounds Dgi-4-xtl, Dgi-12-xtl, and Dgi-Ed-8) from *Daphne giraldii*, (DMSO-*d6*; 500 MHz for ^{1}H and ^{13}C extracted from ^{1}H-^{13}C 2D inverse detected experiments; δ in ppm)

	daphnetin		chrysoeriol		daphneolone	
Position	**δ_H mult (*J* in Hz)**	**δ_C type**	**δ_H mult (*J* in Hz)**	**δ_C type**	**δ_H mult (*J* in Hz)**	**δ_C type**
1					-	196.3 qC
2	-	163.4 qC	-	163.9 qC	2.91 dd (15.0, 5.0) 3.08 dd (15.0, 8.0)	45.3 CH_2
3	6.17 d (9.5)	112.2 CH	6.33 s	103.8 CH	4.05 spt	66.4 CH
4	7.82 d (9.5)	146.7 CH	-	182.0 qC	1.74 m	38.6 CH_2
5	6.99 d (8.5)	120.2 CH	-	157.7 qC	2.63 m 2.76 m	31.0 CH_2
6	6.80 d (8.5)	113.7 CH	6.12 d (3.0)	99.2 CH		
7	-	146.7 CH	-	164.7 qC		
8	-	133.5 CH	6.48 d (3.0)	94.2 CH		
9	-	145.0 qC	-	162.1 qC		
10	-	113.9 qC	-	104.0 qC		
3'-MeO (11)			3.85 s	56.2 O-CH_3		
1'			-	123.5 qC	-	128.4 qC
2'			7.28 d (2.0)	113.3 CH	7.84 d (8.8)	130.2 CH
3'			-	147.0 qC	6.86 d (8.5, 2.0)	114.7 CH
4'			-	147.1 qC	-	161.5 qC
5'			6.85 d (8.0)	112.5 CH	6.86 d (8.5, 2.0)	114.7 CH
6'			7.35 dd (8.0, 2.5)	118.9 CH	7.84 d (8.8)	130.2 CH
1''					-	141.7 qC
2''					7.20 m	127.8 CH
3''					7.26 m	127.3 CH
4''					7.15 m	125.0 CH
5''					7.26 m	127.3 CH
6''					7.20 m	127.8 CH

For ^{13}C shifts, data was extrapolated by HSQC and HMBC contours.

(a)

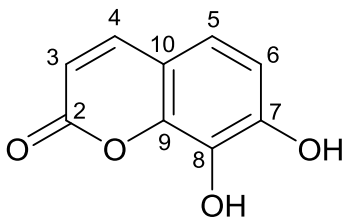

(b)

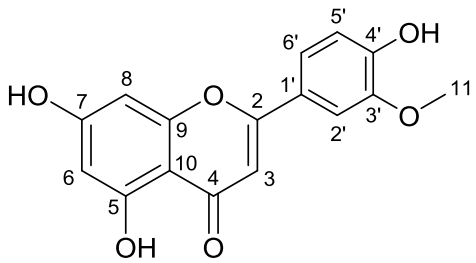

(c)

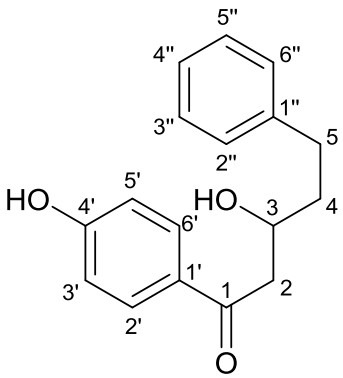

Structures of (**a**) daphnetin, (**b**) chrysoeriol, and (**c**) daphneolone with atom numbering

THE JOURNAL OF BIOLOGICAL CHEMISTRY VOL. 291, NO. 33, pp. 17165–17177, August 12, 2016

Identification of Plant-derived Alkaloids with Therapeutic Potential for Myotonic Dystrophy Type I*

Received for publication, December 14, 2015, and in revised form, June 10, 2016 Published, JBC Papers in Press, June 13, 2016, DOI 10.1074/jbc.M115.710616

Ruben Herrendorff[‡], Maria Teresa Faleschini[§1], Adeline Stiefvater[‡], Beat Erne[‡], Tatiana Wiktorowicz[‡], Frances Kern[‡], Matthias Hamburger[§], Olivier Potterat[§], Jochen Kinter[‡2], and Michael Sinnreich[‡3]

From the [‡]Neuromuscular Research Group, Departments of Neurology and Biomedicine, University Hospital Basel, Klingelbergstrasse 50, 4056 Basel, Switzerland and the [§]Division of Pharmaceutical Biology, Department of Pharmaceutical Sciences, University of Basel, Klingelbergstrasse 50, 4056 Basel, Switzerland

Myotonic dystrophy type I (DM1) is a disabling neuromuscular disease with no causal treatment available. This disease is caused by expanded CTG trinucleotide repeats in the 3′ UTR of the dystrophia myotonica protein kinase gene. On the RNA level, expanded $(CUG)_n$ repeats form hairpin structures that sequester splicing factors such as muscleblind-like 1 (MBNL1). Lack of available MBNL1 leads to misregulated alternative splicing of many target pre-mRNAs, leading to the multisystemic symptoms in DM1. Many studies aiming to identify small molecules that target the $(CUG)_n$-MBNL1 complex focused on synthetic molecules. In an effort to identify new small molecules that liberate sequestered MBNL1 from $(CUG)_n$ RNA, we focused specifically on small molecules of natural origin. Natural products remain an important source for drugs and play a significant role in providing novel leads and pharmacophores for medicinal chemistry. In a new DM1 mechanism-based biochemical assay, we screened a collection of isolated natural compounds and a library of over 2100 extracts from plants and fungal strains. HPLC-based activity profiling in combination with spectroscopic methods were used to identify the active principles in the extracts. The bioactivity of the identified compounds was investigated in a human cell model and in a mouse model of DM1. We identified several alkaloids, including the β-carboline harmine and the isoquinoline berberine, that ameliorated certain aspects of the DM1 pathology in these models. Alkaloids as a compound class may have potential for drug discovery in other RNA-mediated diseases.

Myotonic dystrophy type I (DM1)[4] is the most common muscular dystrophy in the adult population, with a relatively high prevalence of about 1:8000 (1). This autosomal dominantly inherited disease affects multiple organs, most prominently the skeletal muscle, with wasting, weakness, and an inability to relax (myotonia) (1). Currently, there is no effective treatment for this disabling disease. The pathomechanism of DM1 is linked to a CTG_n expansion in the 3′ UTR of the dystrophia myotonica protein kinase (*DMPK*) gene (2, 3), leading to a toxic gain-of-function RNA (4, 5). The mutant DMPK transcript is entrapped within nuclei of affected cells, where it forms aggregates (foci) with splicing factors such as muscleblind-like 1 (MBNL1) (6, 7). Bound to mutant DMPK $(CUG)_n$ RNA, MBNL1 is no longer available for correct splicing of its target pre-mRNAs (8, 9). Thus, the splicing of a multitude of pre-mRNAs is misregulated, including the skeletal muscle chloride channel (*CLCN1*), the insulin receptor (*INSR*), sarcoplasmic/endoplasmic reticulum Ca^{2+} ATPase 1 (*SERCA1*), and cardiac troponin T type 2 (*TNNT2*) pre-mRNA (10–16). Interestingly, the missplicing of some pre-mRNAs can be linked directly to a certain disease symptom, *e.g.* myotonia in the case of the CLCN1 pre-mRNA. MBNL1 sequestration by $(CUG)_n$ RNA causes inclusion of alternative exon 7a, leading to a shift in the open reading frame and to premature termination of translation (12, 13). As a result, functional CLCN1 protein is decreased, which leads to the myotonia characteristic of DM1 (17).

To date, most therapeutic strategies toward DM1 focused either on the development of agents degrading the toxic RNA or blocking its pathogenic interaction with proteins; these strategies are reviewed in Ref. 18. Antisense oligonucleotides targeting the DMPK-$(CUG)_n$ transcripts (5, 19) and viral overexpression of MBNL1 (20) have been shown to reverse the toxic RNA effect *in vitro* and *in vivo*. Compared with the antisense oligonucleotide and gene therapy approaches, an advantage of a suitable small molecule is its potential to penetrate all tissues affected in DM1 patients and its potential oral bioavailability. A variety of small molecules have been described that inhibit the $(CUG)_n$-MBNL1 complex and improve DM1-associated molecular defects *in vitro* and in some cases also *in vivo*. Several approaches were successful in identifying small molecules, such as screening of known nucleic acid binders (21), rational design of small molecules based on the structure of $(CUG)_n$ RNA (22), rational design of oligomers of $(CUG)_n$ RNA binders by modular assembly (23, 24), combinatorial chemistry (25, 26), and high-throughput screening (27, 28).

* This work was funded by the Neuromuscular Research Association Basel, Swiss National Science Foundation, and by Myosuisse. The authors declare that they have no conflicts of interest with the contents of this article.
[1] Supported by Swiss Federal Commission for Scholarship for Foreign Students (FCS) and South African National Research Foundation fellowships.
[2] To whom correspondence may be addressed: Neuromuscular Research Group, Depts. of Neurology and Biomedicine, University Hospital Basel, Klingelbergstr. 50, 4056 Basel, Switzerland. Tel.: 41-61-2671635; E-mail: j.kinter@unibas.ch.
[3] To whom correspondence may be addressed: Neuromuscular Research Group, Depts. of Neurology and Biomedicine, University Hospital Basel, Klingelbergstr. 50, 4056 Basel, Switzerland. Tel.: 41-61-2652525; E-mail: michael.sinnreich@unibas.ch.
[4] The abbreviations used are: DM1, myotonic dystrophy type 1; DMPK, dystrophia myotonica protein kinase; HSA^{LR}, human skeletal α-actin long repeat; qPCR, quantitative PCR; DHB, dihydroberberine; GM, growth medium.

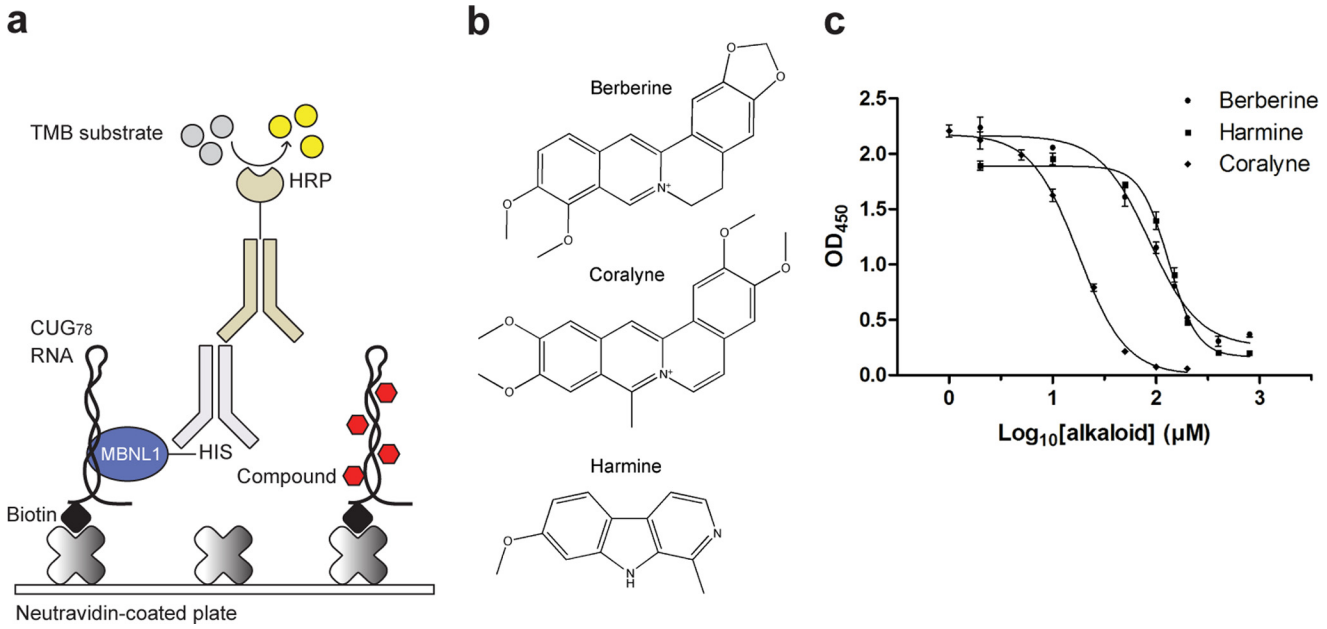

FIGURE 1. **Screening for small molecules of natural origin that disrupt the CUG_{78}-MBNL1 complex *in vitro*.** *a*, the CUG_{78}-MBNL1 inhibition assay detects the amount of MBNL1 bound to CUG_{78}-RNA. *b*, structure of the identified alkaloids berberine, coralyne, and harmine. *c*, CUG_{78}-MBNL1 complex inhibition curves. *OD*, optical density; *TMB*, 3,3′,5,5′-tetramethylbenzidine.

Most of the described $(CUG)_n$ RNA-targeting molecules are synthetic. Only a few small molecules of natural origin have been described, such as neomycin B (21) and lomofungin (27). To our knowledge, our study is the first to focus on small molecules of natural origin and represents the first screening of natural extracts in DM1 drug discovery. As RNA is still a relatively unexploited drug target, natural products present a rich source of new and diverse RNA binders (29). Interestingly, many known RNA-binding drugs are of natural origin, such as antibiotics that target the bacterial ribosomal RNA (30). Hence, it is of interest to investigate natural products in drug discovery for RNA-mediated diseases such as DM1.

We describe here the screening of isolated natural compounds and extracts from plants and fungal strains in a novel CUG_{78}-MBNL1 complex inhibition assay. We identified several alkaloids as CUG_{78}-MBNL1 complex inhibitors. Testing their bioactivity in a human myoblast model of DM1 (31) and in the human skeletal α-actin long repeat (HSA^{LR}) mouse model of DM1 (4) showed that the alkaloids ameliorate certain aspects of the DM1 pathology.

Results

CUG_{78}-MBNL1 Complex Inhibitors of Natural Origin—A collection of 70 isolated natural compounds and a library containing 2128 extracts from plants and fungi were screened with a novel *in vitro* CUG_{78}-MBNL1 complex inhibition assay (Fig. 1*a*). Biotinylated CUG_{78} RNA was immobilized on NeutrAvidin-coated plates that were then co-incubated with MBNL1-HIS and compounds or extracts. The plates were washed to remove unbound components, and MBNL1-HIS in complex with immobilized CUG_{78} RNA was detected via an anti-HIS and a secondary HRP-conjugated antibody. The library of isolated natural compounds was screened at 100 μM concentration and led to the identification of the isoquinoline alkaloid berberine (Fig. 1*b*) as a complex formation inhibitor with an IC_{50} of 86.3 ± 5.8 μM (Fig. 1*c*). Another alkaloid, isaindigotone, showed weak inhibitory activity at 100 μM concentration. From the extract library we identified 21 extracts that inhibited CUG_{78}-MBNL1 complex formation by 40–82% at a concentration of 100 μg/ml compared with solvent-only controls. Seven extracts were chosen for fractionation. To identify the active principles in these extracts, we used an approach referred to as HPLC-based activity profiling. It combines the separation of complex mixtures with spectroscopic data recorded online and with biological information obtained in parallel from time-based microfractionation and a subsequent bioassay (32). In addition, offline microprobe NMR analysis was used to fully establish the structure of active compounds. The alkaloid harmine (Fig. 1*b*) was identified as an active constituent in a methanolic extract from the roots of *Peganum harmala* (Nitrariaceae) (Fig. 2*a*). Besides, two closely related diterpenequinones, methylenetanshinquinone and 1,2-dihydrotanshinquinone, were detected in the active fractions of an ethyl acetate extract from roots of *Salvia miltiorrhiza* (Lamiaceae) (Fig. 2*b*). A commercial sample of harmine had an IC_{50} of 132.4 ± 9.3 μM (Fig. 1*c*), whereas the two diterpenequinones, also commercially obtained, showed weak inhibitory activity at 100 μM concentration. The inhibitory activity of the remaining extracts could be assigned to tannins. These extracts lost their complex inhibitory effect after filtration through a polyamide cartridge to remove polyphenolic tannins.

The alkaloids berberine and harmine were chosen for further study. We tested a small set of structural analogues of berberine and identified coralyne (Fig. 1*b*), a planar berberine derivative, as a stronger CUG_{78}-MBNL1 complex inhibitor with an IC_{50} of 17.8 ± 0.2 μM (Fig. 1, *b* and *c*). As reference compounds, Hoechst 33258 and neomycin B, two known nucleic acid bind-

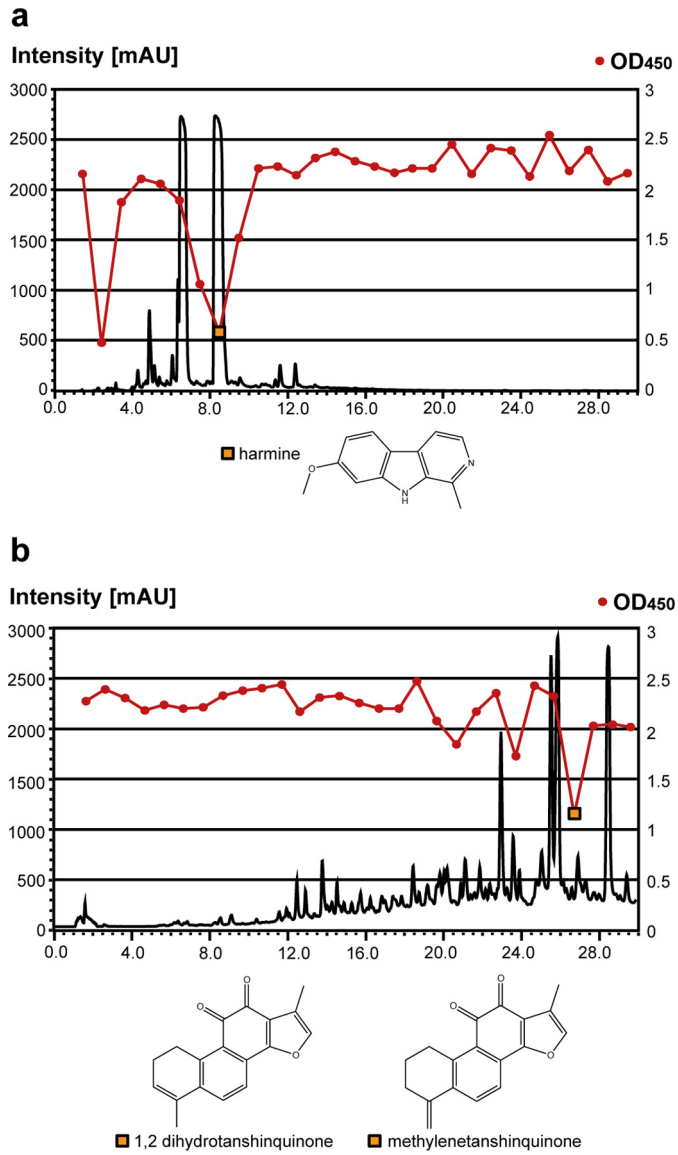

FIGURE 2. *a*, HPLC-based activity profiling of the *P. harmala* methanol extract. Shown on the *y* axis are the online HPLC-UV trace at 254 nm (*black*) and the A_{450} signal from the CUG_{78}-MBNL1 inhibition assay (*red*). The *x* axis shows the time in minutes. 29 fractions were collected, 1 min each. The inhibitory activity of the fraction at minutes 8–9 was assigned to the alkaloid harmine. Based on online MS and UV spectroscopic data, the other major peak eluting at 6.6 min was assigned to harmol. The activity in the early-eluting fraction, 2–3 min, did not correspond to any UV peak and was not further investigated. *OD*, optical density; *mAU*, milli absorbance units. *b*, HPLC-based activity profiling of the ethyl acetate extract of *S. miltiorrhiza*. The inhibitory activity of the fraction at minutes 26–27 was assigned to two diterpenequinone isomers, 1,2-dihydrotanshinquinone and methylenetanshinquinone.

ers, were tested and had IC_{50} values of 195.5 ± 3.0 μM and 5.3 ± 0.6 μM, respectively.

Identified Alkaloids Improve Splicing in Human DM1 Myoblasts—The alkaloids identified in our *in vitro* screening assay were tested for their ability to ameliorate splicing in a human DM1 myoblast cell line containing a CTG_{1300} repeat in the 3′ UTR of the DMPK gene (31). The WT control cell line contained a normal repeat length in the same locus. Differentiated DM1 myoblasts were treated with the identified alkaloids, and alternative splicing was analyzed by a quantitative PCR (qPCR) method using two primer pairs. This method allowed real-time quantitation of the inclusion/exclusion of an investigated alternatively spliced exon.

Berberine improved the splicing of the *TNNT2* pre-mRNA exon 5. In 80 μM berberine-treated DM1 myoblasts, the splicing was close to that of the WT control myoblasts. *TNNT2* pre-mRNA splicing was rescued by 62.1% ± 3.2% ($p = 0.001$, Student's *t* test, 20 μM), 75.1% ± 2.8% ($p = 0.0006$, 40 μM), and 86.2% ± 0.8% ($p = 0.0003$, 80 μM) through berberine treatment (Fig. 3*a*). However, berberine treatment had a negative effect on *INSR* pre-mRNA exon 11 splicing (Fig. 3*a*) in DM1 myoblasts. In contrast to berberine, harmine improved both the splicing of the *TNNT2* pre-mRNA exon 5 by 53.3% ± 3.5% ($p = 0.003$, 20 μM), 76.8% ± 1.6% ($p = 0.0005$, 40 μM), and 66.1% ± 1.2% ($p = 0.0009$, 80 μM), and, furthermore, the splicing of the *INSR* pre-mRNA exon 11 by 6.3% ± 0.3% ($p = 0.003$, 40 μM) and 55.4% ± 3.3% ($p = 0.0003$, 80 μM) (Fig. 3, *a* and *b*). The alternative splicing results obtained with the qPCR method for berberine and harmine were confirmed with classical RT-PCR and visualization of two alternatively spliced isoforms of the *INSR* and *TNNT2* pre-mRNA on 3% agarose gels (Fig. 3, *c* and *d*). The synthetic berberine derivative coralyne and the two diterpenequinones, identified together with harmine during the extract screening, showed no effect on splicing in the DM1 cell model.

To investigate the selectivity of berberine and harmine, we tested their effect on alternative splicing of two genes known to be alternatively spliced but independent of MBNL1, *i.e. ATE1* and *FHL1* (Fig. 3, *e* and *f*) (33). We analyzed exon 7 inclusion in the *ATE1* pre-mRNA, which was close to 33% for the WT cell line and close to 40% in the DM1 cell line. Exon 5 inclusion in the *FHL1* pre-mRNA was close to 0.1–0.2% for both the WT and the DM1 cell line. The levels of alternative exon inclusion in berberine- and harmine-treated (both at 20 μM and 80 μM) myoblasts were in the range of the levels of vehicle-treated WT and DM1 control myoblasts. The qPCR analysis of the harmine effect on *TNNT2* pre-mRNA alternative splicing in WT myoblasts showed an enhancement of MBNL1-dependent splicing analogous to harmine-treated DM1 myoblasts. This effect, however, was only observed with the qPCR method and not visible by the classical RT-PCR method (Fig. 3, *b* and *d*).

The cellular toxicity of berberine and harmine was determined in a viability assay with C2C12 mouse myoblasts. Concentrations (toxicity IC_{50}) were determined at which half of the myoblasts remained viable after 2 days of compound incubation. Berberine yielded a toxicity IC_{50} of 212.1 ± 18.3 μM and harmine one of 123.3 ± 4.6 μM. Mitomycin C was measured as reference compound with a toxicity IC_{50} of 20.4 ± 1.6 μM. Although the IC_{50} and toxicity IC_{50} values were relatively close for both alkaloids, both compounds showed an effect on alternative splicing in the myoblast model at concentrations significantly lower than the IC_{50} and toxicity IC_{50} values, *e.g.* at 20 μM (Fig. 3).

Harmine Reduces Focus Formation in Human DM1 Myoblasts—To examine whether the alkaloids berberine and harmine reduce the sequestration of MBNL1 by $(CUG)_n$ RNA, focus formation was investigated in the two human myoblast cell lines. Immunofluorescence staining in both the WT (nor-

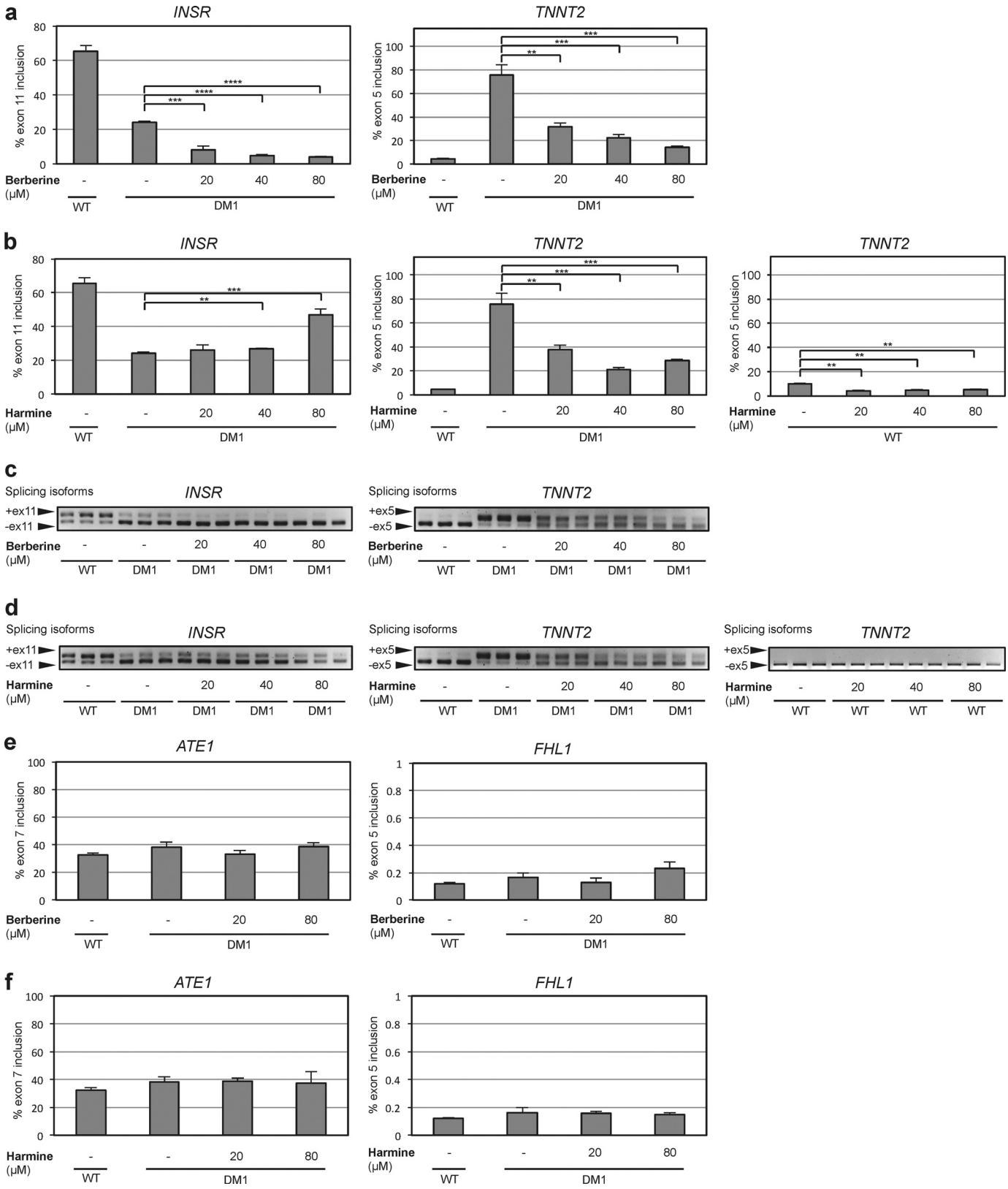

FIGURE 3. **Representative qPCR splicing data for WT and DM1 control myoblasts and treated human myoblasts.** The percentage of alternative exon inclusion is shown. *a*, berberine improves the splicing of the *TNNT2* pre-mRNA but has a detrimental effect on the *INSR* pre-mRNA splicing. *b*, harmine improves the splicing of both the *TNNT2* and of the *INSR* pre-mRNA. Harmine also promotes MBNL1-dependent splicing in treated WT myoblasts, as shown for the *TNNT2* pre-mRNA. *c* and *d*, RT-PCR analysis of *INSR* and *TNNT2* pre-mRNA alternative splicing. Visualized on 3% agarose are two alternative splicing isoforms for both pre-mRNAs in untreated WT and DM1 control myoblasts and DM1 myoblasts treated with (*c*) berberine and (*d*) harmine. The harmine effect on MBNL1-dependent splicing in treated WT myoblasts was not visible with this method, as shown for the *TNNT2* pre-mRNA. *e* and *f*, berberine and harmine do not affect alternative splicing of MBNL1-independently regulated *ATE1* and *FHL1* pre-mRNAs in treated DM1 myoblasts compared with untreated WT and DM1 control myoblasts. **, $p \leq 0.01$; ***, $p \leq 0.001$; ****, $p \leq 0.0001$.

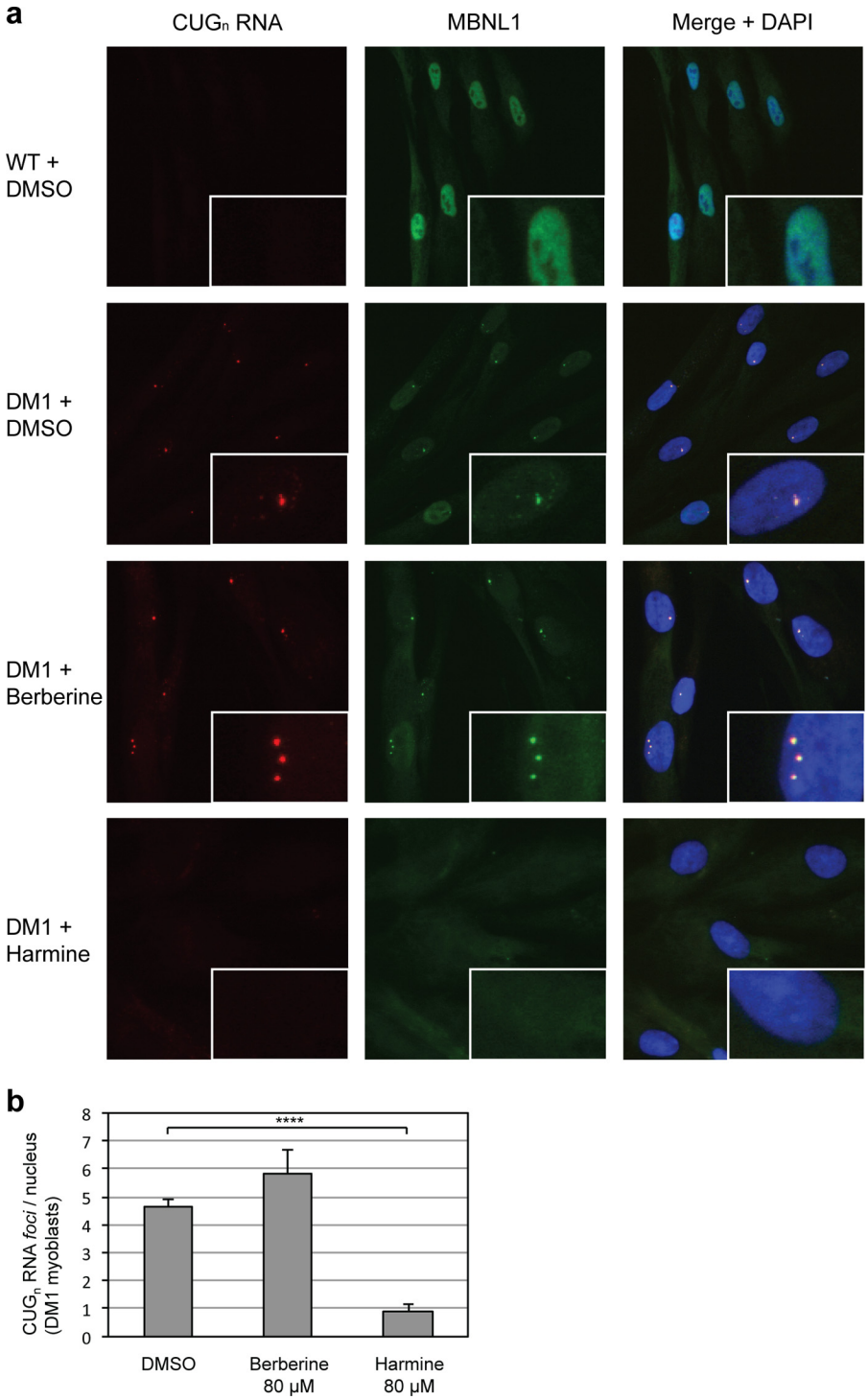

FIGURE 4. **Analysis of foci with FISH and immunofluorescence.** *a*, harmine reduces the amount of foci at 80 μM concentration, whereas berberine does not reduce foci. For each condition, $(CUG)_n$ RNA staining (*red*), MBNL1 staining (*green*), and a merge of both with nuclear DAPI staining (*blue*) is shown. Vehicle-treated control WT and DM1 myoblasts and compound-treated (80 μM) myoblasts are shown. *b*, quantification of the number of foci in human DM1 myoblasts either treated with vehicle or alkaloids at 80 μM. ****, $p \leq 0.0001$.

mal CUG repeat length) and the DM1 (CUG_{1300}) cell line showed that MBNL1 was mainly localized to the nuclei. In the DM1 cells, punctate staining of MBNL1 within the nucleus could be co-localized in foci with $(CUG)_n$ RNA, visualized by fluorescence *in situ* hybridization. Treatment with 80 μM harmine significantly reduced ($p = 0.00005$, Student's *t* test) the quantity of foci in DM1 myoblasts (Fig. 4*a*) to 0.9 $\pm$ 0.2 foci per nucleus compared with DMSO-treated DM1 myoblasts with 4.7 $\pm$ 0.3 foci per nucleus (Fig. 4, *a* and *b*). Harmine-treated myoblasts lost their punctate nuclear MBNL1 staining, indicative of MBNL1 release from the toxic $(CUG)_n$ RNA, although the nuclear MBNL1 staining pattern of WT myoblasts was not regained. We analyzed by Western immunoblotting whether treatment with harmine reduced the levels

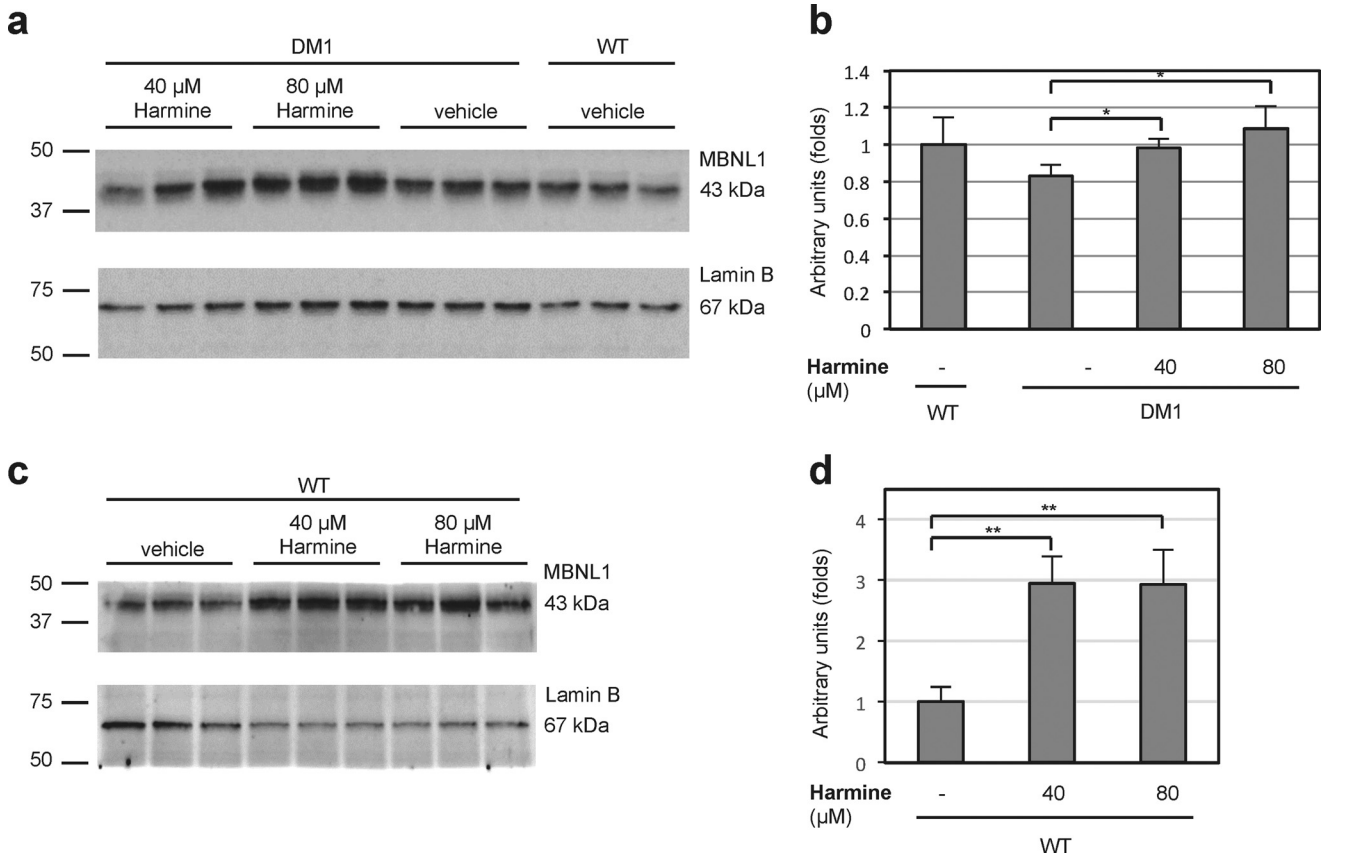

FIGURE 5. *a*, Western blot showing MBNL1 protein levels of DM1 myoblasts treated with 40 and 80 μM harmine, of vehicle-treated DM1 myoblasts, and of vehicle-treated WT myoblasts (*left* to *right*). *b*, quantification of MBNL1 band intensities normalized to lamin B. The means of three replicates for each condition, including the standard deviation, are shown. *c*, Western blot showing MBNL1 protein levels of WT myoblasts treated with vehicle or 40 and 80 μM harmine (*left* to *right*). *d*, quantification of MBNL1 band intensities normalized to lamin B. The means of three replicates for each condition, including the standard deviation, are shown. *, $p \leq 0.05$; **, $p \leq 0.01$.

of MBNL1 in cell lysates of treated DM1 myoblasts to account for the reduced nuclear staining and found that harmine in fact increased the total levels of MBNL1 in treated DM1 myoblasts compared with vehicle-treated control DM1 myoblasts (Fig. 5, *a* and *b*). An increase in MBNL1 levels was also observed in harmine-treated WT myoblasts (Fig. 5, *c* and *d*). 80 μM berberine treatment of DM1 myoblasts led to a statistically insignificant increase ($p = 0.099$) in the number of foci to 5.8 ± 0.9 foci per nucleus in the DM1 myoblast cell line (Fig. 4, *a* and *b*).

Identified Alkaloids Ameliorate Splicing of CLCN1 Pre-mRNA in HSA^{LR} Mice—Next, we treated HSA^{LR} mice, a DM1 model containing a CTG_{250} repeat expressed under a human skeletal actin promoter (4), with the identified alkaloids. The compounds were tested for their ability to restore splicing of CLCN1 (12, 13) and SERCA1 (15) pre-mRNA in quadriceps muscle. MBNL1 promotes the exclusion of the alternatively spliced exon 7a of the CLCN1 pre-mRNA and promotes the inclusion of exon 22 of the SERCA1 pre-mRNA (12, 13, 15). Vehicle-treated WT mice at the age of 10–12 weeks showed a CLCN1 pre-mRNA exon 7a inclusion of 5.0% ± 0.5%, whereas, in vehicle-treated HSA^{LR} mice, the inclusion level was elevated to 40.9% ± 2.5%. The level of SERCA1 pre-mRNA exon 22 inclusion in WT mice was at 83.9% ± 2.9%. In HSA^{LR} mice, exon 22 inclusion was decreased to 24.8% ± 2.7%. We first tested berberine, which, at a dose of 20 mg/kg, led to reduced activity and decreased body temperature, which urged us to lower the dose. Treatment with 5 mg/kg and 10 mg/kg of berberine did not result in any significant splicing improvement. We then tested two close derivatives of berberine, dihydroberberine (DHB) and palmatine, with higher reported LD_{50} values. DHB improved the splicing of the CLCN1 pre-mRNA at a dose of 10 mg/kg by 32.5% ± 2.9% ($p = 0.0008$, Student's *t* test), whereas 5 mg/kg showed no statistically significant effect (Fig. 6*a*). The CLCN1 splicing improvement with 10 mg/kg DHB was confirmed by classical RT-PCR and analysis of splicing isoforms on a 3% agarose gel (Fig. 6*d*). Palmatine treatment improved CLCN1 pre-mRNA splicing at a dose of 40 mg/kg by 34.8% ± 2.1% ($p = 0.0009$) and at a dose of 25 mg/kg by 25.3% ± 0.7% ($p = 0.0017$), whereas 10 mg/kg did not show a significant effect (Fig. 6*b*). Harmine treatment at a dose of 40 mg/kg decreased CLCN1 pre-mRNA exon 7a inclusion by 31.2% ± 1.7% ($p = 0.0003$) and did not significantly improve splicing at a dose of 20 mg/kg (Fig. 6*c*). Side effects observed during harmine treatment were transient tremors. DHB, palmatine, and harmine had no significant effect on SERCA1 pre-mRNA splicing (Fig. 6).

CLCN1 Protein Levels in Quadriceps Muscle of WT, HSA^{LR}, and Treated HSA^{LR} Mice—We examined by Western immunoblotting analysis whether the high-dose alkaloid treatments,

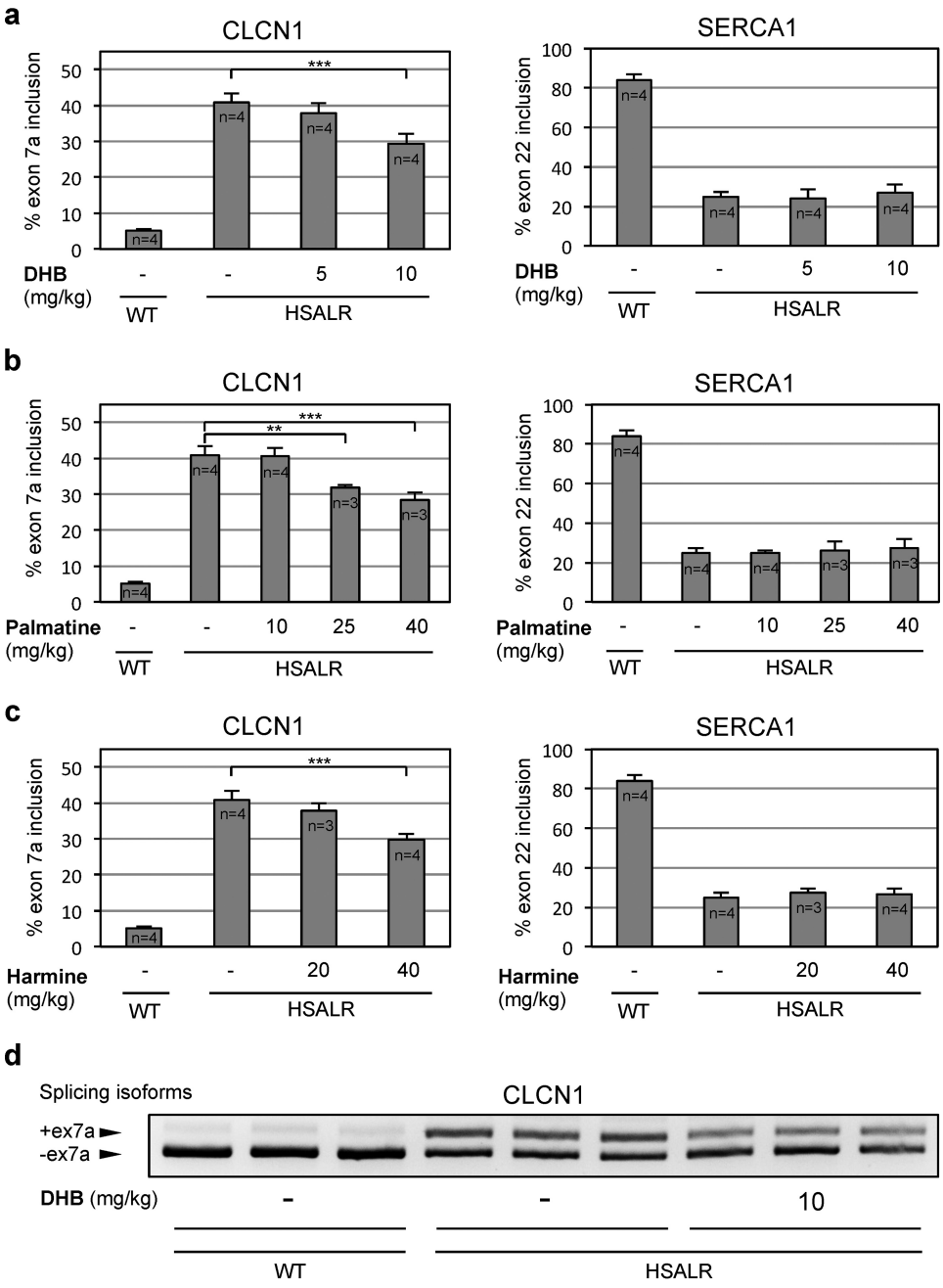

FIGURE 6. **Representative qPCR splicing data for vehicle-treated WT and HSA^{LR} mice and compound-treated HSA^{LR} mice (quadriceps muscle).** Shown is the percentage of exon 7a (*CLCN1*) and exon 22 (*SERCA1*) pre-mRNA inclusion. The alkaloids improve the splicing of CLCN1, whereas the splicing of SERCA1 is unchanged. *a*, DHB treatment. *b*, palmatine treatment. *c*, harmine treatment. *d*, alternative splicing of the CLCN1 pre-mRNA analyzed by RT-PCR and visualized on 3% agarose gel. Shown are two alternative splicing isoforms in vehicle-treated control mice and DHB-treated HSA^{LR} mice. **, $p \leq 0.01$; ***, $p \leq 0.001$.

which had ameliorated CLCN1 pre-mRNA splicing, also increased the protein levels of the full-length CLCN1 channel *in vivo*. CLCN1 protein levels in quadriceps muscle of four vehicle-treated HSA^{LR} mice were decreased by 29.1% ± 12.4% ($p = 0.023$, Student's *t* test, $n = 4$, three immunoblots) compared with four vehicle-treated WT mice (Fig. 7). Treatment of HSA^{LR} mice with 10 mg/kg DHB raised CLCN1 protein levels by 27.1% ± 16.1% ($p = 0.095$, $n = 4$) compared with levels of vehicle-treated HSA^{LR} mice (Fig. 7). Although the CLCN1 protein levels of DHB-treated HSA^{LR} mice were close to WT levels, the effect did not reach statistical significance. Both palmatine and harmine high-dose treatments of 40 mg/kg did not increase the CLCN1 protein levels in HSA^{LR} mice (Fig. 7).

Analysis of Internalized Nuclei in Gastrocnemius Muscle Sections of Vehicle-treated WT, HSA^{LR}, and Harmine-treated HSA^{LR} Mice—Despite the very short treatment duration of only 14–16 h (two injections at a 12-h interval), we wished to examine whether the most promising small molecule, harmine, also improved the histology in gastrocnemius muscle of harmine-treated mice (Fig. 8). Different histological parameters were analyzed, most importantly the percentage of fibers with inter-

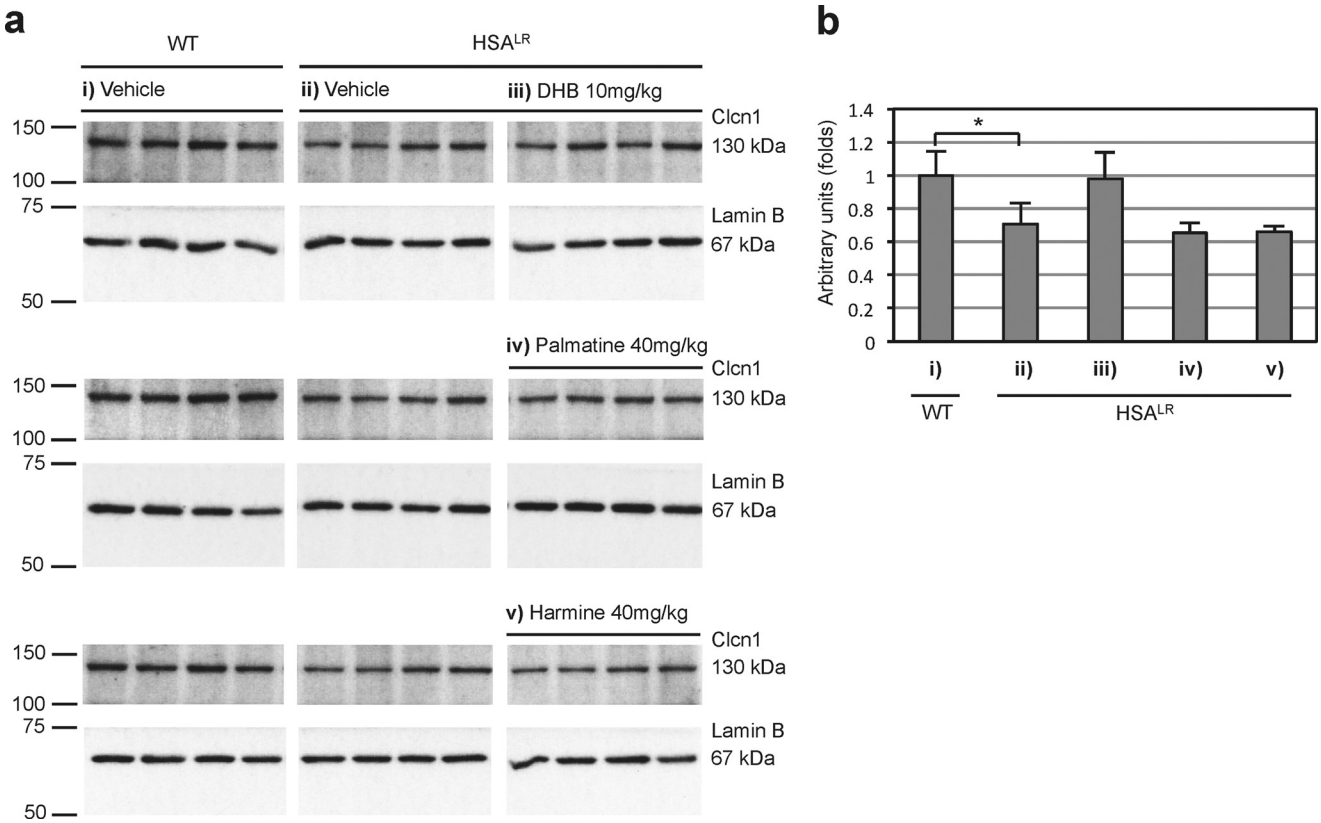

FIGURE 7. *a*, Western blot showing CLCN1 protein levels of (*i*) vehicle-treated WT mice, (*ii*) vehicle-treated HSA^{LR} mice, and (*iii–v*) compound-treated HSA^{LR} mice. *b*, quantification of CLCN1 band intensities normalized to lamin B. The means of four replicates for each condition, including the standard deviation, are shown. *, $p \leq 0.05$.

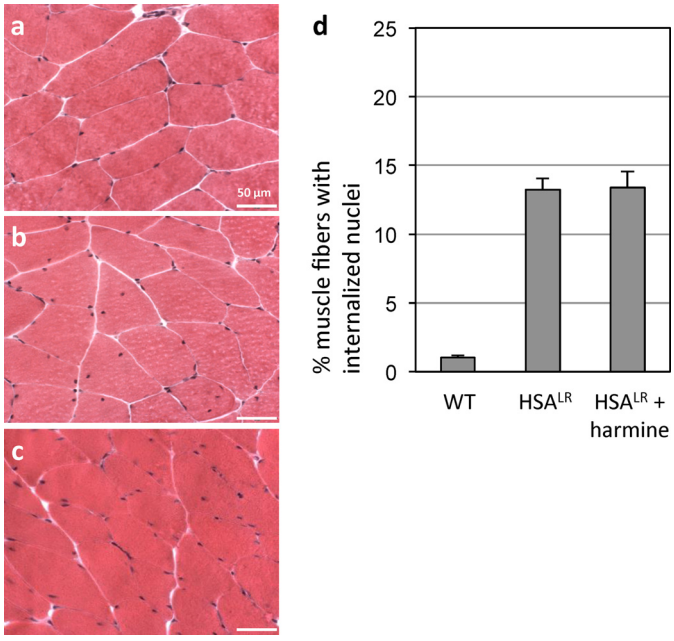

FIGURE 8. Shown is the analysis of internalized nuclei by H&E staining of 8-μm mouse gastrocnemius muscle cross-sections of 10-week-old (*a*) vehicle-treated WT mice, (*b*) vehicle-treated HSA^{LR} mice, and (*c*) HSA^{LR} mice after treatment by two injections of 40 mg/kg harmine at a 12-h interval. *d*, quantitative analysis of the percentage of muscle fibers with internalized nuclei.

nalized nuclei, where no difference was detected between vehicle-treated and harmine-treated HSA^{LR} mice after this short treatment duration.

Discussion

We report the discovery of several plant-derived alkaloids as novel bioactive small molecules with therapeutic potential for DM1. Through inhibition of the $(CUG)_n$-MBNL1 complex, the alkaloids ameliorate certain aspects of the DM1 pathology. Our screening of natural products identified the alkaloids berberine and harmine, which were chosen for further study. Interestingly, both have been described previously to bind to specific RNA structures, such as double-stranded RNA, tRNA, and poly(A) RNA (34–37). The berberine derivative coralyne has been described as a complete intercalator for double-stranded RNA and berberine as a partial intercalator (36). We therefore hypothesize that the binding of these three aromatic alkaloids to the double-stranded $(CUG)_n$ RNA may involve intercalation because of planarity. Aromatic alkaloids such as berberine, coralyne, and harmine might be of particular interest for RNA drug discovery, as they can interact with RNA via stacking (intercalation), hydrogen bonding, or electrostatic interaction (38). To our knowledge, in the context of DM1, no alkaloids have been described so far. An *in vitro* screening study by Chen *et al.* (28) yielded six hits of which four were alkaloids or alkaloid derivatives of the opioid- and ergot alkaloid-type, but none of these alkaloids could be confirmed in a secondary assay .

Berberine and harmine showed partially positive effects on splicing and focus formation in a human DM1 cell line. Harmine showed positive effects in most of the studied models. It inhibited CUG_{78}-MBNL1 complex formation *in vitro* and ameliorated the pre-mRNA splicing of both the *INSR* exon 11

and *TNNT2* exon 5 in the human DM1 myoblast cell line, where it also reduced the formation of foci without decreasing MBNL1 protein levels. Interestingly, harmine enhanced MBNL1-dependent alternative splicing to a comparable relative extent in both DM1 and WT myoblasts, indicating that harmine does not act primarily via $(CUG)_n$-MBNL1 complex disruption but, rather, via another mechanism leading to increased MBNL1 protein levels. We could not detect a significant difference of *TNNT2* pre-mRNA splicing in myotubes upon harmine treatment, although a trend toward MBNL1-mediated alternative splicing was visible (data not shown).

Harmine also improved the splicing of CLCN1 pre-mRNA in the HSA^{LR} DM1 mouse model at a high dose of 40 mg/kg. Even though 40 mg/kg harmine treatment ameliorated CLCN1 splicing in HSA^{LR} mice, it did not affect the histology of these mice. This was, however, expected because of the short treatment duration of only 14–16 h. Berberine did not perform as well as harmine in the studied models. Although it was a stronger CUG_{78}-MBNL1 complex inhibitor than harmine, it only improved the splicing of the *TNNT2* pre-mRNA in the DM1 myoblast cell line, whereas the splicing of the *INSR* pre-mRNA was worsened in treated DM1 myoblasts. This undesirable splicing effect of berberine might be due to insufficient selectivity of berberine for the $(CUG)_n$ RNA over the MBNL1 binding motifs in pre-mRNAs and, therefore, interference with MBNL1-mediated splicing. MBNL1-targeted pre-mRNAs as the toxic DMPK-$(CUG)_n$ transcripts have similar MBNL1 binding motifs (39). Interestingly, the berberine derivative coralyne was an even stronger CUG_{78}-MBNL1 complex inhibitor than berberine but showed no effect on splicing in the DM1 cell model. Coralyne is a nonspecific intercalator for double-stranded RNA (36). Its insufficient selectivity for the $(CUG)_n$ RNA over other double-stranded RNAs might be the reason for lacking specific bioactivity. Like coralyne, the two identified diterpenequinones, methylenetanshinquinone and 1,2-dihydrotanshinquinone, lacked bioactivity. As the two planar diterpenequinones were poorly water-soluble, they precipitated at higher concentrations in the screening assay and precipitated from solution in cell culture at concentrations of 20 and 40 μM. Among all identified compounds during our screening of natural products, planarity and aromaticity turned out to be common features, and the partly double-stranded $(CUG)_n$ RNA target selects for planar molecules with intercalating properties.

The evaluation of the alkaloids berberine, dihydroberberine, palmatine, and harmine in the HSA^{LR} mouse model showed promising results. Most interestingly, two alkaloids of the berberine type, DHB and palmatine, and the alkaloid harmine significantly improved the splicing of the CLCN1 pre-mRNA in this mouse model. The alkaloid DHB was the most active alkaloid, as it improved CLCN1 exon 7a splicing at a dose of 10 mg/kg. However, these alkaloids are not suited for therapeutic application themselves. Their relatively low potency and toxicity are issues that require medicinal chemistry optimization. Berberine has been described as an inhibitor of complex I in the mitochondrial respiratory chain (40). Hence, decreased metabolic activity might account for the side effects we observed upon treatment with berberine and its derivatives at high doses, *i.e.* reduced activity and decreased body temperature. The effect of berberine on thermoregulation in mice has been described previously by Jiang *et al.* (41). In harmine-treated mice we observed tremors after administration. Harmine has been described as a tremorogenic substance (42). Berberine, its derivatives DHB and palmatine, as well as harmine exert CNS effects given that they are monoamine oxidase inhibitors (43, 44). These side effects need to be addressed by medicinal chemistry modifications. However, the fact that these alkaloids penetrate the blood-brain barrier stirs hope for a future small-molecule therapy that also ameliorates the DM1-associated CNS pathology. Moreover, the identified molecules help to further understand the characteristics of small molecules that interact with toxic $(CUG)_n$ RNA and provide new chemical scaffolds for medicinal chemistry studies. Particularly harmine, with its low molecular weight of 212.25 Da, offers an appealing starting point for chemical modifications. Harmine furthermore represents an interesting molecule, as its biological effect is likely not mediated only by liberation of MBNL1 from toxic $(CUG)_n$ RNA, which was initially assumed based on results from the *in vitro* CUG_{78}-MBNL1 inhibition screening assay, but mainly via another, yet unidentified mechanism leading to an increase in MBNL1 protein levels in treated myoblasts. This effect will be investigated in more detail in follow-up studies. Our study thus contributes to further progress in small-molecule drug discovery for this disabling neuromuscular disease.

Experimental Procedures

Statistical Analysis—Unless otherwise stated, results are expressed as mean ± S.D. of $n \geq 3$ independent experiments. Comparisons between two conditions were performed using Student's *t* test with a 0.05 confidence level accepted for statistical significance (*, $p \leq 0.05$; **, $p \leq 0.01$; ***, $p \leq 0.001$; ****, $p \leq 0.0001$).

Compounds and Extracts—The compounds and extracts screened in this study were part of natural product libraries established at the Division of Pharmaceutical Biology of the University of Basel. One library contained 70 pure natural compounds as 10 mM solutions in DMSO, and a second library consisted of 2128 extracts from plants and fungi archived as 10 mg/ml solutions in DMSO (32). Harmine hydrochloride was purchased from TCI Europe (H0002). Berberine chloride (B3251), palmatine chloride hydrate (361615), and coralyne sulfoacetate (S424536) were obtained from Sigma-Aldrich. Dihydroberberine (80429) was purchased from PhytoLab GmbH. Methylenetanshinquinone (QP-393) and 1,2-dihydrotanshinquinone (QP-1166) were obtained from Quality Phytochemicals LLC (East Brunswick, NJ). The reference substances neomycin B (N1876), Hoechst 33258 (B2883), and mitomycin C (M4287) were ordered from Sigma-Aldrich.

MBNL1 Preparation—MBNL1 cDNA (an isoform with amino acids 1–382) was kindly provided by Maurice Swanson (9) (University of Florida). The pGEX-6P-MBNL1-N-His (amino acids 1–253) construct used in this study was cloned according to Yuan *et al.* (9), and protein expression and purification were performed similar to the procedure published by Yuan *et al.* (9). MBNL1-HIS was stored in a buffer containing 10 mM Tris (pH 7.4), 50 mM NaCl, and 1 mM DTT. Protein concentration was determined with a NanoDrop spectrophotom-

eter and a BCA assay (Sigma). The purity of MBNL1-HIS was evaluated by means of SDS-PAGE followed by Coomassie staining. MBNL1-HIS aliquots were snap-frozen in liquid nitrogen and stored at −70 °C.

CUG_{78} RNA Preparation—Genomic DNA was isolated from a patient blood sample (with informed consent) with the Puregene Blood Core Kit B (Qiagen) according to the protocol of the manufacturer. A CTG_{78}-containing genomic DMPK fragment was PCR-amplified with HOT Start DNA polymerase (Solis BioDyne) and the following primers: DMPK forward, 5′CAGCTCCAGTCCTGTGATCC3′; DMPK reverse, 5′CTGGCCGAAAGAAAGAAATG3′. The amplicon was agarose gel-purified with the QIAquick gel extraction kit (Qiagen). The purified DNA fragment was cloned by TA cloning with the pCR II-TOPO plasmid vector in Dh5α bacterial cells. The plasmid was purified with the QIAprep spin miniprep kit (Qiagen) and used as a template for PCR amplification with the following primers: T7 CUG forward, 5′TAATACGACTCACTATAGGCAGCTCCAGTCCTGTGATCC3′; and T7 CUG reverse, 5′TAATACGACTCACTATAGGCTGGCCGAAAGAAAGAAATG3′. The amplified DNA was purified with the QIAquick PCR purification kit (Qiagen). 200 ng of DNA was used as a template for *in vitro* RNA transcription with the MEGAscript T7 transcription kit (Ambion). CUG_{78} RNA was biotin-labeled by addition of 1.875 mM biotin-14-CTP (37.5 nmol). RNA quality and purity was tested by visualization of RNA on 8 M urea/Tris borate-EDTA 5% polyacrylamide gels.

CUG_{78}-MBNL1 Inhibition Assay—Wash steps were performed at room temperature with 150 μl of wash buffer/well (25 mM Tris (pH 7.4), 80 mM NaCl, 1 mM $MgCl_2$, 0.5 mM DTT, 0.05% Tween 20, 1.5 mg/ml BSA, and diethylpyrocarbonate-treated water) and incubation steps with 50 μl of incubation buffer/well (wash buffer + 25 units/ml RNasin (Promega)) at 30 °C on a BIOSAN plate shaker at 300 rpm. Reacti-Bind NeutrAvidin-coated 96-well plates (Pierce) were prewashed once. Wash buffer was removed, and incubation buffer containing 25 ng of biotinylated CUG_{78} RNA was added/well. After incubation for 1 h, the plates were washed twice. Wash buffer was removed, and 45 μl of incubation buffer containing 300 ng of MBNL1-HIS was added, followed by addition of 5 μl of 10× concentrated compound or 5 μl of DMSO/water for controls. After washing wells twice, mouse anti-HIS antibody (1:2000, GE Healthcare, 27-4710-01) was incubated for 1 h. Two washes preceded 1-h incubation with goat anti-mouse-HRP antibody (1:8000, Jackson ImmunoResearch Laboratories, 115-035-174). After two final wash steps, 70 μl of 3,3′,5,5′-tetramethylbenzidine substrate (Thermo Scientific) was added/well at room temperature. The colorimetric reaction was performed at 30 °C and 700 rpm for 3–5 min and stopped with 70 μl of 0.15 M H_2SO_4/well. The optical density was read at 450-nm wavelength with a Molecular Devices plate reader. Inhibition curves were fitted with Prism® software.

HPLC-based Activity Profiling of Extracts—HPLC-based activity profiling was performed on a Waters 2695 Alliance separation module equipped with a Waters 996 photodiode array detector and a C18 SunFire column (3.0 × 150 mm, 3.5 μm). The mobile phase consisted of 0.1% formic acid in H_2O (A) and MeCN (B). A gradient of 5–100% B in 30 min was applied. The flow rate was 0.4 ml/min. 900 μg of extract was injected in three portions, and time-based microfractions were collected into a deep-well 96-well microtiter plate (29 fractions of 60 s each) with a Gilson FC204. The microtiter plate was dried in a Genevac EZ-2 evaporating system at 35 °C overnight. The dried fractions were taken up in 16 μl of DMSO, and 2 μl was used in the CUG_{78}-MBNL1 inhibition assay.

Myoblast Splicing Assay—Two human fibroblast cell lines with a doxycycline-inducible MyoD construct for differentiation into myoblasts were kindly provided by Denis Furling (Université Pierre et Marie Curie-Paris, Paris, France) (31). The WT control cell line was derived from a 19-year-old healthy individual with a normal CTG repeat length in the DMPK locus, whereas the DM1 cell line was derived from an 11-year-old individual with a CTG_{1300} repeat length in the same locus. Fibroblasts were grown in growth medium (GM; 1× DMEM with 1× GlutaMax, 10% FBS (Gibco), 30 mM HEPES, and 50 μg/ml gentamycin (Sigma)) at 37 °C under 5% CO_2. 50,000 cells/well were seeded in 6-well plates and grown for 3 days. Cells were washed with 1× DMEM, and then differentiation medium (GM with 5 μg/ml doxycycline) was added. After 24 h in differentiation medium, the cells were washed with 1× DMEM and treated for 24 h with either compound or DMSO in differentiation medium. The cells were washed with 1× PBS, and total RNA was extracted with TRI reagent (Sigma) according to the protocol of the manufacturer. 500 ng of RNA was used for reverse transcription with the SuperScript III first-strand synthesis system for RT-RCR (Invitrogen), according to the protocol of the manufacturer with random hexamer primers. Pre-mRNA targets were chosen based on prior studies of small molecules in cellular and *in vivo* models of DM1 (21). 1 μl of cDNA was used for qPCR with 40 amplification cycles of 15 s at 95 °C, 15 s at 61 °C, and 20 s at 72 °C. qPCR was performed with two primer pairs, one primer pair only amplifying splicing variants that contain an investigated alternative exon and the other primer pair amplifying all possible splicing variants (pan): *INSR*, 5′GACCTGGTCTCCACCATTCG3′ (forward), 5′CACCAGTGCCTGAAGAGGTT3′ (reverse exon), and 5′ACGAAAACCACGTTGTGCAG3′ (reverse pan); *TNNT2*, 5′CAGCTGCTGTTCTGAGGGAG3′ (forward), 5′CTGCTCGTCTTCGTCCTCTC3′ (reverse exon), and 5′CCTCGTACTCTTCCACCACC3′ (reverse pan). *β-ACTIN* was used as a control gene with the following primers: forward, 5′CCAACCGCGAGAAGATGA3′; reverse, 5′CCAGAGGCGTACAGGGATAG3′. MBNL1-independent splicing of *ATE1* and *FHL1* (33) was analyzed using the following primers: *ATE1*, 5′GGGTTTCCAGGCTCAAGGTC3′ (forward), 5′TGAACTGCGAACTTGGTGGA3′ (reverse exon), and 5′TGTGTGATGCATTCTCTGGTAA3′ (reverse pan); *FHL1*, 5′ATGCCGATTGCTTTGTGTGT3′ (forward), 5′CTGGGTGGCTCACTCTTGAC3′ (reverse exon), and 5′TCTTGCATCCAGCACACTTCT3′ (reverse pan). Amplification was done with HOT FIREPol EvaGreen qPCR mixture (Solis BioDyne) on an Applied Biosystems StepOnePlus real-time PCR machine. The amount of the splicing variant, including the investigated

alternative exon, was quantified relative to the amount of the pan-amplicon, which gave a percentage of exon inclusion.

For classical RT-PCR, 1 μl of cDNA was used for PCR with 40 amplification cycles of 15 s at 95 °C, 15 s at 61 °C, and 20 s at 72 °C. The following primer pairs were used: *INSR*, 5′CCAAAGACAGACTCTCAGAT3′ (forward) and 5′AACATCGCCAAGGGACCTGC3′ (reverse); *TNNT2*, 5′ATAGAAGAGGTGGTGGAAGAGTAC3′ (forward) and 5′GTCTCAGCCTCTGCTTCAGCATCC3′ (reverse). Amplification was done with HOT Start DNA polymerase (Solis BioDyne) on an Applied Biosystems PCR machine. The PCR products were run on 3% agarose gels stained with RedSafe (iNtRON). Gels were imaged with a Gel Doc XR+ (Bio-Rad).

Myoblast Viability Assay—C2C12 mouse myoblasts were plated in 96-well plates in GM (4000 cells/well, 100 μl/well) and grown overnight. Compounds/DMSO were then added in GM. After incubation for 48 h, the CellTiter-Blue® reagent (Promega) was added according to the protocol of the manufacturer. Fluorescence was measured with an Infinite F500 plate reader (Tecan) with an excitation/emission wavelength of 535/590 nm. Signal concentration curves were fitted with Prism® software to determine toxicity IC_{50} values.

FISH and Immunofluorescence—15,000 fibroblasts/well were grown for 24 h in GM on 0.3% gelatin-coated coverslips (24-well dishes). Cells were washed with 1× DMEM and differentiated in DM for 24 h. Washing with 1× DMEM preceded the compound/vehicle incubation in DM for 24 h. Coverslip washing, permeabilization of myoblasts, FISH and immunostaining with MBNL1 antibody (A2764, a kind gift from Charles Thornton, University of Rochester) was performed according to the procedure of Warf *et al.* (21). Wash buffer I contained 1× PBS and 0.05% Triton X-100. Coverslips were blocked in buffer (wash buffer I and 3% BSA, 15 min, room temperature) before MBNL1 antibody incubation. 1:750 diluted goat anti-rabbit DyLight 488 antibody (Jackson ImmunoResearch Laboratories, 111-485-144) was added in wash buffer I (1 h, room temperature). Myoblasts were stained with 1:20,000 DAPI in wash buffer I (5 min, room temperature). Coverslips were mounted on glass slides with FluorSave reagent (Calbiochem). Cells were imaged using a Leica DMRE fluorescence microscope. For quantification, the amount of foci was counted for 3 × 50 randomly chosen nuclei from three experiments.

Treatment of Mice—HSA^{LR} transgenic mice in line 20b were kindly provided by C. Thornton. FVB/N (WT) control mice were obtained from the animal facility of the Department of Biomedicine, University Hospital Basel, Switzerland. Age- and gender-matched groups of a minimum of three mice (10–12 weeks old, male) of WT or HSA^{LR} mice were treated by two intraperitoneal injections of compound/vehicle (12-h interval). Harmine hydrochloride was administered in saline and berberine chloride, dihydroberberine, and palmatine chloride hydrate in 5% DMSO/PBS. Mice were sacrificed 2–4 h after the second injection. Dissected quadriceps muscle was powdered after freezing in liquid nitrogen. Animal studies were conducted in accordance with the Animal Research Authorities (Canton Basel-Stadt, Switzerland, permit no. 2632).

Mouse Skeletal Muscle Splicing Assay—Powdered quadriceps muscle tissue was taken up in TRI reagent (Sigma) and was grinded with a Polytron® (Kinematica) for 30 s at 4 °C. Insoluble material was removed by centrifugation at 12,000 rpm (10 min, 4 °C). From the supernatant, RNA was extracted with TRI reagent (Sigma) according to the protocol of the manufacturer. The qPCR amplification protocol was analogous to the myoblast qPCR protocol with the following primer pairs: CLCN1, 5′GGGCGTGGGATGCTACTTTG3′ (forward exon), 5′CTGACATCCTGACAGTGGGC3′ (forward pan), and 5′AGGACACGGAACACAAAGGC3′ (reverse); SERCA1, 5′GCCCTGGACTTTACCCAGTG3′ (forward), 5′ACGGTTCAAAGACATGGAGGA3′ (reverse exon), and 5′CCTCCAGATAGTTCCGAGCA3′ (reverse pan). Pre-mRNA targets were chosen based on prior studies of small molecules in cellular and *in vivo* models of DM1 (21). Classical RT-PCR was performed analogously to the myoblast splicing assay with the following primers: CLCN1, 5′GGAATACCTCACACTCAAGGCC3′ (forward) and 5′CACGGAACACAAAGGCACTGAATGT3′ (reverse); SERCA1, 5′GCTCATGGTCCTCAAGATCTCAC3′ (forward) and 5′GGGTCAGTGCCTCAGCTTTG3′ (reverse).

Western Blotting Detection of CLCN1 Protein from Mouse Skeletal Muscle—Proteins were extracted from powdered mouse quadriceps muscle according to Dimauro *et al.* (45) to obtain the nuclear/membrane fraction. Instead of NET, radioimmunoprecipitation assay+ buffer (50 mM Tris HCL (pH 8.0), 150 mM NaCl, 1% Nonidet P-40, 0.5% sodium deoxycholate, 1% Triton X-100, 0.1% SDS, and 10% glycerol) was used, containing protease and phosphatase inhibitor tablets (Roche). Protein concentrations were determined with a BCA assay (Sigma). 10-μg samples were separated by Tris/glycine SDS-PAGE on 8% gels and analyzed by Western blotting using Protran BA85 nitrocellulose membranes (GE Healthcare), rabbit polyclonal antibody against the N terminus of full-length CLCN1 (1:1000, a kind gift from Thomas Cooper, Baylor College of Medicine) (13), and HRP-tagged goat anti-rabbit secondary antibody (1:10000, Jackson ImmunoResearch Laboratories, 111-035-003). To detect lamin B (loading control), goat polyclonal anti-lamin B antibody (1:1000, Santa Cruz Biotechnology, sc-6216) and HRP-tagged swine anti-goat antibody (1:10,000, Life Technologies, ACI3404) were used. All antibodies were incubated in 1× TBS, 3% BSA, 0.1% Tween 20, and 0.08% SDS. Membranes were incubated for 5 min with LumiGLO (KPL) chemiluminescent substrate and exposed to Super RX films (Fuji).

Western Blotting Detection of MBNL1 Protein from Myoblasts—Human fibroblasts were cultured, differentiated into myoblasts, and treated in 6-well plates as described above for the myoblast splicing assay. Myoblasts were washed with 1× PBS, harvested in 1× PBS, and centrifuged for 10 min at 4 °C and 15,000 rpm, and then the pellet was resuspended in 100 μl of radioimmune precipitation assay+ buffer containing protease and phosphatase inhibitor tablets (Roche). After 2-h incubation on a wheel at 4 °C, the samples were centrifuged for 10 min at 4 °C and 12,000 rpm. Protein concentrations in supernatants were determined with a BCA assay (Sigma). 10-μg samples were separated by Tris/glycine SDS-PAGE on 12% gels. Western blotting was performed as described above using 1:5000 diluted A2764 anti-MBNL1 antibody and anti-rabbit

secondary antibody (1:10,000, Jackson ImmunoResearch Laboratories, 111-035-003).

Histological Analysis of Internalized Nuclei—8-μm cryostat cross-sections from gastrocnemius mouse muscle were stained with H&E and analyzed for the percentage of muscle fibers with internalized nuclei.

Author Contributions—R. H. conducted the screening, the splicing and focus evaluation, as well as the *in vivo* experiments. He obtained part of the funding, analyzed the results, and wrote the paper. M. T. F. performed the workup of the plant and fungus extracts, including their chemical analysis, and participated in writing of the paper. J. K. established MBNL1 protein expression and purification and supervised the experiments. F. K. and A. S. provided technical assistance. B. E. and T. W. performed the histological analysis of mouse skeletal muscle. M. S. conceived the idea for this project, secured funding, and supervised the project. O. P. and M. H. established the natural product library and profiling approach and supervised the characterization of natural products.

Acknowledgments—We thank D. Furling and the platform for immortalization of human cells from the Institut de Myologie (Paris, France) for the DM1 and control fibroblast cell lines, T. Cooper for the CLCN1 antibody, M. Swanson for the MBNL1 cDNA, and C. Thornton for the HSA^{LR} mice and the MBNL1 antibody.

References

1. Machuca-Tzili, L., Brook, D., and Hilton-Jones, D. (2005) Clinical and molecular aspects of the myotonic dystrophies: a review. *Muscle Nerve* **32,** 1–18
2. Mahadevan, M., Tsilfidis, C., Sabourin, L., Shutler, G., Amemiya, C., Jansen, G., Neville, C., Narang, M., Barceló, J., and O'Hoy, K. (1992) Myotonic-dystrophy mutation: an unstable CTG repeat in the 3′ untranslated region of the gene. *Science* **255,** 1253–1255
3. Brook, J. D., McCurrach, M. E., Harley, H. G., Buckler, A. J., Church, D., Aburatani, H., Hunter, K., Stanton, V. P., Thirion, J. P., and Hudson, T. (1992) Molecular basis of myotonic dystrophy: expansion of a trinucleotide (CTG) repeat at the 3′ end of a transcript encoding a protein kinase family member. *Cell* **69,** 385–385
4. Mankodi, A., Logigian, E., Callahan, L., McClain, C., White, R., Henderson, D., Krym, M., and Thornton, C. A. (2000) Myotonic dystrophy in transgenic mice expressing an expanded CUG repeat. *Science* **289,** 1769–1773
5. Wheeler, T. M., Sobczak, K., Lueck, J. D., Osborne, R. J., Lin, X., Dirksen, R. T., and Thornton, C. A. (2009) Reversal of RNA dominance by displacement of protein sequestered on triplet repeat RNA. *Science* **325,** 336–339
6. Taneja, K. L., McCurrach, M., Schalling, M., Housman, D., and Singer, R. H. (1995) Foci of trinucleotide repeat transcripts in nuclei of myotonic-dystrophy cells and tissues. *J. Cell Biol.* **128,** 995–1002
7. Davis, B. M., McCurrach, M. E., Taneja, K. L., Singer, R. H., and Housman, D. E. (1997) Expansion of a CUG trinucleotide repeat in the 3′ untranslated region of myotonic dystrophy protein kinase transcripts results in nuclear retention of transcripts. *Proc. Natl. Acad. Sci. U.S.A.* **94,** 7388–7393
8. Miller, J. W., Urbinati, C. R., Teng-Umnuay, P., Stenberg, M. G., Byrne, B. J., Thornton, C. A., and Swanson, M. S. (2000) Recruitment of human muscleblind proteins to (CUG)(n) expansions associated with myotonic dystrophy. *EMBO J.* **19,** 4439–4448
9. Yuan, Y., Compton, S. A., Sobczak, K., Stenberg, M. G., Thornton, C. A., Griffith, J. D., and Swanson, M. S. (2007) Muscleblind-like 1 interacts with RNA hairpins in splicing target and pathogenic RNAs. *Nucleic Acids Res.* **35,** 5474–5486
10. Philips, A. V., Timchenko, L. T., and Cooper, T. A. (1998) Disruption of splicing regulated by a CUG-binding protein in myotonic dystrophy. *Science* **280,** 737–741
11. Lin, X., Miller, J. W., Mankodi, A., Kanadia, R. N., Yuan, Y., Moxley, R. T., Swanson, M. S., and Thornton, C. A. (2006) Failure of MBNL1-dependent post-natal splicing transitions in myotonic dystrophy. *Hum. Mol. Genet.* **15,** 2087–2097
12. Mankodi, A., Takahashi, M. P., Jiang, H., Beck, C. L., Bowers, W. J., Moxley, R. T., Cannon, S. C., and Thornton, C. A. (2002) Expanded CUG repeats trigger aberrant splicing of ClC-1 chloride channel pre-mRNA and hyperexcitability of skeletal muscle in myotonic dystrophy. *Mol. Cell* **10,** 35–44
13. Charlet-B, N., Savkur, R. S., Singh, G., Philips, A. V., Grice, E. A., and Cooper, T. A. (2002) Loss of the muscle-specific chloride channel in type 1 myotonic dystrophy due to misregulated alternative splicing. *Mol. Cell* **10,** 45–53
14. Savkur, R. S., Philips, A. V., and Cooper, T. A. (2001) Aberrant regulation of insulin receptor alternative splicing is associated with insulin resistance in myotonic dystrophy. *Nat. Genet.* **29,** 40–47
15. Hino, S., Kondo, S., Sekiya, H., Saito, A., Kanemoto, S., Murakami, T., Chihara, K., Aoki, Y., Nakamori, M., Takahashi, M. P., and Imaizumi, K. (2007) Molecular mechanisms responsible for aberrant splicing of SERCA1 in myotonic dystrophy type 1. *Hum. Mol. Genet.* **16,** 2834–2843
16. Ho, T. H., Charlet-B, N., Poulos, M. G., Singh, G., Swanson, M. S., and Cooper, T. A. (2004) Muscleblind proteins regulate alternative splicing. *EMBO J.* **23,** 3103–3112
17. Berg, J., Jiang, H., Thornton, C. A., and Cannon, S. C. (2004) Truncated ClC-1 mRNA in myotonic dystrophy exerts a dominant-negative effect on the Cl current. *Neurology* **63,** 2371–2375
18. Krzyzosiak, W. J., Sobczak, K., Wojciechowska, M., Fiszer, A., Mykowska, A., and Kozlowski, P. (2012) Triplet repeat RNA structure and its role as pathogenic agent and therapeutic target. *Nucleic Acids Res.* **40,** 11–26
19. Lee, J. E., Bennett, C. F., and Cooper, T. A. (2012) RNase H-mediated degradation of toxic RNA in myotonic dystrophy type 1. *Proc. Natl. Acad. Sci. U.S.A.* **109,** 4221–4226
20. Kanadia, R. N., Shin, J., Yuan, Y., Beattie, S. G., Wheeler, T. M., Thornton, C. A., and Swanson, M. S. (2006) Reversal of RNA missplicing and myotonia after muscleblind overexpression in a mouse poly(CUG) model for myotonic dystrophy. *Proc. Natl. Acad. Sci. U.S.A.* **103,** 11748–11753
21. Warf, M. B., Nakamori, M., Matthys, C. M., Thornton, C. A., and Berglund, J. A. (2009) Pentamidine reverses the splicing defects associated with myotonic dystrophy. *Proc. Natl. Acad. Sci. U.S.A.* **106,** 18551–18556
22. Arambula, J. F., Ramisetty, S. R., Baranger, A. M., and Zimmerman, S. C. (2009) A simple ligand that selectively targets CUG trinucleotide repeats and inhibits MBNL protein binding. *Proc. Natl. Acad. Sci. U.S.A.* **106,** 16068–16073
23. Pushechnikov, A., Lee, M. M., Childs-Disney, J. L., Sobczak, K., French, J. M., Thornton, C. A., and Disney, M. D. (2009) Rational design of ligands targeting triplet repeating transcripts that cause RNA dominant disease: application to myotonic muscular dystrophy type 1 and spinocerebellar ataxia type 3. *J. Am. Chem. Soc.* **131,** 9767–9779
24. Childs-Disney, J. L., Hoskins, J., Rzuczek, S. G., Thornton, C. A., and Disney, M. D. (2012) Rationally designed small molecules targeting the RNA that causes myotonic dystrophy type 1 are potently bioactive. *ACS Chem. Biol.* **7,** 856–862
25. Gareiss, P. C., Sobczak, K., McNaughton, B. R., Palde, P. B., Thornton, C. A., and Miller, B. L. (2008) Dynamic combinatorial selection of molecules capable of inhibiting the (CUG) repeat RNA-MBNL1 interaction *in vitro*: discovery of lead compounds targeting myotonic dystrophy (DM1). *J. Am. Chem. Soc.* **130,** 16254–16261
26. Ofori, L. O., Hoskins, J., Nakamori, M., Thornton, C. A., and Miller, B. L. (2012) From dynamic combinatorial "hit" to lead: *in vitro* and *in vivo* activity of compounds targeting the pathogenic RNAs that cause myotonic dystrophy. *Nucleic Acids Res.* **40,** 6380–6390
27. Hoskins, J. W., Ofori, L. O., Chen, C. Z., Kumar, A., Sobczak, K., Nakamori, M., Southall, N., Patnaik, S., Marugan, J. J., Zheng, W., Austin, C. P., Disney, M. D., Miller, B. L., and Thornton, C. A. (2014) Lomofungin and dilomofungin: inhibitors of MBNL1-CUG RNA binding with distinct cellular effects. *Nucleic Acids Res.* **42,** 6591–6602
28. Chen, C. Z., Sobczak, K., Hoskins, J., Southall, N., Marugan, J. J., Zheng, W., Thornton, C. A., and Austin, C. P. (2012) Two high-throughput

screening assays for aberrant RNA-protein interactions in myotonic dystrophy type 1. *Anal. Bioanal. Chem.* **402,** 1889–1898
29. Koehn, F. E., and Carter, G. T. (2005) The evolving role of natural products in drug discovery. *Nat. Rev. Drug Discov.* **4,** 206–220
30. Wilson, D. N. (2014) Ribosome-targeting antibiotics and mechanisms of bacterial resistance. *Nat. Rev. Microbiol.* **12,** 35–48
31. Chaouch, S., Mouly, V., Goyenvalle, A., Vulin, A., Mamchaoui, K., Negroni, E., Di Santo, J., Butler-Browne, G., Torrente, Y., Garcia, L., and Furling, D. (2009) Immortalized skin fibroblasts expressing conditional MyoD as a renewable and reliable source of converted human muscle cells to assess therapeutic strategies for muscular dystrophies: validation of an exon-skipping approach to restore dystrophin in Duchenne muscular dystrophy cells. *Hum. Gene Ther.* **20,** 784–790
32. Potterat, O., and Hamburger, M. (2014) Combined use of extract libraries and HPLC-based activity profiling for lead discovery: potential, challenges, and practical considerations. *Planta Med.* **80,** 1171–1181
33. Mykowska, A., Sobczak, K., Wojciechowska, M., Kozlowski, P., and Krzyzosiak, W. J. (2011) CAG repeats mimic CUG repeats in the misregulation of alternative splicing. *Nucleic Acids Res.* **39,** 8938–8951
34. Kumar, G. S. (2012) RNA targeting by small molecules: binding of protoberberine, benzophenanthridine and *Aristolochia* alkaloids to various RNA structures. *J. Biosci.* **37,** 539–552
35. Nafisi, S., Malekabady, Z. M., and Khalilzadeh, M. A. (2010) Interaction of β-carboline alkaloids with RNA. *DNA Cell Biol.* **29,** 753–761
36. Islam, M. M., Chowdhury, S. R., and Kumar, G. S. (2009) Spectroscopic and calorimetric studies on the binding of alkaloids berberine, palmatine and coralyne to double stranded RNA polynucleotides. *J. Phys. Chem. B* **113,** 1210–1224
37. Cetinkol, O. P., and Hud, N. V. (2009) Molecular recognition of poly(A) by small ligands: an alternative method of analysis reveals nanomolar, cooperative and shape-selective binding. *Nucleic Acids Res.* **37,** 611–621
38. Thomas, J. R., and Hergenrother, P. J. (2008) Targeting RNA with small molecules. *Chem. Rev.* **108,** 1171–1224
39. Warf, M. B., and Berglund, J. A. (2007) MBNL binds similar RNA structures in the CUG repeats of myotonic dystrophy and its pre-mRNA substrate cardiac troponin T. *RNA* **13,** 2238–2251
40. Turner, N., Li, J.-Y., Gosby, A., To, S. W., Cheng, Z., Miyoshi, H., Taketo, M. M., Cooney, G. J., Kraegen, E. W., James, D. E., Hu, L.-H., Li, J., and Ye, J.-M. (2008) Berberine and its more biologically available derivative, dihydroberberine, inhibit mitochondrial respiratory complex I: a mechanism for the action of berberine to activate AMP-activated protein kinase and improve insulin action. *Diabetes* **57,** 1414–1418
41. Jiang, J.-F., Wang, Y.-G., Hu, J., Lei, F., Kheir, M. M., Wang, X.-P., Chai, Y.-S., Yuan, Z.-Y., Lu, X., Xing, D.-M., Du, F., and Du, L.-J. (2013) Novel effect of berberine on thermoregulation in mice model induced by hot and cold environmental stimulation. *PLoS ONE* 10.1371/journal.pone.0054234
42. Guan, Y. B., Louis, E. D., and Zheng, W. (2001) Toxicokinetics of tremorogenic natural products, harmane and harmine, in male Sprague-Dawley rats. *J. Toxicol. Env. Health A* **64,** 645–660
43. Lee, S. S., Kai, M., and Lee, M. K. (1999) Effects of natural isoquinoline alkaloids on monoamine oxidase activity in mouse brain: inhibition by berberine and palmatine. *Med. Sci. Res.* **27,** 749–751
44. Herraiz, T., González, D., Ancín-Azpilicueta, C., Arán, V. J., and Guillén, H. (2010) β-Carboline alkaloids in *Peganum harmala* and inhibition of human monoamine oxidase (MAO). *Food Chem. Toxicol.* **48,** 839–845
45. Dimauro, I., Pearson, T., Caporossi, D., and Jackson, M. J. (2012) A simple protocol for the subcellular fractionation of skeletal muscle cells and tissue. *BMC Res. Notes* **5,** 513–513

Identification of Plant-derived Alkaloids with Therapeutic Potential for Myotonic Dystrophy Type I

Ruben Herrendorff, Maria Teresa Faleschini, Adeline Stiefvater, Beat Erne, Tatiana Wiktorowicz, Frances Kern, Matthias Hamburger, Olivier Potterat, Jochen Kinter and Michael Sinnreich

J. Biol. Chem. 2016, 291:17165-17177.
doi: 10.1074/jbc.M115.710616 originally published online June 13, 2016

Thieme

The Dual Edema-Preventing Molecular Mechanism of the *Crataegus* Extract WS 1442 Can Be Assigned to Distinct Phytochemical Fractions

Authors

Simone Fuchs[1,2*], Iris Bischoff[1*], Elisabeth A. Willer[2], Jacqueline Bräutigam[1], Martin F. Bubik[2], Clemens A. J. Erdelmeier[3], Egon Koch[3], Maria T. Faleschini[4], Maria De Mieri[4], Milena Bauhart[4], Stefan Zahler[2], Andreas Hensel[5], Matthias Hamburger[4], Olivier Potterat[4], Robert Fürst[1]

Affiliations

1 Institute of Pharmaceutical Biology, Goethe University Frankfurt/Main
2 Pharmaceutical Biology, Department of Pharmacy, Center for Drug Research, University of Munich
3 Preclinical Research, Dr. Willmar Schwabe GmbH & Co. KG, Karlsruhe
4 Division of Pharmaceutical Biology, University of Basel, Basel, Switzerland
5 Institute of Pharmaceutical Biology and Phytochemistry, University of Münster

Key words

Crataegus spp., Rosaceae, endothelial permeability, bioactivity-guided fractionation, oligomeric procyanidins, intracellular calcium levels, cortactin activation

received September 27, 2016
revised November 16, 2016
accepted December 2, 2016

Bibliography

DOI http://dx.doi.org/10.1055/s-0042-123388
Published online December 22, 2016 | Planta Med 2017; 83: 701–709 © Georg Thieme Verlag KG Stuttgart · New York | ISSN 0032-0943

Correspondence

Robert Fürst, PhD
Institute of Pharmaceutical Biology, Biocenter, Goethe University Frankfurt/Main
Max-von-Laue-Str. 9, 60438 Frankfurt/Main
Phone: + 49 69 79 82 96 55, Fax: + 49 6 97 98 76 32 96 55
fuerst@em.uni-frankfurt.de

Supporting information available online at http://www.thieme-connect.de/products

ABSTRACT

The hawthorn (*Crataegus* spp.) extract WS 1442 is used against mild forms of chronic heart failure. This disease is associated with endothelial barrier dysfunction and edema formation. We have recently shown that WS 1442 protects against this dysfunction by a dual mechanism: it both promotes endothelial barrier integrity by activation of a barrier-enhancing pathway (cortactin activation) and inhibits endothelial hyperpermeability by blocking a barrier disruptive pathway (calcium signaling). In this study, we aimed to identify the bioactive compounds responsible for these actions by using a bioactivity-guided fractionation approach. From the four fractions generated from WS 1442 by successive elution with water, 95% ethanol, methanol, and 70% acetone, only the water fraction was inactive, whereas the other three triggered a reduction of endothelial hyperpermeability. Analyses of intracellular calcium levels and cortactin phosphorylation were used as readouts to estimate the bioactivity of subfractions and isolated compounds. Interestingly, only the ethanolic fraction interfered with the calcium signaling, whereas only the methanolic fraction led to an activation of cortactin. Thus, the dual mode of action of WS 1442 could be clearly assigned to two distinct fractions. Although the identification of the calcium-active substance(s) was not successful, we could exclude an involvement of phenolic compounds. Cortactin activation, however, could be clearly attributed to oligomeric procyanidins with a distinct degree of polymerization. Taken together, our study provides the first approach to identify the active constituents of WS 1442 that address different cellular pathways leading to the inhibition of endothelial barrier dysfunction.

* These authors contributed equally to this work.

ABBREVIATIONS

CHF	chronic heart failure
ECs	endothelial cells
HMEC	human microvascular endothelial cell
HUVEC	human umbilical vein endothelial cell
OPC	oligomeric procyanidin

Introduction

CHF is a progressive and severe cardiovascular pathology. Extracts of different hawthorn (*Crataegus*) species are used as an adjuvant treatment of CHF. The most widely studied *Crataegus* extract WS 1442 is approved for the treatment of mild forms of CHF according to the New York Heart Association functional class II [1]. The efficacy of WS 1442 was proven in various clinical trials [2, 3] and is based on its positive inotropic, antiarrhythmic, vasodilating, and cardioprotective actions [4–6]. One of the various symptoms of CHF is the formation of peripheral edema. This symptom is not only based on the altered hydrostatic pressure due to an increased cardiac preload, but is also caused by the inflammation-associated occurrence of endothelial barrier dysfunction. Interestingly, treatment with WS 1442 has been reported to improve ankle edema in CHF [7, 8]. Recently, our group provided evidence that WS 1442 protects against edema formation by directly affecting the endothelium. *In vitro* experiments revealed that WS 1442 inhibits thrombin-induced endothelial barrier dysfunction in human ECs. WS 1442 also showed a barrier-protecting activity *in vivo* in a murine model of endothelial hyperpermeability. Analysis of the effects of WS 1442 on key regulators of the endothelial barrier function gave detailed insights into the dual action of the extract (▶ **Fig. 1**): WS 1442 blocks barrier disruptive pathways on the one hand, and activates barrier-stabilizing mechanisms on the other hand. The thrombin-evoked rise of intracellular calcium levels ($[Ca^{2+}]_i$), and the activation of protein kinase C (PKC) and RhoA were markedly reduced by WS 1442. Apart from the abrogation of the stimuli-induced impairment of barrier function, the extract *per se* activated a barrier-stabilizing cascade by increasing endothelial cAMP levels leading to the activation of the Epac1/Rap1 signaling pathway. By stimulating the cAMP cascade, WS 1442 increased the activity of Rac1, resulting in the cortactin-mediated induction of a cortical F-actin ring that finally stabilized endothelial barrier integrity [9]. Interestingly, WS 1442 alone increased basal $[Ca^{2+}]_i$ without affecting endothelial permeability, but reduced the rise of $[Ca^{2+}]_i$ induced by barrier-disruptive stimuli [10].

OPCs and flavonoids have been described as the pharmacologically most important secondary metabolites in the extract [11]. However, individual compounds responsible for the protection against barrier dysfunction have not been identified up to now. Therefore, we aimed to shed light on the bioactive group(s) of compounds responsible for the positive effects of WS 1442 on barrier integrity of thrombin-induced endothelial cells *in vitro*. To identify the bioactive principle(s), an iterative bioactivity-guided fractionation procedure was used. For the assessment of bioactivity, measurements of thrombin-induced endothelial hyperpermeability, cytosolic calcium levels, and activation of cortactin in human endothelial cells were used as readout parameters.

Results and Discussion

WS 1442 was separated into four different fractions (A–D). Fraction A contained non-phenolic and aliphatic compounds, while small phenolic compounds and flavonoids were present in fraction B. OPCs were identified in fraction C, and fraction D consisted of polymeric procyanidins (▶ **Fig. 2A**). Since we have previously shown that WS 1442 significantly reduces the thrombin-evoked macromolecular permeability [9], we were interested in identifying the fraction responsible for this effect. Thus, ECs were treated with each fraction and, subsequently, the thrombin-induced macromolecular permeability was analyzed as an indicator for vascular leakage and, thus, edema formation [12]. The flux of fluorescence-labeled dextran through a thrombin-activated monolayer of HMECs was monitored after 30 min. Pretreatment (30 min) of HMECs with fractions B, C, or D evoked a significant decrease of the macromolecular permeability (▶ **Fig. 2B**), whereas the decrease triggered by fraction A was slight and statistically not significant. Thus, procyanidins, small phenolic compounds, and flavonoids might be responsible for the barrier-protecting action of WS 1442. In fact, both classes of secondary plant metabolites have already been reported to act against endothelial barrier dysfunction [13, 14]. Taken together, our results suggest that the barrier-protecting effect of WS 1442 is based not only on one group of secondary metabolites.

WS 1442 has been previously shown to protect against endothelial barrier dysfunction via cortactin activation (phosphorylation at tyrosine 421) and by blocking the thrombin-induced rise of $[Ca^{2+}]_i$ levels. Therefore, these two systems were used as a readout parameter to estimate the bioactivity of each fraction. Immunofluorescence stainings of phosphorylated cortactin revealed that only fraction C induced a rim of activated cortactin at the border of endothelial cells (▶ **Fig. 3A**). In contrast, only fraction B was able to prevent the thrombin-induced peak of $[Ca^{2+}]_i$ (▶ **Fig. 3B**). These results indicate that the dual modes of action of WS 1442 can be clearly assigned to two distinct fractions. While fraction B, i.e., small phenolic compounds and flavonoids, seems to be responsible for the inhibition of barrier disruptive signaling, the activating effects of the extract on the barrier-stabilizing pathway might be attributed exclusively to oligomeric procyanidins (▶ **Fig. 3C**). Interestingly, although polymeric procyanidins (fraction D) were able to act against endothelial hyperpermeability, this fraction did not cause any alteration in the two signaling pathways. This might point towards other, as yet unidentified, targets that are addressed by fraction D.

To track the constituents responsible for the activity, fraction B was submitted to a process referred to as HPLC-based profiling [15]. This approach combines physicochemical data recorded online with biological information obtained in parallel from time-based HPLC microfractionation. An aliquot of fraction B was separated by semipreparative HPLC, and the resulting nine subfrac-

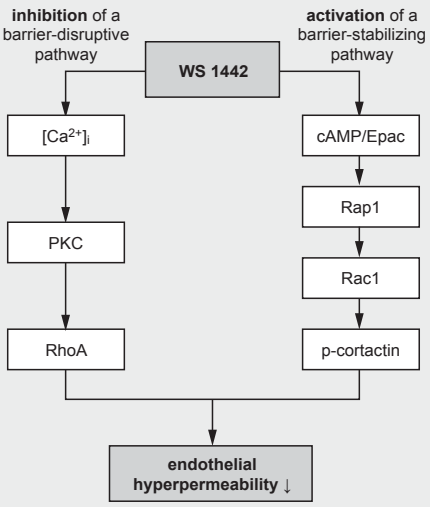

▶ **Fig. 1** WS 1442 prevents endothelial hyperpermeability via a dual mechanism. The hawthorn extract inhibits the barrier disruptive pathway by reduction of the thrombin-evoked intracellular calcium rise, PKC, and RhoA activity on the one hand. On the other hand, the barrier protective signaling was activated by increasing cAMP levels, the activation of the Rap1/Rac1signaling, and cortactin rearrangement at the borders of the endothelial cells.

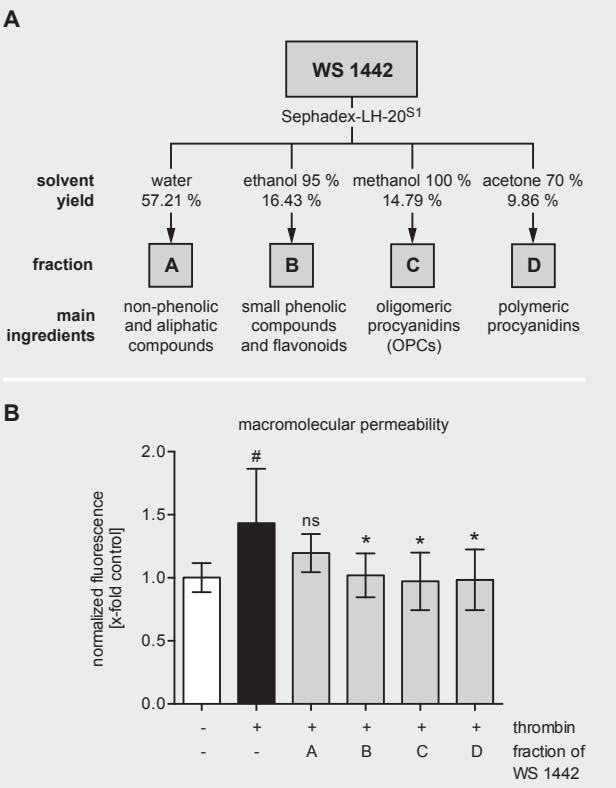

▶ **Fig. 2** Influence of fractions of WS 1442 on the thrombin-induced endothelial hyperpermeability. **A** Fractionation scheme of WS 1442. **B** HMECs were left untreated or pretreated with WS 1442 fractions A–D (A: 57 µg/mL, B: 17 µg/mL, C: 12 µg/mL, D: 8 µg/mL) for 30 min. To measure the flux of FITC-labeled dextran (1 mg/mL) across the endothelial monolayer, a Transwell two-compartment system was used. FITC-dextran was added at time point t = 0 min and, subsequently, thrombin (1 U/mL) was applied to the upper compartment. After 30 min, samples were taken from the lower compartment. Data are expressed as the mean ± SD. * $P \leq 0.05$ (one-way ANOVA followed by Dunnett's post hoc test) vs. thrombin (black bar). # $P \leq 0.05$ (one-way ANOVA followed by Dunnett's post hoc test) vs. control (white bar), n = 3; n. s. = not significantly different compared to thrombin.

tions were analyzed for their interference with the thrombin-evoked increase of $[Ca^{2+}]_i$. The activity was recovered in a subfraction eluted with 100% acetonitrile (▶ **Fig. 4A**). Importantly, phenolic compounds, in particular flavonoids, eluted earlier and could thus be excluded as active principles (▶ **Fig. 4A**). The separation of fraction B by two successive steps of preparative HPLC afforded a lipophilic active fraction containing terpenic constituents (data not shown). The low amounts of material, however, precluded additional separation steps and identification of the active compounds. Therefore, the further characterization of active substances was performed starting from the whole extract WS 1442, since it was available in larger amounts. The extract was partitioned between ethyl acetate (EtOAc) and water. Fractionation of the EtOAc-soluble portion (E) by column chromatography on silica gel afforded two fractions, E-7 and E-8 (▶ **Fig. 4B, C**), which were able to block the $[Ca^{2+}]_i$ peak and trigger the typical (nontoxic) increase of $[Ca^{2+}]_i$. Unfortunately, no active fractions could be obtained after the further separation of E-7 (data not shown). However, purification of fraction E-8 by semipreparative HPLC on an RP-18 column resulted in three active subfractions (E-8/4, E-8/5, and E-8/6; ▶ **Fig. 4B, D**), which were characterized by NMR, GC-MS, and HPLC-MS analysis. These subfractions each consisted of a mixture of triterpenes and fatty acids. According to GC-MS analysis, the major fatty acids in all fractions were palmitic acid and stearic acid (**Fig. 1S**, Supporting Information). As to the triterpenes, hyptatic acid A could be identified as the main triterpene in fraction E-8/5, with a content of approx. 50% according to the ^{1}H-NMR spectrum (**Fig. 2S**, Supporting Information). Triterpenes detected in fractions E-8/4 and E-8/6 (**Fig. 3S**, Supporting Information) could not be identified. Pure hyptatic acid A, stearic acid, and palmitic acid were tested for their influence on the thrombin-evoked rise of $[Ca^{2+}]_i$, but none of the compounds was found to be active (**Fig. 4S**, Supporting Information). These constituents represent, according to NMR and GC-MS analysis, approx. 90% of the active fraction E-8/5. The low amounts of active fractions precluded further separation. Some other triterpenes that had been isolated during the fractionation of WS 1442, such as pomolic acid, corosolic acid, oleanolic acid, and ursolic acid, were also inactive (data not shown). Taken together, we could exclude that the action of WS 1442 on $[Ca^{2+}]_i$ is based on small phenolic compounds and flavonoids. However, the exact nature of the active compounds remains unresolved. Synergetic effects of extract constituents cannot be excluded.

Immunofluorescence stainings of ECs treated with six subfractions of fraction C revealed that only the subfractions C-3 and C-5

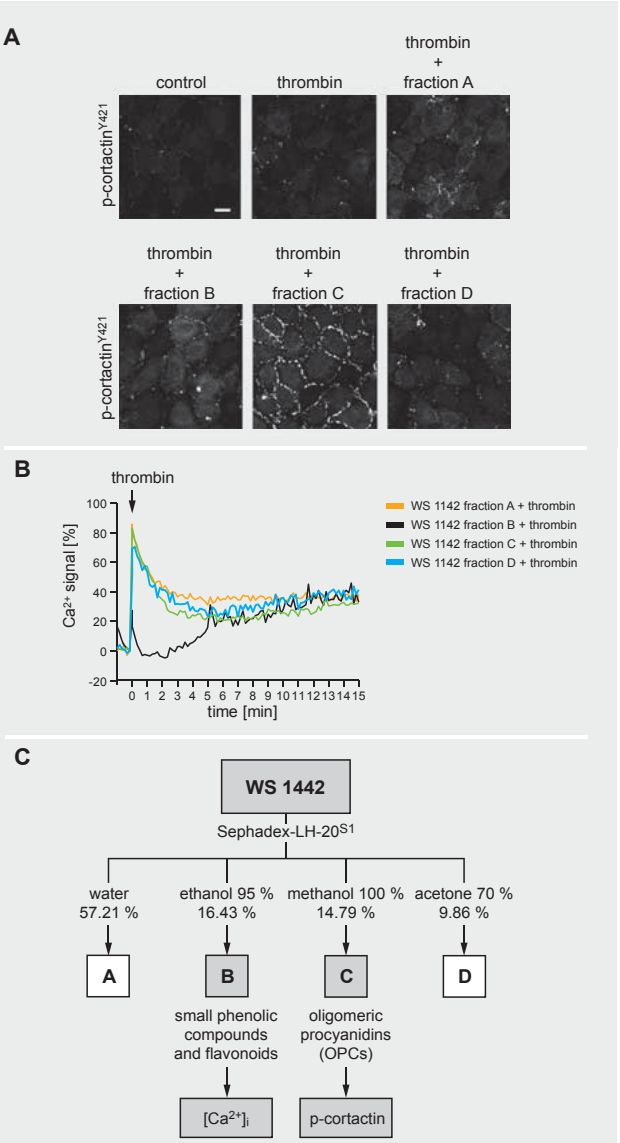

▶ **Fig. 3** Influence of the WS 1442 fractions on cortactin activation and thrombin-induced $[Ca^{2+}]_i$. **A** HUVECs were pretreated for 30 min with WS 1442 fractions A–D (A: 57 µg/mL, B: 17 µg/mL, C: 12 µg/mL, D: 8 µg/mL) prior to treatment with thrombin (1 U/mL, 30 min). Control cells were treated with DMSO as the vehicle control. The increase of cortactin phosphorylation was determined with an antibody against Tyr421-phosphorylated cortactin. Images were taken by confocal microscopy with a 40-fold magnification. One representative image out of three independently performed experiments (n = 3) is shown. Scale bar represents 20 µm. **B** Confluent HUVECs were pretreated for 30 min with fractions A–D (A: 57 µg/mL, B: 17 µg/mL, C: 12 µg/mL, D: 8 µg/mL). Changes of $[Ca^{2+}]_i$ were detected by fluorescence microscopy using Fura-2-AM (2 µM) in a static tempered system (37 °C). Thrombin (1 U/mL) was added at time point t = 0 min. Basal $[Ca^{2+}]_i$ was set as 100% and the $[Ca^{2+}]_i$ increase is shown; n = 3. **C** Scheme of WS 1442 fractions A–D. Active fractions B and C are highlighted.

triggered the phosphorylation of cortactin (▶ **Fig. 5A, B**). To obtain more information on the bioactive compounds, C-3 and C-5 were further fractionated into six and four subfractions, respectively, and again analyzed for cortactin activation. Unfortunately, the bioactivity could not be narrowed down, but was found to be broadly distributed. The five subfractions C-3/2 to C-3/6 (▶ **Fig. 5C**) and the three subfractions C-5/1, C-5/3, and C-5/4 (▶ **Fig. 5D**) were active. To circumvent this issue, we decided to use OPCs with different degrees of polymerization (DP2 to DP10) that had been previously isolated from hawthorn leaves with flowers [16]. Four out of nine OPC clusters (DP5–DP6 and DP8–DP9) were found to induce the phosphorylation of cortactin (▶ **Fig. 6**). Numerous studies previously demonstrated that OPC containing extracts reduce edema formation in animal models [17, 18]. However, none of them elucidates the specific phytochemical compound that positively regulates endothelial barrier functions. Our study presents an unique approach identifying certain OPC clusters to be highly bioactive compounds in WS 1442 that stabilize the endothelial barrier integrity. We want to point out that our conclusions based on these *in vitro* findings cannot simply be applied to the *in vivo* or human situation. It is not very likely that OPCs consisting of more than three monomers are readily absorbed. In contrast, plasma levels of dimeric and trimeric procyanidins (e.g., procyanidin dimers B1 or B2 or the trimer C2) have been reported in animal or human plasma after oral administration of different OPC-containing products [19–21]. There is a lack of data on the absorption of OPCs with higher degrees of polymerization. However, we want to emphasize that it is also not clear whether DP5/6 and DP8/9 exert their pharmacological *in vitro* effects as whole molecules or, e.g., as metabolites resulting from the enzymatic environment. Therefore, there is an uncertainty about the precise molecules that exert the *in vitro* action and also about the question as to whether these compounds can enter the cell.

Taken together, we could demonstrate that the dual mechanism by which WS 1442 exerts its barrier-protecting function can be clearly assigned to certain groups of secondary metabolites. Bioactivity-guided fractionation of WS 1442 revealed that the extract's influence on $[Ca^{2+}]_i$ was not due to phenolic compounds, in particular flavonoids. The calcium active subfractions mostly contained triterpenes and fatty acids. However, none of the pure compounds tested from these groups showed any activity. Thus, one may speculate that a mixture of these compounds, or other (minor) substances, is responsible for the influence of $[Ca^{2+}]_i$. In contrast, distinct OPC clusters were found to be responsible for the cortactin activating property of WS 1442. In conclusion, our study supports the principle of phytotherapy, namely that a multi-compound mixture is able to address different cellular signaling pathways that jointly lead to a beneficial therapeutic effect.

Materials and Methods

Compounds

The *Crataegus* special extract WS 1442 (lot no. 289 N001) was kindly provided by Dr. Willmar Schwabe GmbH & Co. KG (Karlsruhe, Germany). A voucher specimen is deposited under the lot

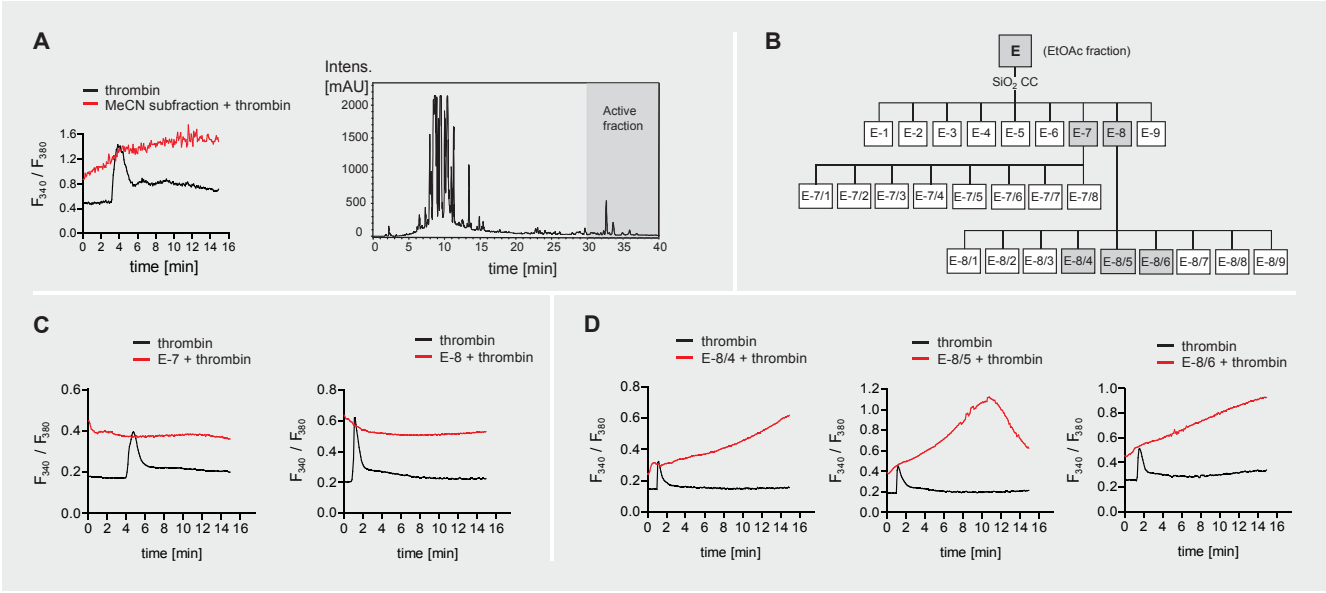

▶ **Fig. 4** Interference of fractions with the thrombin-evoked increase of $[Ca^{2+}]$. **A** Confluent HUVECs were pretreated for 30 min with the MeCN subfraction (5 µg/mL). HPLC-based activity profiling of fraction B. UV trace at 254 nm. Activity was recovered in the fraction collected from 30 to 40 min. For chromatographic conditions, see Material and Methods. **B** Scheme of fractionation and activity distribution (active fractions in grey). **C** Confluent HUVECs were pretreated for 30 min with fractions E-7 and E-8 (10 µg/mL). **D** Confluent HUVECs were pretreated for 30 min with fractions E-8/4, E-8/5, and E-8/6 (10 µg/mL). Changes of $[Ca^{2+}]_i$ were detected by fluorescence microscopy using Fura-2-AM (2 µM) in a static tempered system (37 °C). Thrombin (1 U/mL) was added exactly at time point t = 1 min after initiating the experiment. One representative experiment out of three independently performed experiments (n = 3) is shown.

number at the company. WS 1442 is a dry extract from hawthorn leaves with flowers with a drug extract ratio of 4–6.6 : 1 using ethanol (45 % w/w) as the extraction solvent. WS 1442 is adjusted to a content of 17.3–20.1 % of OPCs. WS 1442, fractions, and OPC clusters were solubilized in DMSO (≥ 99.9 %; Sigma-Aldrich) and stored at − 20 °C. Substances were diluted (concentrations as described in the respective passages) without exceeding a final DMSO concentration of 0.1 %. Hyptatic acid A was kindly provided by Prof. Yongxian Cheng (Kunming Institute of Botany, Chinese Academy of Sciences). The purity was > 95 % according to NMR analysis. Stearic acid (purity > 98.5 %) and palmitic acid (purity > 99 %) were purchased from Sigma-Aldrich and were dissolved in DMSO. Accustain, bovine serum albumin, fluorescein isothiocyanate (FITC)-dextran (40 kDa), thrombin, and Triton X-100 were obtained from Sigma-Aldrich. Fura-2-AM ester was purchased from Biotrend.

Cell culture

Primary HUVECs were purchased from PELOBiotech. The human microvascular endothelial cell line CDC/EU.HMEC-1 [22] was kindly provided by the Centers for Disease Control and Prevention (CDC). HMECs were exclusively used in the permeability assay. ECs were cultured in EC growth medium (ECGM, PELOBiotech), which was supplemented with 10 % heat-inactivated FBS (Biochrom), 100 U/mL penicillin (PAN-Biotech), 100 µg/mL streptomycin (PAN-Biotech), and 0.25 µg/mL amphotericin B (PAN-Biotech) under constant humidity at 37 °C in an atmosphere containing 95 % air and 5 % CO_2.

Macromolecular permeability assay

Macromolecular endothelial permeability was investigated using HMECs in a two-compartment system (Transwell plate with inserts; Corning Life Sciences). The assay was performed as previously reported [9]. Briefly, cells were seeded onto Transwell inserts (pore size 0.4 µm, 12 mm diameter, polyester membrane) until confluency. FITC-dextran (40 kDa; 1 mg/mL) was applied to the upper compartment of the Transwell chamber at t = 0 min and cells were treated as indicated. After 30 min, the samples were taken out of the lower compartment to determine fluorescence intensity with a SpectraFluor Plus plate reader (Tecan).

Cytosolic calcium imaging

Changes in cytosolic calcium levels were determined by ratiometrical analysis with the fluorescent dye Fura-2-AM as previously reported [10]. In brief, HUVECs were grown on 8-well µ-slides (ibidi GmbH) to reach a monolayer. Cells were incubated in HEPES buffer (138 mM NaCl, 10 mM HEPES, 10 mM glucose, 5 mM KCl, 2 mM $CaCl_2$, and 1 mM $MgCl_2$, pH adjusted to 7.4) with Fura-2-AM (2 µM) for 30 min, washed and treated as indicated. Measurements were performed at 37 °C and fluorescence intensity was obtained by a Zeiss Axiovert 200 inverted microscope with a Polychrome V monochromator and an IMAGO-QE camera (TILL Photonics) or with a Leica DMI6000 B microscope and a DFC365FX camera (Leica Microsystems GmbH). Images were taken every 5 seconds and data analysis was performed using TILLvisION software (version 4.0.1.2, TILL Photonics) or LAS X software (version 1.0.12269.0, Leica Microsystems GmbH). Each data point of the different graphs was calculated from a randomly cho-

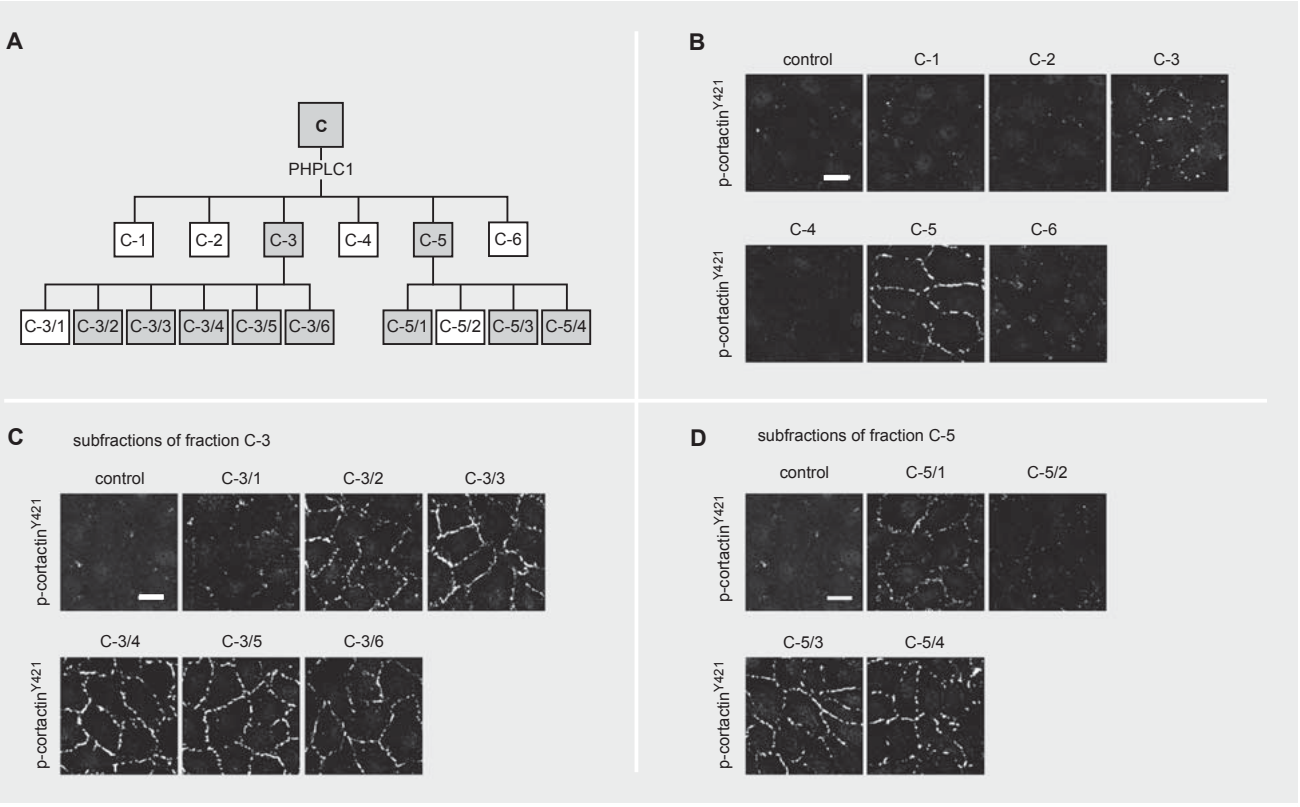

▶ **Fig. 5** Bioactivity-guided subfractionation of fraction C. **A** Scheme of subfractionation and activity distribution (active subfractions in grey). **B** A confluent HUVEC monolayer was either left untreated or was treated for 15 min with WS 1442 fraction C (12 µg/mL) or with one of the different subfractions (C-1 to C-6) (5 µg/mL). Immunocytochemistry and confocal microscopy of Tyr421-phosphorylated cortactin was subsequently performed. C-3 and C-5 are the most potent subfractions, both leading to a strong phosphorylation of cortactin. **C, D** Confluent HUVECs were either left untreated or were treated with 5 µg/mL for 15 min with one of the different WS 1442 subfractions of fraction C-3 (C-3/1 to C-3/6) or with one of the different subfractions of fraction C-5 (C-5/1 to C-5/4). Images were obtained by confocal microscopy (magnification: 40-fold) after immunocytochemical staining of Tyr421-phosphorylated cortactin. One representative image out of three independently performed experiments (n = 3) is shown. Scale bar represents 20 µm.

sen rectangle containing ≥ 30 adjacent cells and thereby mean values were expressed.

Immunocytochemistry and confocal laser scanning microscopy

HUVECs were cultured until confluency on 8-well µ-slides (ibidi GmbH). After treatment as indicated, cells were washed, fixed with Accustain, and permeabilized using Triton X-100 (0.2%). The following antibodies were used: rabbit anti-phospho-cortactin^{Y421} (New England Biolabs GmbH) as the primary antibody and Alexa Fluor 488 goat anti-rabbit (Life Technology GmbH) as the secondary antibody. Stained cells were finally embedded in FluorSave mounting medium (Merck Millipore). Images were obtained with a Zeiss LSM 510 Meta confocal laser-scanning microscope.

Fractionation of the *Crataegus* extract WS 1442

140 g of WS 1442 (lot no. 289 N001) were fractionated using Sephadex LH-20 column (11.5 cm × 150 cm; Pharmacia) chromatography by sequential elution with the following eluents: demineralized water, ethanol 95% (v/v), methanol 100%, and acetone-water 70% (v/v) (organic solvents were of analytical grade from Merck). The complete volume of each individual eluent was collected in a single fraction to give fractions A (yield 80.1 g), B (yield 23.0 g), C (yield 20.7 g), and D (yield 13.8 g), respectively.

HPLC-based activity profiling of fraction B

To localize the activity in fraction B, semipreparative HPLC was performed on an Agilent 1100 instrument equipped with a PDA detector. An aliquot (50 mg) of fraction B was separated in four portions on a SunFire C18 column (5 µm, 150 × 10 mm i. d.; Waters) equipped with a precolumn (10 × 10 mm i. d.). The mobile phase consisted of water with 0.1% HCOOH (A) and MeCN (B). A gradient of 5 to 100% B in 30 min was used, followed by 100% MeCN for 10 min. The flow rate was 4 mL/min. Nine fractions were collected between 1.5 and 40.0 min. Activity was recovered in the last fraction (4.4 mg, t_R 30–40 min).

Fractionation of the extract WS 1442 to identify active compounds in fraction B

The extract WS 1442 (48 g) was partitioned between H_2O (900 mL) and EtOAc (3 × 900 mL). The organic layers were combined and dried under reduced pressure. The EtOAc-soluble frac-

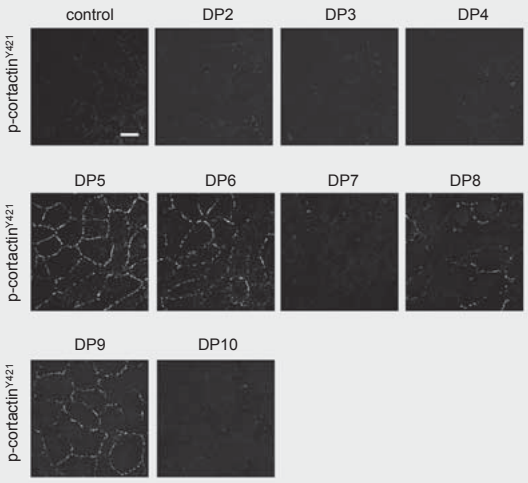

▶ **Fig. 6** The bioactivity distribution could be narrowed down to the highly active OPC clusters DP5, DP6, DP8, and DP9. Increasing cortactin phosphorylation at the cell border of HUVECs was analyzed by immunocytochemistry. Confluent HUVECs were either left untreated or treated for 15 min with OPC clusters with rising degrees of polymerization (DP2-DP10) (5 µg/mL). Images were obtained by confocal microscopy (magnification: 40-fold) after immunocytochemical staining of Tyr421-phosphorylated cortactin. One representative image out of three independently performed experiments (n = 3) is shown. The scale bar represents 20 µm.

tion (8.34 g, fraction E) was separated by silica gel CC (75 × 6 cm i.d. column) with $CHCl_3$-MeOH mixtures of increasing polarity (97 : 3 to 9 : 1). The resulting fractions were analyzed by TLC and combined to nine fractions according to the similarity of the chromatograms. Fraction E-8 (92 mg) was dissolved in DMSO-THF 1 : 1 at a concentration of 100 mg/mL, and separated by semipreparative HPLC on a C18 SunFire HPLC column (10.0 × 150 mm; 5 µm; Waters). The mobile phase consisted of H_2O (A) and MeCN (B). A gradient of 5–100 % B in 30 min, with a 5 min 100 % B wash, was applied. The flow rate was 4.0 mL/min. Detection was set at UV 288 nm. Aliquots of 100 µL each were injected. Nine fractions were obtained (fractions E-8/1 to E-8/9) by using a combination of peak-based and time-based collection. Activity was found in fractions E-8/4 (t_R 19.2–19.4 min, 0.7 mg), E-8/5 (t_R 21.1–22.1 min, 1.9 mg), and E-8/6 (t_R 25.7–25.9 min, 2.0 mg). Fraction E-7 (141 mg) was separated following the same chromatographic conditions as for fraction E-8, but with detection at UV 247 nm. Eight fractions were collected, but no activity could be recovered in any of them. ^{1}H-NMR spectra of active fractions and the reference compound hyptatic acid A were recorded on an Avance III spectrometer (Bruker) equipped with a 1-mm TXI microprobe.

Subfractionation of fraction C

12 g of fraction C were further fractionated by using the preparative HPLC system (VWR International); column: 350 × 50 mm packed with YMC RP-18 ODS-AQ 15 µm (Phenomenex). Elution with methanol 30 % (v/v) afforded six fractions (C-1 to C-6), namely C-1 (0.8 g), C-2 (0.7 g), C-3 (2.7 g), C-4 (3.6 g), C-5 (1.8 g), and C-6 (2.3 g). Fractions C-3 (2.0 g) and C-5 (1.36 g) were further separated over a Sephadex LH-20 column (70 × 4.25 cm; Pharmacia). Methanol 100 % was used as the eluent. The flow rate was 1 mL/min, and fractions of 15 min were collected and combined to fractions C-3/1 (90 mg), C-3/2 (240 mg), C-3/3 (260 mg), C-3/4 (310 mg), C-3/5 (350 mg), C-3/6 (670 mg), C-5/1 (260 mg), C-5/2 (360 mg), C-5/3 (380 mg), and C-5/4 (380 mg).

Isolation of oligomeric oligomeric procyanidin clusters

Hawthorn leaf and flower (Crataegi folium cum flore) dried plant material according to the specification of the European Pharmacopoeia [European Pharmacopoeia Version 8.0 (2015) Hawthorn leaf and flower, version 01/2010 : 1432] were obtained from Caesar-Loretz GmbH (Ch. No. 52467097). Reference samples (Voucher No. IPBP240) are stored at the Institute of Pharmaceutical Biology and Phytochemistry (University of Münster, Germany). An acetone-water (7 : 3) extract and the water-soluble part of this extract were prepared from hawthorn leaf and flower plant material as recently described in detail [23]. Of the lyophilized acetone-water extract, 1.3 g dissolved in 10 mL MeOH-water (1 : 9 v/v) were fractionated by medium-pressure liquid chromatography (MPLC) on RP-18, 18–32 µm, 100 Å, 460 × 26 mm (Büchi Labortechnik GmbH) at a flow rate of 9 mL/min (pump BESTA E100; BESTA Technik GmbH). A step gradient of MeOH 30 % (460 mL), MeOH 50 % (480 mL), and MeOH 100 % (510 mL) was used. Fractionation: pre-run 200 mL, discarded (no OPCs detectable by TLC); fractions 1–15 (590 mL), discarded (no OPCs detectable by TLC); fractions 16–24 (238 mL), OPCs detectable by TLC (named as “F1”; 0.09 g); fractions 25–51 (632 mL), OPCs detectable by TLC (named as “F2”; 0.14 g); fractions 52–62 (234 mL), OPCs detectable by TLC (named as “F3”; 0.06 g); fractions 63–84 (780 mL), discarded (no OPCs detectable by TLC). For further fractionation, the MPLC fraction “F2” was used, which had been obtained in a yield of 10.8 % (w/w) related to the acetone-water extract [16].

Preparative HPLC for isolation of oligomeric procyanidins from F2

136 mg of MPLC fraction F2, dissolved in acetonitrile-water (1 : 1), were fractionated by HPLC into distinct OPC clusters (total OPC yield 41.6 mg). Yield of cluster DP2 was 6 mg, DP3 7 mg, DP4 6.5 mg, DP5 5.6 mg, DP6 5.4 mg, DP7 4 mg, DP8 3 mg, DP9 2.5 mg, and DP10 1.6 mg. HPLC was performed using two Waters 515 HPLC pumps, Waters dual λ absorbance detector, Waters pump control module, software Millenium32 (Waters), and degasser uniflows degasys DG-2410 (Optilab). Stationary phase: Uptisphere 120 Å, bonding OH, 6 µm, 250 × 21.2 mm ID (Interchim). Mobile phase A: acetonitrile; mobile phase B: MeOH-water (95 : 5 v/v); elution gradient [min (% A)]: initial (100), 0–30 (100 → 60), 30–40 (60, isocratic), 40–45 (60 → 50), 45–50 (50 → 0), 50–55 (0, isocratic), 55–60 (0 → 100), 60–70 (100, isocratic). The flow rate was 10 mL/min and detection λ was 280 nm [16].

Analytical characterization of oligomeric procyanidins by MS

The molecular weight of OPCs was determined by ESI-MS in the negative ion mode (Bruker Daltonics micrOTOF; Bruker). MS spectroscopy was performed exemplarily on OPC clusters DP2, DP4, and DP7: OPC cluster DP2, found *m/z* 577.1349 $(M - H)^-$, calculated *m/z* 577.1352; OPC cluster DP4, found *m/z* 1153.2601 $(M - H)^-$, calculated *m/z* 1153.2608; OPC cluster DP7, found *m/z* 1008.2137 $(M - H)^-$, calculated *m/z* 1008.2224 [16].

Purity control of oligomeric procyanidin clusters (HPLC on diol and RP-18 phase)

Purity control of OPC clusters by HPLC was performed using Waters Alliance with Waters 996 PAD and Waters 2475 multi-λ fluorescence detector and the software Empower 2 (Waters). Stationary phase 1: Uptisphere 120 Å, bonding OH, 6 µm, 250 × 4.6 mm ID (Interchim); detection PAD 200–400 nm, FLD λ_{exc} 280 nm, λ_{em} 316 nm; column temperature 40 °C; injection volume 10 µL; test sample dissolved in acetonitrile-water (1 : 1); flow rate 0.8 mL/min. Mobile phase A: acetonitrile-acetic acid (98 : 2 v/v); mobile phase B: MeOH-water-acetic acid (95 : 3 : 2 v/v/v); elution gradient [min (% A)]: initial (100), 0–38 (100 → 60), 38–45 (isocratic), 45–50 (60 → 0), 60–65 (isocratic), 65–70 (0 → 100). Stationary phase 2: Phenomenex 100 Å, Luna 5 µm, 250 × 3.0 mm ID (Phenomenex); detection PAD 200–400 nm; column temperature 40 °C; injection volume 10 µL. Flow gradient: 0 min 0.9 mL/min, 50 min 0.9 mL/min, 55 min 1.0 mL/min, 60 min 1.0 mL/min, 65 min 0.9 mL/min. Mobile phase A: water + TFA 0.1 % (1 : 1 v/v); mobile phase B: acetonitrile; elution gradient: 0 min 95 % A, 50 min 50 % A, 55 min 0 % A, 60 min 0 % A, 65 min 95 % A. ^{13}C-NMR spectroscopy was performed by using 100 mg of the polymer fraction in MeOH-d_4 (VWR International GmbH) over 60 h using a Varian UNITY Plus 600 (Varian, Inc.) [16].

Statistical analysis

All experiments were independently performed three times (n = 3). In the case that nothing else is mentioned, bar graph data are expressed as means ± SD. Statistical analysis was performed with the software Prism (version 5.04; GraphPad Software). One-way analysis of variance (ANOVA) followed by Dunnett's post-hoc test was used. P values ≤ 0.05 were considered statistically significant.

Supporting information

The GC-MS analysis of fatty acids in fractions E-8/4, E-8/5, and E-8/6, ^{1}H NMR spectra of hyptatic acid A and fractions E-8/4, E-8/5, and E-8/6 as well as measurements of the action of palmitic acid, stearic acid, and hyptatic acid A on endothelial calcium levels are available as Supporting Information.

Acknowledgements

Thanks are due to Prof. Yongxian Cheng, State Key Laboratory of Phytochemistry and Plant Resources in West China, Kunming Institute of Botany, Chinese Academy of Sciences, for the generous gift of a sample of hyptatic acid A, and to Orlando Fertig (Division of Pharmaceutical Biology, University of Basel) for performing the GC-MS analysis of the fatty acids. We thank Dr. Ilse Zündorf for her help in preparing the figures. This work was funded, in part, by the German Research Foundation (DFG, FU691/7-1).

Conflict of Interest

Clemens Erdelmeier and Egon Koch are employees of the company that manufactures WS 1442.

References

[1] Tauchert M. Efficacy and safety of *Crataegus* extract WS 1442 in comparison with placebo in patients with chronic stable New York Heart Association class-III heart failure. Am Heart J 2002; 143: 910–915

[2] Pittler MH, Guo R, Ernst E. Hawthorn extract for treating chronic heart failure. Cochrane Database Syst Rev 2008; 1: CD005312

[3] Zapfe jr. G. Clinical efficacy of *Crataegus* extract WS 1442 in congestive heart failure NYHA class II. Phytomedicine 2001; 8: 262–266

[4] Asher GN, Viera AJ, Weaver MA, Dominik R, Caughey M, Hinderliter AL. Effect of hawthorn standardized extract on flow mediated dilation in prehypertensive and mildly hypertensive adults: a randomized, controlled cross-over trial. BMC Complement Altern Med 2012; 12: 26

[5] Idris-Khodja N, Auger C, Koch E, Schini-Kerth VB. *Crataegus* special extract WS 1442 prevents aging-related endothelial dysfunction. Phytomedicine 2012; 19: 699–706

[6] Schmidt U, Kuhn U, Ploch M, Hubner WD. Efficacy of the Hawthorn (*Crataegus*) preparation LI 132 in 78 patients with chronic congestive heart failure defined as NYHA functional class II. Phytomedicine 1994; 1: 17–24

[7] Eggeling T, Regitz-Zagrosek V, Zimmermann A, Burkart M. Baseline severity but not gender modulates quantified *Crataegus* extract effects in early heart failure – a pooled analysis of clinical trials. Phytomedicine 2011; 18: 1214–1219

[8] Härtel S, Kutzner C, Westphal E, Limberger M, Burkart M, Ebner-Priemer U, Kohl-Bareis M, Bös K. Effects of endurance exercise training and *Crataegus* extract WS 1442 in patients with heart failure with preserved ejection fraction – a randomized controlled trial. Sports 2014; 2: 59–75

[9] Bubik MF, Willer EA, Bihari P, Jürgenliemk G, Ammer H, Krombach F, Zahler S, Vollmar AM, Fürst R. A novel approach to prevent endothelial hyperpermeability: the *Crataegus* extract WS 1442 targets the cAMP/Rap1 pathway. J Mol Cell Cardiol 2012; 52: 196–205

[10] Willer EA, Malli R, Bondarenko AI, Zahler S, Vollmar AM, Graier WF, Fürst R. The vascular barrier-protecting hawthorn extract WS 1442 raises endothelial calcium levels by inhibition of SERCA and activation of the IP3 pathway. J Mol Cell Cardiol 2012; 53: 567–577

[11] Chatterjee SS, Koch E, Jaggy H, Krzeminski T. *In vitro* and *in vivo* studies on the cardioprotective action of oligomeric procyanidins in a *Crataegus* extract of leaves and blooms. Arzneimittelforschung 1997; 47: 821–825

[12] Horan KL, Adamski SW, Ayele W, Langone JJ, Grega GJ. Evidence that prolonged histamine suffusions produce transient increases in vascular permeability subsequent to the formation of venular macromolecular leakage sites. Proof of the Majno-Palade hypothesis. Am J Pathol 1986; 123: 570–576

[13] Robert AM, Tixier JM, Robert L, Legeais JM, Renard G. Effect of procyanidolic oligomers on the permeability of the blood-brain barrier. Pathol Biol (Paris) 2001; 49: 298–304

[14] Fan Y, Wu DZ, Gong YQ, Zhou JY, Hu ZB. Effects of calycosin on the impairment of barrier function induced by hypoxia in human umbilical vein endothelial cells. Eur J Pharmacol 2003; 481: 33–40

[15] Potterat O, Hamburger M. Combined use of extract libraries and HPLC-based activity profiling for lead discovery: potential, challenges, and practical considerations. Planta Med 2014; 80: 1171–1181

[16] Hellenbrand N, Sendker J, Lechtenberg M, Petereit F, Hensel A. Isolation and quantification of oligomeric and polymeric procyanidins in leaves and flowers of Hawthorn (*Crataegus* spp.). Fitoterapia 2015; 104: 14–22

[17] Blazso G, Gabor M, Rohdewald P. Antiinflammatory activities of procyanidin-containing extracts from *Pinus pinaster* Ait. after oral and cutaneous application. Pharmazie 1997; 52: 380–382

[18] Dongmo AB, Kamanyi A, Anchang MS, Chungag-Anye Nkeh B, Njamen D, Nguelefack TB, Nole T, Wagner H. Anti-inflammatory and analgesic properties of the stem bark extracts of *Erythrophleum suaveolens* (Caesalpiniaceae), Guillemin & Perrottet. J Ethnopharmacol 2001; 77: 137–141

[19] Holt RR, Lazarus SA, Sullards MC, Zhu QY, Schramm DD, Hammerstone JF, Fraga CG, Schmitz HH, Keen CL. Procyanidin dimer B2 [epicatechin-(4beta-8)-epicatechin] in human plasma after the consumption of a flavanol-rich cocoa. Am J Clin Nutr 2002; 76: 798–804

[20] Sano A, Yamakoshi J, Tokutake S, Tobe K, Kubota Y, Kikuchi M. Procyanidin B1 is detected in human serum after intake of proanthocyanidin-rich grape seed extract. Biosci Biotechnol Biochem 2003; 67: 1140–1143

[21] Tsang C, Auger C, Mullen W, Bornet A, Rouanet JM, Crozier A, Teissedre PL. The absorption, metabolism and excretion of flavan-3-ols and procyanidins following the ingestion of a grape seed extract by rats. Br J Nutr 2005; 94: 170–181

[22] Ades EW, Candal FJ, Swerlick RA, George VG, Summers S, Bosse DC, Lawley TJ. HMEC-1: establishment of an immortalized human microvascular endothelial cell line. J Invest Dermatol 1992; 99: 683–690

[23] Zumdick S, Petereit F, Luftmann H, Hensel A. Preparative isolation of oligomeric procyanidins from Hawthorn (*Crataegus* spp.). Pharmazie 2009; 64: 286–288